

**ANALYTICAL AND LASER SCANNING TECHNIQUES TO DETERMINE  
SHAPE PROPERTIES OF AGGREGATES USED IN PAVEMENTS**

**JULIUS JOSEPH KOMBA**

**A dissertation submitted in partial fulfilment of the requirements of the  
degree of**

**MASTER OF ENGINEERING (TRANSPORTATION ENGINEERING)**

**In the**

**FACULTY OF ENGINEERING**

**UNIVERSITY OF PRETORIA**

**June 2013**

## **DISSERTATION SUMMARY**

### **ANALYTICAL AND LASER SCANNING TECHNIQUES TO DETERMINE SHAPE PROPERTIES OF AGGREGATES USED IN PAVEMENTS**

**JULIUS JOSEPH KOMBA**

**Supervisor:** Professor W.J.vdM Steyn  
**Co- Supervisor:** Doctor J.K Anochie-Boateng  
**Department:** Civil Engineering  
**University:** University of Pretoria  
**Degree:** Master of Engineering (Transportation Engineering)

#### **SUMMARY:**

Pavement layers are constructed using a combination of materials, of which rock aggregates constitute a larger proportion. Current understanding is that the performance of pavements is dependent on the aggregate shape properties which include form, angularity and surface texture. However, direct and accurate measurements of aggregate shape properties remain a challenge. The current standard test methods used to evaluate aggregate shape properties cannot measure these properties accurately. Among the reasons contributing to the difficulties in the determination of aggregate shape properties is irregular shapes of aggregate particles. Therefore, current research efforts focus on developing accurate, reliable and innovative techniques for evaluation of aggregate shape properties.

The work presented in this dissertation contributes to the current innovative research at the Council for Scientific and Industrial Research (CSIR) in South Africa, to automate the measurement of aggregate shape properties. The CSIR's present research is aimed at improving pavement performance through better materials characterisation, using laser scanning and advanced modelling techniques. The objective of this study was to investigate improved techniques for the determination of aggregate shape properties using analytical and laser scanning techniques.

A three-dimensional (3-D) laser scanning device was used for scanning six types of aggregate samples commonly used for construction of pavements in South Africa. The laser scan data were processed to reconstruct 3-D models of the aggregate particles. The models were further analysed to determine the shape properties of the aggregates. Two analysis approaches were used in this study. The first approach used the aggregate's physical properties (surface area, volume and orthogonal dimensions) measured by using laser scanning technique to compute three different indices to describe the form of aggregates. The computed indices were the sphericity computed by using surface area and volume of an aggregate particle, the sphericity computed by using orthogonal dimensions of an aggregate particle, and the flat and elongated ratio computed by using longest and smallest dimensions of an aggregate particle. The second approach employed a spherical harmonic analysis technique to analyse the aggregate laser scan data to determine aggregate form, angularity and surface texture indices. A MATLAB<sup>TM</sup> code was developed for analysis of laser scan data, using the spherical harmonic analysis technique.

The analyses contained in this dissertation indicate that the laser-based aggregate shape indices were able to describe the shape properties of the aggregates studied. Furthermore, good correlations were observed between the spherical harmonic form indices and the form indices determined by using the aggregate's physical properties. This shows that aggregate laser scanning is a versatile technique for the determination of various indices to describe aggregate shape properties.

Further validation of the laser-based technique was achieved by correlating the laser-based aggregate form indices with the results from two current standard tests; the flakiness index and the flat and elongated particles ratio tests. The laser-based form indices correlated linearly with both, the flakiness index and the flat and elongated particles ratio test results. The observed correlations provide an indication of the validity of laser-based aggregate shape indices. It is concluded that the laser based scanning technique could be employed for direct and accurate determination of aggregate shape properties.

## DECLARATION

I, the undersigned hereby declare that:

I understand what plagiarism is and I am aware of the University's policy in this regard;

The work contained in this thesis is my own original work;

I did not refer to work of current or previous students, lecture notes, handbooks or any other study material without proper referencing;

Where other people's work has been used this has been properly acknowledged and referenced;

I have not allowed anyone to copy any part of my thesis;

I have not previously in its entirety or in part submitted this thesis at any university for degree.

### **Signature of student**

#### **Name of student**

Julius Joseph Komba

#### **Student number**

26431620

#### **Date**

June 2013

## ACKNOWLEDGEMENT

I wish to express my appreciation to the following organisations and individuals who made this dissertation possible:

- a) Prof. W.J.vdM Steyn, my supervisor for his guidance and support during the study.
- b) Dr. J.K Anochie-Boateng, My co-supervisor and Principal Investigator of the CSIR's project on laser scanning and modelling of aggregates for his guidance and support during the study.
- c) The Council for Scientific and Industrial Research (CSIR) through its R&D office for funding this research through Strategic Research Panel (SRP) project TA 2011-001. The CSIR's Parliamentary Grant (PG) for 2012/2013 also supported this study.
- d) Dr. James W Maina, Pavement Design and Construction group manager at the CSIR for many discussions and his encouragement during the study.
- e) Dr. Martin Mgangira, for many discussions during the study.
- f) Mr. Colin Fisher, for his assistance with MATLAB<sup>TM</sup> software.
- g) My colleagues at the CSIR, Transport Infrastructure Engineering (TIE) Competency Area for their support and useful discussion during the study.
- h) CSIR Built Environment Pavement material laboratory staff for their assistance and support during the study.
- i) My parents, brothers and sisters for their encouragement and support during the study.

## TABLE OF CONTENTS

1	INTRODUCTION .....	1-1
1.1	Background .....	1-1
1.2	Problem definition.....	1-2
1.3	Objectives of the study .....	1-3
1.4	Scope of the study .....	1-3
1.5	Methodology .....	1-3
1.6	Organisation of the dissertation.....	1-4
2	LITERATURE REVIEW .....	2-1
2.1	Introduction .....	2-1
2.2	Coarse aggregate shape properties .....	2-1
2.3	Influence of aggregate shape properties on pavement performance .....	2-3
2.4	Current standard tests and specifications for coarse aggregates .....	2-4
2.4.1	Evaluation of form .....	2-4
2.4.2	Evaluation of angularity .....	2-7
2.4.3	Evaluation of surface texture.....	2-8
2.4.4	Limitations of the current standard tests .....	2-8
2.5	Advanced measurement of aggregate shape properties.....	2-9
2.5.1	Image-based technique .....	2-9
2.5.2	Laser-based technique .....	2-13
2.6	Characterisation of coarse aggregate shape properties.....	2-16
2.6.1	Form indices .....	2-16
2.6.2	Angularity indices .....	2-18
2.6.3	Surface texture indices .....	2-19
2.6.4	Mathematical-based analysis of aggregate shape properties .....	2-21
2.6.5	Fourier analysis .....	2-21
2.6.6	Spherical harmonics analysis .....	2-23
2.6.7	Wavelet transform .....	2-24
2.7	Summary .....	2-26
3	METHODOLOGY .....	3-1
3.1	Introduction .....	3-1
3.2	Material selection and sample preparation .....	3-1
3.3	Laser scanning of aggregates .....	3-3
3.4	Determination of laser-based aggregate shape properties .....	3-5
3.5	Validation of aggregate shape properties .....	3-6
3.6	Summary .....	3-6
4	LABORATORY TESTING AND LASER SCANNING RESULTS .....	4-1
4.1	Introduction .....	4-1

4.2	Laboratory test results .....	4-1
4.3	Results of scanned aggregate particles .....	4-4
4.4	Grading of the aggregate particles selected for laser scanning .....	4-15
4.5	Summary .....	4-20
5	DATA ANALYSIS AND DISCUSSIONS .....	5-1
5.1	Introduction .....	5-1
5.2	Quantification of aggregate form indices by using physical properties .....	5-1
5.2.1	Sphericity computed using surface area and volume .....	5-2
5.2.2	Sphericity computed using orthogonal dimensions.....	5-4
5.2.3	Flat and elongated ratio .....	5-6
5.2.4	Discussion of the laser-based form indices results.....	5-8
5.3	Quantification of aggregate shape properties by using spherical harmonic analysis .....	5-9
5.3.1	Pre-processing of laser scan data.....	5-9
5.3.2	Determination of spherical harmonic coefficients .....	5-13
5.3.3	Validation of the computation of harmonic coefficients and radii.....	5-15
5.3.4	Spherical harmonics form indices .....	5-28
5.3.5	Spherical harmonics angularity indices.....	5-31
5.3.6	Spherical harmonics surface texture indices .....	5-34
5.4	Correlation of spherical harmonics form indices with other form indices .....	5-37
5.5	Validation of the laser-based form indices.....	5-47
5.5.1	Correlation of flakiness index with laser-based form indices .....	5-47
5.5.2	Correlation of flat and elongated particles ratio with laser-based form indices ...	5-51
5.6	Selection of aggregates for pavement construction.....	5-58
5.7	Summary .....	5-59
6	CONCLUSIONS AND RECOMMENDATIONS .....	6-1
6.1	Conclusions .....	6-1
6.2	Recommendations .....	6-3
7	REFERENCES .....	7-1
8	APPENDIX A: AGGREGATE SCAN RESULTS .....	8-1
9	APPENDIX B: MATLAB CODE FOR ANALYSIS OF LASER SCAN DATA .....	9-1
10	APPENDIX C: EFFECT OF DEGREE ( <i>l</i> ) VALUE ON CONVERGENCE.....	10-1

## LIST OF TABLES

Table 2.1: Flakiness index specifications .....	2-5
Table 2.2: Specifications for flat and elongated particles .....	2-6
Table 2.3: Specifications for angularity .....	2-7
Table 3.1: Aggregate samples .....	3-2
Table 4.1: Grading analysis and standard laboratory test results .....	4-2
Table 4.2: Scan results of 19.0 mm granite aggregate particles.....	4-8
Table 5.1: Statistical parameters for sphericity computed using surface area and volume.....	5-3
Table 5.2: Statistical parameters for sphericity computed using orthogonal dimensions.....	5-5
Table 5.3: Statistical parameters for flat and elongated ratio.....	5-7
Table 5.4: Criteria for identification of the quadrant of the vertex.....	5-13
Table 5.5: Criteria for computation of angle $\alpha$ .....	5-13
Table 5.6: Spherical Harmonics .....	5-14
Table 5.7: Effect of varying degree ( $l$ ).....	5-17
Table 5.8: Form indices for different degree ( $l$ ) Values.....	5-29
Table 5.9: Statistical parameters for spherical harmonic form index.....	5-30
Table 5.10: Comparison of angularity indices.....	5-33
Table 5.11: Comparison of surface texture indices.....	5-36
Table 8.1: Scan results of 19.0 mm granite aggregate particles.....	8-1
Table 8.2: Scan results of 13.2 mm granite aggregate particles.....	8-2
Table 8.3: Scan results of 9.5 mm granite aggregate particles.....	8-3
Table 8.4: Scan results of 6.7 mm granite aggregate particles.....	8-4
Table 8.5: Scan results of 4.75 mm granite aggregate particles.....	8-5
Table 8.6: Scan results of 19.0 mm tillite aggregate particles.....	8-6
Table 8.7: Scan results of 13.2 mm tillite aggregate particles.....	8-7
Table 8.8: Scan results of 9.5 mm tillite aggregate particles.....	8-8
Table 8.9: Scan results of 6.7 mm tillite aggregate particles.....	8-9
Table 8.10: Scan results of 4.75 mm tillite aggregate particles.....	8-10
Table 8.11: Scan results of 19.0 mm quartzite aggregate particles.....	8-11
Table 8.12: Scan results of 13.2 mm quartzite aggregate particles.....	8-12
Table 8.13: Scan results of 9.5 mm quartzite aggregate particles.....	8-13
Table 8.14: Scan results of 6.7 mm quartzite aggregate particles.....	8-14
Table 8.15: Scan results of 4.75 mm quartzite aggregate particles.....	8-15
Table 8.16: Scan results of 19.0 mm hornfels aggregate particles.....	8-16
Table 8.17: Scan results of 13.2 mm hornfels aggregate particles.....	8-17
Table 8.18: Scan results of 9.5 mm hornfels aggregate particles.....	8-18
Table 8.19: Scan results of 6.7 mm hornfels aggregate particles.....	8-19
Table 8.20: Scan results of 4.75 mm hornfels aggregate particles.....	8-20
Table 8.21: Scan results of 19.0 mm alluvial gravel aggregate particles.....	8-21
Table 8.22: Scan results of 13.2 mm alluvial gravel aggregate particles.....	8-22
Table 8.23: Scan results of 9.5 mm alluvial gravel aggregate particles.....	8-23
Table 8.24: Scan results of 6.7 mm alluvial gravel aggregate particles.....	8-24
Table 8.25: Scan results of 4.75 mm alluvial gravel aggregate particles.....	8-25
Table 8.26: Scan results of 19.0 mm RA aggregate particles.....	8-26
Table 8.27: Scan results of 13.2 mm RA aggregate particles.....	8-27
Table 8.28: Scan results of 9.5 mm RA aggregate particles.....	8-28
Table 8.29: Scan results of 6.7 mm RA aggregate particles.....	8-29
Table 8.30: Scan results of 4.75 mm RA aggregate particles.....	8-30



## LIST OF FIGURES

Figure 2.1: Fundamental aggregate shape properties .....	2-2
Figure 2.2: Flakiness index test apparatus.....	2-5
Figure 2.3: Proportional caliper device. ....	2-6
Figure 2.4 Angular and non-angular aggregate particles. ....	2-7
Figure 2.5: Chart for visual evaluation of roundness of aggregate . ....	2-10
Figure 2.6: Chart for visual evaluation of sphericity of aggregate .....	2-11
Figure 2.7: The University of Illinois Aggregate Image Analyser .....	2-12
Figure 2.8: The Aggregate Imaging System . ....	2-13
Figure 2.9: Laser-based Aggregate Scanning System .....	2-14
Figure 2.10: A 3-D laser scanning device at the CSIR. ....	2-15
Figure 2.11: Actual and scanned aggregate particles .....	2-15
Figure 2.12: Representation of an aggregate particle for Fourier analysis.....	2-22
Figure 3.1: Aggregate scanning process. ....	3-4
Figure 3.2: Procedures for laser based-based determination of aggregate shape properties. ....	3-5
Figure 4.1: Grading analysis results. ....	4-3
Figure 4.2: Actual and modelled 19.0 mm for granite, tillite and quartzite. ....	4-5
Figure 4.3: Actual and modelled 19.0 mm for hornfels, alluvial gravel and RA. ....	4-6
Figure 4.4: Surface area and volume of granite. ....	4-9
Figure 4.5: Surface area and volume of tillite. ....	4-10
Figure 4.6: Surface area and volume of quartzite. ....	4-11
Figure 4.7: Surface area and volume of hornfels. ....	4-12
Figure 4.8: Surface area and volume of alluvial gravel. ....	4-13
Figure 4.9: Surface area and volume of RA. ....	4-14
Figure 4.10: Flat and elongated particle passing through a sieve with the intermediate size greater than the sieve size.....	4-15
Figure 4.11: Grading curves for granite and tillite. ....	4-17
Figure 4.12: Grading curves for quartzite and hornfels. ....	4-18
Figure 4.13: Grading curves for alluvial gravel and RA. ....	4-19
Figure 5.1: Distributions of sphericity computed using surface area and volume. ....	5-4
Figure 5.2: Distributions of sphericity computed using orthogonal dimensions.....	5-5
Figure 5.3: Distributions of flat and elongated ratio. ....	5-7
Figure 5.4: Mesh model of scanned spherical object. ....	5-10
Figure 5.5: Mesh model of scanned aggregate particle.....	5-10
Figure 5.6: Surface point data of scanned aggregate particle.....	5-11
Figure 5.7: Relationship between Cartesian and polar coordinate systems. ....	5-12
Figure 5.8: Average absolute errors for a spherical object.....	5-18
Figure 5.9: Average absolute errors for a cubical aggregate.....	5-19
Figure 5.10: Average absolute errors for an elongated aggregate.....	5-20
Figure 5.11: Radii determined from the laser scans and radii computed by using the spherical harmonic technique for a spherical object.....	5-22
Figure 5.12: Radii determined from the laser scans and radii computed by using the spherical harmonic technique for a cubical aggregate.....	5-23
Figure 5.13: Radii determined from the laser scans and radii computed by using the spherical harmonic technique for an elongated aggregate.....	5-24
Figure 5.14: Radii determined from the laser scans versus radii computed by using the spherical harmonic technique for a spherical object.....	5-25
Figure 5.15: Radii determined from the laser scans versus radii computed by using the spherical harmonic technique for a cubical aggregate.....	5-26
Figure 5.16: Radii determined from the laser scans versus radii computed by using the spherical harmonic technique for an elongated aggregate.....	5-27
Figure 5.17: Distribution of spherical harmonic form index.....	5-30

Figure 5.18: Distribution of spherical harmonic angularity index. ....	5-32
Figure 5.19: Distribution of spherical harmonic surface texture index. ....	5-35
Figure 5.20: Spherical harmonic form index versus sphericity computed using volume and surface area for granite. ....	5-38
Figure 5.21: Spherical harmonic form index versus sphericity computed using volume and surface area for tillite. ....	5-39
Figure 5.22: Spherical harmonic form index versus sphericity computed using volume and surface area for quartzite. ....	5-39
Figure 5.23: Spherical harmonic form index versus sphericity computed using volume and surface area for hornfels. ....	5-40
Figure 5.24: Spherical harmonic form index versus sphericity computed using volume and surface area for alluvial gravel. ....	5-40
Figure 5.25: Spherical harmonic form index versus sphericity computed using volume and surface area for RA. ....	5-41
Figure 5.26: Spherical harmonic form index versus sphericity computed using orthogonal dimensions for granite. ....	5-41
Figure 5.27: Spherical harmonic form index versus sphericity computed using orthogonal dimensions for tillite. ....	5-42
Figure 5.28: Spherical harmonic form index versus sphericity computed using orthogonal dimensions for quartzite. ....	5-42
Figure 5.29: Spherical harmonic form index versus sphericity computed using orthogonal dimensions for hornfels. ....	5-43
Figure 5.30: Spherical harmonic form index versus sphericity computed using orthogonal dimensions for alluvial gravel. ....	5-43
Figure 5.31: Spherical harmonic form index versus sphericity computed using orthogonal dimensions for RA. ....	5-44
Figure 5.32: Spherical harmonic form index versus flat and elongated ratio for granite. ....	5-44
Figure 5.33: Spherical harmonic form index versus flat and elongated ratio for tillite. ....	5-45
Figure 5.34: Spherical harmonic form index versus flat and elongated ratio for quartzite. ....	5-45
Figure 5.35: Spherical harmonic form index versus flat and elongated ratio for hornfels. ....	5-46
Figure 5.36: Spherical harmonic form index versus flat and elongated ratio for alluvial gravel. 5-46	
Figure 5.37: Spherical harmonic form index versus flat and elongated ratio for RA. ....	5-47
Figure 5.38: Flakiness index versus sphericity computed by using volume and surface area. ....	5-49
Figure 5.39: Flakiness index versus sphericity computed by using orthogonal dimensions. ....	5-49
Figure 5.40: Flakiness index versus flat and elongated ratio. ....	5-50
Figure 5.41: Flakiness index versus spherical harmonic form index. ....	5-50
Figure 5.42: Flat and elongated particles ratio (proportional caliper set at 5:1) versus sphericity computed by using volume and surface area. ....	5-52
Figure 5.43: Flat and elongated particles ratio (proportional caliper set at 5:1) versus sphericity computed by using orthogonal dimensions. ....	5-52
Figure 5.44: Flat and elongated particles ratio determined using the standard method (proportional caliper set at 5:1) versus the laser-based flat and elongated ratio. ....	5-53
Figure 5.45: Flat and elongated particles ratio determined using the standard method (proportional caliper set at 5:1) versus spherical harmonic form index. ....	5-53
Figure 5.46: Flat and elongated particles ratio (proportional caliper set at 3:1) versus sphericity computed by using volume and surface area. ....	5-54
Figure 5.47: Flat and elongated particles ratio (proportional caliper set at 3:1) versus sphericity computed by using orthogonal dimensions. ....	5-54
Figure 5.48: Flat and elongated particles ratio determined using the standard method (proportional caliper set at 3:1) versus laser-based flat and elongated ratio. ....	5-55
Figure 5.49: Flat and elongated particles ratio determined using the standard method (proportional caliper set at 3:1) versus spherical harmonic form index. ....	5-55

Figure 5.50: Flat and elongated particles ratio (proportional caliper set at 2:1) versus sphericity computed by using volume and surface area.....	5-56
Figure 5.51: Flat and elongated particles ratio (proportional caliper set at 2:1) versus sphericity computed by using orthogonal dimensions. ....	5-56
Figure 5.52: Flat and elongated particles ratio determined using the standard method (proportional caliper set at 2:1) versus laser-based flat and elongated ratio. ....	5-57
Figure 5.53: Flat and elongated particles ratio determined using the standard method (proportional caliper set at 2:1) versus spherical harmonic form index. ....	5-57
Figure 10.1: Radii determined from laser scans and radii computed using spherical harmonic technique for 19 mm spherical object ( $l=5$ and $10$ ). ....	10-1
Figure 10.2: Radii determined from laser scans and radii computed using spherical harmonic technique for 19 mm spherical object ( $l=15$ and $20$ ). ....	10-2
Figure 10.3: Radii determined from laser scans and radii computed using spherical harmonic technique for 19 mm spherical object ( $l=25$ ). ....	10-3
Figure 10.4: Radii determined from laser scans and radii computed using spherical harmonic technique for 13 mm spherical object ( $l=5$ and $10$ ). ....	10-4
Figure 10.5: Radii determined from laser scans and radii computed using spherical harmonic technique for 13 mm spherical object ( $l=15$ and $20$ ). ....	10-5
Figure 10.6: Radii determined from laser scans and radii computed using spherical harmonic technique for 13 mm spherical object ( $l=25$ ). ....	10-6
Figure 10.7: Radii determined from laser scans and radii computed using spherical harmonic technique for 13.2 mm aggregate particle ( $l=5$ and $10$ ). ....	10-7
Figure 10.8: Radii determined from laser scans and radii computed using spherical harmonic technique for 13.2 mm aggregate particle ( $l=15$ and $20$ ). ....	10-8
Figure 10.9: Radii determined from laser scans and radii computed using spherical harmonic technique for 13.2 mm aggregate particle ( $l=25$ ). ....	10-9
Figure 10.10: Radii determined from laser scans and radii computed using spherical harmonic technique for 9.5 mm aggregate particle ( $l=5$ and $10$ ). ....	10-10
Figure 10.11: Radii determined from laser scans and radii computed using spherical harmonic technique for 9.5 mm aggregate particle ( $l=15$ and $20$ ). ....	10-11
Figure 10.12: Radii determined from laser scans and radii computed using spherical harmonic technique for 9.5 mm aggregate particle ( $l=25$ ). ....	10-12
Figure 10.13: Radii determined from laser scans and radii computed using spherical harmonic technique for 6.7 mm aggregate particle ( $l=5$ and $10$ ). ....	10-13
Figure 10.14: Radii determined from laser scans and radii computed using spherical harmonic technique for 6.7 mm aggregate particle ( $l=15$ and $20$ ). ....	10-14
Figure 10.15: Radii determined from laser scans and radii computed using spherical harmonic technique for 6.7 mm aggregate particle ( $l=25$ ). ....	10-15
Figure 10.16: Radii determined from laser scans and radii computed using spherical harmonic technique for 4.75 mm aggregate particle ( $l=5$ and $10$ ). ....	10-16
Figure 10.17: Radii determined from laser scans and radii computed using spherical harmonic technique for 4.75 mm aggregate particle ( $l=15$ and $20$ ). ....	10-17
Figure 10.18: Radii determined from laser scans and radii computed using spherical harmonic technique for 4.75 mm aggregate particle ( $l=25$ ). ....	10-18

## LIST OF ABBREVIATIONS

ACV	- Aggregate Crushing Value
AI	- Angularity Index
AIMS	- Aggregate Imaging System
ASTM	- American Society of Testing and Materials
BRD	- Bulk Relative Density
COLTO	- Committee of Land Transportation Officials
CSIR	- Council for Scientific and Industrial Research
CSRA	-Committee of State Road Authorities
DOT	- Department of Transport
FER	- Flat and Elongated Ratio
FI	- Flakiness Index
HMA	- Hot Mix Asphalt
LASS	- Laser-based Aggregate Scanning System
PG	- Parliamentary Grant
PI	- Particle Index
PSV	- Polishing Stone Value
RA	- Recycled Aggregate
R&D	- Research and Development
SANS	- South African National Standards
SHRP	- Strategic Highway Research Program
SRP	- Strategic Research Panel
SUPERPAVE	- Superior Performing Asphalt Pavements
TMH	- Technical Methods for Highways
TRH	- Technical Recommendations for Highways
TIE	- Transport Infrastructure Engineering
10% FACT	- Ten per cent Fine Aggregate Crushing Test
2-D	- Two-Dimensional
3-D	- Three-Dimensional
USA	- Unites States of America
UIAIA	- University of Illinois Aggregate Image Analyser

# **1 INTRODUCTION**

## **1.1 Background**

Rock aggregates constitute a larger proportion (about 95 per cent by mass) of the materials used for construction of roads and airport pavements. Therefore, the performance of pavements is highly dependent on aggregates. The key aggregate shape properties that are influential to the performance of pavements are form, angularity and surface texture (Al-Rousan et al, 2007). Aggregate form describes the overall three dimensional (longest, intermediate and shortest) shape of an aggregate particle. Angularity describes the sharpness of corners, whereas surface texture describes smoothness or roughness of an aggregate particle. Current understanding is that the pavement performance indicators affected by aggregate shape properties include permanent deformation, shear resistance, skid resistance, stiffness, fatigue resistance, stability and workability of Hot Mix Asphalt (HMA) mixes (Button et al, 1990; Barksdale and Itani, 1994; Yeggoni et al, 1994; Taute et al 2001; Chen et al, 2005; Pan et al, 2005; Pan et al, 2006 and Arasan et al, 2011).

In order to ensure good performance, modern pavement design guidelines specify the required aggregate shape properties. For instance, the USA Strategic Highway Research Program (SHRP) through its Superior Performing Asphalt Pavements (SUPERPAVE) design of asphalt mixes specify the coarse aggregate shape properties in terms of flat and elongated particles ratio, angularity and surface texture (Asphalt Institute, 1996). South African specifications for coarse aggregates shape properties are contained in various guidelines and specifications such as the interim guidelines for design of Hot Mix Asphalt (HMA) (Taute et al, 2001), TRH 8 and the Standard Specifications for Road and Bridge Works for State Road Authorities (CSRA, 1998)

In South Africa, the coarse aggregate form is currently evaluated manually using the flakiness index test. The test procedures are contained in Technical Methods for Highways (TMH 1) Method B3 (TMH 1, 1986). The aggregate form can also be evaluated using flat and elongated particles ratio. The American Society of Testing and Materials (ASTM) standard procedure ASTM D 4791 is the current standard test method for determination of flat and elongated aggregate particles (ASTM D 4791, 2010). For evaluation of aggregate angularity, counting the number of fractured aggregate faces (ASTM D 5821, 2006) is recommended. The aggregate surface texture is measured indirectly using the particle index (ASTM D 3398, 2006). Although these standard methods supported the current understanding of the influence of aggregate shape

properties on pavement performance, they have several limitations including the use of a manual approach (subjective in nature), time consuming and laborious (TMH 1, 1986; ASTM D 4791, 2010; ASTM D 5821, 2006 and ASTM D 3398, 2006). Also, the current methods quantify aggregate shape properties indirectly, resulting in a lack of a direct relationship with fundamental aggregate properties governing pavement performance (Masad and Button, 2000; Tutumluer et al, 2000; Masad, 2003; Prowell et al, 2005 and Masad et al, 2007).

Current research efforts to address the limitations of the existing standard test methods are employing advanced technologies such as imaging and laser scanning. The South African Council for Scientific and Industrial Research (CSIR) is currently pursuing research project on pavement materials. The research objective is to improve pavements performance through better evaluation and modelling of aggregate shape properties. This will be achieved through the use of laser scanning and advanced modelling techniques. This dissertation contributes towards the CSIR's broader research in quantification of aggregate shape properties by a using laser scanning technique.

## **1.2 Problem definition**

Limitations of the current standard test methods used for determination of coarse aggregate shape properties including form, angularity and surface texture necessitate the need for developing advanced techniques. The current standard methods have not been able to quantify the key aggregate shape properties accurately. Irregularity of aggregate shapes is among the reasons creating challenges for direct and accurate quantification of aggregate shape properties, using the current standard methods. Consequently, the pavement performance indicators have been related to the aggregate shape properties indirectly. Direct and accurate determination of aggregate shape properties is required in order to better understand the effects of aggregate shape properties on pavement performance, hence improving pavement design. Advanced techniques such as three-dimensional (3-D) aggregate laser scanning could be used to obtain accurate aggregate shape properties, hence addressing the limitations of the current standard methods.

### **1.3 Objectives of the study**

The objectives of the study are:

- To investigate the use of improved techniques for the determination of coarse aggregate shape properties using an advanced laser-based scanning technique, and
- To validate the proposed laser-based aggregate shape properties.

### **1.4 Scope of the study**

The scope of the study is summarised as follows:

- Selection of aggregate samples;
- Scanning of aggregates using the 3-D laser scanning device at CSIR;
- Processing of scan data to reconstruct 3-D models of the aggregates;
- Analyses of the laser scan results to determine aggregate shape properties, and
- Validation of the laser-based aggregate shape properties using the current standard test methods.

Specifically:

- The study focuses on quantification of coarse aggregate shape properties only, i.e. aggregates larger than 4.75 mm.
- Linkage of the quantified aggregate shape properties with pavement performance indicators was not part of this study.

### **1.5 Methodology**

Six types of aggregates used for construction of pavements in South Africa and sourced from six commercial quarries were selected for the study. The materials selection ensured that aggregates with varying shape properties were included in the study. Representative samples were obtained from each aggregate type by means of rifling, and basic aggregate tests were carried out. The tests included grading analyses, flakiness index, flat and elongated particles ratio, bulk density, Aggregate Crushing Value (ACV) and 10 per cent Fines Aggregate Crushing Test (10 % FACT).

From the graded aggregate samples, 30 particles were randomly selected from each of the coarser sieve sizes (4.75, 6.7, 9.5, 13.2 and 19.0 mm) for laser scanning. 150 particles were

scanned for each aggregate type or overall a total of 900 aggregate particles were scanned for the six types of aggregates studied. A 3-D laser scanning device was used for scanning aggregate particles, and the data were processed to reconstruct 3-D models of aggregate particles. The 3-D models were further analysed to quantify aggregate shape properties, using two different analyses approaches identified during a literature review conducted during the study. Indices to describe aggregate shape properties based on the laser scanning approach were determined.

Lastly, it was necessary to validate the laser-based aggregate shape indices. The laser-based form indices were validated by correlating them with flakiness index and flat and elongated particles ratio test results. The flakiness index and flat and elongated particles ratio are the current standard tests used to evaluate aggregate form properties. The laser-based angularity and surface texture indices were validated by comparing the angularity and surface texture of aggregates visually, with the computed indices.

## **1.6 Organisation of the dissertation**

The dissertation consists of six chapters:

- Chapter 1 provides the background information of the study;
- Chapter 2 provides a review of the currently available knowledge on the main aspects covered in this dissertation;
- Chapter 3 discusses the research methodology followed including material selection and sample preparation, laser scanning of the aggregates, determination and validation of the laser-based shape properties of aggregates;
- Chapter 4 presents the results of laboratory tests and laser scanning without detailed analysis;
- Chapter 5 presents the analyses and discussions of the results;
- Chapter 6 provides conclusions and recommendations of the study, and
- List of references and appendices A, B and C follow at the end of the dissertation report.



## **2 LITERATURE REVIEW**

### **2.1 Introduction**

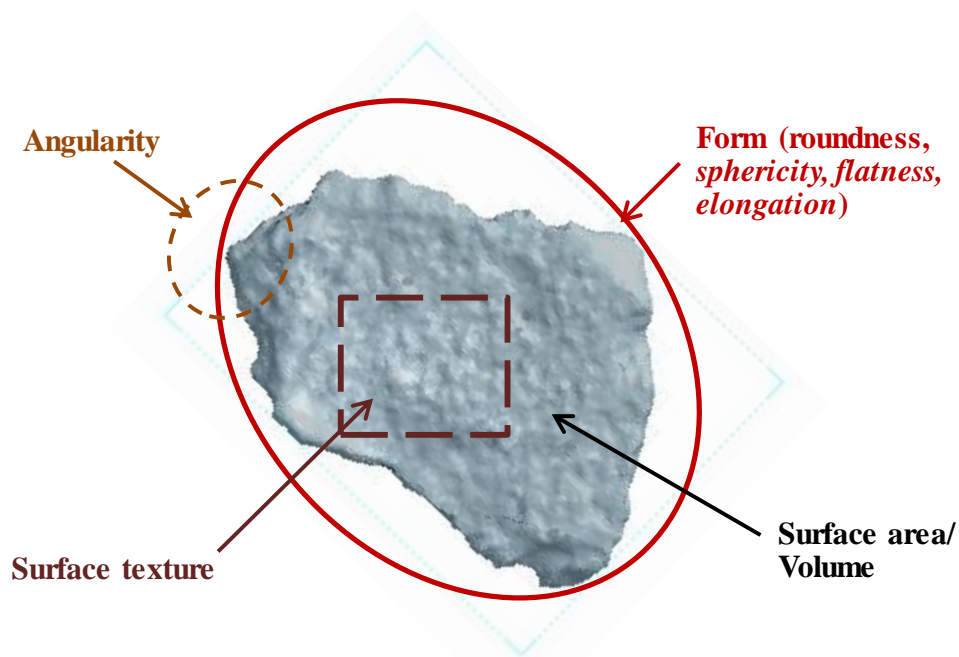
In this Chapter, a literature review of the current available knowledge on the main aspects covered in the dissertation is provided. The literature covers the following areas:

- Fundamental coarse aggregate shape properties;
- Influence of aggregate shape properties on the performance of pavements;
- Current standard tests on coarse aggregate, specifications and limitations;
- Advanced measurement of aggregate shape properties using image and laser-based scanning techniques, and
- Characterisation of coarse aggregate shape properties.

### **2.2 Coarse aggregate shape properties**

The shape or morphology of aggregate particles is distinguished by using three independent fundamental properties (i.e. form, angularity and surface texture). These properties are defined based on their scales with respect to an aggregate particle size. Aggregate form describes the overall three dimensional (longest, intermediate and shortest) shape of an aggregate particle. For example, the form of an aggregate can be spherical, cubical, flat and elongated. Angularity of an aggregate particle describes the sharpness of corners. Crushed aggregate particles have sharp corners compared to uncrushed aggregate particles such as river gravels. Aggregate surface texture describes smoothness or roughness of an aggregate particle.

Previous research studies have used different terminologies to describe the three fundamental aggregate properties. In some literature, the aggregate form, angularity and surface texture are referred to as shape, roundness and roughness respectively. This study describes aggregate shape properties as form, angularity and surface texture. Figure 2.1 illustrates the three fundamental aggregate shape properties, recently defined by Anochie-Boateng et al (2011c).



**Figure 2.1: Fundamental aggregate shape properties (Anochie-Boateng et al, 2011c).**

Coarse aggregates commonly used for construction of pavements may be crushed aggregates, natural gravel (uncrushed) or Recycled Aggregates (RA). Crushed aggregates are obtained by crushing the three primary rock types (igneous, sedimentary and metamorphic). Gravel aggregates are naturally occurring deposits found on land, rivers or seabed. Whereas, RA is obtained by crushing used asphalt to reclaim the aggregate. Currently, crushed aggregates constitute a larger proportion of aggregates used for construction of pavements in South Africa. However, economic and environmental benefits warrant the use of RA for construction purposes (Rahal, 2007; TRH 21, 2009).

The shape properties of crushed aggregates depend on three main factors. These factors include the properties of the parent rock, the type of crusher being used and the way in which the crusher is operated (Prowell et al, 2005; SBM, 2012). Some sedimentary rocks have weaker strength in one direction (anisotropy) due to mineral cleavage or parallel weak layers. Such rocks may produce flat and elongated particles when crushed (SBM, 2012). Other rock types such as quartzite and basalt produce aggregates with fractured surfaces as they fracture in a conchoidal manner (Prowell et al, 2005).

Crushers commonly used for the production of aggregates are grouped into two categories. These categories are compression-type and impact crushers (Collis and Fox, 1985). The main difference between the two is the mechanism in which the crushing load is applied. Compression-type crushers, which include jaw, gyratory and cone crushers, compress a rock until it breaks. On the other hand, an impact crusher consists of rotating hammers which transfer kinetic energy to a rock by striking it until it breaks (Collis and Fox, 1985 and SBM, 2012). The mechanism in which the crushing load is applied affects the shape properties of the produced aggregates. Compression-type crushers tend to produce flat and elongated particles and impact crushers produce cubical aggregates (Prowell et al, 2005).

### **2.3 Influence of aggregate shape properties on pavement performance**

Significant research studies to investigate the influence of aggregate shape properties on the performance of pavements have been conducted. Pavement performance indicators affected by aggregate shape properties include permanent deformation, shear resistance, skid resistance, stiffness, fatigue resistance, stability and workability of HMA mixes (Button et al, 1990; Barksdale and Itani, 1994; Yeggoni et al, 1994; Taute et al 2001; Chen et al, 2005; Pan et al, 2005; Pan et al, 2006 and Arasan et al, 2011).

Arasan et al (2011) evaluated the mechanical properties of asphalt mixes manufactured by using aggregates with different shape properties. They found that asphalt mixes containing spherical aggregates have higher stability, workability and resistance to permanent deformation compared to HMA mixes containing flat and elongated aggregates. Flat and elongated particles tend to lock up (resist re-orientation) resulting to difficulties in compaction. Furthermore, the tendency of flat and elongated particles to break during compaction may result into difficulties in achieving voids requirements in HMA mixes, due to aggregate degradation which may change the grading. For the same reasons, the interim guidelines for the design of HMA in South Africa recommends avoidance of flat and elongated particles in HMA mixes (Taute et al, 2001). The SUPERPAVE mix design procedures recommend minimum use of flat and elongated particles in HMA mixes due to their tendency to break down during compaction and under traffic loading (Asphalt Institute, 2006).

Button et al (1990) investigated the influence of aggregate shape on rutting in asphalt pavements. They found that crushed aggregates improve rutting resistance when compared to smooth aggregates. Chen et al (2005) investigated the influence of coarse aggregate shape on

the strength of asphalt mixes. They found that cubical aggregates provide improved rutting resistance. On the other hand, flat and elongated aggregate particles result in asphalt mixes with low shear deformation resistance.

Pan et al (2005) investigated the effect of coarse aggregate morphology on the resilient modulus of asphalt mixes. In their study, angularity and surface texture indices quantified by using image analysis were correlated to resilient modulus of asphalt mixes. They found that coarse aggregates with high angularity and surface texture improve the resilient modulus of asphalt mixes.

A study on the influence of aggregate shape on pavement base layer behaviour conducted by Barksdale and Itani (1994) showed that crushed aggregates result in improved resilient modulus and shear strength. Another study conducted by Pan et al (2006) focused on investigating the influence of aggregate angularity and surface texture on the resilient behaviour of unbound granular materials. Their findings indicated that angular and rough textured aggregates improve interlock and frictional properties.

It is evident that coarse aggregate shape properties have significant effects on the performance of pavements. Therefore, proper characterisation of aggregate shape properties is essential in order to improve the performance of pavements.

## **2.4 Current standard tests and specifications for coarse aggregates**

### **2.4.1 Evaluation of form**

The standard test method used to evaluate the form of aggregates for road construction in South Africa is the flakiness index test. Flakiness index test procedures are contained in Technical Methods for Highways (TMH 1) Method B3 (TMH 1, 1986). Under the new South African National Standards (SANS), the method will be replaced by SANS 3001-AG4 (SANS, 2009). The test procedures start with performing grading analysis on the aggregate sample to be tested. Each aggregate particle retained on a specific sieve size is then passed through a corresponding rectangular slot of a flakiness gauge. The particles passing the slots are regarded as flaky, whereas particles which do not pass are considered being non-flaky. Flakiness index (in percentage) is calculated by dividing the mass of aggregates passing the slots by the total mass of the sample. The test provides an indication of the flatness of aggregate particles. Excessive use of flaky particles in pavement construction is not recommended due to their tendency of

breaking down during compaction and under traffic loading (DOT Draft TRH8, 1987; Asphalt Institute, 1996; Taute et al, 2001 and Arasan et al, 2011).

Figure 2.2 shows a photograph of the flakiness index test apparatus. The specifications for flakiness index in South Africa contained in the Committee of Land Transportation Officials (COLTO and the Draft TRH8: Design and use of hot-mix asphalt in pavements documents are presented in Table 2.1 (CSRA, 1998; TRH8, 1987).



**Figure 2.2: Flakiness index test apparatus.**

**Table 2.1: Flakiness index specifications (CSRA, 1998; TRH8, 1987).**

<b>COLTO Specification: Maximum flakiness index</b>				
Nominal size of aggregate (mm)	Surfacing aggregate		Rolling-in-chip (all grades)	Base (all grades)
	Grade 1	Grade 2		
19.0	25	30	20	35
13.2	25	30	20	35
9.5	30	35	-	-
6.7	30	35	-	-
<b>TRH8 Specification: Maximum flakiness index</b>				
	Surfacing	Overlays	Base	Levelling
	30	35	20	20

The form of aggregate particles can also be evaluated by using the flat and elongated particle test. Similar to the flakiness index test, the flat and elongated particle test provides an indication of the flatness and elongation of aggregates. The method is recommended in SUPERPAVE for evaluation of aggregate form (Asphalt Institute, 1996). The test procedures are contained in the

American Society of Testing and Materials (ASTM) standard procedure ASTM D 4791 (ASTM D 4791, 2010). In this method, a proportional caliper device set at a pre-defined ratio is used to measure the ratios of longest to the shortest dimensions of an aggregate particle. The SUPERPAVE mix design procedures recommend a ratio of 5:1 to be used for determination of the flat and elongated particles ratio. The flat and elongated particles ratio is calculated by dividing the mass of flat and elongated particles by the total mass of the sample, and is expressed as a percentage. Table 2.2 shows SUPERPAVE specifications for flat and elongated particles for HMA mixes (Asphalt Institute, 1996). Figure 2.3 shows a photograph of a proportional caliper device used for testing flat and elongated particles.

**Table 2.2: Specifications for flat and elongated particles (Asphalt Institute, 1996).**

Traffic (Million ESALs)	Maximum flat and elongated particles (%)
< 0.3	-
< 1	-
< 3	10
< 10	10
< 30	10
< 100	10
≥ 100	10



**Figure 2.3: Proportional caliper device.**

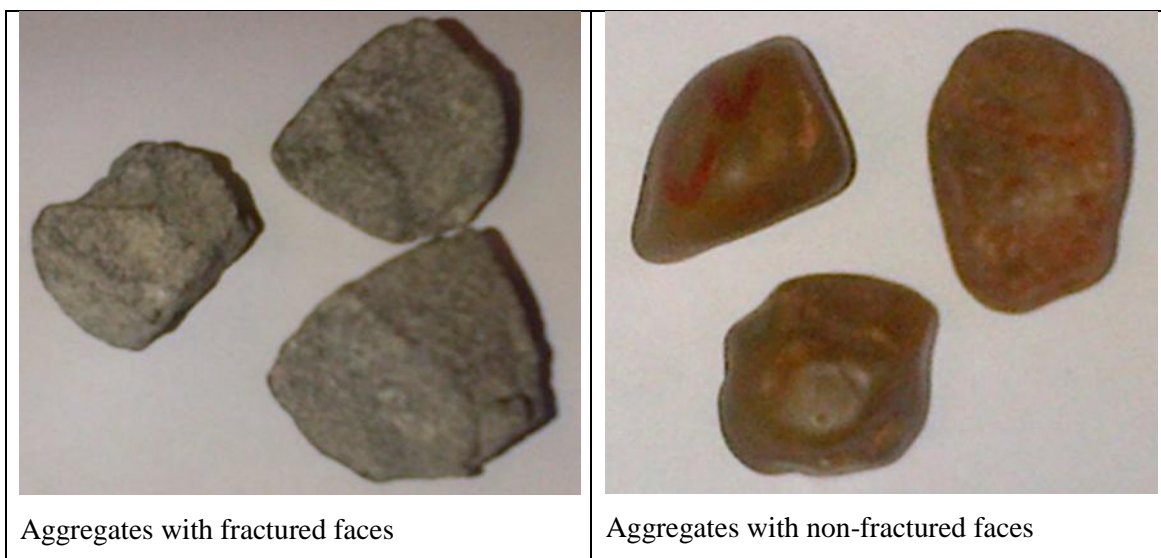
## 2.4.2 Evaluation of angularity

Currently, the standard test method used to evaluate angularity of aggregates is based on counting the number of fractured faces of aggregate particles. The test procedures are contained in the ASTM D 5821 test method (ASTM D 5821, 2006). Using this method, an aggregate particle is visually inspected to establish the number of fractured faces. The face of an aggregate particle is considered fractured if the area of fractured face is at least 25 percentage of the greatest projection of a particle at a given orientation (2-D image) (ASTM D 5821, 2006). Once fractured and non-fractured aggregate particles have been identified, the percentage of fractured particles is calculated by dividing the mass of fractured particles by the total mass of the sample. Table 2.3 shows SUPERPAVE specifications for coarse aggregate angularity. Figure 2.4 shows an example of aggregates with fractured faces and non-fractured faces.

**Table 2.3: Specifications for angularity (Asphalt Institute, 1996).**

Traffic (Million ESALs)	Depth from surface	
	Less than 100 mm	More than 100 mm
< 0.3	55/-	-/-
< 1	65/-	-/-
< 3	75/-	50/-
< 10	85/80	60/-
< 30	95/90	80/75
< 100	100/100	95/90
≥ 100	100/100	100/100

Note: "85/80" Means 85 percentage of the coarse aggregate has one or more fractured faces and 80 percentage has two or more fractured faces.



**Figure 2.4 Angular and non-angular aggregate particles.**

### **2.4.3 Evaluation of surface texture**

Currently, there is no direct method dedicated for evaluation of surface texture of coarse aggregate. The ASTM D 3398 (2006) test method is currently used to provide an indication of both form and surface texture. The test measures voids in aggregate and computes a particle index parameter that provides combined characterisation of aggregate form and surface texture.

### **2.4.4 Limitations of the current standard tests**

The current standard tests used to evaluate coarse aggregate shape properties have several limitations. Masad (2003) argued that the flat and elongated particles ratio test (ASTM D 4791) gives a single index, which is less descriptive and does not reflect the distribution of particle dimensions in a sample.

In South Africa, the coarse aggregate form is currently evaluated using the flakiness index test. Anochie-Boateng et al (2011b) pointed out that the slots of the gauge used to conduct the test may allow aggregate with considerable variations in form to pass. Similar to the ASTM D 4791 test method, the flakiness index test gives a single index which does not provide sufficient information to distinguish the form of the aggregate particle.

The accuracy and repeatability of the current test method used to evaluate aggregate angularity (ASTM D 5821) is also questionable. Prowell et al (2005) pointed out that the technician performing the angularity test may fail to decide whether the area of fractured face of an aggregate particle is at least 25 percentage of the projection of a particle at a given orientation. Hence the method is subjective, which may affect the accuracy and repeatability of the test results.

The current ASTM D 3398 test method does not provide characterisation of aggregate surface texture in a direct manner. The test relies on relating voids in the aggregate to form and surface texture. In addition, the test method gives one index to describe both aggregate form and surface texture. The aggregate form and surface texture are two independent properties. Therefore, they should ideally be evaluated separately.

Other limitations of the current standard methods include; subjectivity due to the use of a manual approach, time consuming and laborious, inter-laboratory variability, low repeatability



and lack of a direct relationship with the fundamental properties governing the performance of pavements (Masad and Button, 2000; Tutumluer et al, 2000; Masad, 2003; Prowell et al, 2005 and Masad et al, 2007).

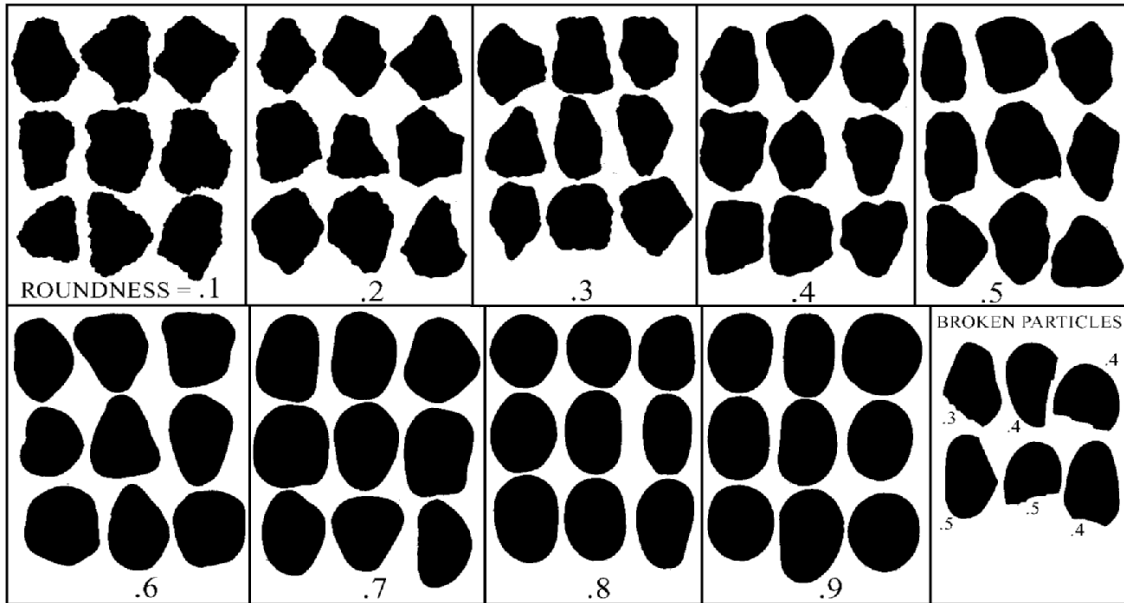
These limitations may lead to major consequences. Masad (2003) pointed out that the limitations of the current standard methods may result in inconsistency in predicting to what extent the aggregate form, angularity and surface texture affect pavement performance.

## **2.5 Advanced measurement of aggregate shape properties**

Aggregate imaging and laser scanning are among advanced techniques that have been investigated to address limitations of the current methods used to evaluate aggregate shape properties. These techniques are considered to be superior to the current methods due to: efficiency, evaluation speed, ability to be automated hence eliminating human subjectivity and ability to relate the measured aggregate shape properties to fundamental properties affecting pavement performance (Masad and Button, 2000; Tutumluer et al, 2000; Masad, 2003; Wang et al, 2005; Masad et al, 2007 Anochie-Boateng et al, 2012). This section reviews recent developments in aggregate imaging and laser scanning techniques.

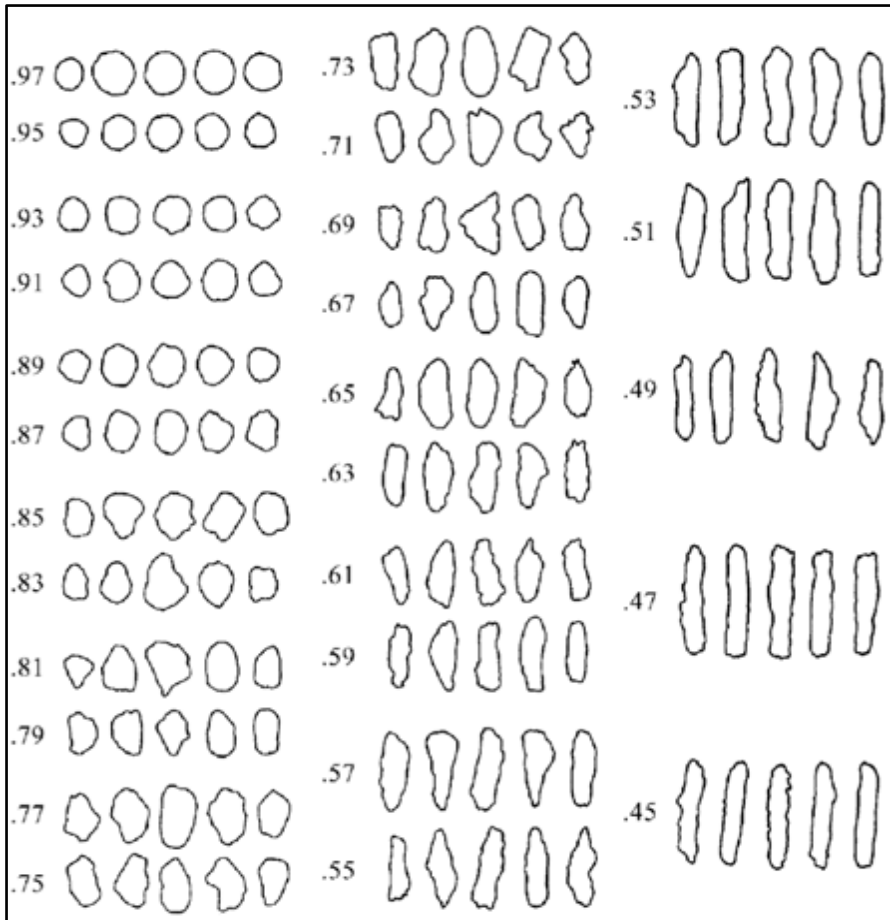
### **2.5.1 Image-based technique**

The concept of using images to characterize aggregate shape properties started in the 1940s. Krumbein (1941) developed a chart for visual evaluation of 2-D angularity of granular materials in terms of roundness. Roundness is a parameter that gives an indication of the angularity of an aggregate particle. The roundness chart developed by Krumbein (1941) is used to assess (visually) similarity of aggregate particles with images presented in Figure 2.5 and assigned a roundness value. The roundness value of round shaped aggregate particles approaches 1, whereas that of non-round particles approach zero.



**Figure 2.5: Chart for visual evaluation of roundness of aggregate (Krumbein, 1941).**

Rittenhouse (1943) developed a chart for visual assessment the form of the aggregates in terms of sphericity. Sphericity is a parameter that describes the overall form of an aggregate particle. Aggregate particles are visually assessed for similarity with particle presented in Figure 2.6 (Rittenhouse, 1943) and assigned a sphericity number. As the form of aggregate particles becomes spherical, the sphericity number approaches 1, whereas sphericity of flat and elongated particles approaches zero.



**Figure 2.6: Chart for visual evaluation of sphericity of aggregate (Rittenhouse, 1943).**

The roundness and sphericity evaluation charts developed by Krumbein (1941) and Rittenhouse (1943) respectively are based on 2-D images of aggregate particles. Although these charts may be capable to describe variation in aggregate form and angularity, the fact that the approach is based on 2-D images has some limitations. For example, different 2-D views of the same aggregate particle projected from a different orientation may result in different roundness or sphericity numbers.

Recent developments in image-based techniques for quantification of aggregate shape properties are based on capturing images of aggregate particles by using high resolution cameras. The captured images are analysed to quantify aggregate shape properties. Internationally, research efforts to develop and evaluate the image-based technique for quantification of aggregate shape properties have been growing significantly (Masad and Button, 2000; Tutumluer et al, 2000; Masad, 2003 and Wang et al, 2005).

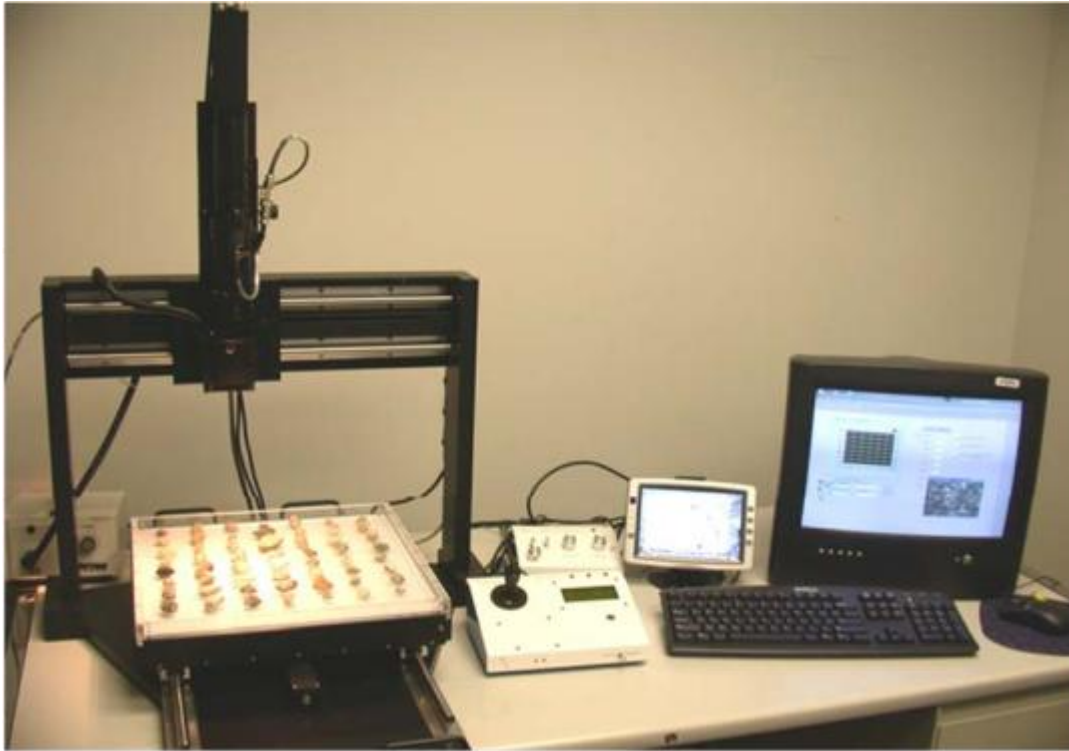
Tutumluer et al (2000) developed the University of Illinois Aggregate Image Analyser (UIAIA) to provide improved and automated measurement of coarse aggregate shape properties. The UIAIA shown in Figure 2.7 makes use of three cameras to capture aggregate images from three orthogonal directions. Use of three cameras in the UIAIA ensures collection of 3-D information required for accurate determination of the volume of an aggregate particle (Tutumluer et al, 2003). The UIAIA has been used extensively to measure dimensions, volume, surface area and quantify aggregate shape properties including the flat and elongated ratio, angularity and surface texture (Tutumluer et al, 2000; Rao et al, 2001, Rao et al, 2002; Rao et al, 2003; Tutumluer et al, 2003 and Pan, 2006). In the US, the UIAIA has been proposed as a test method for measuring volume, flat and elongated ratio, angularity and surface texture of coarse aggregates (Masad et al, 2007).



**Figure 2.7: The University of Illinois Aggregate Image Analyser (Tutumluer et al, 2003).**

Another imaging system that has been used for measurement of aggregate shape properties is the Aggregate Imaging System (AIMS), developed by Masad (2003). The AIMS is used to measure shape properties of coarse and fine aggregates. The system as shown in Figure 2.8 consists of a camera, video microscope, lighting systems, aggregate tray, computer automated data acquisition system and processing software for analysis of aggregate shape properties (Masad, 2003 and Masad, 2004). Masad et al (2007) evaluated test methods for characterising

aggregate shape properties. They proposed the use of AIMS as suitable for quantification of aggregate form, angularity and surface texture.



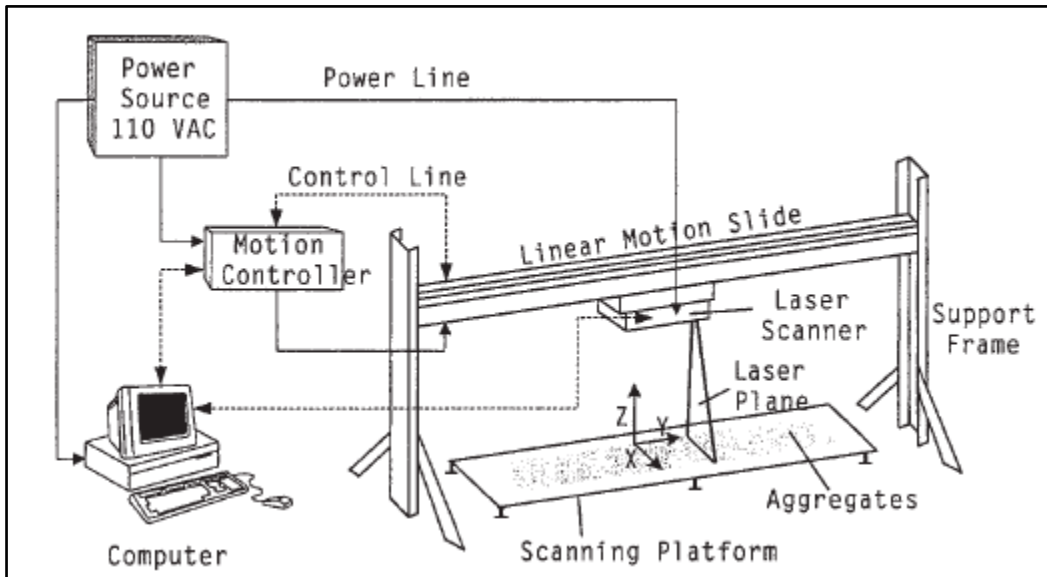
**Figure 2.8: The Aggregate Imaging System (Masad et al, 2007).**

Although aggregate imaging has been used extensively for direct measurement of aggregate shape properties and has provided a better understanding of distinction between aggregate form, angularity and surface texture, the technique has some limitations. The main limitation is that most available image based systems provide information that facilitate characterisation of aggregate form, angularity and surface texture in 2-D. In reality, an aggregate particle is a 3-D object. Therefore, characterisation of aggregate shape properties should ideally be based on 3-D information. The use of more advanced techniques such as the laser scanning could alleviate some limitations of image-based aggregate analysis.

### **2.5.2 Laser-based technique**

Three-dimensional (3-D) laser-based scanning is another technique that has been used for measurement of aggregate shape properties. Kim et al (2001) developed the Laser-based Aggregate Scanning System (LASS) consisting of a linear line scanner, a linear motion slide and a computer shown in Figure 2.9. LASS captures x, y and z coordinates of an aggregate

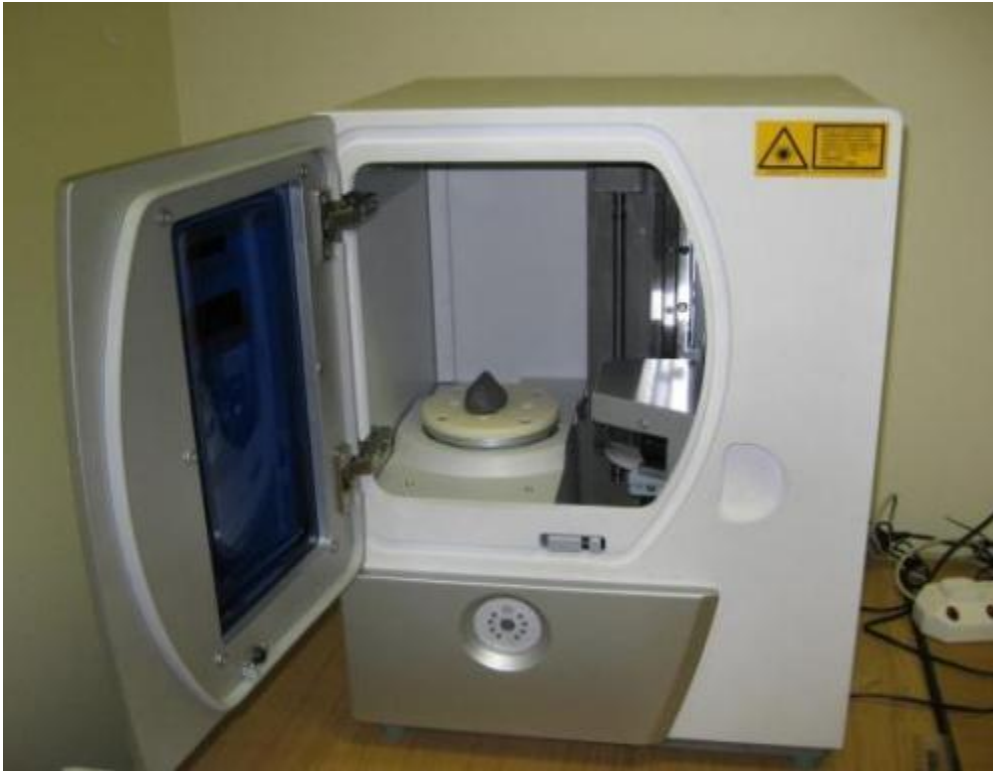
particle. The data captured by using LASS have been used to quantify form, angularity and surface texture of aggregate particles (Kim et al, 2002).



**Figure 2.9: Laser-based Aggregate Scanning System (Kim et al, 2001).**

Recently, Pan and Tutumluer (2010) used a 3-D laser scanning device to validate the surface area of aggregates measured by using the image-based technique. Hayakawa and Oguchi (2005) used a laser scanning device to evaluate sphericity and roundness of gavel particles.

The CSIR is currently pursuing a research project in the use of 3-D laser scanning and advanced modelling techniques to characterise aggregate shape properties. A 3-D laser scanning device at the CSIR's pavement material laboratory has been evaluated for measurement of aggregate shape properties (Anochie-Boateng et al, 2010). The device has been successfully used to measure surface areas of aggregates used in typical South African HMA mixes (Anochie-Boateng et al, 2011a). Furthermore, new approaches for determination of flakiness index (Anochie-Boateng et al, 2011b) and flat and elongated particles ratio (Anochie-Boateng et al, 2011c) of aggregates were recently developed based on the aggregate volume instead of the mass. Figure 2.10 shows a photograph of the 3-D laser scanning device at the CSIR. An example of actual and scanned aggregate particles is shown in Figure 2.11.



**Figure 2.10: A 3-D laser scanning device at the CSIR.**



(a) Actual aggregates



(b) Scanned and processed aggregates

**Figure 2.11: Actual and scanned aggregate particles (Anochie-Boateng et al, 2011b).**

The main advantage of the laser scanning approach is the ability to capture 3-D information of the aggregate particles, hence allowing for more realistic and accurate quantification of aggregates shape properties. Generally, research on quantification of aggregates shape properties based on the laser scanning technique is not advanced as compared to the image-based approach. However, the laser-based approach has the potential to address some

limitations of the image-based approach of which most of the limitations are based on 2-D analysis of images.

## 2.6 Characterisation of coarse aggregate shape properties

The application of image and laser-based techniques to quantify shape properties of aggregates is divided into two main processes. The first process involves acquisition/capturing of the aggregate image or laser scan data. The second process involves analysis of the images or laser scan data to quantify shape properties of the aggregate. Research efforts aimed at employing imaging and laser scanning have led to the development of several indices for quantifying fundamental aggregate shape properties.

### 2.6.1 Form indices

Several indices to quantify aggregate form properties have been proposed. Most form indices are computed by using three dimensions of an aggregate particle (longest, intermediate and shortest dimensions), surface area and volume.

Masad (2003) developed AIMS to measure aggregate shape properties and proposed computation of sphericity and shape factor to describe aggregate form using Equations 2.1 and 2.2 respectively. The Equations 2.1 and 2.2 use three orthogonal dimensions of an aggregate particle.

$$Sphericity = \sqrt[3]{\frac{d_s \cdot d_l}{d_L^2}} \quad 2.1$$

$$Shape\ Factor = \frac{d_s}{\sqrt{d_L \cdot d_l}} \quad 2.2$$

Where:

$d_L$  = Longest dimension of an aggregate particle;

$d_l$  = Intermediate dimension of an aggregate particle, and

$d_s$  = Shortest dimension of an aggregate particle.

From Equation 2.1 it can be seen that, for equal dimensional aggregate particles such as round aggregates, the sphericity approaches a value of 1.



Rao et al (2001) used aggregate's dimensions measured by using an imaging technique to compute flat and elongated ratio of an aggregate particle by using Equation 2.3.

$$\text{Flat and elongated ratio} = \frac{d_L}{d_s} \quad 2.3$$

Where:

$d_L$  = Longest dimension of an aggregate particle, and

$d_s$  = Shortest dimension of an aggregate particle.

From Equation 2.3 it can be seen that, for equal dimensional aggregate particles such as round aggregates, the flat and elongated ratio approaches a value of 1. As an aggregate particle becomes flatter, the flat and elongated ratio increases.

Lin and Miller (2005) used an X-ray technique to measure volume and surface area of aggregate particles and computed sphericity ( $\psi$ ) by using Equation 2.4.

$$\text{Sphericity } (\psi) = \frac{\sqrt[3]{36\pi V^2}}{A} \quad 2.4$$

Where:

$V$  = Volume of an aggregate particle, and

$A$  = Surface area of an aggregate particle.

Sphericity defined by using Equation 2.4 approaches 1 as the form of an aggregate becomes spherical.

Aggregate form can also be defined in terms of roundness ( $\rho$ ) computed by using Equation 2.5 (Al-Rousan et al, 2007).

$$\text{Roundness } (\rho) = \frac{p^2}{4\pi A} \quad 2.5$$

Where:

$p$  = Perimeter of the projection of an aggregate particle at a given orientation, and

$A$  = Area of an equivalent circle.

Masad et al (2001) proposed another form index parameter that is based on incremental change in the aggregate particle radius, defined by Equation 2.6.

$$Form\ Index = \sum_{\theta=0}^{\theta=360-\Delta\theta} \left| \frac{R_{\theta+\Delta\theta} - R_{\theta}}{R_{\theta}} \right| \quad 2.6$$

Where:

$R$  = Radius of an aggregate particle at a given direction;

$\theta$  = Directional angle, and

$\Delta\theta$  = Incremental different in the angle ( $4^{\circ}$ )

For round shaped aggregates, the form index defined by using Equation 2.6 above becomes zero since there is no change in radius.

Among the form indices described above, the two sphericity parameters (Equation 2.1 and 2.4) and flat and elongated ratio (Equation 2.3) can be computed directly using the data obtained using the 3-D laser scanning device used in this study. Therefore, these indices will further be investigated in this dissertation.

## 2.6.2 Angularity indices

Several indices have been proposed to characterise angularity of aggregate particles. Most of the available angularity indices are based on analysis of 2-D images of aggregate particles.

Masad et al (2001) proposed the radius method for analysis of aggregate angularity. The method is based on measuring the radius of the projection of an aggregate particle at a given orientation (2-D images) and that of an equivalent ellipse. Using the radius method, the Angularity Index ( $AI$ ) is computed by using Equation 2.7 (Masad et al, 2001).

$$AI = \sum_{\theta=0}^{360-\Delta\theta} \left| \frac{R_{\theta} - R_{EE\theta}}{R_{EE\theta}} \right| \quad 2.7$$

Where:

$R_{\theta}$  = Radius of an aggregate particle at an angle  $\theta$ , and

$R_{EE\theta}$  = Radius of an equivalent ellipse at an angle  $\theta$ .

$\Delta\theta$  = Incremental different in the angle ( $4^{\circ}$ )

Rao et al (2002) presented an approach for computation of aggregate angularity from images measured by using the UIAIA. Using the proposed approach, the angularity ( $A$ ) of one projected side of the image of an aggregate particle, is computed by using Equation 2.8.

$$A = \sum_{e=0}^{170} e * P(e) \quad 2.8$$

Where:

$e$  = Starting angle value for each 10 degree class interval, and

$p(e)$  = Probability of each angle change in the range  $e$  to  $(e+10)$ .

For the three projected sides of an aggregate particle, the Angularity Index ( $AI$ ) is computed as weighted by using Equation 2.9 (Rao et al, 2002).

$$AI = \frac{\sum_{i=1}^3 (Angularity_i \times Area_i)}{\sum_{i=1}^3 Area_i} \quad 2.9$$

Where:

$Angularity_i$  = Angularity of  $i^{th}$  side, and

$Area_i$  = Area of  $i^{th}$  side.

The angularity indices (Equations 2.7 to 2.9) are based on 2-D analysis of image data. These angularity indices may not be appropriate for analysis of the data, measured by using the laser scanning device used in this study. This is because the laser scanning technique results in 3-D models.

### 2.6.3 Surface texture indices

Pan (2006) presented an approach for computing aggregate surface texture by using erosion and dilation. The approach is based on calculating the difference in the area of the projections of a particle at a given orientation after performing a certain number of erosion and dilation cycles. The surface texture of one projected view of an aggregate particle is computed by using Equation 2.10.

$$st_i = \frac{A_1 - A_2}{A_1} \times 100\% \quad 2.10$$

Where:

$st_i$  = Surface texture parameter for each of the three views, (i = 1, 2 and 3);

$A_1$  = Area (in pixels) of the particle image before a certain number of erosion and dilation cycles, and

$A_2$  = Area (in pixels) of the particle image after a certain number of erosion and dilation cycles.

Once the surface texture parameter has been computed for each of the three orthogonal views of an aggregate particle, the surface texture ( $ST$ ) is computed as a weighted average by using Equation 2.11 (Pan, 2006).

$$ST = \frac{st_1(\text{front}) \times \text{Area}(\text{front}) + st_2(\text{top}) \times \text{Area}(\text{top}) + st_3(\text{side}) \times \text{Area}(\text{side})}{\text{Area}(\text{front}) + \text{Area}(\text{top}) + \text{Area}(\text{side})} \quad 2.11$$

Masad (2004) proposed the use of a wavelet method to analyse aggregate surface texture from images measured by using the AIMS. The method is based on describing texture content at a given resolution and decomposition level. Equation 2.12 is used to compute the wavelet texture parameter that describes the surface texture of an aggregate particle (Masad, 2004).

$$\text{Texture Index}_n = \frac{1}{3N} \sum_{i=1}^3 \sum_{j=1}^N (D_{i,j}(x, y))^2 \quad 2.12$$

Where:

$n$  = Decomposition level;

$N$  = Total number of coefficients;

$i$  = 1, 2 or 3 for three directions of texture;

$j$  = Wavelet coefficient, and

$D_{i,j}(x, y)$  = Location of coefficients.

## 2.6.4 Mathematical-based analysis of aggregate shape properties

Various mathematical-based techniques have been used to analyse aggregate shape properties. This section reviews some mathematical-based data analysis techniques which can be used to quantify form, angularity and surface texture.

## 2.6.5 Fourier analysis

Fourier series technique has been used for analysis of aggregate shape properties. The technique has been used in aggregate imaging research to describe aggregate form, angularity and surface texture.

The profile of an aggregate particle such as the one presented in Figure 2.12 can be represented mathematically as a Fourier series by using Equation 2.13. Equation 2.13 is a periodic function describing the radius  $R(\alpha)$  of an aggregate profile, from the centre of mass at a corresponding angle  $\alpha$ . The quantification of aggregate shape properties by using Fourier series is based on solving the coefficients  $a_0$ ,  $a_m$  and  $b_m$  of the Fourier series in Equation 2.13.

$$R(\alpha) = a_0 + \sum_{m=1}^{\infty} (a_m \cos m\alpha + b_m \sin m\alpha) \quad 2.13$$

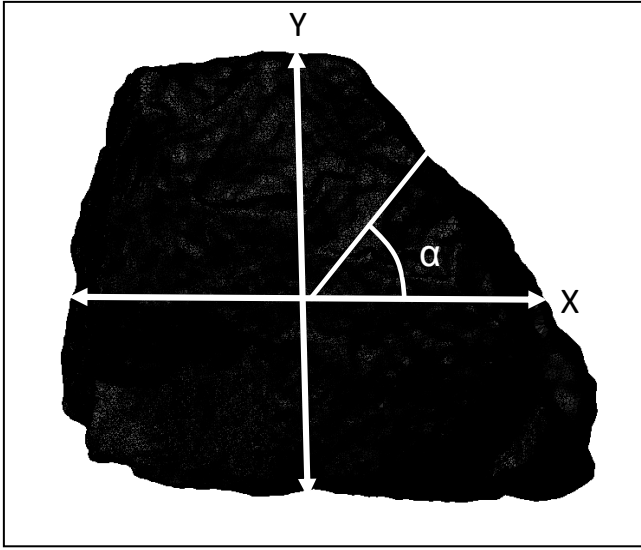
Where:

$R(\alpha)$  = Radius from the centre of the mass of aggregate image;

$\alpha$  = Angle measured from x-axis counter clockwise;

$a_0, a_m$  and  $b_m$  = Coefficients of the Fourier series, and

$m$  = Frequency.



**Figure 2.12: Representation of an aggregate particle for Fourier analysis.**

Mathematically, the coefficients of the Fourier series are normally determined by means of integration techniques using Equations 2.14 to 2.16.

$$a_0 = \frac{1}{2\pi} \int_0^{2\pi} R(\alpha) \delta\alpha \quad 2.14$$

$$a_n = \frac{1}{\pi} \int_0^{2\pi} R(\alpha) \cos(n\theta) \delta\alpha, \quad n = 1, 2, 3 \dots \quad 2.15$$

$$b_n = \frac{1}{\pi} \int_0^{2\pi} R(\alpha) \sin(n\alpha) \delta\alpha, \quad n = 1, 2, 3 \dots \quad 2.16$$

The coefficients of Fourier series may be used to describe form, angularity and surface texture of aggregate particles. Wang et al (2005) proposed Fourier descriptors of aggregate form, angularity and surface texture by using coefficients of the Fourier series. Using the proposed Fourier series analysis technique, the aggregate form, angularity and surface texture are computed by using Equations 2.17, 2.18 and 2.19 respectively. The three equations are based on the fact that the form of an aggregate particle can be quantified at low frequency. On the other hand, angularity and surface texture are quantified at intermediate and high frequencies, respectively.

$$Form = \frac{1}{2} \sum_{m=1}^{m=n} \left[ \left( \frac{a_m}{a_0} \right)^2 + \left( \frac{b_m}{a_0} \right)^2 \right] \quad 2.17$$

$$Angularity = \frac{1}{2} \sum_{m=n+1}^{m=2n} \left[ \left( \frac{a_m}{a_0} \right)^2 + \left( \frac{b_m}{a_0} \right)^2 \right] \quad 2.18$$

$$Texture = \frac{1}{2} \sum_{m=n+1}^{m=\infty} \left[ \left( \frac{a_m}{a_0} \right)^2 + \left( \frac{b_m}{a_0} \right)^2 \right] \quad 2.19$$

The Fourier series analysis discussed thus far is a major advancement towards quantitative quantifications of aggregate shape properties. In this method, a 2-D profile of an aggregate particle is analysed. In reality, an aggregate particle is a 3-D object. Therefore, the quantification of aggregates shape properties should ideally be based on 3-D analysis. Despite that shortcoming, research on 2-D imaging analysis using Fourier series analysis has shown promising results (Wang et al, 2005).

### 2.6.6 Spherical harmonics analysis

Garboczi (2002) proposed a technique for 3-D analysis of aggregate shape using X-ray tomography and spherical harmonic analysis. The proposed technique defines an aggregate particle by using a radial distance function as indicated in Equation 2.20. Equation 2.20 is a function describing surface points of an aggregate in 3-D.

$$R(\beta, \alpha) = \sum_{l=0}^{l_{max}} \sum_{m=-l}^l a_{lm} Y_l^m(\beta, \alpha) \quad 2.20$$

$$0 \leq \beta \leq \pi, 0 \leq \alpha \leq 2\pi$$

Where:

$R(\alpha, \beta)$  = Radius from the centre of mass to the surface of an aggregate particle;

$\beta$  = Angle measured from positive z-axis;

$\alpha$  = Angle measured from positive x-axis;

$l$  = Degree;

$m$  = Order;

$a_{lm}$  = Scalar coefficient, and

$Y_l^m(\beta, \alpha)$  = Harmonic functions of degree  $l$  and order  $m$ .

The quantification of aggregate form, angularity and surface texture by using the harmonic analysis technique is based on solving the coefficient  $a_{lm}$  in Equation 2.20. Garboczi (2002) proposed the use of an integral shown in Equation 2.21, to evaluate the coefficient  $a_{lm}$  in Equation 2.20.

$$a_{lm} = \int_0^{2\pi} \int_0^{\pi} d\alpha d\beta \sin(\beta) r(\beta, \alpha) Y_l^{m*} \quad 2.21$$

By using coefficient  $a_{lm}$  in Equation 2.20, Masad et al (2005) proposed three descriptors computed by using Equations 2.22, 2.23 and 2.24 to quantify aggregate form, angularity and surface texture respectively.

$$Form = \sum_{l=0}^5 \sum_{m=-l}^l |a_{lm}| \quad 2.22$$

$$Angularity = \sum_{l=6}^{25} \sum_{m=-l}^l |a_{lm}| \quad 2.23$$

$$Form = \sum_{l=25}^{l_{max}} \sum_{m=-l}^l |a_{lm}| \quad 2.24$$

The spherical harmonic analysis technique described above makes use of data acquired by using X-ray tomography technique. Similar approach could be used for analysis of aggregate laser scans data. Therefore, this dissertation also investigated analysis of aggregate laser scan data using spherical harmonic analysis.

### 2.6.7 Wavelet transform

The 3-D surface points of an aggregate particle can be defined with polar coordinates by using radial distance (R), horizontal angles  $\alpha$  and vertical angle  $\beta$ . Kim et al (2002) used a laser-based aggregate scanning system and developed a method for quantification of aggregate shape properties using the wavelet transform technique. In a polar coordinate system, an aggregate particle can be described by a wavelet transform using Equation 2.25 (Kim et al, 2002).



$$f(\alpha, \beta) = \sum_{i=-\infty}^{\infty} \sum_{j=-\infty}^{\infty} \sum_{k=-\infty}^{\infty} \sum_{l=0}^2 d_{i,j,k,l} W_{i,j,k,l}(\alpha, \beta) \quad 2.25$$

$$i, j, k \in z, l \in [0, 2]$$

Where:

$f(\alpha, \beta)$  = Radius from the Centre of mass;

$\alpha$  = Horizontal angle;

$\beta$  = Vertical angle;

$d_{i,j,k,l}$  = Wavelet coefficient, and

$W_{i,j,k,l}(\alpha, \beta)$  = Translation function.

The wavelet coefficient ( $d_{i,j,k,l}$ ) may be evaluated by using the integral shown in Equation 2.26 (Kim et al, 2002).

$$d_{i,j,k,l} = \int_{-\infty}^{\infty} f(\alpha, \beta) W_{i,j,k,l}(\alpha, \beta) \delta\alpha \delta\beta \quad 2.26$$

After solving the wavelet coefficients ( $d_{i,j,k,l}$ ) in Equation 2.25, the aggregate form, angularity and surface texture are described by using Equations 2.27, 2.28 and 2.29 respectively (Kim et al, 2002).

$$Form = \frac{\sum(d_{0,j,k,l}) + \sum(d_{1,j,k,l})}{R_{average}} \quad 2.27$$

$$Angularity = \frac{\sum(d_{2,j,k,l}) + \sum(d_{3,j,k,l})}{R_{average}} \quad 2.28$$

$$Texture = \frac{\sum(d_{4,j,k,l}) + \sum(d_{5,j,k,l})}{R_{average}} \quad 2.29$$

Where:

$R_{average}$  = Average radius.

## 2.7 Summary

This chapter provided a review of the available information on the main aspects covered in the dissertation. Based on the information covered in this chapter the following conclusions are drawn:

### **Fundamental coarse aggregate shape properties**

The coarse aggregate shape properties identified to be most influential to pavement performance were the aggregate form, angularity and surface texture. These properties vary for different types of aggregates, i.e. natural gravel (uncrushed) or RA. Therefore, the selection of materials for this study ensured that aggregates with different shape properties are included.

### **Influence of aggregate shape properties on the performance of pavements**

The literature review indicated that the influence of shape properties on the performance of pavements is widely documented. With the exception of some studies which have linked the aggregate properties determined by using imaging techniques to pavement performance indicators, most of the studies used aggregate shape properties which are measured based on the current standard methods and these have several limitations. Therefore, the development of techniques that will improve the characterisation of aggregate shape properties is essential. The primary focus of this study is to develop improved techniques for accurate and effective determination of coarse aggregate shape properties using a laser scanning technique. The correlation of the improved coarse aggregate shape properties with pavement performance indicators is not part of the scope of the study.

### **Current standard tests on coarse aggregate, specifications and limitations**

The current standard methods used for determination of coarse aggregate shape properties were discussed, along with their limitations. The need for improved techniques to address the limitations of the current standard methods became evident.

### **Advanced measurement of aggregate shape properties**

Some of the available advanced techniques for measurements of aggregate shape properties have been described. These techniques are generally divided into two categories namely image and laser-based. The equipment available at the CSIR's pavement material laboratory is a 3-D laser scanning device. Therefore, in this study the laser scanning technique was used.

### **Characterisation of coarse aggregate shape properties**

A number of techniques for analysis of image and laser scanning data to characterise coarse aggregate's shape properties have been described. Some of the described techniques might not be relevant or suitable for analysis of data obtained by using the 3-D laser scanning device used in this study. Based on the type of aggregate laser scanning data and ability of the techniques to describe 3-D coarse aggregate shape properties, several analysis techniques were identified to be further investigated in this study. Another reason for selection of these techniques is the fact that the information required as inputs can be obtained using the laser scanning device used in this study. The identified techniques are:

1. Quantification of form using aggregate physical dimensions:
  - The sphericity computed by using the aggregate surface area and volume as defined by Equation 2.4;
  - The sphericity computed by using orthogonal dimensions of the aggregate as defined by Equation 2.1, and
  - The flat and elongated ratio computed using the longest and smallest dimensions of the aggregate as defined by Equation 2.3.
2. Quantification of coarse aggregate form, angularity and surface texture by using a spherical harmonic analysis technique.

### **3 METHODOLOGY**

#### **3.1 Introduction**

The objective of this chapter is to present the methodology followed during the study. The study comprised of the following:

- Selection and sampling of aggregates;
- 3-D laser scanning of aggregates;
- Determination of aggregate shape properties, and
- Performing the current standard tests used to characterise aggregate shape properties to validate the laser-based shape properties.

#### **3.2 Material selection and sample preparation**

Six different types of aggregates commonly used in South African pavements were selected for the study. The aggregates included four types of crushed aggregates (granite, tillite, quartzite and hornfels), one alluvial gravel sample and Recycled Aggregate (RA). The four types of crushed aggregates were sourced from commercial quarries supplying aggregates for pavement construction in South Africa. The crushed aggregate sample selection ensured that aggregates from three primary rock groups (igneous, sedimentary and metamorphic) are included in the study. Alluvial gravel was sourced from Molopo River near Mafikeng and the RA was sourced from the National Asphalt Plant in Durban. Sampling of aggregates at stockpiles was done randomly at different positions as per TMH 5 procedures (TMH 5, 1981). The sample selection ensured that materials with varying shape properties were included in the study. The alluvial gravel was used as a control sample. Alluvial gravel had round shaped particles. The computed shape properties for alluvial gravel particles were expected to differ from other types of aggregates. RA was also used as a control sample, to assess the shape properties of aggregates after being subjected to traffic and compaction. Table 3.1 shows types and sources of the aggregates used in this study.

Representative samples were obtained from each aggregate type by means of rifling and sieve analyses were performed. Following the sieve analyses, a total of 30 particles were selected from aggregates retained on coarser sieve sizes (4.75, 6.7, 9.5, 13.2 and 19.0 mm) for laser scanning. The sieve analyses ensured that different sizes of aggregate particles are selected for

laser scanning. 150 particles of each source or overall 900 aggregate particles were scanned. The particle selection was done such that different aggregate shape properties are represented. For each aggregate type, flat and elongated, angular, round, rough and smooth aggregate particles were visually identified and randomly selected from a population of aggregates.

Other standard laboratory tests performed on the aggregate samples were:

- Flakiness index (TMH1 Method B3);
- Flat and elongated particles ratio (ASTM D 4791);
- Bulk Relative Density (BRD) (TMH1 Method B14);
- Aggregate Crushing Value (ACV) (TMH1 Method B1) , and
- Ten per cent Fines Aggregate Crushing Test (10 % FACT) (TMH1 Method B2).

The flakiness index and flat and elongated particles ratio tests were performed to obtain an indication of the shape properties of the aggregates studied based on the current standard test methods. The flakiness index and flat and elongated particles tests results were also correlated with laser-based aggregate shape indices proposed in this study. The BRD, ACV and 10 % FACT tests were performed to ensure that, the materials studied comply with specifications for aggregate used for construction of pavements in South Africa.

**Table 3.1: Aggregate samples.**

<b>Aggregate type</b>	<b>Rock type</b>	<b>Quarry name</b>	<b>Location</b>
Granite	Igneous	Afrisam Jukskei	Midrand
Tillite	Sedimentary	Afrisam Verulam	Kwazulu Natal
Quartzite	Metamorphic	Afrisam Ferro	Pretoria
Hornfels	Metamorphic	Afrisam Peninsula	Cape Town
Alluvial gravel	N/A	Molopo River	Mafikeng
RA	N/A	National Asphalt Plant	Kwazul Natal

### 3.3 Laser scanning of aggregates

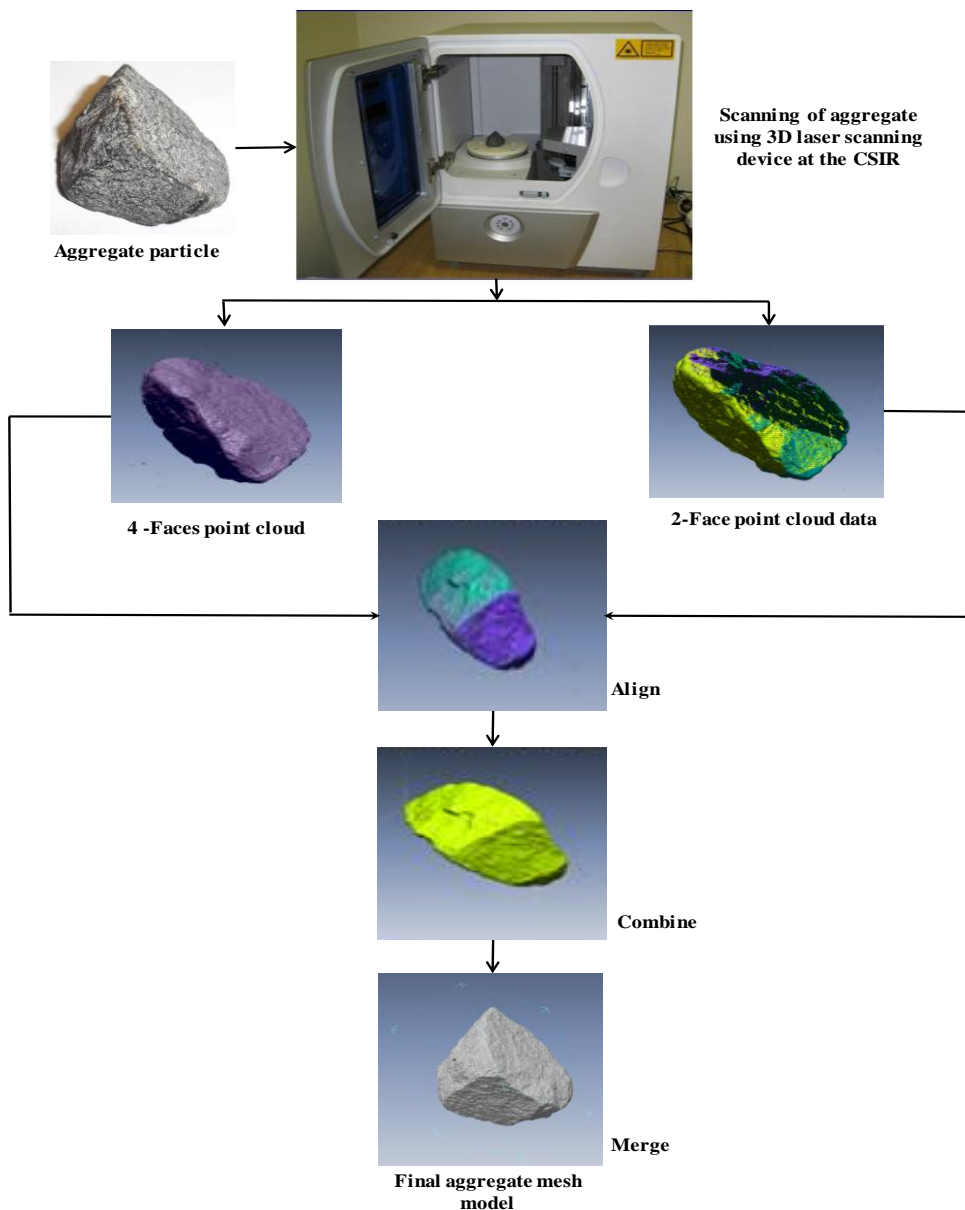
A 3-D laser scanning device available at the CSIR was used to scan aggregate particles, individually. Laser scanning protocol developed at the CSIR was used during aggregate scanning (Anochie-Boateng and Komba, 2010). The 3-D laser scanning device has been integrated with Rapidform data acquisition and processing software. The device operates in rotary and planar scanning modes. Rotary scanning mode is suitable for scanning spherical objects, whereas planar mode is used for scanning non-spherical objects. Aggregates are scanned in planar mode as 3-D solid object with six planes. Four side surfaces of an aggregate particle are scanned first and then the aggregate particle is turned to scan the top and bottom surfaces (i.e. two surfaces). During the scanning process, the laser scanning device captures point cloud data of an aggregate particle at a pre-defined resolution. The maximum scanning resolution of the laser scanner used in this study is 0.1 mm (100  $\mu$ m). Maximum resolution was used for all scanning performed in order to obtain high quality scans of aggregate particles.

The data obtained after completing scanning an aggregate particle are point clouds. Rapidform software was used to process the point cloud data to reconstruct 3-D models of scanned aggregates. The process involves aligning, combining and merging the four side surfaces and two surfaces (top and bottom) scanned separately. After processing the data of scanned aggregate particles, the dimensions (longest, intermediate and shortest), surface area, volume and coordinates of the centre were obtained directly by using Rapidform software. Direct validation and evaluation of the accuracy of the 3-D laser scanning device to measure these aggregate properties has been previously accomplished at the CSIR (Anochie-Boateng et al, 2010 and Anochie-Boateng et al, 2011a). Therefore, validation of the 3-D laser scanning device will not be repeated in this study. Figure 3.1 illustrates procedures for aggregate scanning and processing.

Other information that can be obtained after completing processing of the scanned aggregate particle include the centre of mass, the surface points (vertices) in terms of x, y and z Cartesian coordinates and triangular surfaces known as poly-faces. The x, y and z Cartesian coordinates can be exported to other data processing software such as Microsoft Excel<sup>TM</sup> and MATLAB<sup>TM</sup> for further processing. In this dissertation, MATLAB<sup>TM</sup> was used.

The x, y and z Cartesian coordinates of the surface points and the centre of the mass of an aggregate particle were obtained by using the Rapidform software. The surface points and the centre of mass coordinates are the basic data for the spherical analysis technique to determine

the aggregate shape properties. The commercial software (Rapidform) used for aggregate scanning and pre-processing the laser scans data cannot perform spherical analysis to determine the aggregate shape indices. A separate MATLAB™ code was developed to perform the spherical harmonic analysis and compute aggregate form, angularity and surface texture indices. Detailed information on the development and computations implemented in the MATLAB™ code are described in Chapter 5 Sections 5.3.1 to 5.3.2. The developed MATLAB™ code is presented in Appendix B.



**Figure 3.1: Aggregate scanning process.**

### 3.4 Determination of laser-based aggregate shape properties

The determination of aggregate shape properties by using the laser scanning technique is the core focus of this dissertation. Two different approaches were used to analyse aggregate scan data, to determine their shape properties. The first approach makes use of the aggregate's dimensions (longest dimension, intermediate dimension shortest dimension), surface area and volume to compute indices describing aggregate form.

The second approach is a spherical harmonic analysis of laser scan data to quantify the form, angularity and surface texture of the aggregates. Detailed procedures for pre-processing of the laser scan data and application of the spherical harmonic analysis technique are covered in Chapter 5 of this dissertation. Figure 3.2 shows schematic procedures used for determination of aggregate shape properties.

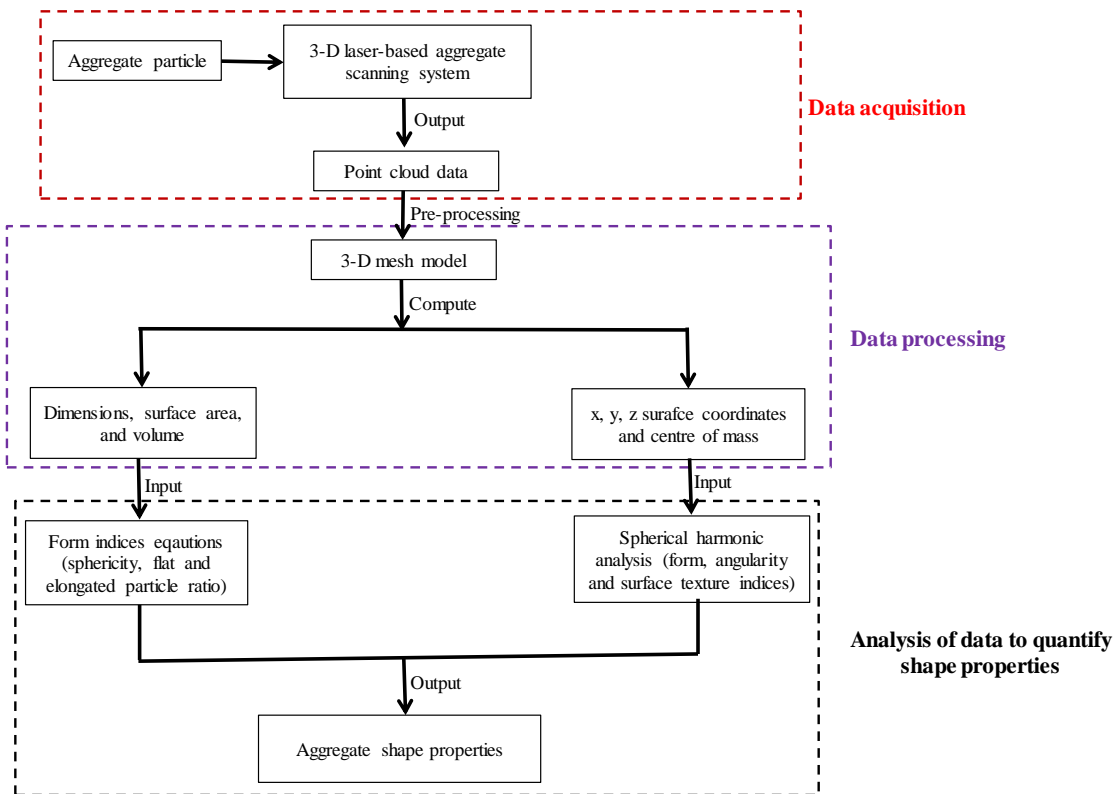


Figure 3.2: Procedures for laser based-based determination of aggregate shape properties.



### **3.5 Validation of aggregate shape properties**

The validation of the laser-based aggregate shape indices was achieved by:

- Correlation between various laser-based aggregate shape indices;
- Correlation of laser-based aggregate shape indices with flakiness index;
- Correlation of laser-based aggregate shape indices with flat and elongated particles ratio, and
- Visual comparison of angularity and surface texture of aggregates with laser-based angularity and surface texture indices.

### **3.6 Summary**

The methodology followed during the study has been discussed. The study consists of material selection and sample preparation, laser scanning of aggregates, determination of aggregate shape properties and validation of the laser-based aggregate shape properties.

## **4 LABORATORY TESTING AND LASER SCANNING RESULTS**

### **4.1 Introduction**

This chapter presents results of laboratory tests and the aggregate laser scanning results without detailed analysis. The results of standard laboratory tests are presented first. Secondly, the results obtained from laser scanning of the aggregates studied are presented. The results of scanned aggregates will be further analysed in Chapter 5 to determine aggregate shape properties. An indication of what the results were used for is also provided in this chapter.

### **4.2 Laboratory test results**

As indicated previously, the laboratory tests performed on aggregate samples prior to laser scanning included grading analyses, flakiness index, flat and elongated particles ratio, bulk relative density, aggregate crushing value and ten per cent Fines Aggregate Crushing value. Test results for the six types of aggregates studied are presented in Table 4.1.

Grading analyses results gave an indication of the distribution of aggregate particles for each of the six types of aggregates studied. Grading analyses also formed the basis for the selection of aggregate particles for laser scanning. The study used aggregate particles retained on different sieve sizes. From the graded aggregate particles, it was possible to select the required aggregate particles for laser scanning.

The flakiness index and flat and elongated particles ratio test results are used in Chapter 5 Section 5.5 to validate the laser-based aggregate form indices. The flakiness index and flat and elongated particles ratio results for the six types of aggregates were correlated with the computed laser-based form indices.

The purpose of other tests including bulk density, aggregate crushing value and ten per cent Fines Aggregate Crushing value were to obtain an indication whether the aggregates studied comply with the specifications for aggregate used for the construction of pavements in South Africa. Detailed analysis of these results is not part of the scope of this dissertation.

**Table 4.1: Grading analysis and standard laboratory test results.**

Material	Granite	Tillite	Quartzite	Hornfels	Alluvial gravel	RA	
<b>Sieve size (mm)</b>	<b>Sieve analysis (Percentage passing)</b>						
53.0					100	100	
37.5	100	100	100	100	95	100	
26.5	98	93	94.2	88	83	100	
19.0	84	78	82.0	70	69	91	
13.2	69	66	68.5	61	49	50	
9.5	57	58	60.9	53	33	38	
6.7	49	48	58.2	44	23	21	
4.75	44	42	52.4	40	17	12	
2.36	34	28	35.3	28	10	7	
1.18	26	20	23.9	21	9	5	
0.600	19	14	17.1	16	9	4	
0.300	13	10	14.6	13	9	3	
0.150	9	8	12.7	11	6	2	
0.075	6.5	5.7	9.2	8.4	2.3	1.3	
<b>Standard laboratory test results</b>							
<b>Flakiness Index (%)</b>	21.7	17.1	34.7	27.2	3.1	28.2	
<b>Flat and elongated particles ratio (%)</b>	<b>5:1</b>	10.3	4.9	12.1	13.2	0.0	0.1
	<b>3:1</b>	31.2	31.7	31.6	25.5	2.4	15.4
	<b>2:1</b>	63.7	63.4	66.7	56.2	40.4	59.7
<b>BRD<sup>1</sup></b>	2.634	2.670	2.650	2.709	2.649	2.504	
<b>ACV (%)</b>	21.6	11.9	16.6	10.7	13.6	9.5	
<b>10% FACT (kN)</b>	180	345	265	378	325	415	

<sup>1</sup>: Bulk Relative Density (BRD) of the aggregates.

Figure 4.1 shows plots of grading analysis results. The plots of grading analysis indicate that the four crushed aggregates (granite, tillite, quartzite and hornfels) are continuously graded. This is primarily due to the fact that a crusher run (full grading as produced from the crusher) sample was obtained from the quarries. On the other hand, alluvial gravel and RA samples are gap graded, with over 80 per cent of the aggregate particles retained on the 4.75 mm sieve. This could be due to the fact the alluvial gravel was collected along a river where there is no guarantee to obtain all fractions. Similarly, the RA was sampled at the plant stockpile; therefore its grading is determined by the fractions contained on a specific stockpile. As indicated before, the focus of this study was on the coarse aggregate (aggregates greater than 4.75 mm). Despite the differences in the grading of crushed aggregates, alluvial gravel and RA sufficient materials for testing and laser scanning were available for all types of aggregates studied.

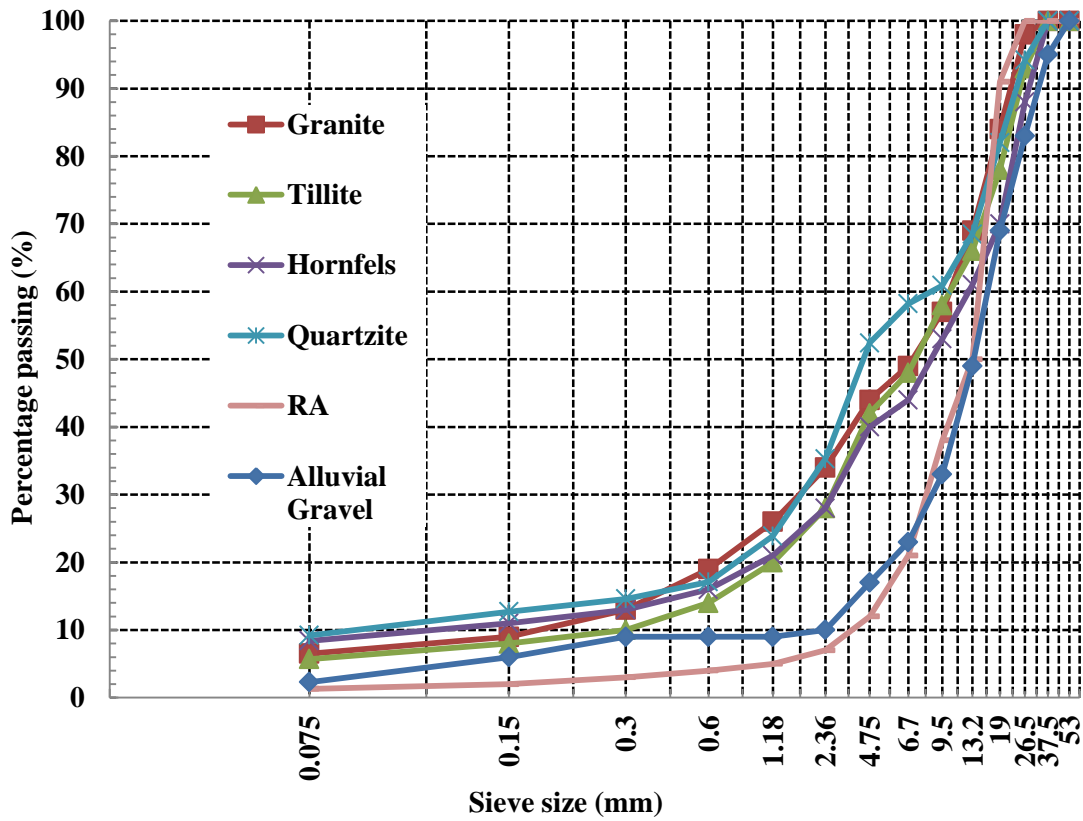


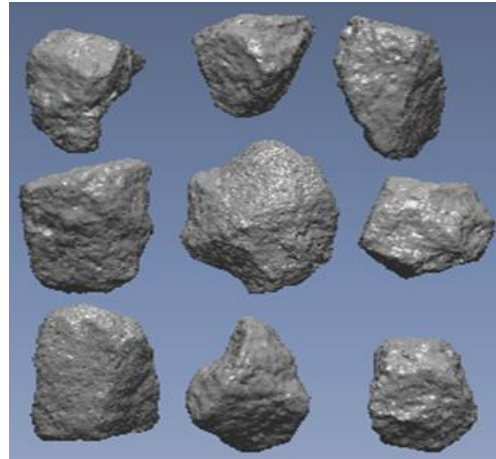
Figure 4.1: Grading analysis results.

### **4.3 Results of scanned aggregate particles**

The results presented in this section forms basic data used for the analyses presented in Chapter 5 Sections 5.2 and 5.3, to determine aggregate shape properties. Figure 4.2 shows photos of 19.0 mm actual aggregates and models of scanned aggregate for granite, tillite and quartzite. Similar samples for hornfels, alluvial gravel and RA are shown in Figure 4.3. From the figures, it is clear that the laser scanning technique is capable of producing aggregate models, which are similar to the actual aggregates. Therefore, it is reliable to analyse the aggregate models to get an indication of the shape properties of the actual aggregates.



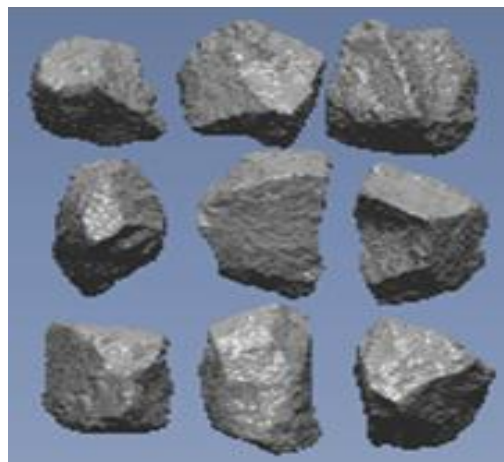
Actual granite aggregates



Modelled granite aggregates



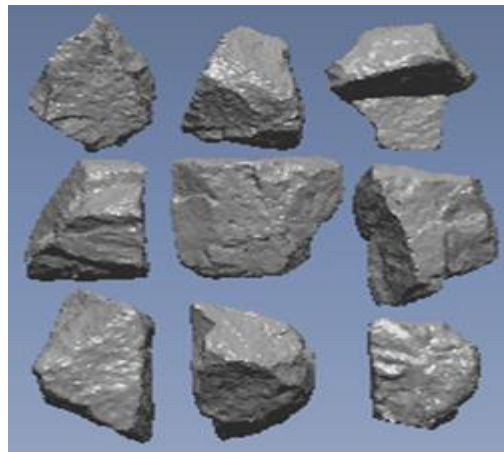
Actual tillite aggregates



Modelled tillite aggregates



Actual quartzite aggregates

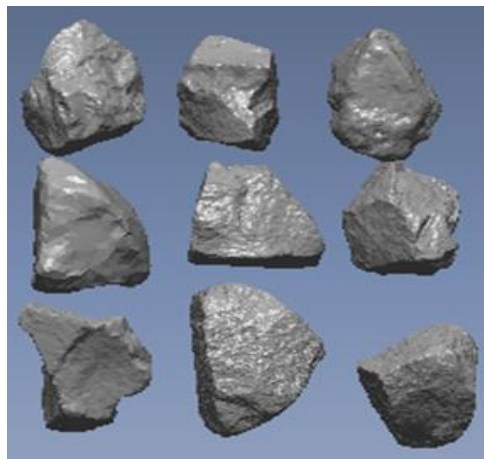


Modelled quartzite aggregates

**Figure 4.2: Actual and modelled 19.0 mm for granite, tillite and quartzite.**



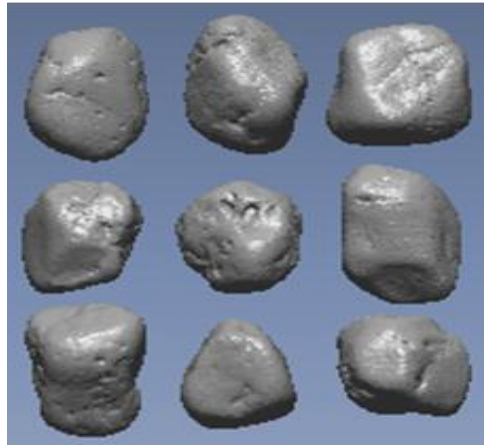
Actual hornfels aggregates



Modelled hornfels aggregates



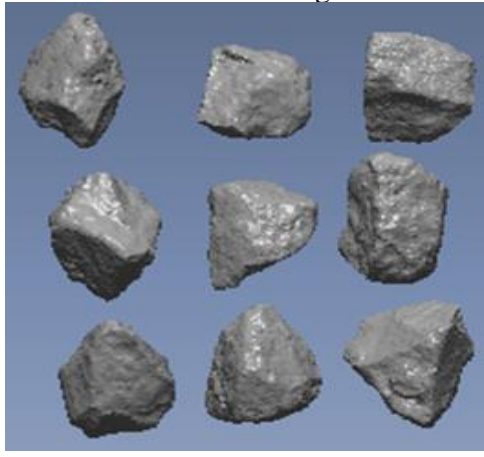
Actual alluvial gravel



Modelled alluvial gravel



Actual RA



Modelled RA

**Figure 4.3: Actual and modelled 19.0 mm for hornfels, alluvial gravel and RA.**

Table 4.2 presents the results of dimensions, coordinates of the centre of mass, surface area and volume of 19.0 mm granite aggregate particles. Appendix A contains the results of the rest of aggregate particles studied. The dimensions, surface area and volume of aggregate particles are used in Chapter 5 Section 5.2 to determine aggregate form indices. The coordinates of the centre of mass are used as input for spherical harmonic analysis of aggregates in Chapter 5 Section 5.3 to determine form, angularity and surface texture indices.

Figures 4.4 to 4.9 show plots of the surface area and volume for the six types of aggregates studied. The plots show that the surface area and volume of aggregates decrease with decreasing size of the sieve on which they are retained, which is the expected trend. It is also observed that the average surface area and volume of different types of aggregates retained on the same sieve size differ significantly. The plots clearly demonstrate the capability of the laser scanning technique to measure surface area and volume properties of aggregates.



**Table 4.2: Scan results of 19.0 mm granite aggregate particles.**

19.0 mm Sieve								
Particle No.	Dimensions (mm)			Centre of mass (mm)			Surface area (mm <sup>2</sup> )	Volume (mm <sup>3</sup> )
	d <sub>L</sub>	d <sub>I</sub>	d <sub>S</sub>	X	Y	Z		
1	39.22	31.87	16.10	-0.42	2.89	13.52	2558.46	7851.52
2	31.35	22.42	19.87	-1.13	2.13	15.66	2146.07	6699.91
3	34.65	27.34	18.50	-0.71	0.84	15.47	2524.83	8805.80
4	35.88	24.43	23.02	-1.48	1.39	16.13	2476.04	8460.95
5	34.01	28.49	19.31	0.62	2.51	14.30	2512.79	8635.04
6	28.02	22.99	21.35	0.38	-0.32	15.95	2035.34	6866.36
7	32.84	22.00	21.17	-1.69	1.49	15.16	1986.29	6128.76
8	26.78	26.33	18.01	-1.36	-0.44	14.85	1880.01	6082.07
9	30.57	21.01	19.76	-2.19	1.04	15.74	1919.39	6102.64
10	24.92	22.39	19.97	-0.90	1.81	15.32	1701.03	5380.24
11	37.00	28.36	15.00	0.66	1.50	13.26	2406.86	7387.02
12	32.56	23.58	14.82	0.37	2.93	13.17	1918.29	5462.13
13	34.41	28.82	18.49	-0.30	2.13	13.93	2231.51	6486.52
14	47.06	29.42	17.29	0.45	0.08	14.59	3298.66	11197.2
15	34.51	25.32	17.23	1.43	0.05	14.30	2331.67	7483.74
16	31.80	30.99	14.39	2.93	-1.44	13.79	2087.39	5896.26
17	48.88	25.45	18.03	1.83	0.05	14.12	2975.01	9593.82
18	46.08	31.87	18.42	3.77	-0.93	14.11	3179.23	9820.76
19	60.25	32.62	21.95	-1.35	-2.22	15.20	3888.95	13142.2
20	52.56	30.31	21.73	-4.05	-1.17	15.71	3149.90	10292.0
21	41.45	27.16	14.34	-0.70	1.74	13.38	2491.10	6882.31
22	37.39	30.87	15.77	-0.35	1.47	13.32	2229.72	5972.80
23	42.18	32.10	13.59	1.64	1.50	13.11	2684.04	6691.75
24	41.44	26.37	12.08	0.43	2.01	12.07	2260.93	5714.88
25	44.97	30.28	9.86	-0.03	1.10	11.07	2641.25	5574.31
26	54.29	30.05	9.45	-1.68	1.82	11.19	2761.07	5458.15
27	44.64	26.68	8.57	-2.00	1.37	10.64	2278.43	4344.42
28	44.55	28.31	9.34	-2.12	2.59	11.04	2505.89	5066.99
29	42.92	30.25	8.80	0.62	1.76	10.69	2053.62	3090.84
30	37.62	33.57	8.99	1.78	2.97	10.36	1799.19	2569.85

d<sub>L</sub> = Longest dimension, d<sub>I</sub> = Intermediate dimension and d<sub>S</sub> = Shortest dimension.

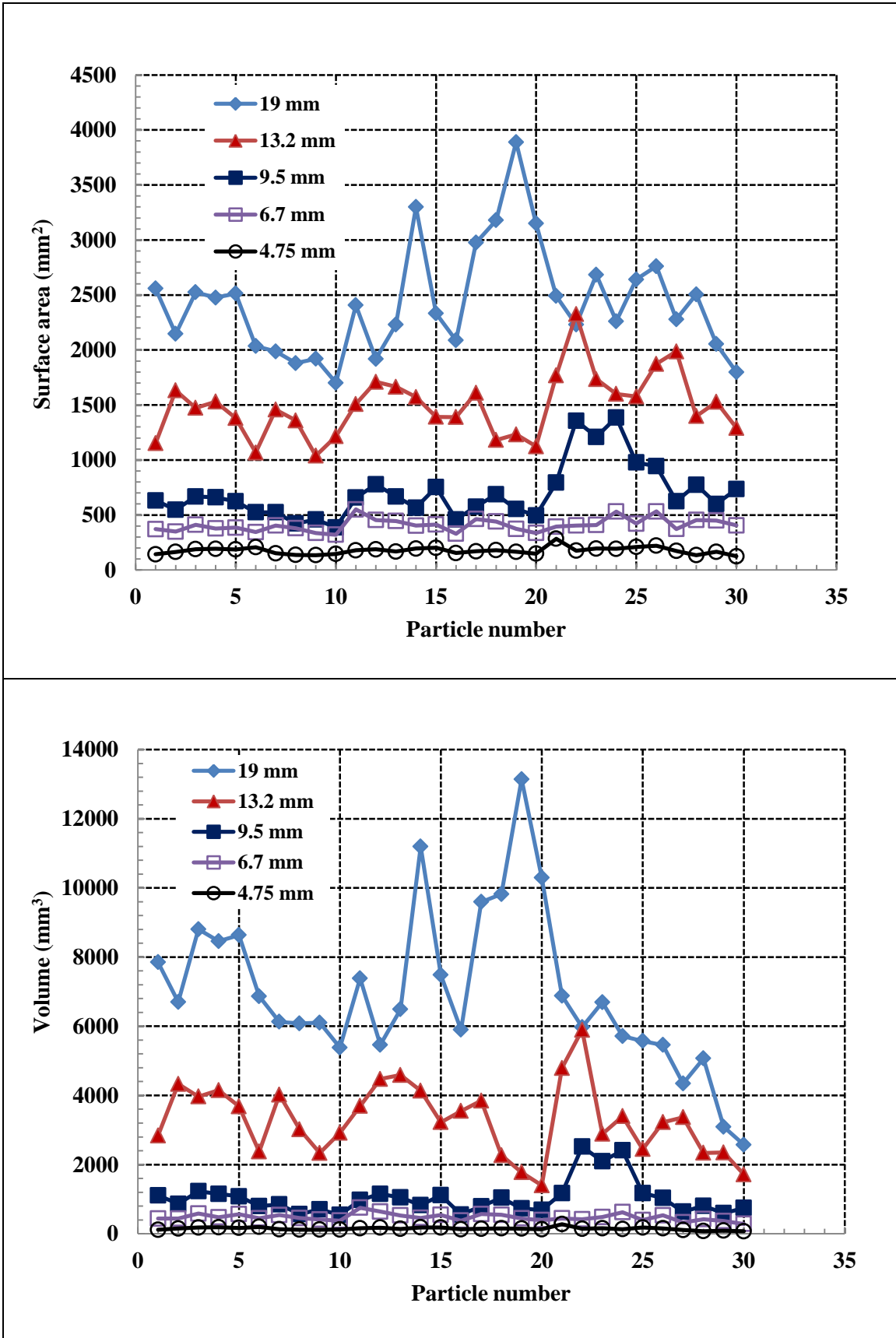


Figure 4.4: Surface area and volume of granite.

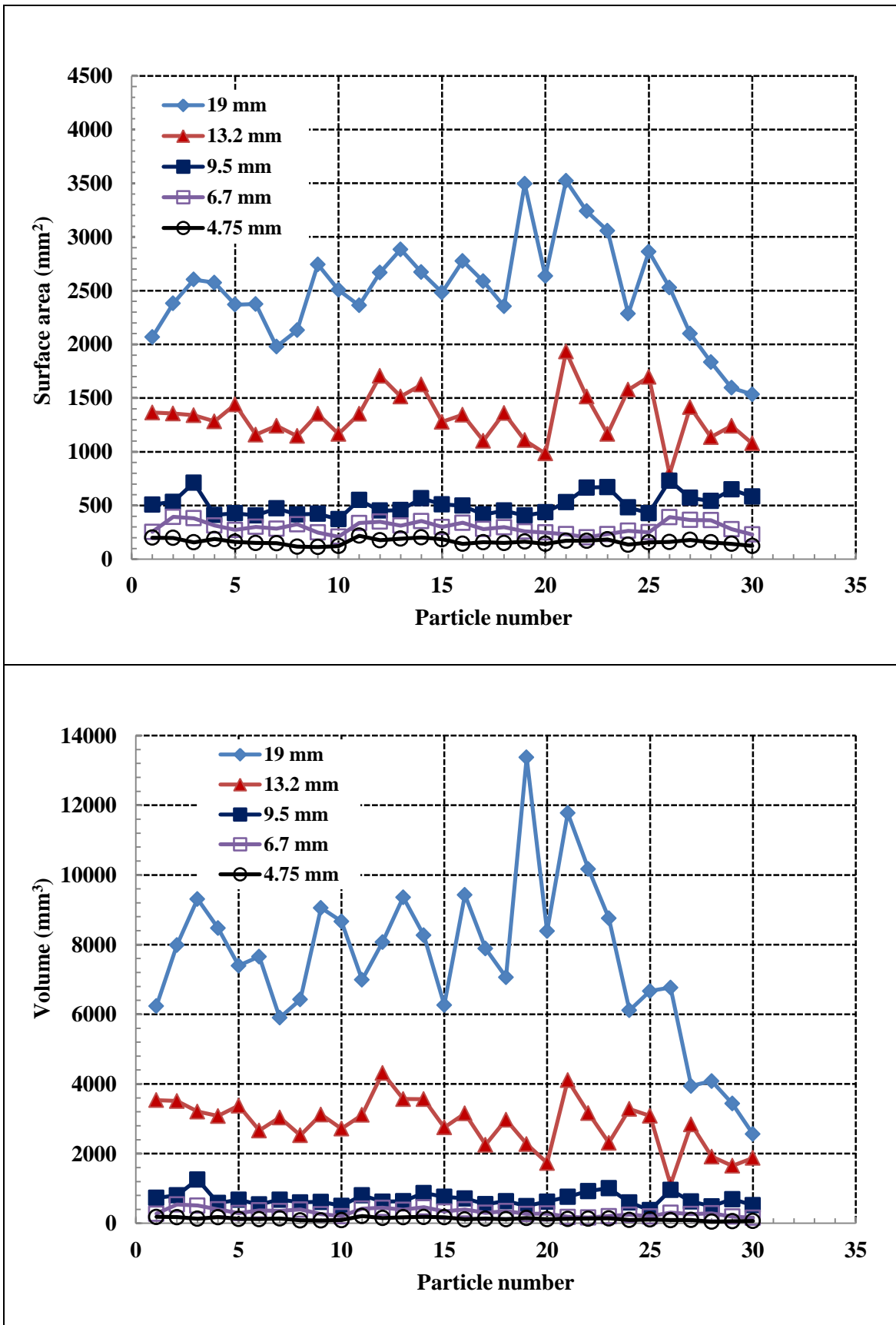


Figure 4.5: Surface area and volume of tillite.

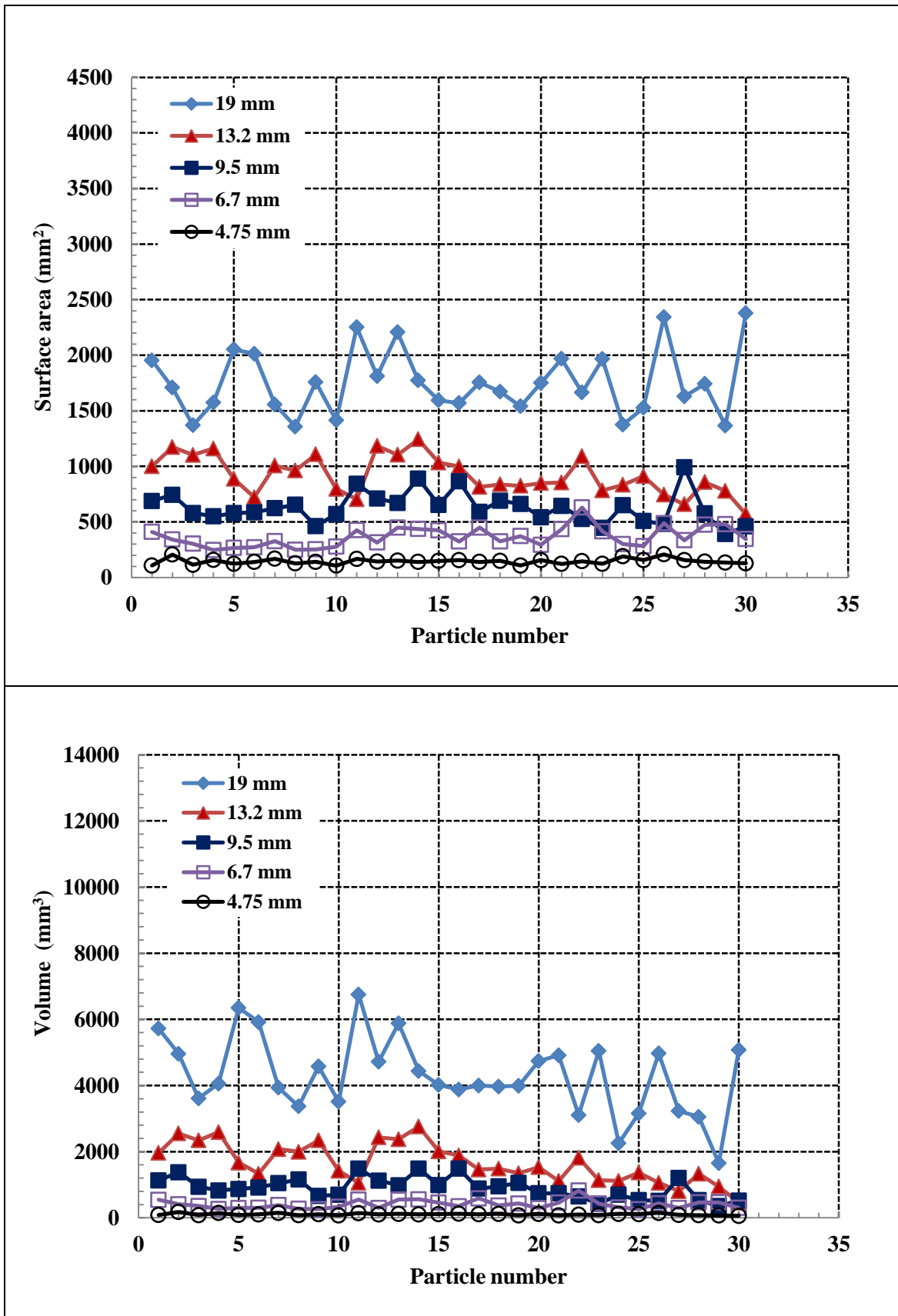


Figure 4.6: Surface area and volume of quartzite.

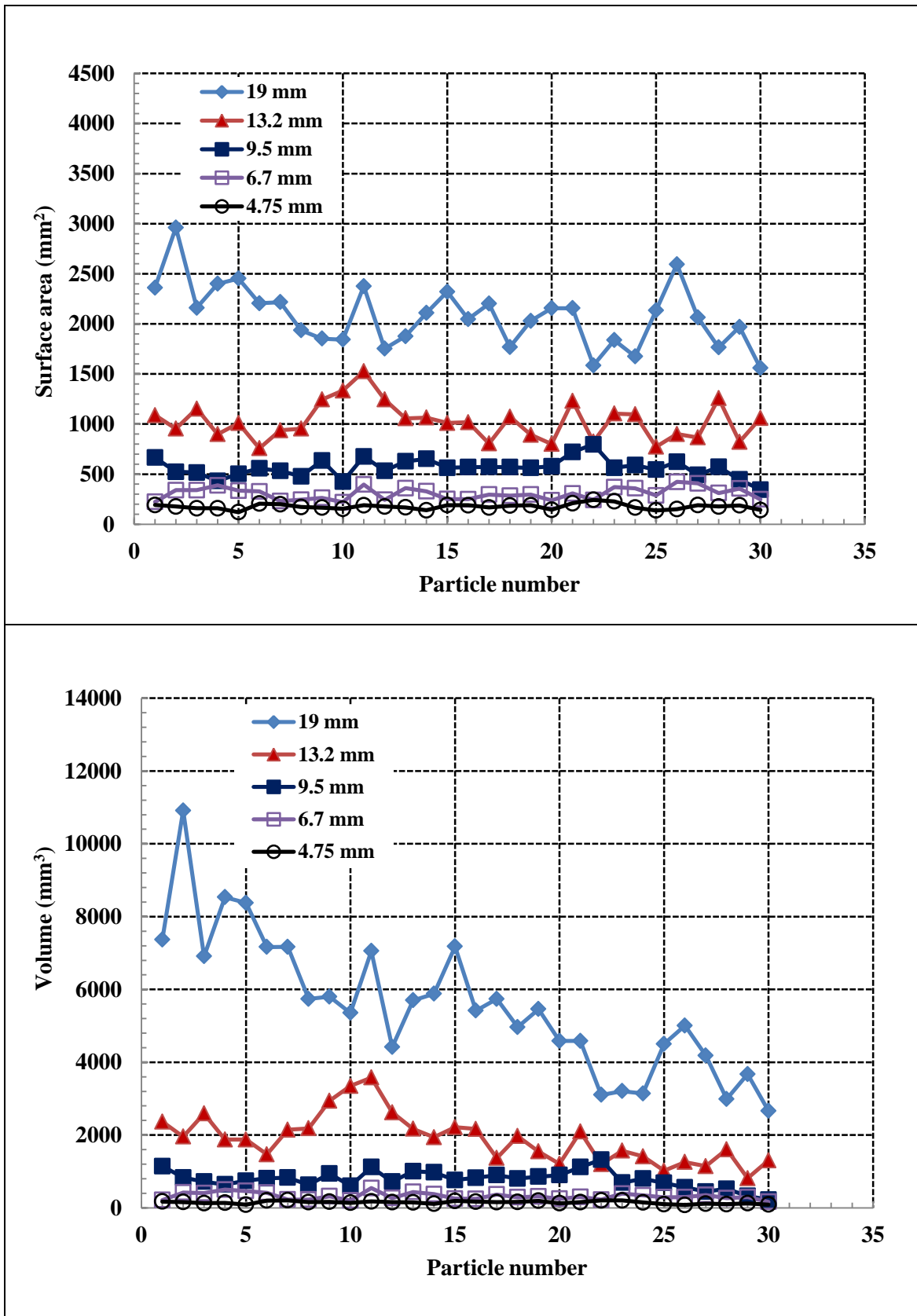


Figure 4.7: Surface area and volume of hornfels.

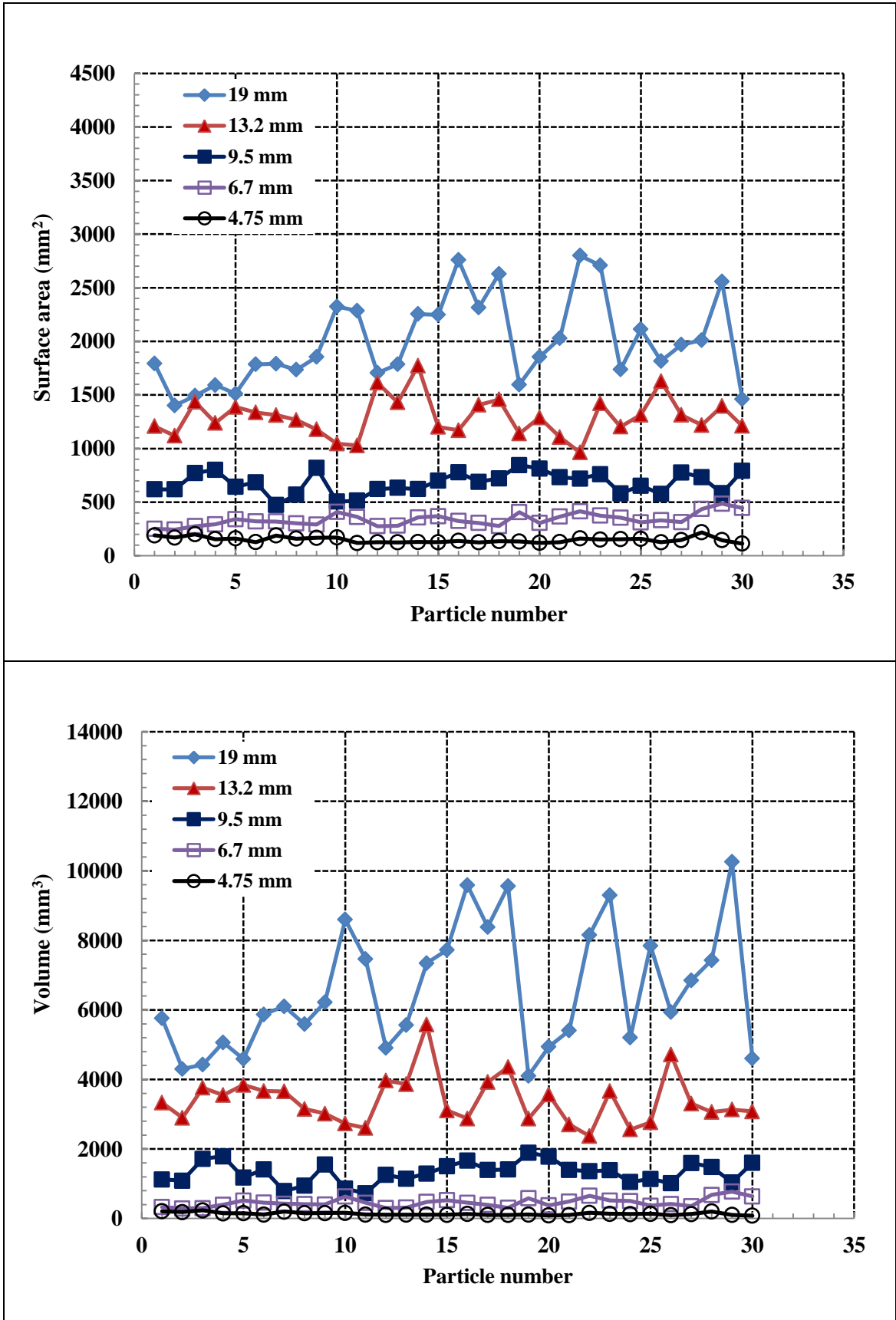


Figure 4.8: Surface area and volume of alluvial gravel.

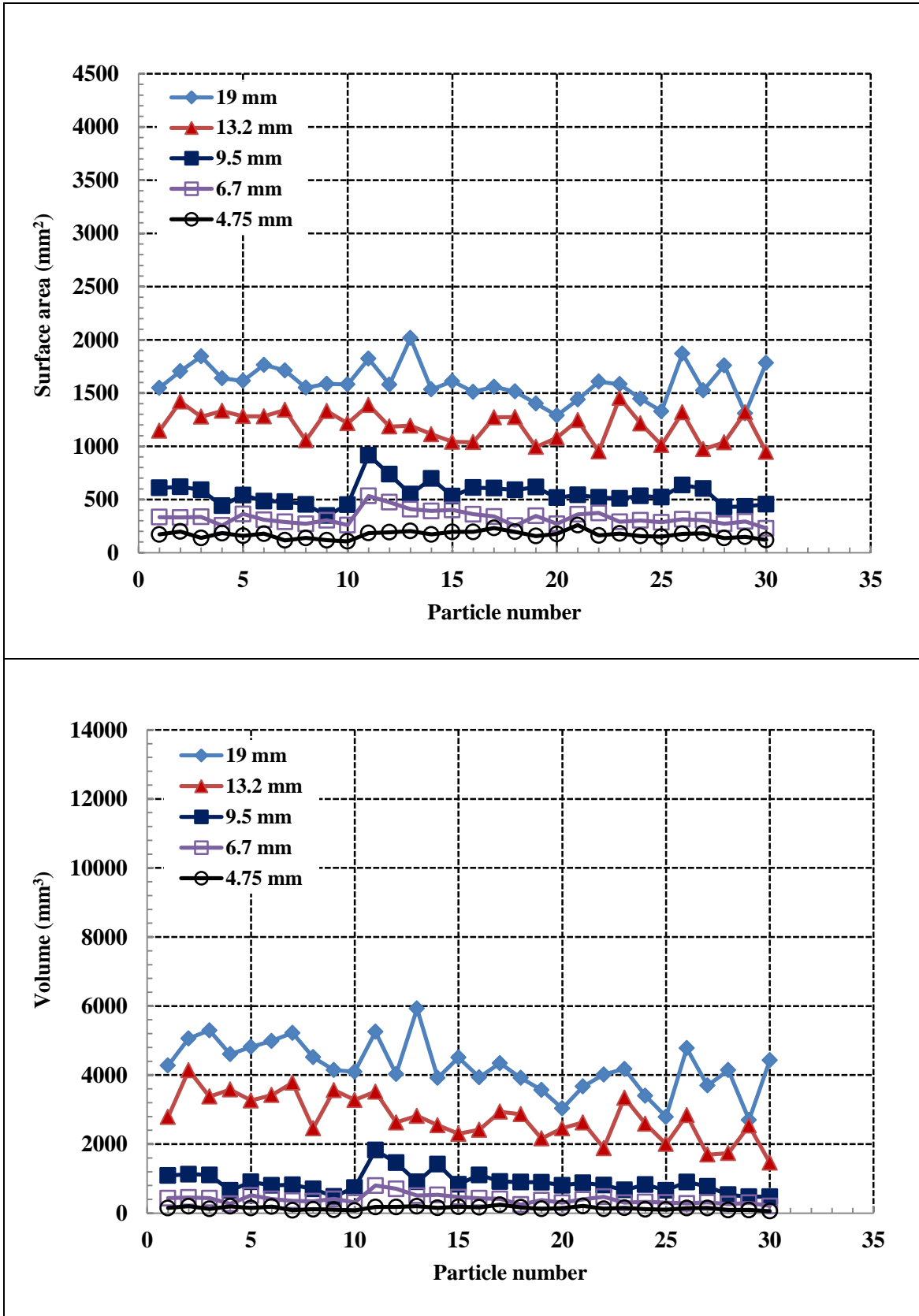


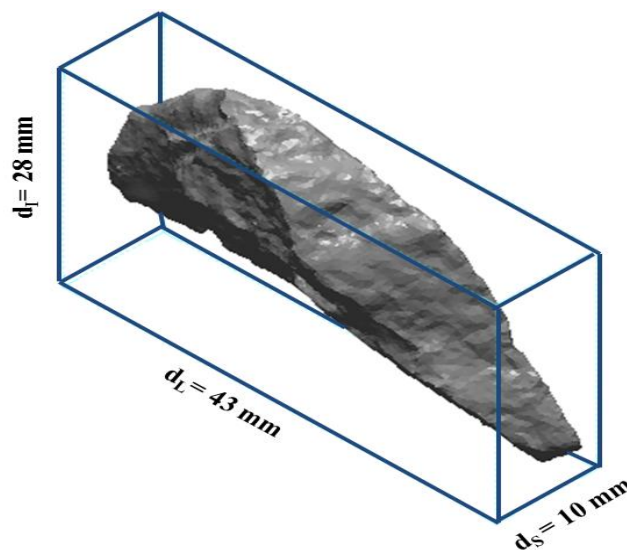
Figure 4.9: Surface area and volume of RA.

#### 4.4 Grading of the aggregate particles selected for laser scanning

As mentioned earlier, the aggregate particles selected for laser scanning are those retained on coarser sieve sizes (4.75, 6.7, 9.5, 13.2 and 19.0 mm). The grading curves of the aggregate particles selected for scanning were determined for each aggregate type by using two different approaches. The first approach is the standard manual method (mechanical sieve shaking in accordance with TMH 1 Method B4). The second approach is based on the dimensions and volume of aggregate particles determined by using the laser scanning technique.

An aggregate particle can be retained on a sieve if the longest dimension ( $d_L$ ) and the intermediate dimension ( $d_I$ ) are greater than the sieve size. In other words, the intermediate dimension controls the sieve on which an aggregate particle can be retained. However, because of irregularity of aggregate shape, some particles with intermediate dimension greater than the sieve size can still pass through the sieve. Flat and elongated particle with intermediate dimension smaller than the diagonal of the square opening are more likely to pass through the sieve opening, even if the intermediate dimension is greater than the sieve size.

Figure 4.10 shows a model of a flat and elongated aggregate particle with both the longest dimension ( $d_L = 43$  mm) and the intermediate dimension ( $d_I = 28$  mm) greater than 19.0 mm. Based on the longest dimension and the intermediate dimension criteria, the particle shown in Figure 4.10 should be retained on the 19.0 mm sieve, but it passed through the sieve in the standard test procedures.



**Figure 4.10: Flat and elongated particle passing through a sieve with the intermediate size greater than the sieve size.**



The determination of the grading curves by using the laser scans results makes use of the ratio by volume as opposed to the ratio by mass used in the standard manual method (TMH 1 Method B4). Aggregate particles from the same parent rock can be assumed to have the same specific gravity. Therefore, the ratio by mass is equivalent to the ratio by volume. The following are the procedures for determination of the grading curves:

- Obtain the longest and the intermediate dimensions of individual aggregate particles after completing scanning and pre-processing the scans data by using the Rapidform software;
- Establish whether the sieve on which each aggregate particle is retained. The longest and the intermediate dimensions should be greater than the sieve on which the particle is retained. In addition, check whether the particle passed through the sieve above which it is retained by ensuring that the intermediate dimension is less than the diagonal of the square opening of the sieve;
- Compute the volume of the aggregates retained on each sieve (19.0, 13.2, 9.5, 6.7 and 4.75 mm);
- Compute the total volume of the whole aggregate sample;
- Computed the percentage of the aggregate particles retained on the sieve size by dividing the volume of aggregate on a specific sieve by the total volume of the aggregate sample, and multiply by 100, and
- Finally, compute the percentage of the aggregate particles passing through each size.

Figures 4.11 to 4.13 show grading curves of the aggregates used in the study. With the exception of quartzite and tillite, the grading curves determined by using the laser scans results closely follow the grading curves determined by using the standard manual method. Despite the limitation of the use of the intermediate dimension criteria particularly for flat and elongated aggregate particles, the intermediate dimension of an aggregate particle appears to control the sieve size on which the aggregate particles are retained. This is in agreement with the finding of other studies in aggregate imaging (Rao et al, 2001).

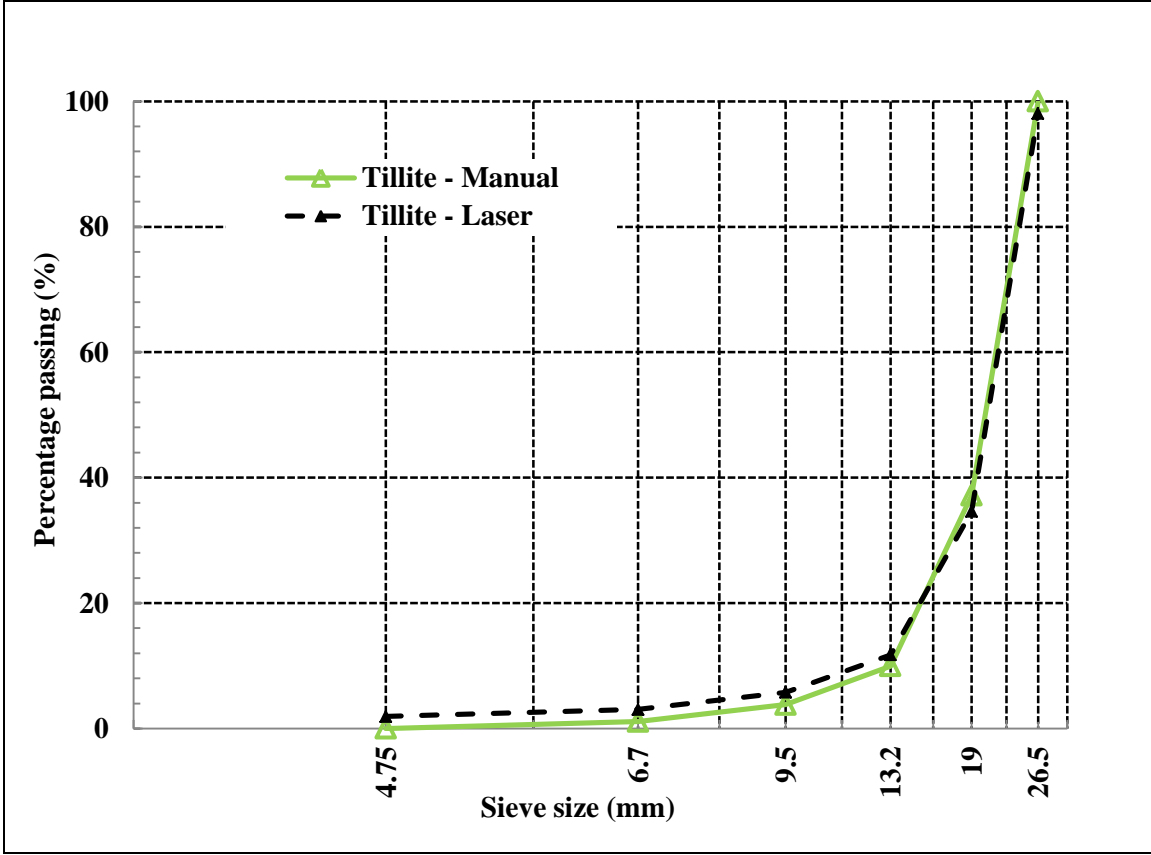
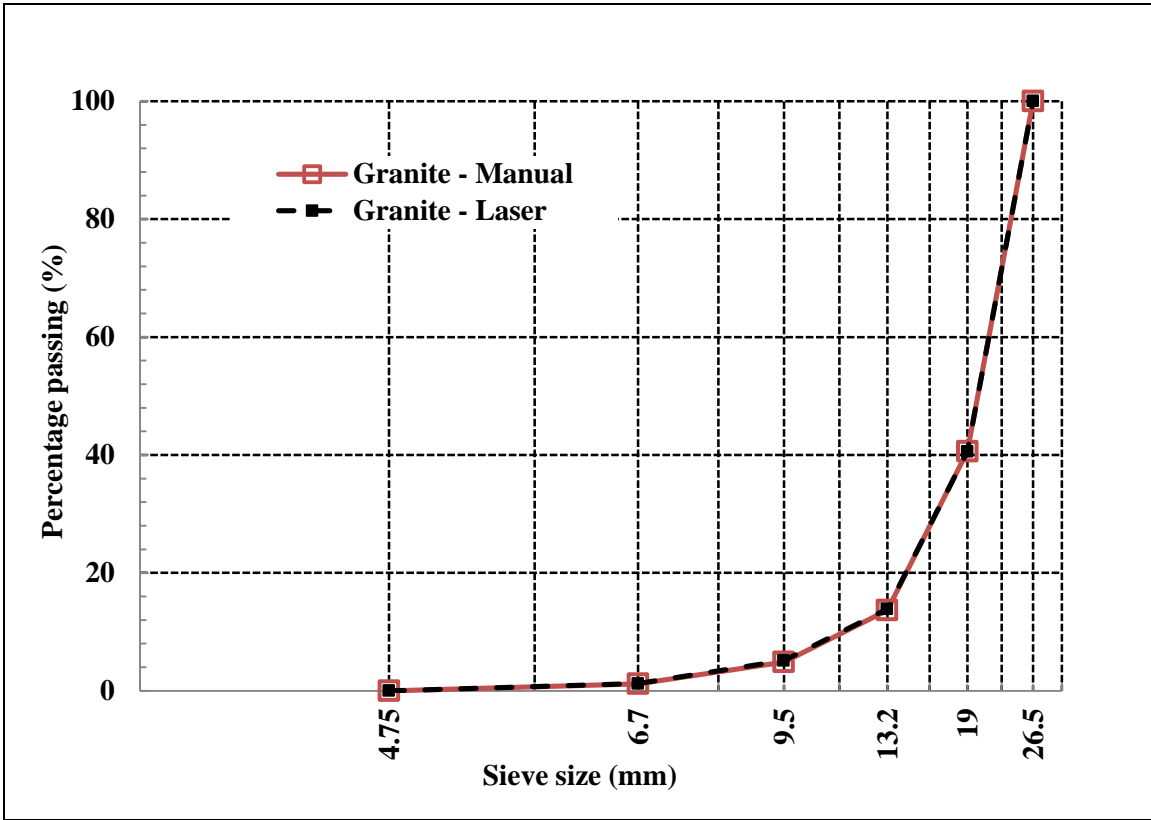


Figure 4.11: Grading curves for granite and tillite.

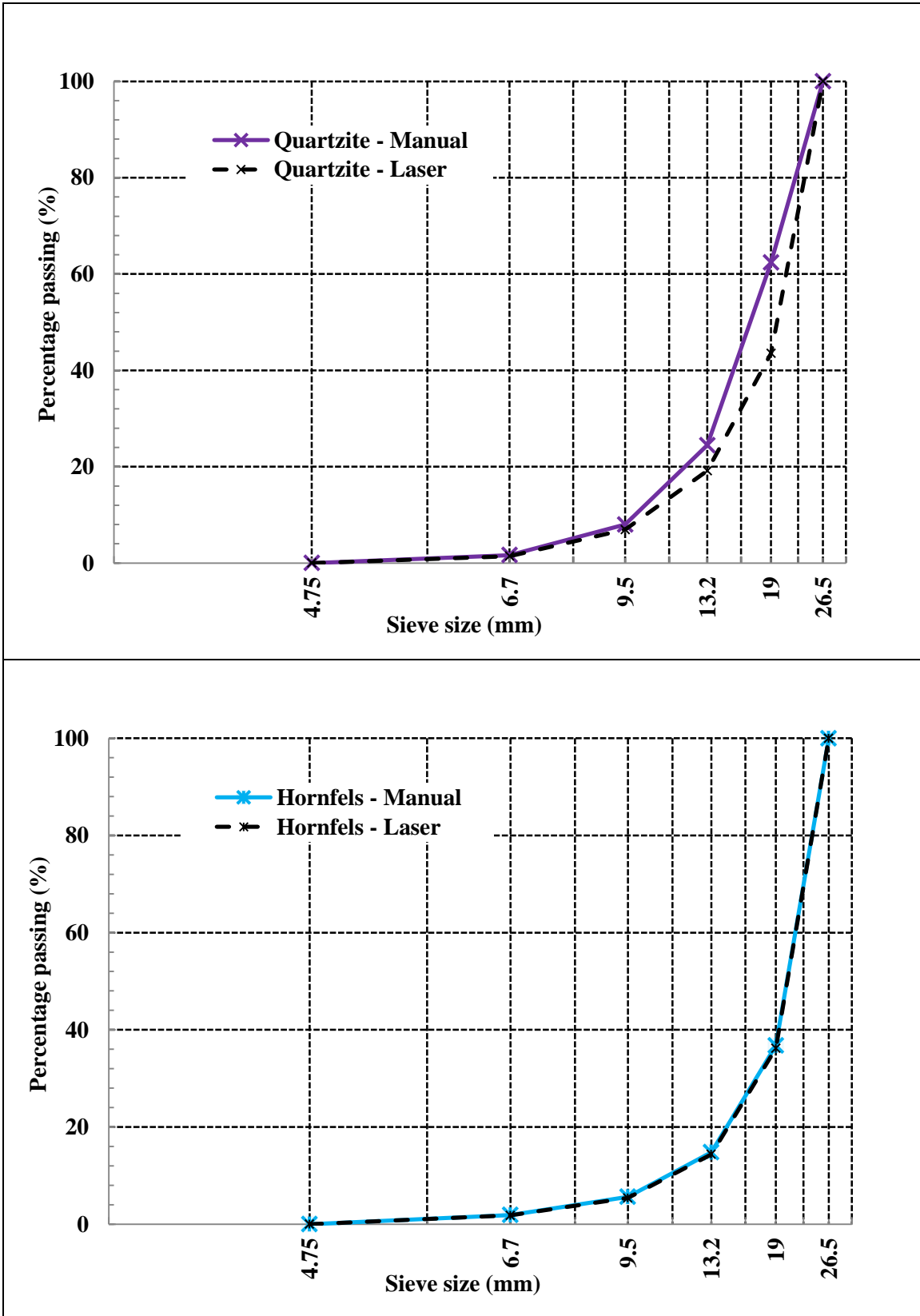


Figure 4.12: Grading curves for quartzite and hornfels.

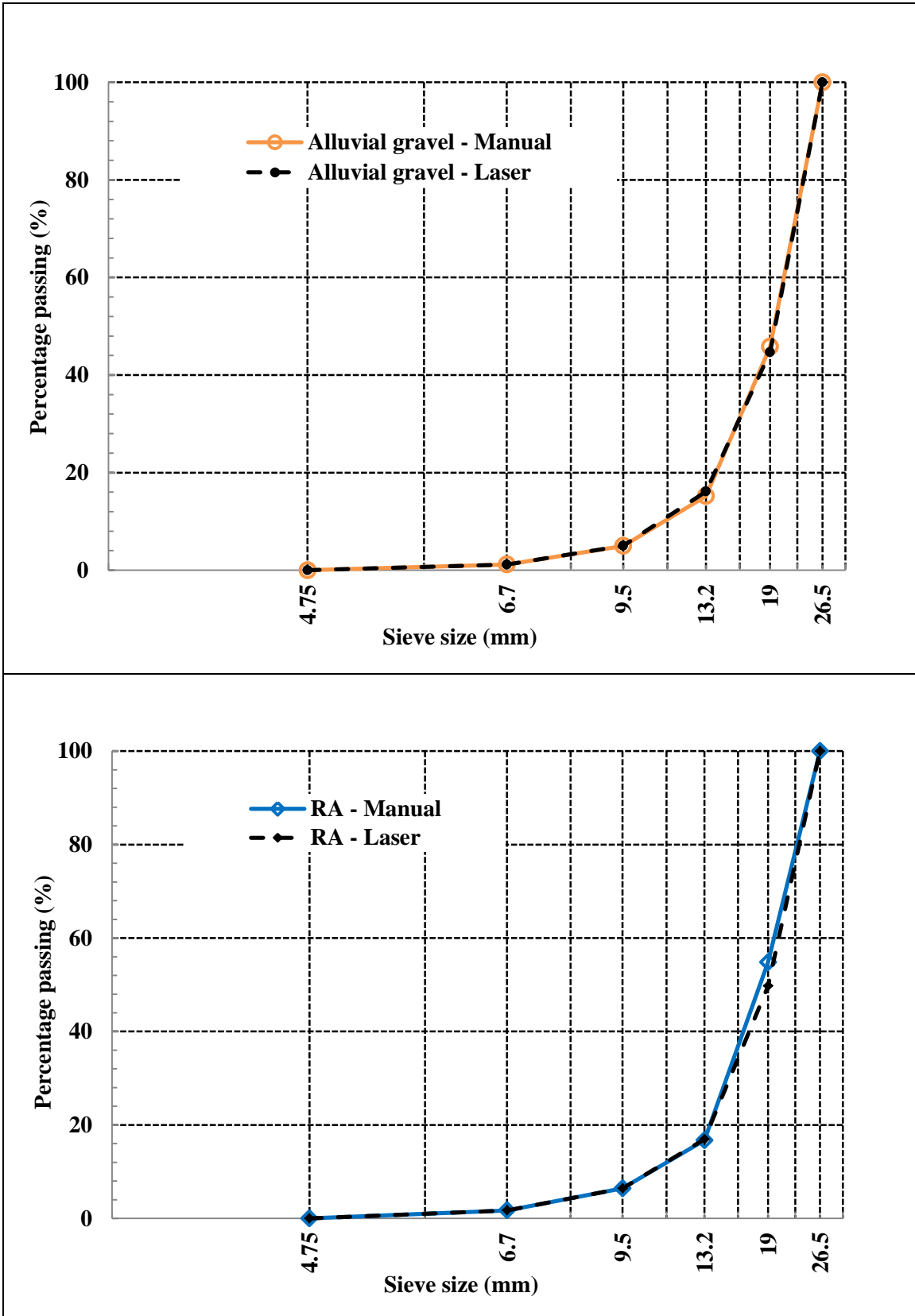


Figure 4.13: Grading curves for alluvial gravel and RA.

## 4.5 Summary

Chapter 4 presented the laboratory and laser scanning test results without detailed analysis. The results forms basic data used for the analyses presented in Chapter 5 Sections 5.2 to 5.5. The presented results are used as follows:

- The dimensions (longest dimensions, intermediate dimension and shortest dimension) of aggregate particles presented in Table 4.2 are used in Chapter 5 Section 5.2.1 to compute sphericity of aggregate particles.
- The surface area and volume results presented in Table 4.2 and Figures 4.4 to 4.9 are used to compute sphericity values in Chapter 5 Section 5.2.2;
- The dimensions and volume of the aggregate particles were also used to determine grading curves of the aggregates presented earlier in Chapter 4 Section 4.4;
- The x, y and z coordinates presented in Table 4.2 are used as inputs for spherical harmonic analysis to compute form, angularity and surface texture indices in Chapter 5 Section 5.3, and
- The flakiness index and flat and elongated particles ratio results presented in Table 4.1 are used for correlations with laser-based form indices in Chapter 5 Section 5.5.

## **5 DATA ANALYSIS AND DISCUSSIONS**

### **5.1 Introduction**

The objectives of this chapter are to conduct data analysis and discuss of the results obtained during the study. The analysis of the laser scan data is performed using two different approaches namely:

- Determination of aggregate form indices by using physical properties, and
- Determination of aggregate form, angularity and surface texture by using spherical harmonic analysis.

The validation of the laser-based aggregate form indices was performed by correlation with the flakiness index (TMH1 Method B3) and the flat and elongated particles ratio (ASTM D 4791) tests. These are the current standard test methods used to characterise form properties of aggregates. Detailed discussions on the test methods were provided in the literature survey conducted for this study (Chapter 2 Section 2.4). Validation of angularity and surface texture indices of the aggregates is based on visual assessment of selected aggregate particles in comparison with spherical harmonic analysis results.

### **5.2 Quantification of aggregate form indices by using physical properties**

The literature survey conducted during the study revealed that aggregate parameters measured using the laser scanning technique could be used to compute indices to describe aggregate shape properties. Aggregate physical parameters measured by the laser scanning device used in this study include the dimensions (i.e. longest dimension, intermediate dimension and shortest dimension), surface area and volume. It is important to emphasise that the evaluation of the capability and accuracy of the laser scanning device to measure these parameters has been accomplished in previous studies, and was not repeated in this study (Anochie-Boateng et al, 2010; Anochie-Boateng et al, 2011a).

Three different form indices computed by using the aggregate's physical properties were selected for further investigation. These selected form indices are:

- Sphericity computed using surface area and volume as defined by Equation 2.4;

- Sphericity computed using orthogonal dimensions of an aggregate particle as defined by Equation 2.1, and
- Flat and elongated ratio computed using the longest dimension and the shortest dimension of an aggregate particle as defined by Equation 2.3.

### 5.2.1 Sphericity computed using surface area and volume

The surface area and volume of individual aggregate particles were used to compute a sphericity parameter that describes the form of the aggregate using Equation 2.4. The sphericity computed by using Equation 2.4 approaches a maximum value of 1 for round shaped aggregate particles. Therefore, for the types of aggregates used in this study, the alluvial gravel sample was expected to yield higher sphericity values. Table 5.1 shows the sphericity statistical parameters (average, standard deviation and standard error) for the six types of the aggregates studied. The average surface area and volume of each aggregate size are also included in Table 5.1. The sphericity statistical parameters were computed for each aggregate size, as well as for each aggregate type. For each aggregate size the statistical parameters were computed by using results of 30 aggregate particles, whereas for each aggregate type the statistical parameters were computed by using results of 150 aggregate particles.

The results presented in Table 5.1 indicates that the average sphericity of alluvial gravel was the highest followed by that of RA. For the crushed aggregate types, the average sphericity of tillite was relatively higher followed by that of hornfels. The average sphericity of granite and hornfels was similar. It was also observed that there no consistent trend with regard to changes in sphericity values of different aggregate sizes for the same aggregate type.

Figure 5.1 shows the distributions of the sphericity computed using surface area and volume. The sphericity distributions are plotted for 150 particles studied for each aggregate type. Included in the figure are sphericity values of 15 spherical objects. The spherical objects had different sizes and were manufactured by using different types of materials (steel, ceramic, rubber and plastic). As expected all the spherical objects plotted closer to a value of one. For the six types of materials studied, alluvial gravel has higher sphericity values with a distribution ranging from 0.700 to 0.948, followed by RA with a distribution ranging from 0.604 to 0.896. Overall, the sphericity distributions of crushed aggregate particles did not differ significantly. Tillite has relatively higher sphericity values, followed by hornfels, granite and quartzite.

It was also observed that the distribution of sphericity values for different aggregate types may differ significantly; despite their average values being closer to each other. Therefore, a single average parameter such as flakiness index and flat and elongated particles ratio as used in the current standard test methods cannot accurately differentiate shape properties of different aggregate samples. Therefore, the use of an advanced technique such as aggregate laser scanning used in this study provides more information required to distinguish the form properties of different aggregate samples.

**Table 5.1: Statistical parameters for sphericity computed using surface area and volume.**

Aggregate type	Sieve size (mm)	Average surface area (mm <sup>2</sup> )	Average volume (mm <sup>3</sup> )	Sphericity for each aggregate size			Sphericity for each aggregate type		
				Average	Standard deviation	Standard error	Average	Standard deviation	Standard error
Granite	19.0	2430.43	6971.38	0.722	0.108	0.020	0.725	0.097	0.008
	13.2	1492.52	3298.78	0.715	0.111	0.020			
	9.5	701.78	1032.89	0.709	0.099	0.018			
	6.7	409.12	474.80	0.721	0.085	0.015			
	4.75	176.03	146.32	0.759	0.073	0.013			
Tillite	19.0	2506.87	7549.43	0.732	0.066	0.012	0.741	0.083	0.007
	13.2	1325.67	2860.89	0.731	0.068	0.012			
	9.5	509.44	688.59	0.743	0.088	0.016			
	6.7	295.87	316.76	0.752	0.092	0.017			
	4.75	162.40	128.02	0.747	0.101	0.018			
Quartzite	19.0	1754.39	4294.94	0.723	0.084	0.015	0.725	0.076	0.006
	13.2	919.68	1659.92	0.719	0.072	0.013			
	9.5	627.43	899.86	0.708	0.077	0.014			
	6.7	364.59	405.28	0.730	0.072	0.013			
	4.75	145.18	106.28	0.746	0.073	0.013			
Hornfels	19.0	2078.77	5558.34	0.717	0.098	0.018	0.732	0.093	0.008
	13.2	1025.36	1897.67	0.713	0.101	0.018			
	9.5	562.36	782.20	0.719	0.092	0.017			
	6.7	305.61	321.84	0.742	0.085	0.016			
	4.75	175.72	148.78	0.769	0.082	0.015			
Alluvial gravel	19.0	1997.25	6570.52	0.848	0.056	0.010	0.848	0.046	0.004
	13.2	1294.01	3389.60	0.842	0.048	0.009			
	9.5	678.40	1319.66	0.852	0.037	0.007			
	6.7	338.06	458.44	0.844	0.042	0.008			
	4.75	148.85	136.08	0.852	0.049	0.009			
RA	19.0	1601.22	4241.75	0.788	0.039	0.007	0.790	0.059	0.005
	13.2	1190.62	2767.47	0.793	0.061	0.011			
	9.5	552.42	884.91	0.797	0.068	0.012			
	6.7	328.60	397.09	0.787	0.055	0.010			
	4.75	169.43	146.52	0.785	0.070	0.013			

Note: For each aggregate type the statistical parameters were computed using results of 150 particles.



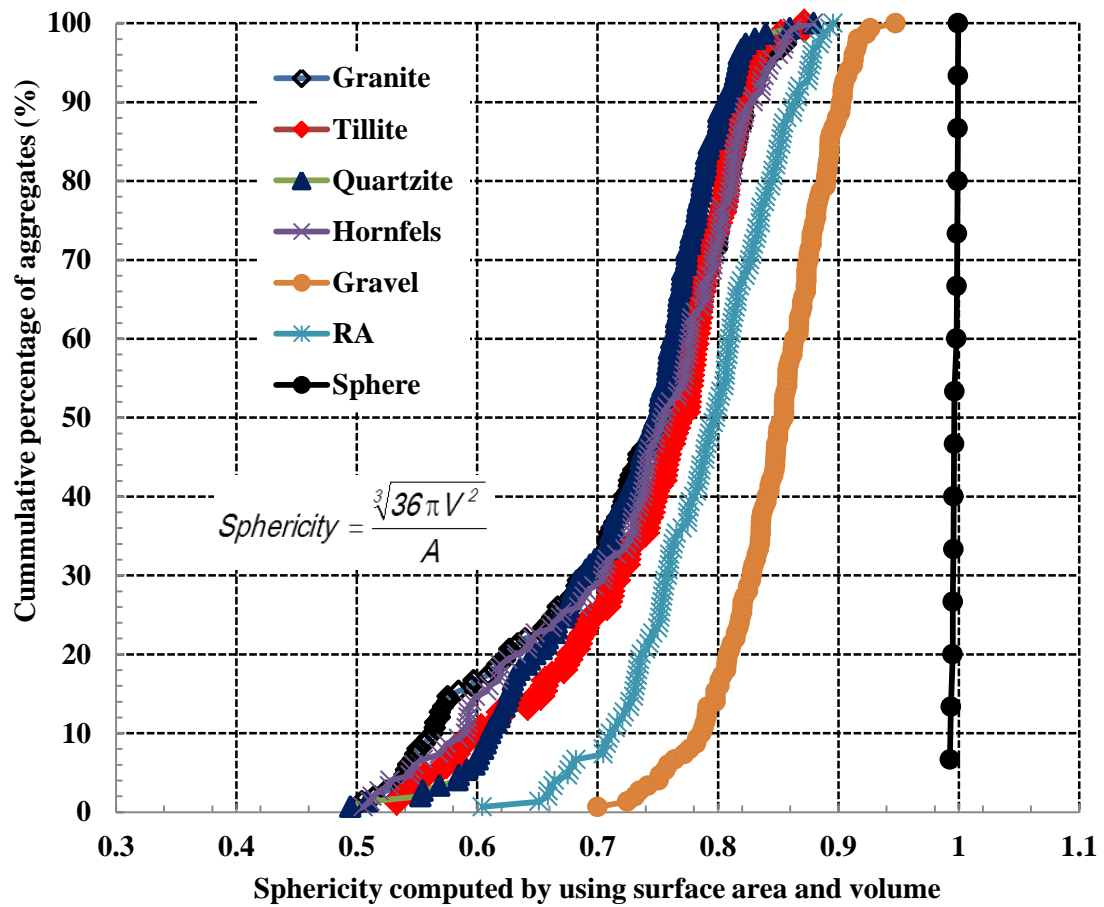


Figure 5.1: Distributions of sphericity computed using surface area and volume.

### 5.2.2 Sphericity computed using orthogonal dimensions

The orthogonal dimensions of individual aggregate particles were used to compute another sphericity parameter that is defined using Equation 2.1. For equal dimensional particles such as round aggregates, the computed sphericity approaches a maximum value of 1. Consequently, the alluvial gravel sample is expected to have higher sphericity values. Table 5.2 shows statistical sphericity parameters (average, standard deviation and standard error) for the six types of aggregates studied. As expected, the average sphericity of alluvial gravel was the highest followed by that of RA. For the crushed aggregate types, the average sphericity of tillite was relatively higher followed by that of hornfels, granite and quartzite.

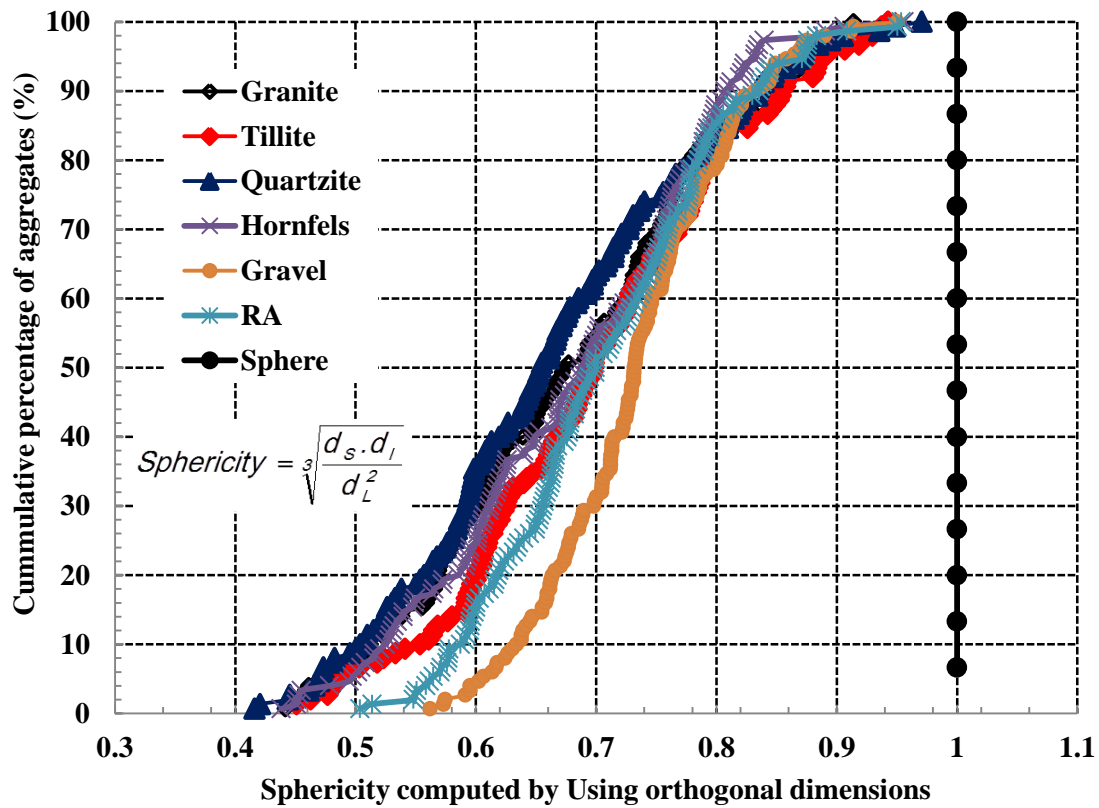
Figure 5.2 shows plots of the distributions of sphericity computed using orthogonal dimensions. For sphericity values greater than 0.8, the distributions of sphericity for all types of aggregates

are similar. For sphericity values smaller than 0.8, alluvial gravel has higher sphericity values followed by RA, tillite, hornfels, granite and quartzite. The results of 15 spherical objects are also plotted in Figure 5.2. All the spherical objects have a sphericity value of 1, which was expected.

**Table 5.2: Statistical parameters for sphericity computed using orthogonal dimensions.**

Aggregate type	Average	Standard deviation	Standard error
Granite	0.679	0.121	0.010
Tillite	0.701	0.116	0.009
Quartzite	0.665	0.123	0.010
Hornfels	0.680	0.110	0.009
Alluvial gravel	0.734	0.076	0.006
RA	0.707	0.093	0.008

*Note:* For each aggregate type the statistical parameters were computed using results of 150 particles.



**Figure 5.2: Distributions of sphericity computed using orthogonal dimensions.**

Comparing the results presented in Tables 5.2 and 5.3, as well as plots presented in Figures 5.1 and 5.2, there is a significant difference between the sphericity values computed by using the two different approaches. It should be noted that the definitions of the sphericity are different. The sphericity results presented in Table 5.2, and Figure 5.1 are based on volume and surface area of the aggregate particles (Equation 2.4), whereas the sphericity results presented in Table 5.3 and Figure 5.2 are based on the dimensions (longest dimension, intermediate dimension, and shortest dimension) (Equation 2.1). Possible reason for the differences in the sphericity values computed by using the two definitions is the accurate characterization of surface areas and volumes of irregular aggregate particles. This is a main benefit of using 3-D laser scanning technology. The ability of the laser scanning technology to capture 3-D information of the irregular aggregate particles allows for more realistic and accurate determination of aggregate form properties.

### **5.2.3 Flat and elongated ratio**

The longest and shortest dimensions of aggregate particles were used to compute the flat and elongated ratio using Equation 2.3. The flat and elongated ratio statistical parameters for the six types of aggregates studied are presented in Table 5.3. For equal dimensional aggregate particles, the flat and elongated ratio approaches a minimum value of 1. This means the alluvial gravel sample is expected to have lower flat and elongated ratio values as compared to other types of aggregates studied. As expected, the average flat and elongated ratio of alluvial gravel was the lowest, followed by RA. The averages of the flat and elongated ratio values of crushed aggregates are similar. The average flat and elongated ratio of granite is the lowest, followed by tillite, hornfels and quartzite.

Figure 5.3 shows plots of the distributions of flat and elongated ratio for all aggregates studied and 15 spherical objects. All the spherical objects have flat and elongated ratios of 1, which was expected. Generally, alluvial gravel has lower flat and elongated ratio values followed by RA and tillite. Hornfels, granite, and quartzite have almost similar distributions of flat and elongated ratio values.

Table 5.3: Statistical parameters for flat and elongated ratio.

Aggregate type	Average	Standard deviation	Standard error
Granite	2.500	1.099	0.090
Tillite	2.510	1.238	0.101
Quartzite	2.630	1.145	0.094
Hornfels	2.596	1.169	0.095
Alluvial gravel	1.943	0.433	0.035
RA	2.283	0.686	0.056

Note: For each aggregate type the statistical parameters were computed using results of 150 particles.

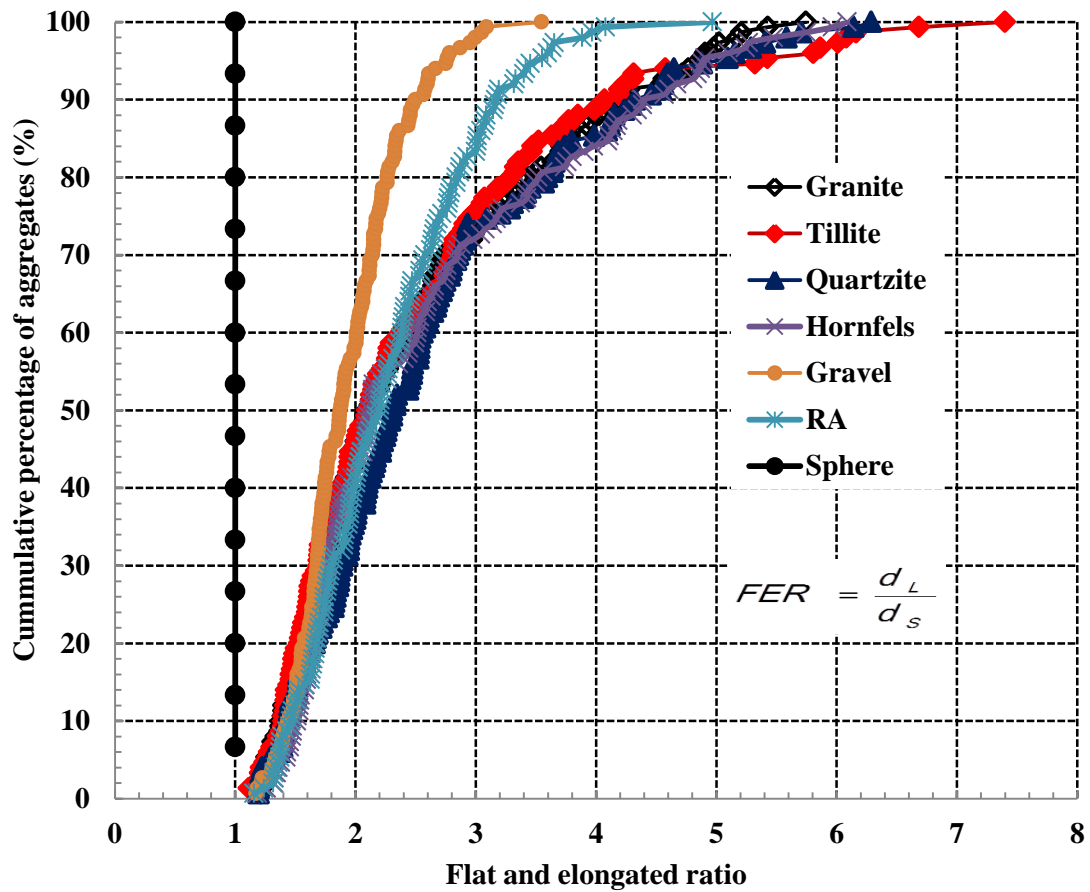


Figure 5.3: Distributions of flat and elongated ratio.

#### 5.2.4 Discussion of the laser-based form indices results

Based on the statistical analysis results presented earlier in Tables 5.1 to 5.3 and distributions of laser-based form indices plotted in Figures 5.1 to 5.3, the following can be deduced:

- The laser-based form indices were capable to distinguish the form properties of the six types of the aggregates studied;
- All the laser-based form indices clearly showed that the distributions of form properties of the crushed aggregates (granite, tillite, quartzite and hornfels) differ from that of alluvial gravel and RA;
- A wider distribution of form indices were observed for crushed aggregates compared to alluvial gravel and RA;
- The laser-based form indices showed that the distributions of form properties of the crushed aggregate particles do not differ significantly;
- The distribution of sphericity indices computed by using surface area and volume, distinguished the form properties of the six types of aggregates clearer than other form indices. This may be due to the fact that the indices were computed using volume and surface area which represent the overall 3-D form of aggregates. On the other hand, the sphericity computed by using orthogonal dimensions and flat and elongated ratio indices are based on dimensions, which do not necessarily represent the overall 3-D form of aggregates.
- Overall, the ranking of the form properties of the six types of the aggregates was similar for the three laser-based form indices, and
- As expected, the form indices for 15 spherical objects were close to a value of 1, hence strengthening the validity and the accuracy of the laser scanning technique.

### 5.3 Quantification of aggregate shape properties by using spherical harmonic analysis

The spherical harmonic analysis is another technique used to determine form, angularity and surface texture of the aggregates. The technique was introduced in Section 2.6.6. In this section, procedures for analysis of laser scan data by using the spherical harmonic analysis technique are described in detail.

#### 5.3.1 Pre-processing of laser scan data

The aggregate models were exported into surface point asc file format. The exported data are surface points or vertices in terms of Cartesian coordinates (x, y and z). Critical examination of the laser scan data revealed that the origin of the Cartesian coordinate system do not correspond to the centre of mass of the scanned aggregate as shown in Figures 5.4 and 5.5. Figure 5.4 is a screenshot of Rapidform software showing a mesh model of the scanned spherical object. The origin of the Cartesian coordinate system and other spherical object properties including the dimensions of the bounding box, surface area, volume and coordinates of the centre of the mass are also displayed. Similarly, an example of the mesh model of a scanned aggregate particle and its properties is shown in Figure 5.5. Figure 5.6 shows a model of the same aggregate particle to illustrate the surface point data.

The spherical harmonic analysis technique employed in this study requires the origin of the coordinates of the surface points to correspond with the centre of the mass. Therefore, the surface point data (x, y and z) were transformed such that the origin of the Cartesian coordinate system corresponds to the centre of the mass of the scanned aggregate/object. The translation relation presented in Equation 5.1 was used.

$$(x_T, y_T, z_T) = ((x - x_c), (y - y_c), (z - z_c)) \quad 5.1$$

Where:

(x, y, z) = Coordinates of the vertices;

(x<sub>c</sub>, y<sub>c</sub>, z<sub>c</sub>) = Coordinate of the centre of the mass of the aggregate particle, and

(x<sub>T</sub>, y<sub>T</sub>, z<sub>T</sub>) = Transformed coordinates of the vertices.

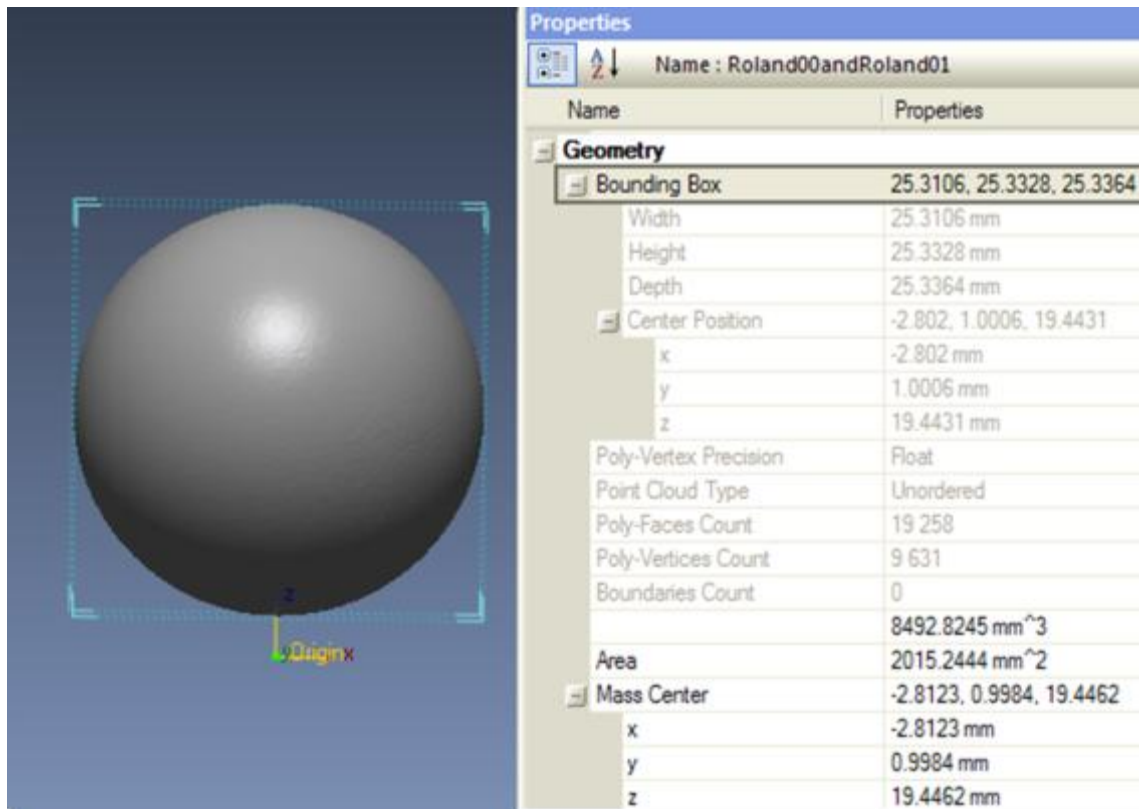


Figure 5.4: Mesh model of scanned spherical object.

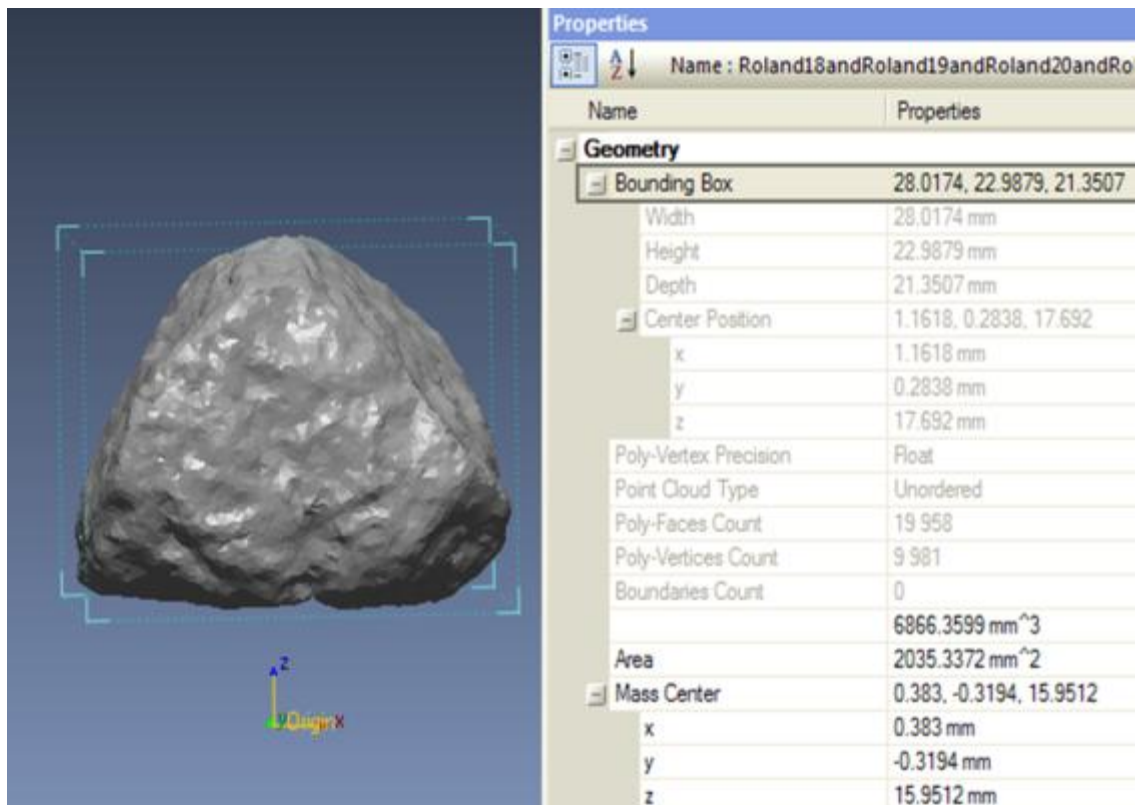
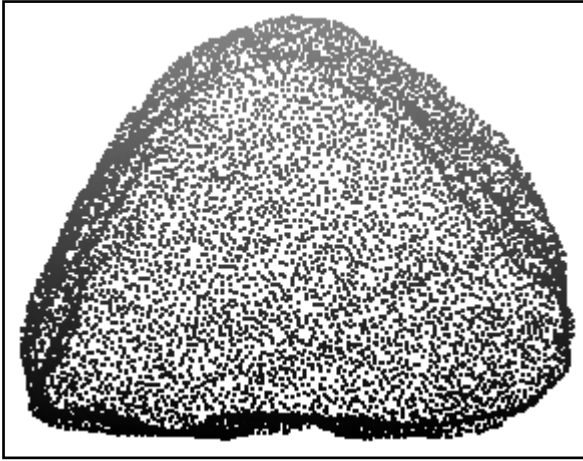


Figure 5.5: Mesh model of scanned aggregate particle.



**Figure 5.6: Surface point data of scanned aggregate particle.**

The spherical harmonic analysis technique makes use of a polar coordinate system. Using a polar coordinate system, the surface point data can be defined in terms of radius ( $R$ ), the horizontal angle ( $\alpha$ ) and the vertical angle ( $\beta$ ) (Figure 5.7). The radius is measured from the centre of the mass of an aggregate particle. Following transformation of the surface points such that the origin of the Cartesian coordinate system corresponds to the mass centre (Equation 5.1), the surface point data were converted to a polar coordinate system. The radius ( $R$ ) of each surface point was computed by using Equation 5.2. The horizontal angle ( $\alpha$ ) and the vertical angle ( $\beta$ ) were computed using spherical polar coordinate relations show in Equations 5.3 and 5.4 respectively.

$$R = \sqrt{((x_T)^2 + (y_T)^2 + (z_T)^2)} \quad 5.2$$

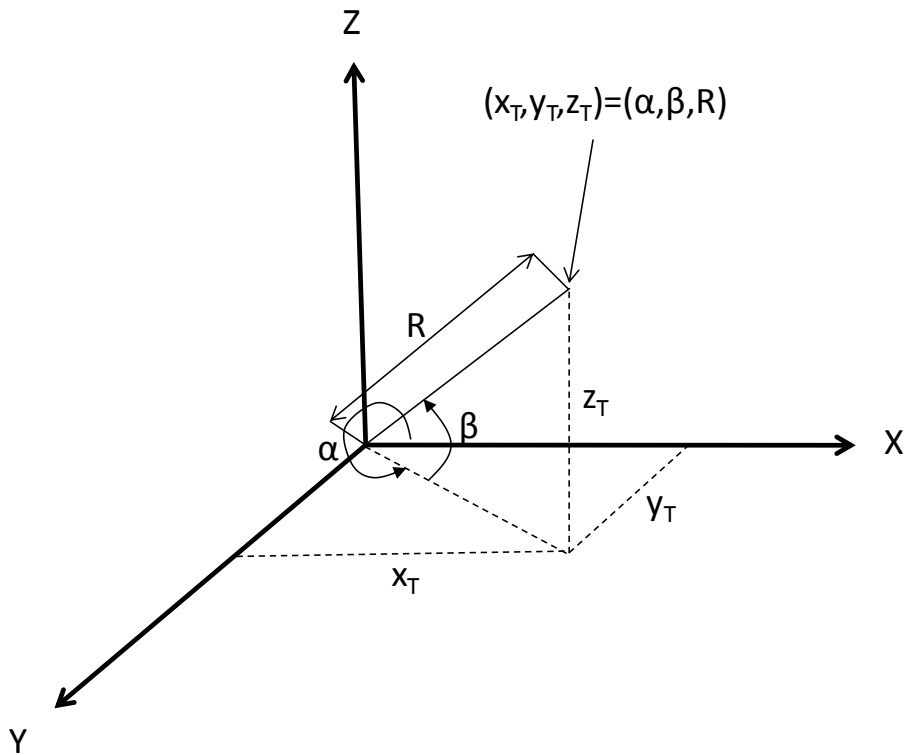
$$\alpha = \arctan \frac{y_T}{x_T} \quad 5.3$$

$$\beta = \arccos \frac{z_T}{R} \quad 5.4$$

Where:

( $x_T$ ,  $y_T$  and  $z_T$ ) = Transformed coordinates of the vertices.





**Figure 5.7: Relationship between Cartesian and polar coordinate systems.**

In order to compute the horizontal angles ( $\alpha$ ), it was necessary to identify the quadrant of each surface point in an eight quadrant system. A standard two-dimensional (2-D) x-y plane with x and y-axis has four quadrants. Introduction of a z-axis to define the elevation of the data points in space results in 8 quadrants. Starting from the positive x-axis of a standard 2-D x-y plane and rotating towards the counter clockwise direction, quadrants 1 to 4 have positive z values. Similarly, quadrants 5 to 8 have negative z values. The identification of the quadrant to which a specific surface point belongs is based on the sign of the  $x_T$ ,  $y_T$ ,  $z_T$  coordinates (Table 5.4).

Following identification of the quadrant on which each surface point is located, the horizontal angles ( $\alpha$ ) were computed based on the criteria shown in Table 5.5. The computation of vertical angle ( $\beta$ ) using Equation 5.4 is independent on the quadrant in which the surface point is located. At this stage the angles  $\alpha$  and  $\beta$ , and radius ( $R$ ) required to represent each surface point in a polar coordinate system can be computed.

**Table 5.4: Criteria for identification of the quadrant of the vertex.**

Quadrant number	Coordinate sign		
	$x_T$ Coordinate	$y_T$ Coordinate	$z_T$ Coordinate
1	Positive	Positive	Positive
2	Negative	Positive	Positive
3	Negative	Negative	Positive
4	Positive	Negative	Positive
5	Positive	Positive	Negative
6	Negative	Positive	Negative
7	Negative	Negative	Negative
8	Positive	Negative	Negative

**Table 5.5: Criteria for computation of angle  $\alpha$ .**

Quadrant number	$\alpha$ (Radians)
1 and 5	$\arctan( y / x )$
2 and 6	$\pi/2 + \arctan( x / y )$
3 and 7	$\pi + \arctan( y / x )$
4 and 8	$3\pi/2 + \arctan( x / y )$

### 5.3.2 Determination of spherical harmonic coefficients

The determination of aggregate shape properties by using spherical harmonic analysis is based on solving the coefficients of the spherical harmonic equation (Equation 2.20). The equation describes the radii of an aggregate particle, and can be written in terms of summation of the product of the harmonic coefficients ( $a_{lm}$ ) and harmonic function ( $Y_l^m$ ) evaluated at each degree ( $l$ ) and order ( $m$ ) as presented in Equation 5.5.

$$R(\beta, \alpha) = a_{00}Y_0^0(\beta, \alpha) + a_{1-1}Y_1^{-1}(\beta, \alpha) + a_{10}Y_1^0(\beta, \alpha) + a_{11}Y_1^1(\beta, \alpha) + \dots + a_{lm}Y_l^m(\beta, \alpha) \quad 5.5$$

In Equation 5.5, the angles  $\alpha$  and  $\beta$ , and radius ( $R$ ) of each surface point of the scanned aggregate particle can be obtained numerically as described in Section 5.3.2. The harmonic function ( $Y_l^m$ ) can also be evaluated numerically by using relations such as Condon-Shortley Phase (Arfken and Webber, 1995). The equations for computation of the first few spherical harmonics up to degree ( $l$ ) equals 2, are presented in Table 5.6. Evaluation of the harmonic functions for higher degrees could be tedious. In this dissertation, the MATLAB<sup>TM</sup> was used.

**Table 5.6: Spherical Harmonics (Condon-Shortly Phase) (Arfken and Webber, 1995).**

Degree (l)	Order (m)	Function
0	0	$Y_0^0(\beta, \alpha) = \frac{1}{\sqrt{4\pi}}$
1	-1	$Y_1^{-1}(\beta, \alpha) = \sqrt{\frac{3}{8\pi}} \sin \beta e^{-i\alpha}$
1	0	$Y_1^0(\beta, \alpha) = \sqrt{\frac{3}{4\pi}} \cos \beta$
1	1	$Y_1^1(\beta, \alpha) = -\sqrt{\frac{3}{8\pi}} \sin \beta e^{i\alpha}$
2	-2	$Y_2^{-2}(\beta, \alpha) = \sqrt{\frac{5}{96\pi}} 3 \sin^2 \beta e^{-2i\alpha}$
2	-1	$Y_2^{-1}(\beta, \alpha) = \sqrt{\frac{5}{24\pi}} 3 \sin \beta \cos \beta e^{-i\alpha}$
2	0	$Y_2^0(\beta, \alpha) = \sqrt{\frac{5}{4\pi}} \left( \frac{3}{2} \cos \beta - \frac{1}{2} \right)$
2	1	$Y_2^1(\beta, \alpha) = -\sqrt{\frac{5}{24\pi}} 3 \sin \beta \cos \beta e^{i\alpha}$
2	2	$Y_2^2(\beta, \alpha) = -\sqrt{\frac{5}{96\pi}} 3 \sin^2 \beta e^{2i\alpha}$

After computing the radii ( $R$ ) and spherical harmonics for each surface point of an aggregate particle, the only unknowns in Equation 5.5 are the spherical harmonic coefficients ( $a_{lm}$ ) which could be obtained by optimization using a least square method or by solving a linear matrix system. In this study, the coefficients were determined using a linear matrix method. Using matrix notation, Equation 5.5 can be expressed as indicated in Equation 5.6.

$$R = a_{lm} \times Y_l^m \tag{5.6}$$

Where:

$R$  = Column vector representing radii at each corresponding  $\beta$  and  $\alpha$ ;

$a_{lm}$  = Vector representing the coefficients to be determined, and

$Y_l^m$  = Spherical harmonics.

The number of rows in the matrix defined by Equation 5.6 is equal to the number of aggregate surfaces points to be analysed. Some aggregate particles had a larger number of surface data points. Therefore, solving the spherical harmonic coefficients ( $a_{lm}$ ) by using traditional methods could be tedious.

In order to facilitate the analysis of the aggregate shape properties, a MATLAB<sup>TM</sup> code was developed to perform all the computations described in Sections 5.3.1 and 5.3.2. The developed MATLAB<sup>TM</sup> code is presented in Appendix B. The main steps implemented in the MATLAB<sup>TM</sup> code are:

- Transforming surface point data such that the origin corresponds to the mass centre;
- Computing radius ( $R$ ), angles  $\alpha$  and  $\beta$ ;
- Computing spherical harmonics;
- Solving spherical harmonic coefficients using the matrix method, and
- Determination of the aggregate form, angularity and surface texture indices.

The spherical harmonic coefficients were determined by solving Equation 5.6. The coefficients were used to compute the spherical harmonic form indices to describe aggregate form, angularity and surface texture using Equations 2.22 to 2.24, respectively. In this study, the form, angularity and surface texture are defined at degree ( $l$ ) values of 5, 20 and 25 respectively. Detailed validation of these values is discussed in Section 5.3.3. The indices were normalized by dividing by the first coefficient ( $a_{00}$ ) to eliminate the effect of particle size as suggested by Kutay et al (2011).

### **5.3.3 Validation of the computation of harmonic coefficients and radii**



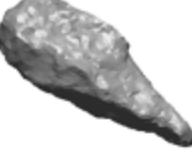
The form, angularity, and surface texture indices are defined at different degree ( $l$ ) values. At a lower degree ( $l$ ), the spherical harmonic coefficients could be used to estimate the radii ( $R$ ) defining the overall shape of an aggregate particle. As the degree ( $l$ ) is increased, more accurate radii ( $R$ ) are obtained hence providing information about the angularity and surface texture of an aggregate. To illustrate this concept, the scan results of a spherical object, and two aggregate particles (cubical and elongated) were analysed to determine the spherical harmonic coefficients by using the developed MATLAB<sup>TM</sup> code. The determined spherical harmonic coefficients were used to compute the radius of each surface point by using Equation 5.5. The analyses were

performed by using different  $l$  values ( $l = 5, 10, 15, 20$  and  $25$ ). The capability of the spherical harmonic technique to compute the radii was assessed by plotting the following three graphs:

- Errors (difference between radius determined from the laser scans and radius computed by using the spherical harmonic technique) for each surface point (Figures 5.8 to 5.10);
- Radius determined from the laser scans and radius computed by using the spherical harmonic technique at each surface point on the same graph for different  $l$  values (Figures 5.11 to 5.13), and
- Radius determined from the laser scans versus radius computed by using the spherical harmonic technique at each surface point (Figures 5.14 to 5.16).

Table 5.7 shows scanned models of the spherical object and two aggregate particles. The diameter of the spherical object is 25 mm. The two aggregates were sampled from granite particles retained on the 19.0 mm sieve. Included in the table are the average absolute errors, and average percentage errors which are indicated in brackets. The error is defined as the absolute value of the difference between the radius determined from laser scans and radius computed using spherical harmonic technique for each surface point. Moving horizontally across the table ( $l = 5$  to  $25$ ), the average absolute error decreases. This indicates that for higher  $l$  values, the radii determined from laser scans and radii computed using spherical harmonic technique are approximately the same. For each  $l$  value smaller average absolute errors were computed for a spherical object. This indicates that for spherical objects, lower  $l$  values are sufficient to ensure that the radii determined from laser scans and radii computed using spherical harmonic technique are approximately the same. The highest average absolute errors were computed for an elongated aggregate compared to a cubical aggregate. This indicates that convergence is much quicker for cubical aggregate particles. Overall, smallest absolute errors were computed at  $l$  of 25 for spherical object and aggregate particles, indicating that the radii determined from laser scans and radii computed using spherical harmonic technique are approximately equal.

**Table 5.7: Effect of varying degree ( $l$ ).**

Description	Model	Average absolute error- Difference between radii determined from the laser scans and radii computed by using the spherical harmonic technique (mm)				
		$l=5$	$l=10$	$l=15$	$l=20$	$l=25$
<b>Spherical object</b>		0.0073 (0.059 %)	0.0071 (0.057 %)	0.0068 (0.055 %)	0.0067 (0.053 %)	0.0063 (0.051 %)
<b>Cubical aggregate</b>		0.3940 (3.236 %)	0.2196 (1.793 %)	0.1505 (1.221 %)	0.1137 (0.919 %)	0.0841 (0.675 %)
<b>Elongated aggregate</b>		1.3180 (8.267 %)	0.6984 (4.197 %)	0.5187 (3.245 %)	0.2662 (1.479 %)	0.1553 (0.789 %)

Figures 5.8 to 5.10 show plots of absolute errors for each surface point for a spherical object, cubical and elongated aggregate particles, respectively for different  $l$  values. From the figures, the following observations can be made:

- Smallest absolute errors were observed for the spherical object, followed by the cubical the aggregate and elongated aggregate, and
- The convergence rate is dependent on the shape of the aggregate/object. For the spherical object, lower  $l$  values could ensure that the radius determined from the laser scans and radius computed by using the spherical harmonic technique is approximately equal. This means that both  $l$  equal to 5 and 25 could reasonable compute the radii. On the other hand, as the aggregate particle becomes elongated, higher  $l$  values are required to ensure that the radii determined from the laser scans and radii computed by using the spherical harmonic technique are approximately equal.

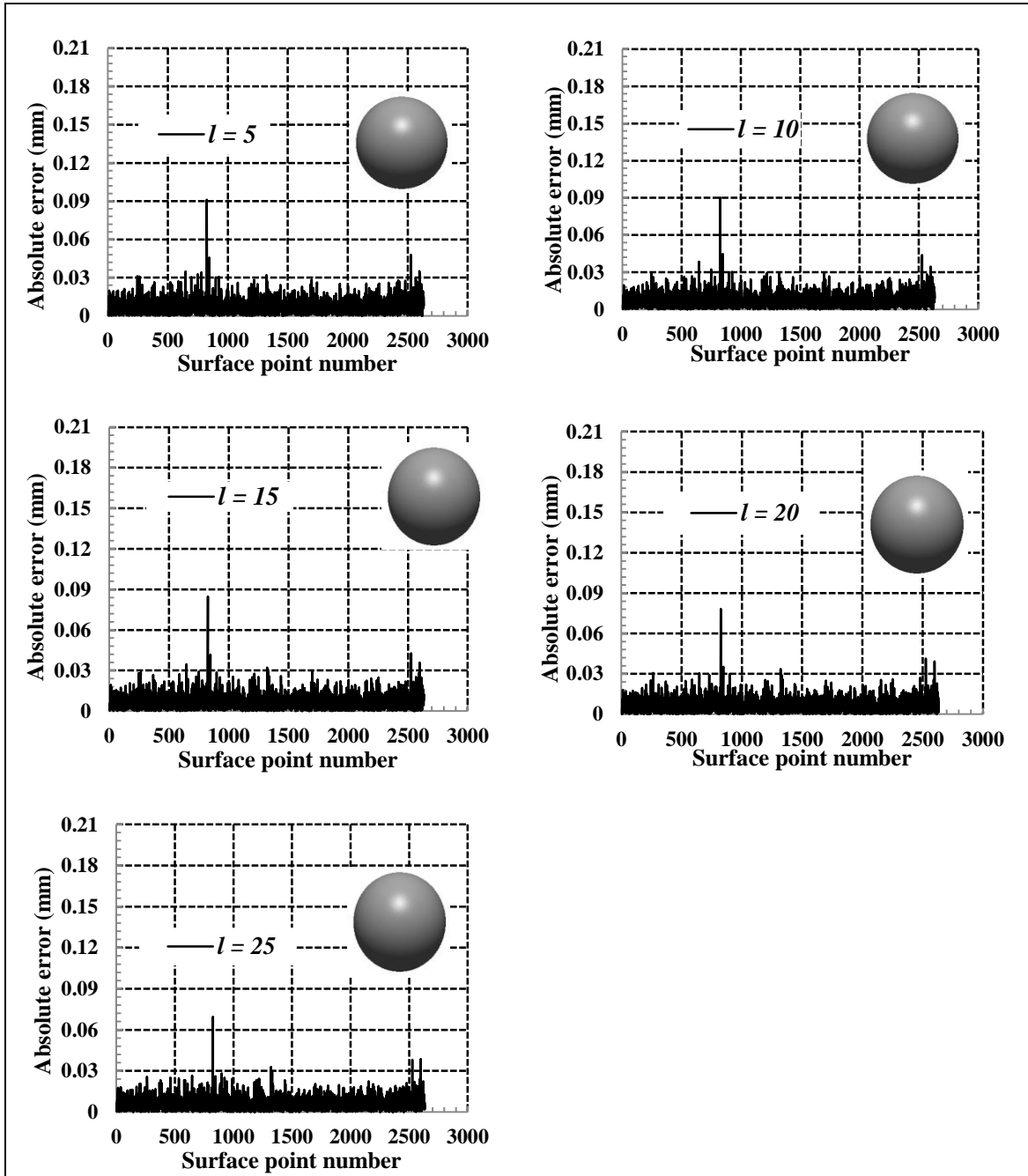


Figure 5.8: Average absolute errors for a spherical object.

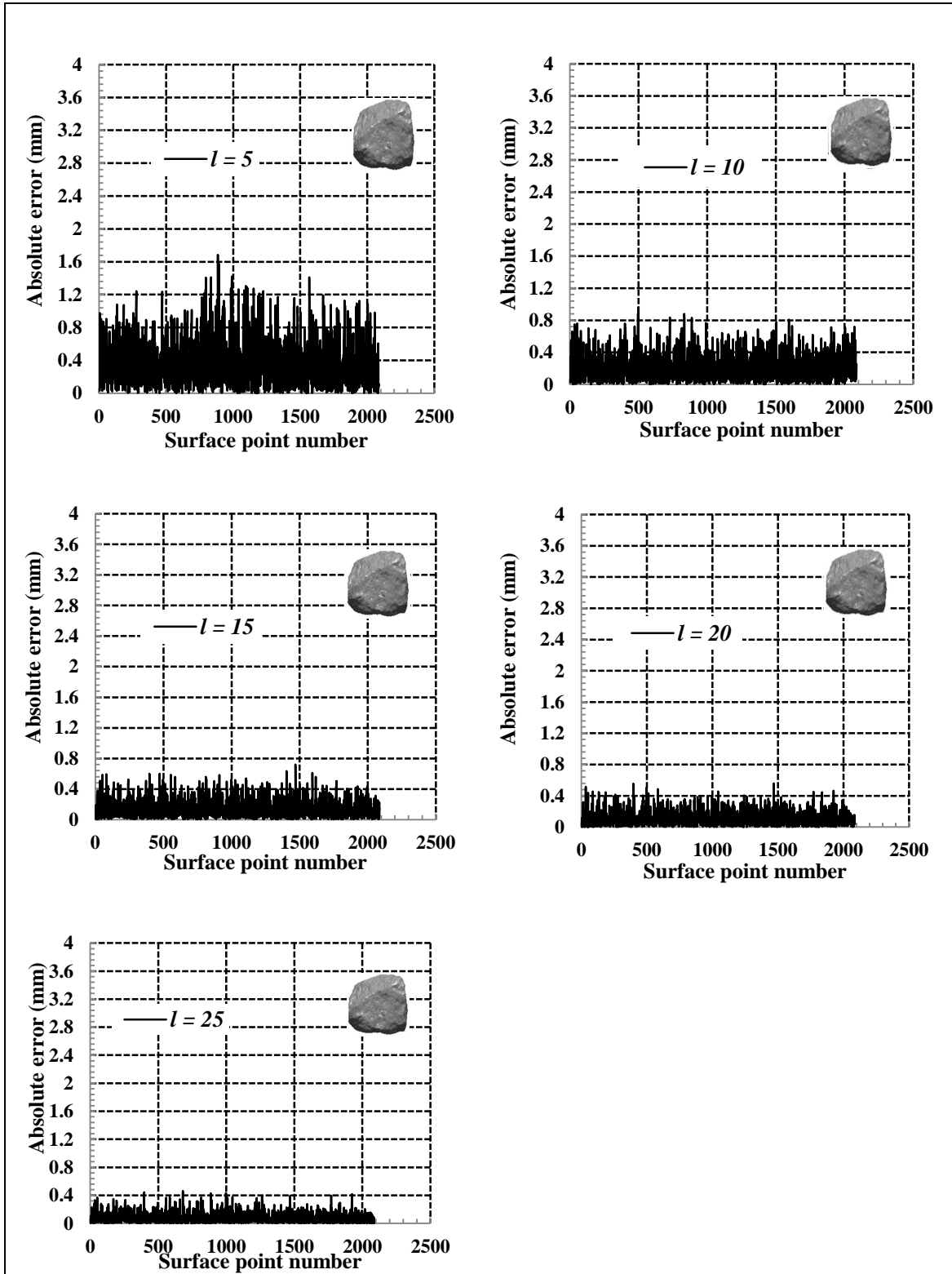


Figure 5.9: Average absolute errors for a cubical aggregate.



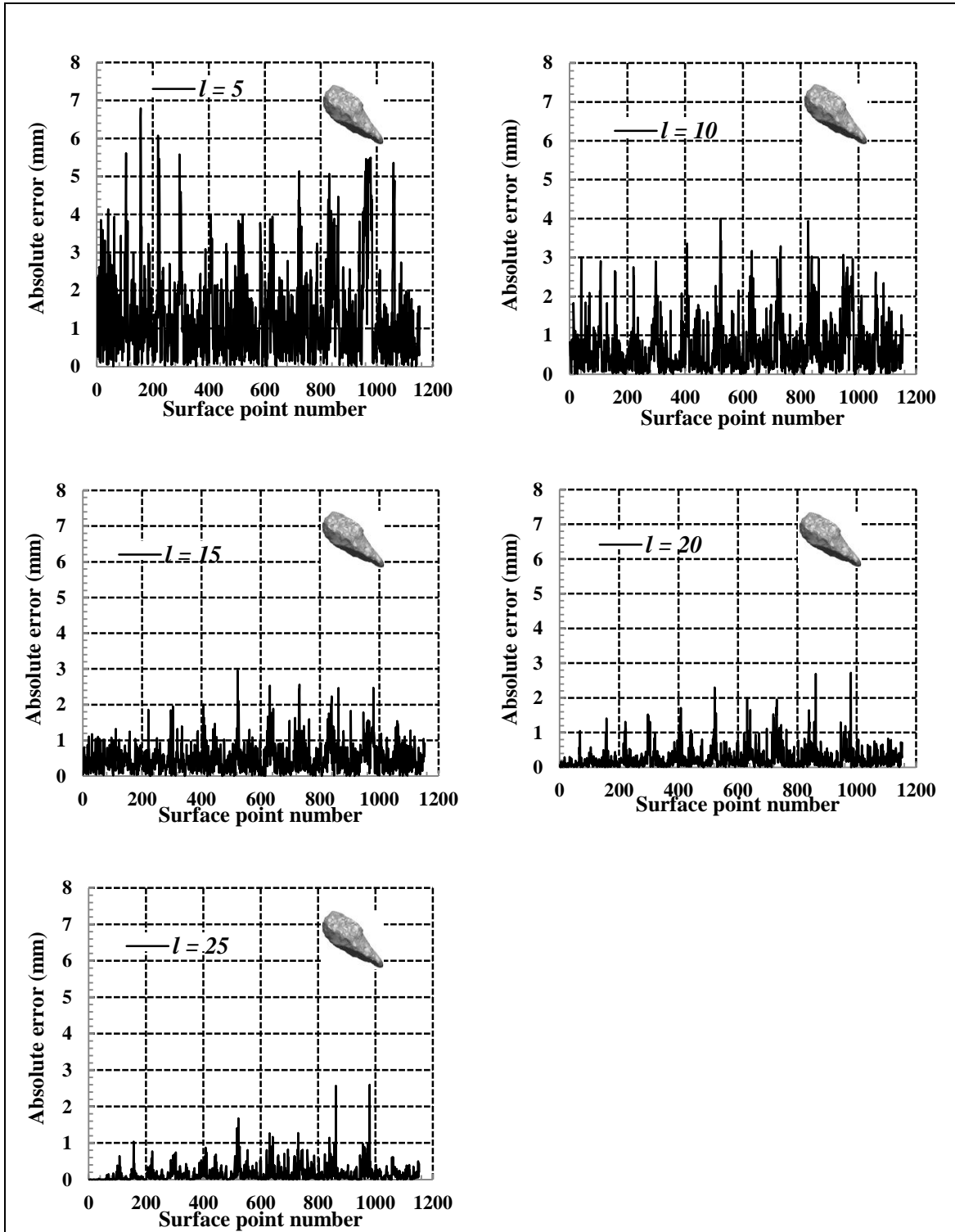


Figure 5.10: Average absolute errors for an elongated aggregate.

The second validation approach used was to plot the radii determined from the laser scans and radii computed by using the spherical harmonic technique for different  $l$  values. Figures 5.11 to 5.13 show plots for a spherical object, cubical and elongated aggregates, respectively. For a spherical object, all the  $l$  values showed similar results, where the radii determined from the laser scans and the radii computed by using the spherical harmonic technique were the same. The radii of the spherical object obtained at different surface points were found to be relatively constant (12.2 mm). This is expected and is in agreement with the known radius of the spherical object, measured by using a vernier caliper. For aggregate particles, as  $l$  increases, the radii determined from laser scans and radii computed using spherical harmonic technique become similar.

The third validation approach was to plot the radius determined from the laser scans versus radius computed by using the spherical harmonic technique of all surface points for a spherical object, cubical and elongated aggregate particles. Figures 5.14 to 5.16 show results for different  $l$  values. As before, the radii of the spherical object were approximately equal. This is expected because the radius of a spherical object is a constant value. For cubical and elongated aggregates, the plots were scattered for lower  $l$  values. As the  $l$  values increases, the radii determined from the laser scans and radii computed by using the spherical harmonic technique appeared similar.

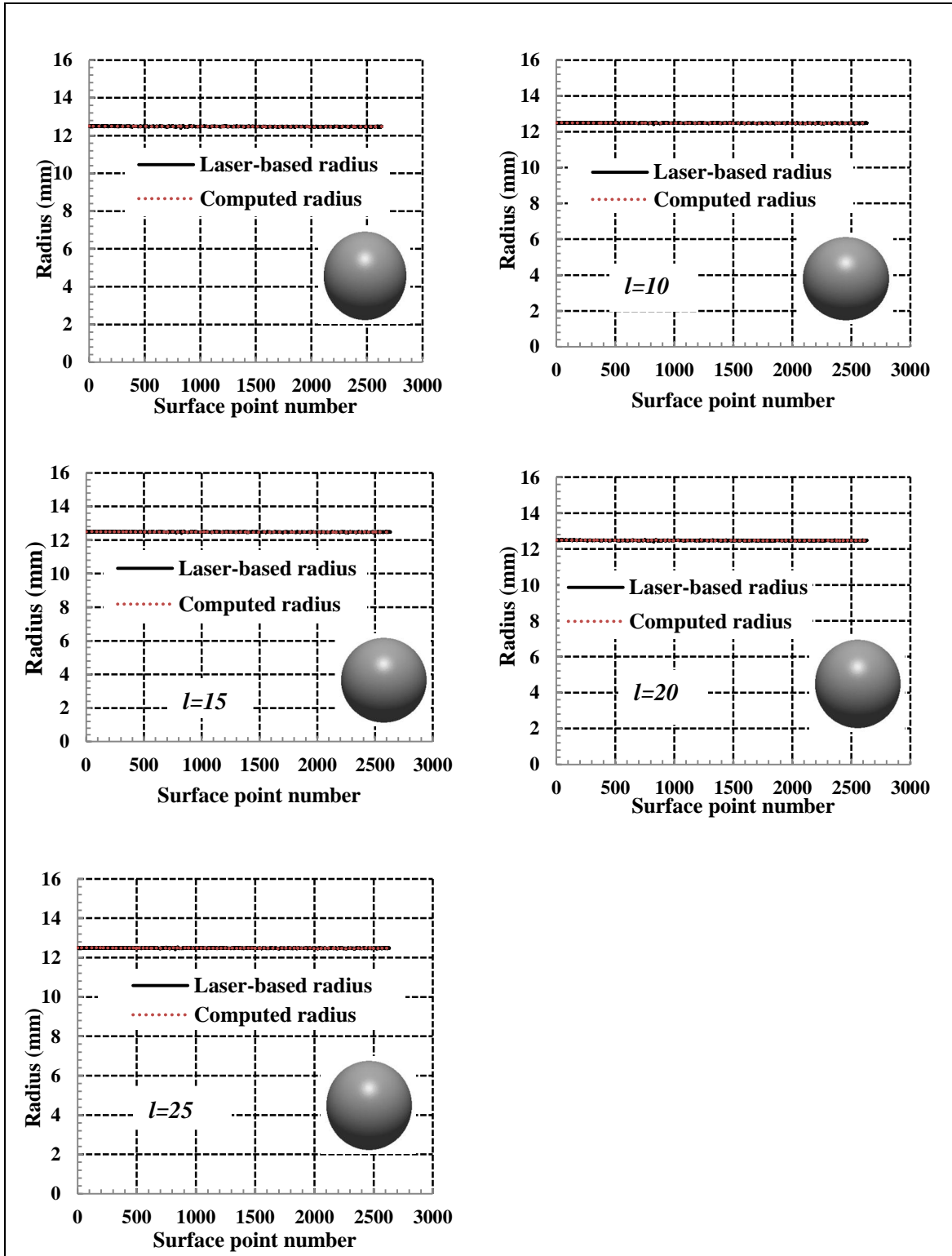


Figure 5.11: Radii determined from the laser scans and radii computed by using the spherical harmonic technique for a spherical object.

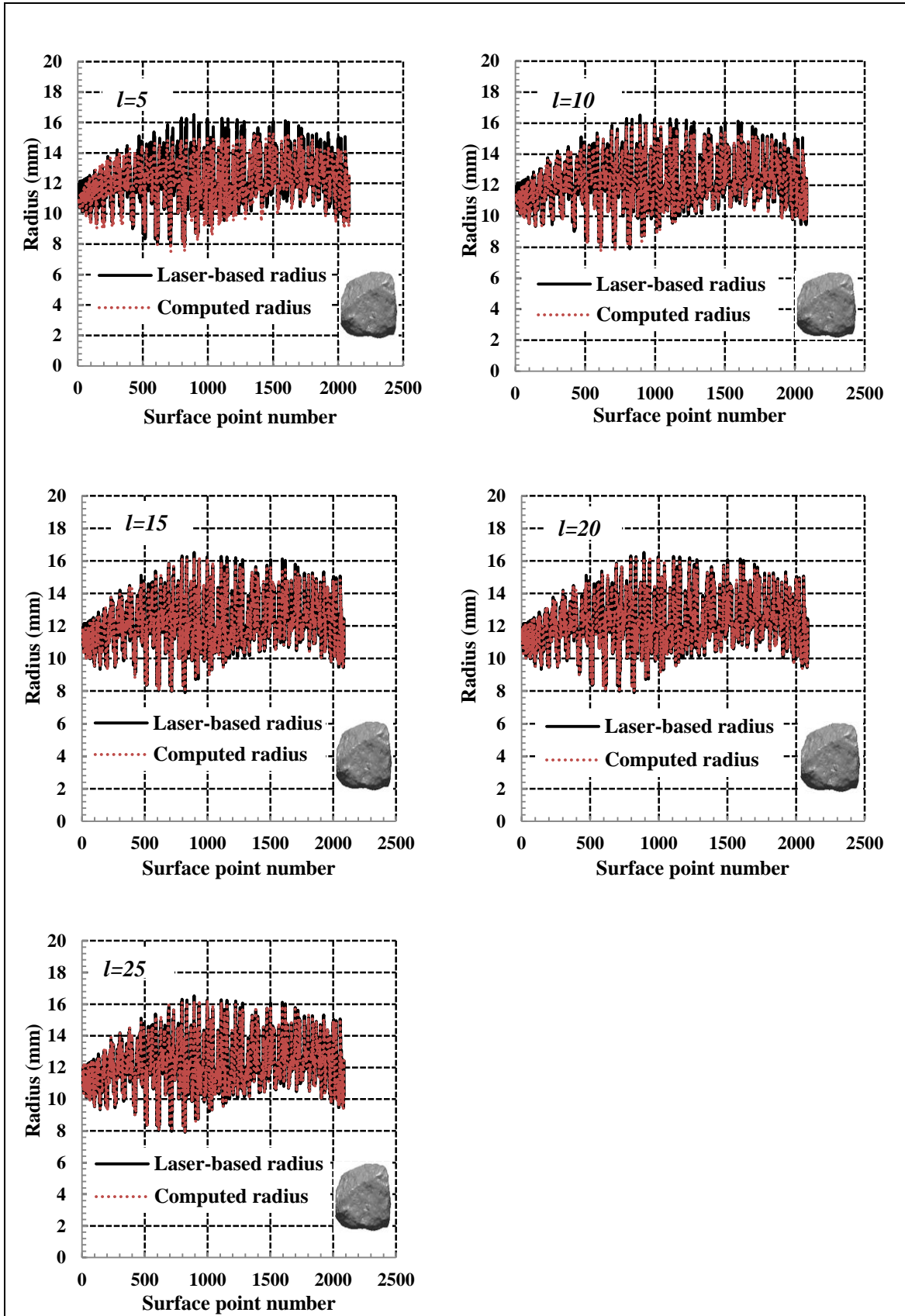


Figure 5.12: Radii determined from the laser scans and radii computed by using the spherical harmonic technique for a cubical aggregate.

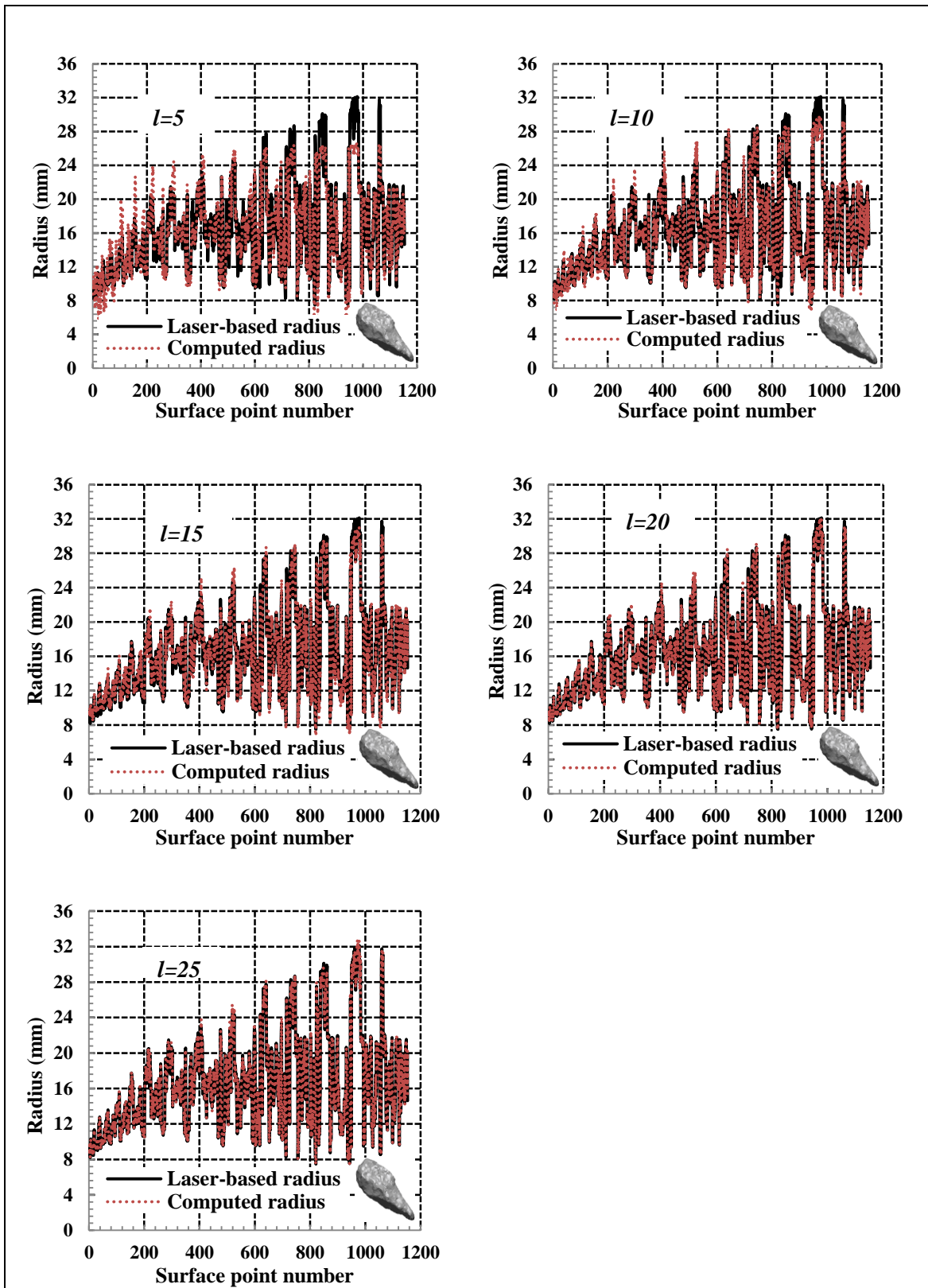


Figure 5.13: Radii determined from the laser scans and radii computed by using the spherical harmonic technique for an elongated aggregate.

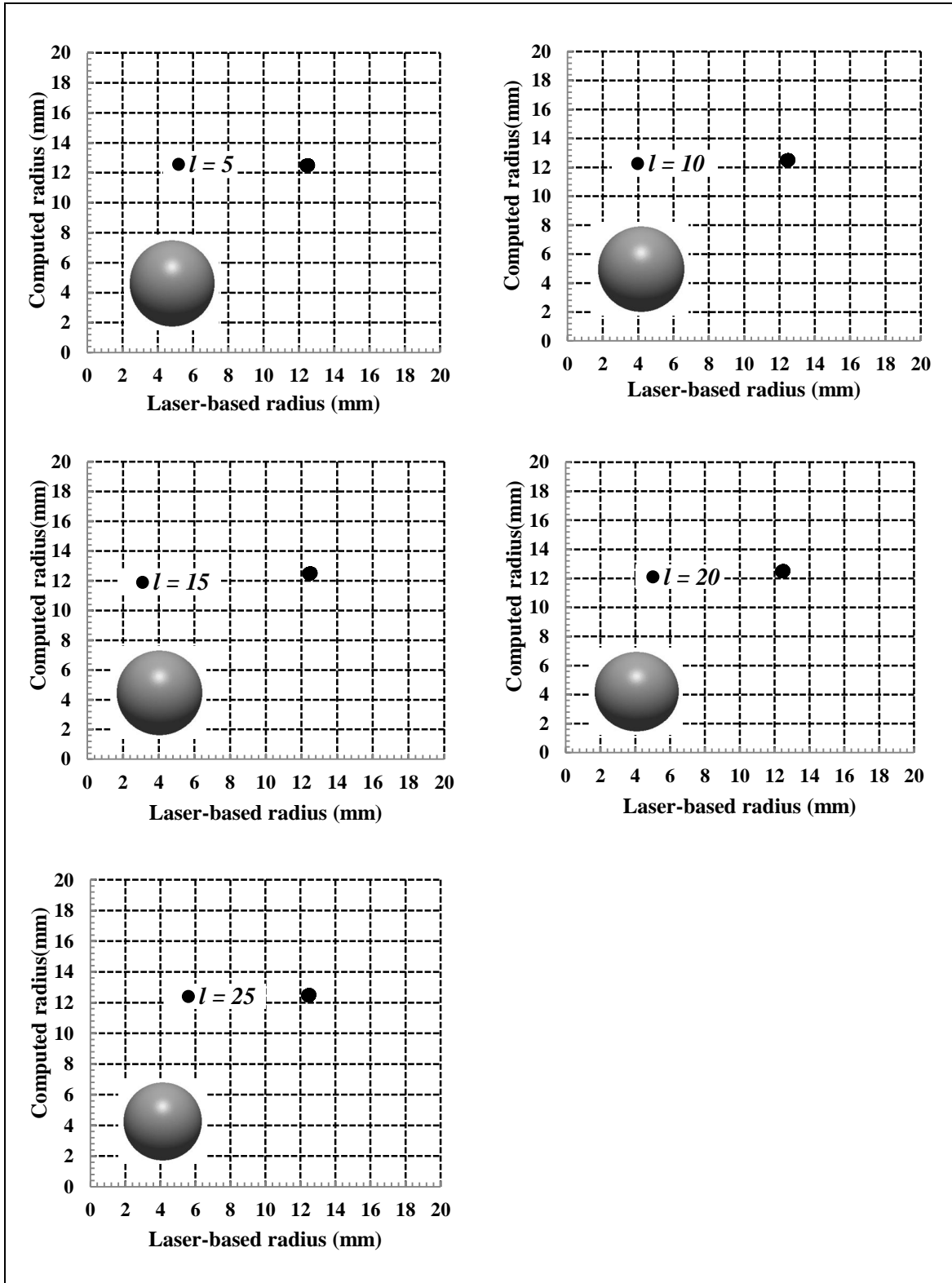


Figure 5.14: Radii determined from the laser scans versus radii computed by using the spherical harmonic technique for a spherical object.

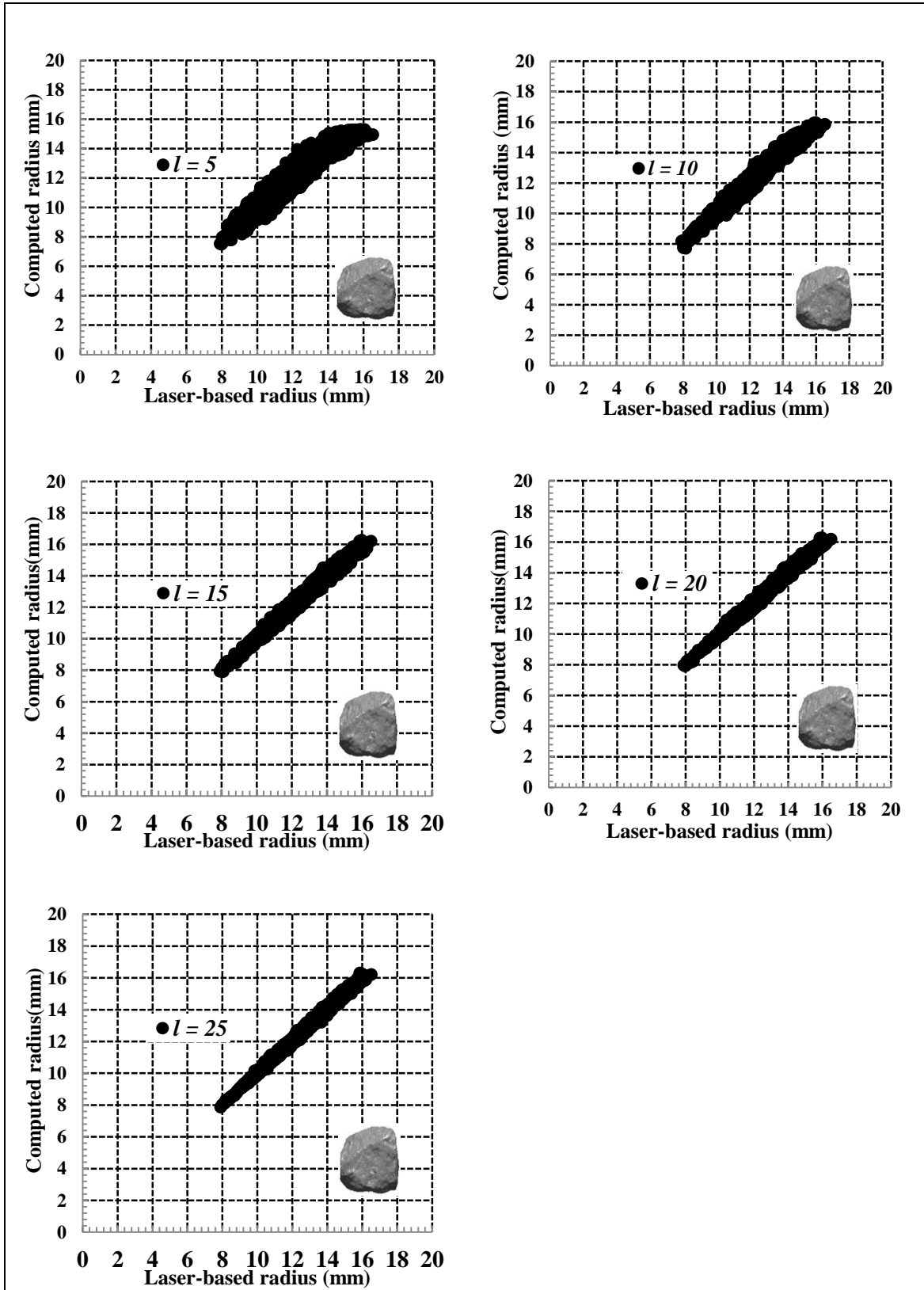


Figure 5.15: Radii determined from the laser scans versus radii computed by using the spherical harmonic technique for a cubical aggregate.

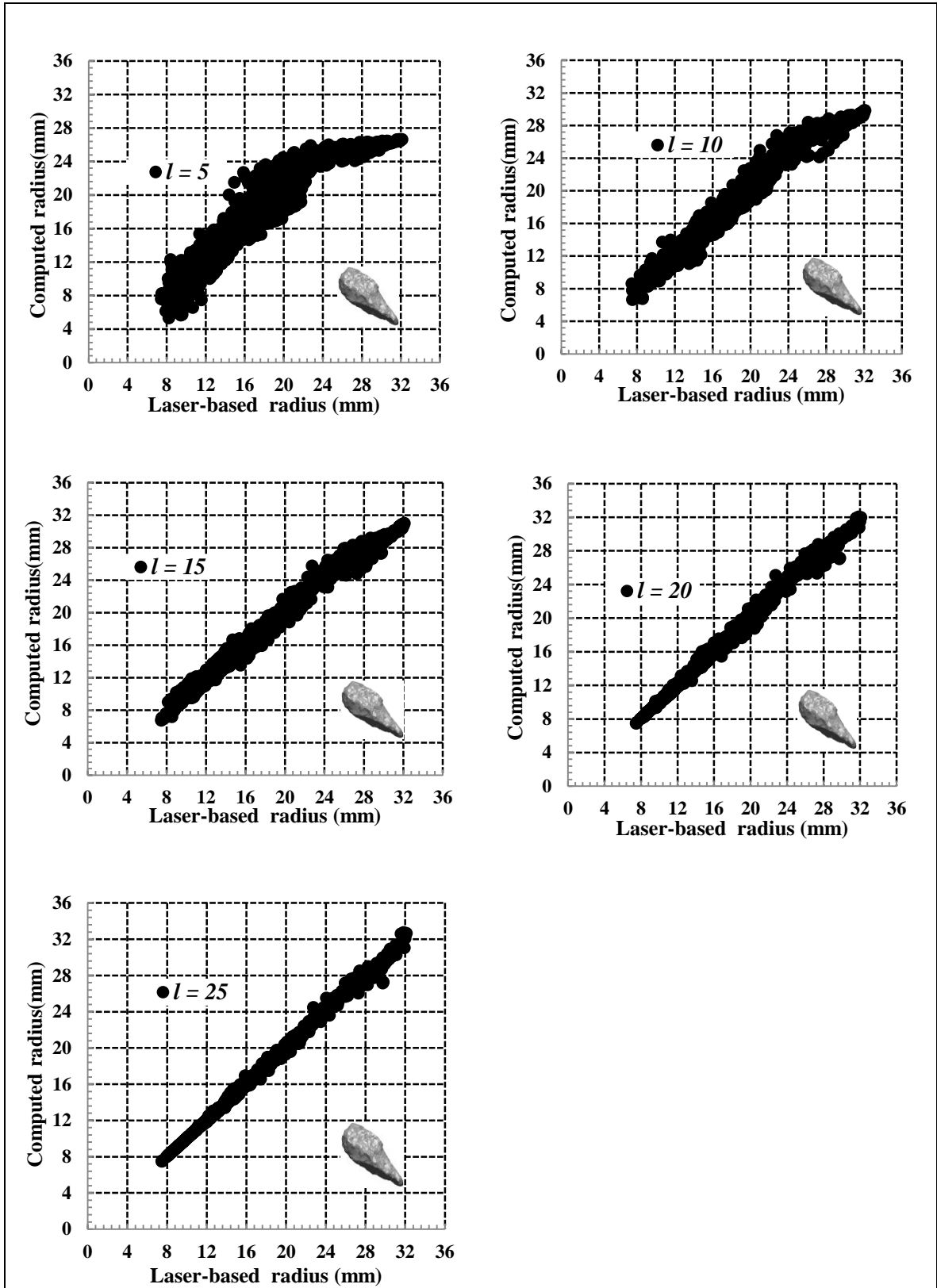


Figure 5.16: Radii determined from the laser scans versus radii computed by using the spherical harmonic technique for an elongated aggregate.



In order to assess the influence of the size of aggregate/object on the rate of convergence, two additional spherical objects (19 mm and 13 mm diameter) and aggregate particles of different sizes were analysed. The aggregate were sampled from granite particles retained on the 13.2, 9.5, 6.7 and 4.75 mm sieves. The plots are presented in Appendix C. Only plots the radii determined from laser scans and radii computed using spherical harmonic technique on the same graph are shown. It was concluded that the convergence occurs regardless of aggregate size. It was also found that the convergence rate depends on the size of aggregate/object. For larger aggregate particles, higher  $l$  values are required to ensure that the difference (error) between the actual and computed radius is small. For small aggregate particles, the radii determined from laser scans and radii computed using spherical harmonic technique were observed to be equal at relatively lower  $l$  values. For example, an aggregate particle retained on the 4.75 mm sieve showed convergence at an  $l$  value of 20.

The maximum size of the aggregates used in the study was 19.0 mm. For this size, convergence occur at an  $l$  value of 25. Therefore,  $l$  equal to 25 was selected in this study for computation of surface texture indices. Form and angularity indices were computed using  $l$  equal to 5 and 20 respectively. Further validation of the capability of  $l = 5$  to distinguish aggregate with different form is presented in Section 5.3.4.

#### **5.3.4 Spherical harmonics form indices**

The MATLAB<sup>TM</sup> code developed for this study was described in Section 5.3.2 and presented in Appendix B. The code was used to compute spherical harmonic form indices of all the aggregates studied. The spherical harmonic form indices were computed using a degree ( $l$ ) value of 5. In order to establish whether  $l$  equal to 5 is sufficient to distinguish aggregate with different form properties, a spherical object and four different aggregate particles of varying shapes (round to flat and elongated) were analysed using degree values ranging from 1 to 5. The spherical object had a diameter of 25 mm, whereas all the aggregates were retained on the 19.0 mm sieve. The results are presented in Table 5.8. The scanned models are included in the table. It can be seen that moving vertically down in Table 5.8, the form indices increase from 1, indicating that the method is capable of differentiating aggregates with different forms. For a degree value of 5, the form index of a rounded aggregate differed significantly from that of flat aggregate, indicating that at this degree value, the spherical harmonic analysis can be used to differentiate aggregates with different forms. Therefore, a degree of 5 was used for the analysis of form indices for all aggregates studied.

**Table 5.8: Form indices for different degree ( $l$ ) Values.**




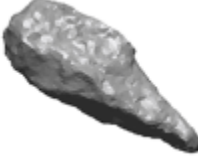

Description	Model	$l=1$	$l=2$	$l=3$	$l=4$	$l=5$
Spherical object		1.0003	1.0008	1.0014	1.0016	1.0016
Round granite		1.0283	1.1555	1.3379	1.4586	1.5144
Cubical granite		1.0295	1.1351	1.2560	1.3268	1.4028
Elongated granite		1.0968	1.6624	1.9302	2.1936	2.3079
Flat and elongated granite		1.0987	2.8833	3.5230	3.0995	3.2838

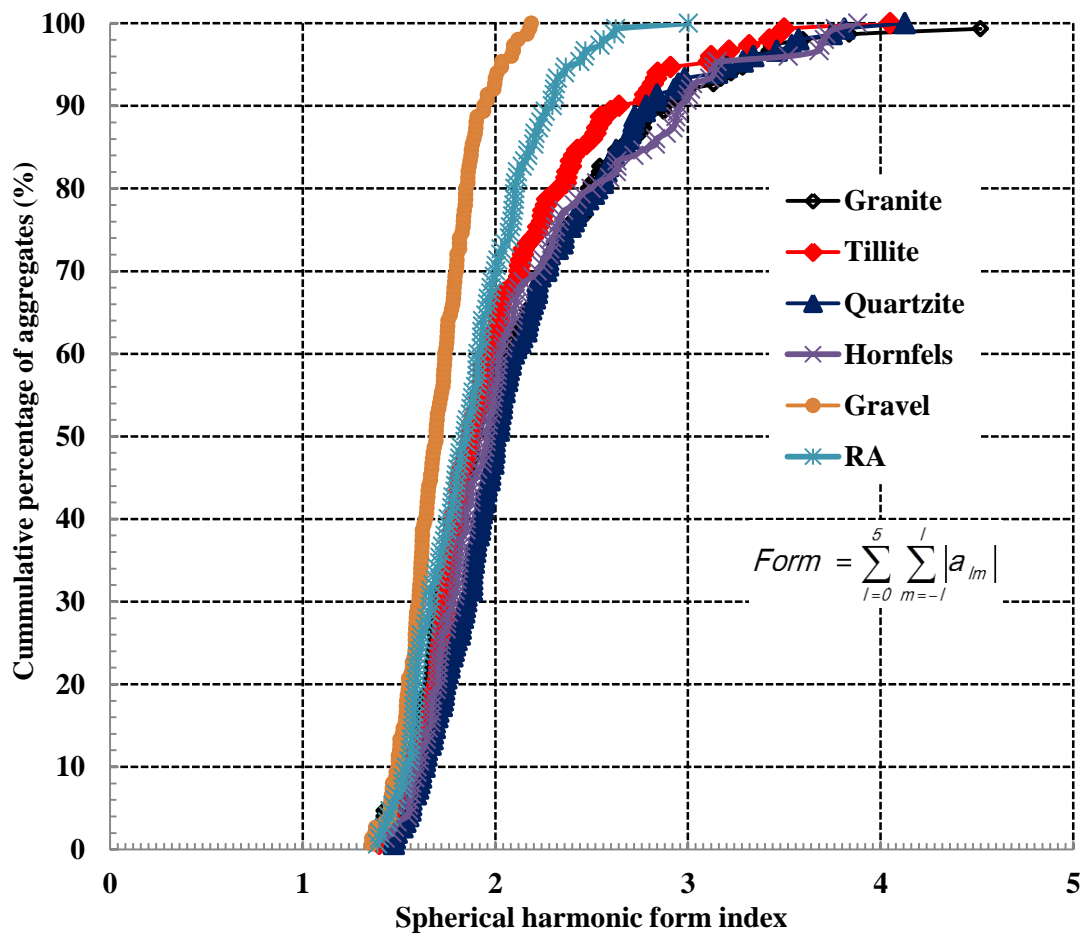
Table 5.9 shows statistical parameters of spherical harmonic form indices for the six types of aggregates studied. All the parameters were computed by using results of 150 aggregate particles studied for each aggregate type. As expected, the average sphericity of alluvial gravel was the lowest followed by that of RA. For the crushed aggregate types, the average sphericity of tillite was relatively lower followed by that of granite, hornfels and quartzite.

Figure 5.17 shows plots of the distributions of spherical harmonic form indices. It can be seen that alluvial gravel has lower form indices with a distribution ranging from 1.358 to 2.232, followed by RA with a distribution ranging from 1.390 to 3.004. The sphericity distributions of crushed aggregate particles did not differ significantly. However, it is noted that crushed aggregates (hornfels, granite and quartzite) have a wider range compared to alluvial gravel and RA.

**Table 5.9: Statistical parameters for spherical harmonic form index.**

Aggregate type	Average	Standard deviation	Standard error
Granite	2.088	0.56	0.046
Tillite	2.027	0.473	0.039
Quartzite	2.153	0.515	0.042
Hornfels	2.140	0.572	0.047
Alluvial gravel	1.713	0.178	0.015
RA	1.875	0.299	0.024

*Note:* For each aggregate type the statistical parameters were computed using results of 150 particles.



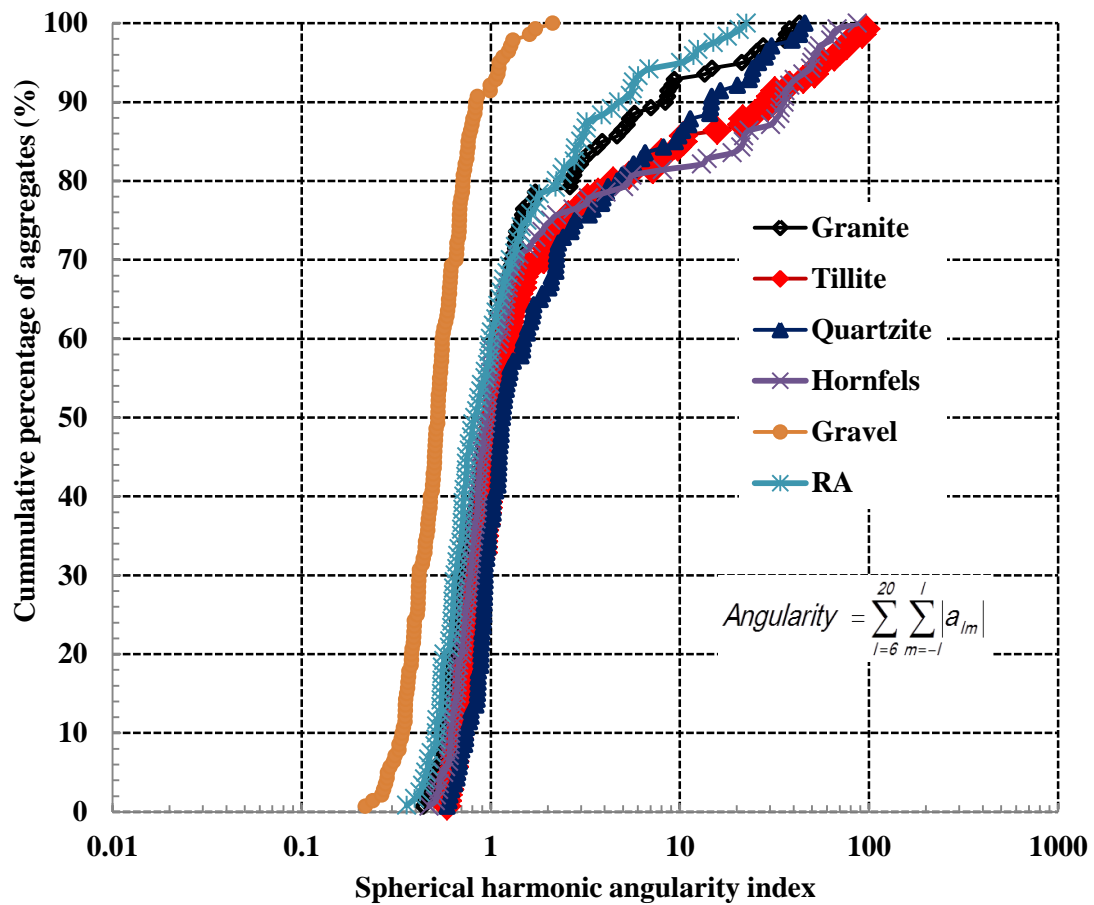
**Figure 5.17: Distribution of spherical harmonic form index.**

### 5.3.5 Spherical harmonics angularity indices

The developed MATLAB<sup>MT</sup> code was used for the analysis of laser scan data and to compute spherical harmonic angularity indices of individual aggregate particles. All the angularity indices were computed using Equation 2.23, with a maximum  $l$  value of 20. Ideally, spherical objects or round shaped aggregates are expected to have angularity index values close to zero. For the six types of aggregates used in this study, the alluvial gravel sample had the most rounded particles. It was expected that the angularity indices for alluvial gravel should be the smallest, compared to other aggregate types.

Figure 5.18 shows plots of the distributions of the angularity indices for the six types of aggregates studied. The alluvial gravel sample had the smallest angularity indices. Approximately 90 per cent of the alluvial gravel particles had angularity indices less than a value of 1. Overall, the RA sample had smaller angularity indices compared to the crushed aggregates. This may be due to the fact that RA is a used material and the angular corners have been broken down due to traffic loading and compaction. Approximately 60 per cent of the RA particles had angularity indices less than a value of 1. For crushed aggregates, the distributions at lower angularity indices did not differ significantly. However, for angularity values greater than 2, it was observed that granite is less angular, followed by quartzite, tillite and hornfels.






Another important observation that deserves a comment is the range of angularity indices for the six types of materials studied. The Alluvial gravel samples had a smaller range (from 0.218 to 2.127), followed by the RA sample (from 0.366 to 22.47). All the crushed aggregates showed a wider distribution of angularity indices. Approximately 30 per cent of the crushed aggregates had angularity indices between 3 and 100. It was further observed that higher angularity indices were obtained for the elongated aggregate particles. The reason for a wider distribution of the angularity indices for crushed aggregates may be the presence of a larger amount of elongated aggregate particles.



**Figure 5.18: Distribution of spherical harmonic angularity index.**

Further validation of the spherical harmonic angularity indices was based on a visual inspection. A spherical object, two round shaped aggregates and two angular aggregate particles were visually identified and selected. The angularity indices for the spherical object and the aggregate particles were determined. The photos of the spherical object and the aggregate particles are shown in Table 5.10. Included in the table are spherical harmonic angularity indices. As expected, the angularity index for the spherical object was approaching zero. It is also observed that the round shaped aggregates have lower angularity indices compared to the angular aggregate particles, which was expected. The observed trend clearly indicates that the spherical harmonic analysis technique is able to distinguish aggregate particles with different angularities.

**Table 5.10: Comparison of angularity indices.**

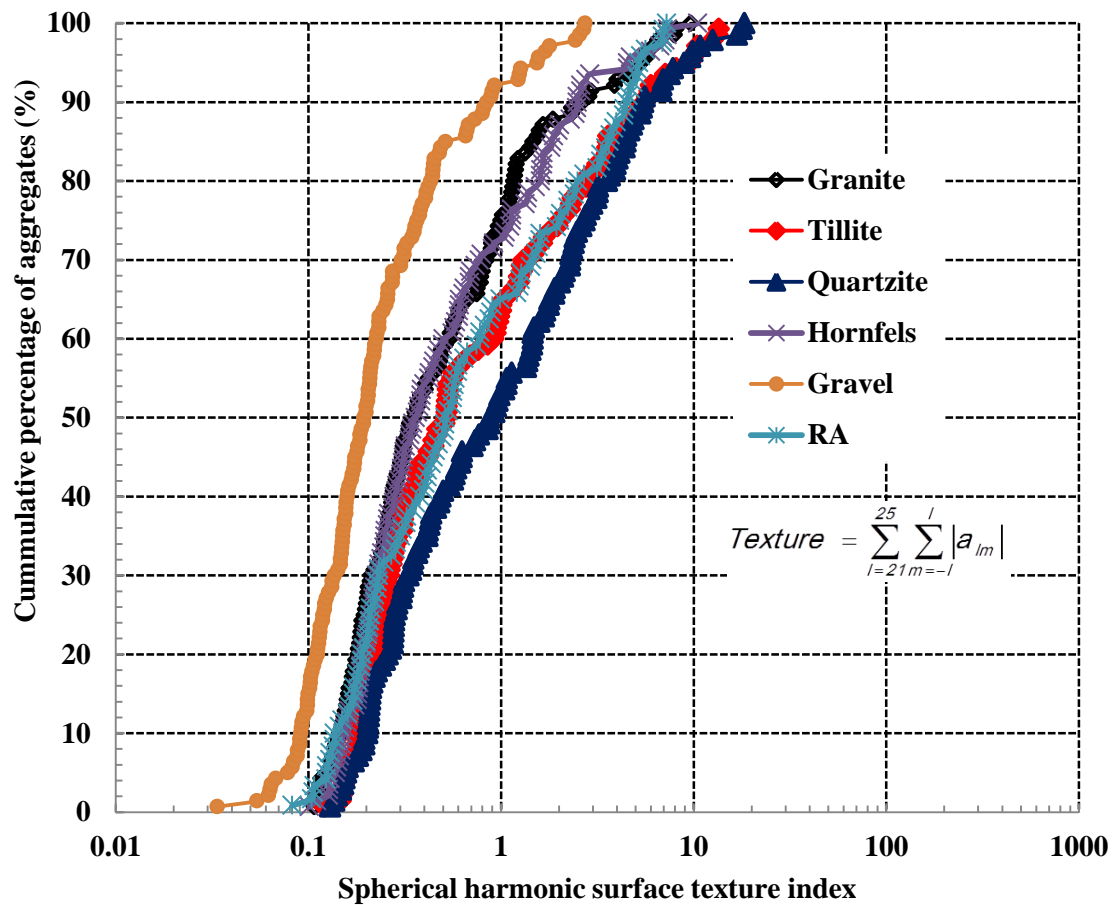
Description	Actual photo	Angularity index
Spherical object		0.0036
Round aggregate particles		0.3905
		0.4357
Angular aggregate particles		0.6268
		1.0127

### 5.3.6 Spherical harmonics surface texture indices

All the spherical harmonic surface texture indices were computed using Equation 2.24, with a maximum  $l$  value of 25. Perfect spherical and smooth aggregates/objects are expected to have surface texture indices values close to zero. For the six types of aggregates used in this study, the alluvial gravel sample was generally smoother compared to the rest of the aggregates studied.

Figure 5.19 shows plots of the distributions of the surface texture indices for the six types of aggregates studied. As expected, smaller surface texture indices were computed for alluvial gravel (alluvial gravel sample was smoother). Overall, the surface texture indices computed for both granite and hornfels were found to be the second smallest, followed by tillite and RA. The highest surface texture indices were computed for the quartzite aggregate. Over 90 per cent of the alluvial gravel particles had surface texture indices values of less than 1. On the other hand, the aggregates with surface texture indices values less than 1 for the rest of the aggregate studied ranged from 50 per cent for quartzite to 75 per cent for granite.

Similar to form and angularity indices, wider distributions of surface texture indices were observed for crushed aggregates (approximately from 0.1 to 10), whereas the range for alluvial gravel continued to be the smallest (approximately from 0.03 to 3). Unlike the distribution of form and angularity indices (Figures 5.17 and 5.18) on which the RA ranked just after the alluvial gravel, it is interesting to note that the distribution of surface texture for RA was almost in between the crushed aggregates. It should be mentioned that some bitumen binder, still remaining on the RA, might have affected the computed surface texture.








**Figure 5.19: Distribution of spherical harmonic surface texture index.**

Similar to the angularity indices, the validation of the surface texture indices relied on a comparison of the alluvial gravel particles with the rest of the aggregate types studied. Alluvial gravel particles were smoother compared to the rest of the aggregates studied. It was expected that their surface texture indices would differ from the rest of the aggregates studied. Table 5.11 shows photos of a smooth spherical object, two smooth round shaped aggregates and rough aggregate particles. Included in the table are spherical harmonic surface texture indices. The spherical object has a surface texture index approaching a value of zero, which was expected. The smooth round shaped aggregates had lower surface texture indices values compared to round aggregate particles. This confirms the ability of the spherical harmonic analysis technique to distinguish aggregates with different surface textures.



**Table 5.11: Comparison of surface texture indices**

Description	Actual photo	Surface texture index
Spherical object		0.0019
Smooth aggregate particles		0.1511
		0.1365
Rough aggregate particles		0.8301
		1.0183

## 5.4 Correlation of spherical harmonics form indices with other form indices

In order to get an indication of the capability of each of the laser-based form indices to distinguish the aggregates with different form properties, the spherical harmonic form indices were correlated with each of the form indices computed by using the aggregate's physical properties. The results indicated that linear models were the best to relate the spherical harmonic form indices with laser-based form indices computed by using the aggregate's physical dimensions. The following correlations were performed:

- Correlation between spherical harmonic form indices with sphericity computed by using surface area and volume;
- Correlation between spherical harmonic form indices with sphericity computed by using orthogonal dimensions, and
- Correlation between spherical harmonic form indices with flat and elongated ratios.

Figures 5.20 to 5.37 show correlations of spherical harmonic form indices with form indices computed by using the aggregate's physical properties. Good correlation was observed for all six types of aggregates studied. The spherical harmonic form indices decrease linearly with increasing sphericity computed by using the surface area and volume (Figures 5.20 to 5.25). The spherical harmonic form indices also decrease with increasing sphericity computed by using orthogonal dimensions (Figures 5.26 to 5.31). On the other hand, the spherical harmonic form indices increase linearly with increasing flat and elongated ratio (Figures 5.32 to 5.37). The observed trends agree with the theory underlying each of the form indices.

Overall, the correlations of the spherical harmonic form indices with the sphericity computed using the surface area and volume results from laser scanning results was the strongest, followed by the flat and elongated ratio. The correlation between the spherical harmonic form index and the sphericity computed by using three orthogonal dimensions was the weakest for all types of the aggregates studied. The reasons for the best correlations between the spherical harmonic form indices and the sphericity computed using the surface area and volume could be due to the fact that both indices are computed based on information that represents the overall 3-D form of aggregate particles. The observed good correlations confirm and strengthen the capability of the aggregate laser scanning technique to determine various form indices describing the aggregate form properties.

It is again observed that the alluvial gravel and RA showed the weakest correlations compared to crushed aggregates (granite, tillite, quartzite and hornfels). This may be due to the fact that the crushed aggregates showed a wider distribution of form indices compared to alluvial gravel and RA.

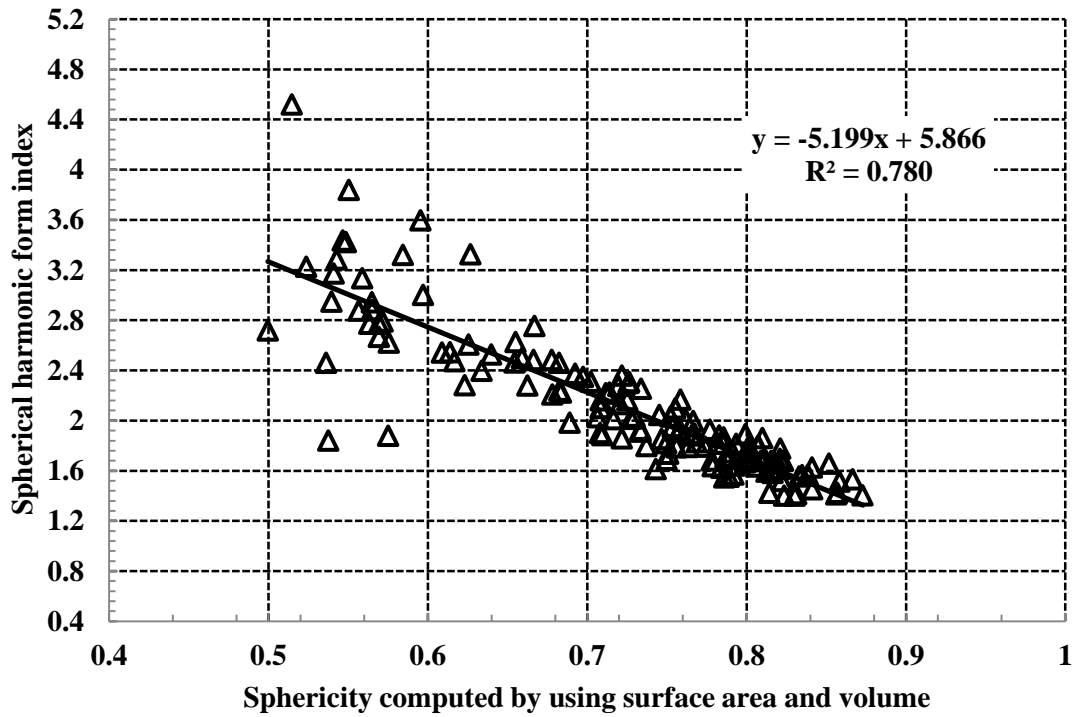


Figure 5.20: Spherical harmonic form index versus sphericity computed using volume and surface area for granite.

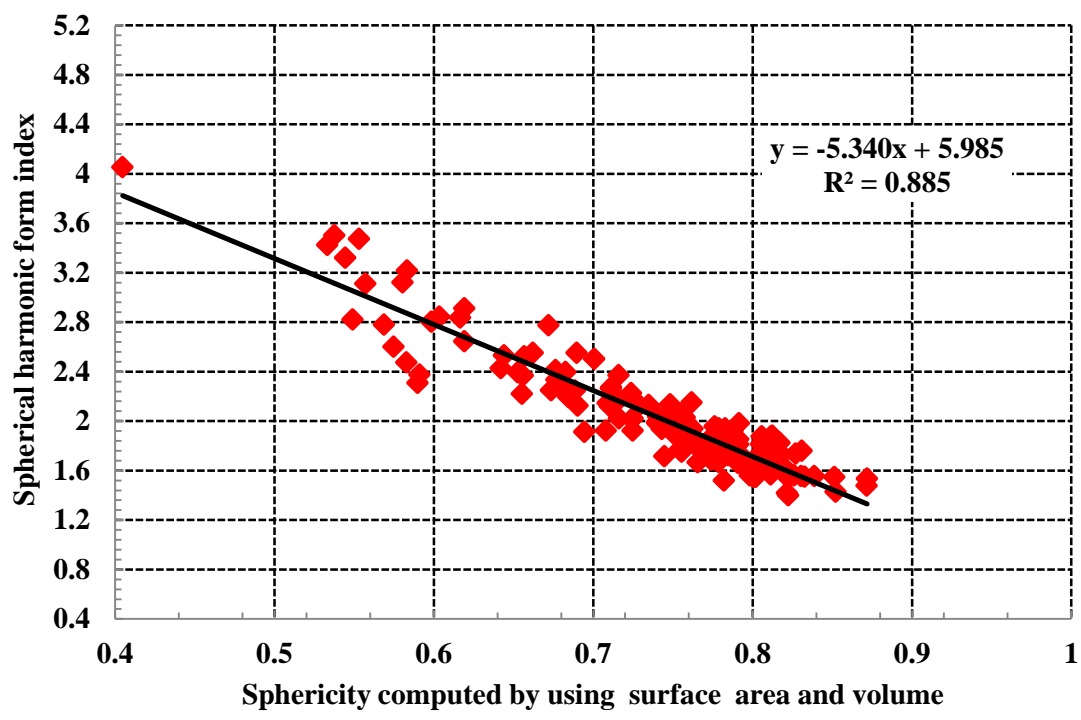


Figure 5.21: Spherical harmonic form index versus sphericity computed using volume and surface area for tillite.

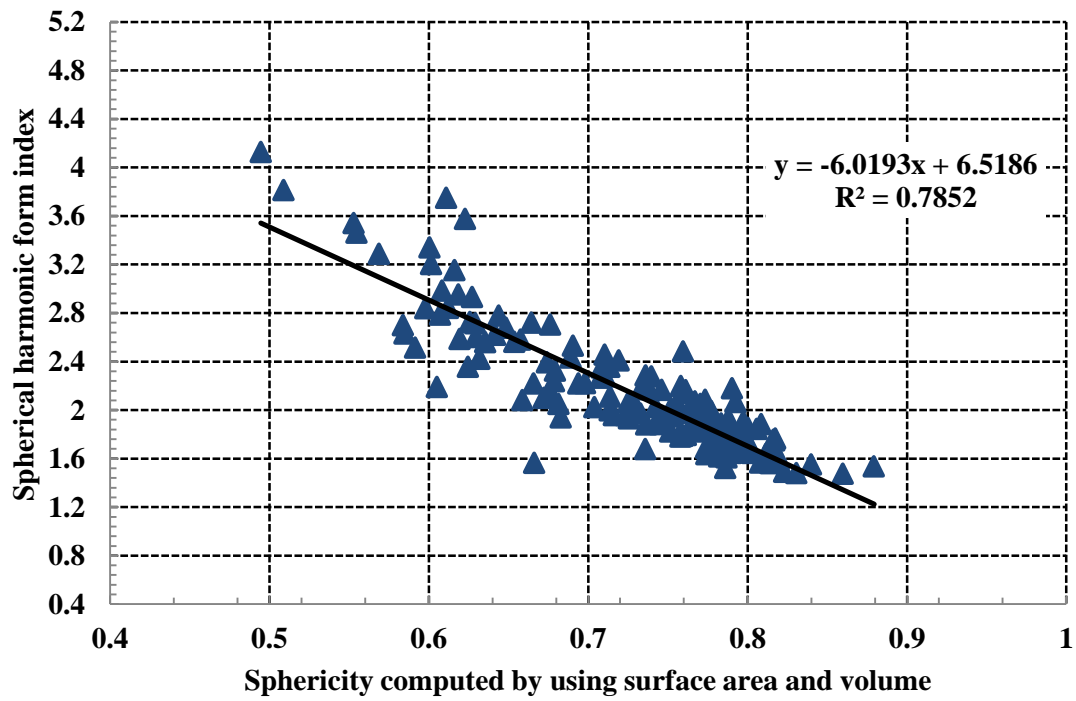


Figure 5.22: Spherical harmonic form index versus sphericity computed using volume and surface area for quartzite.

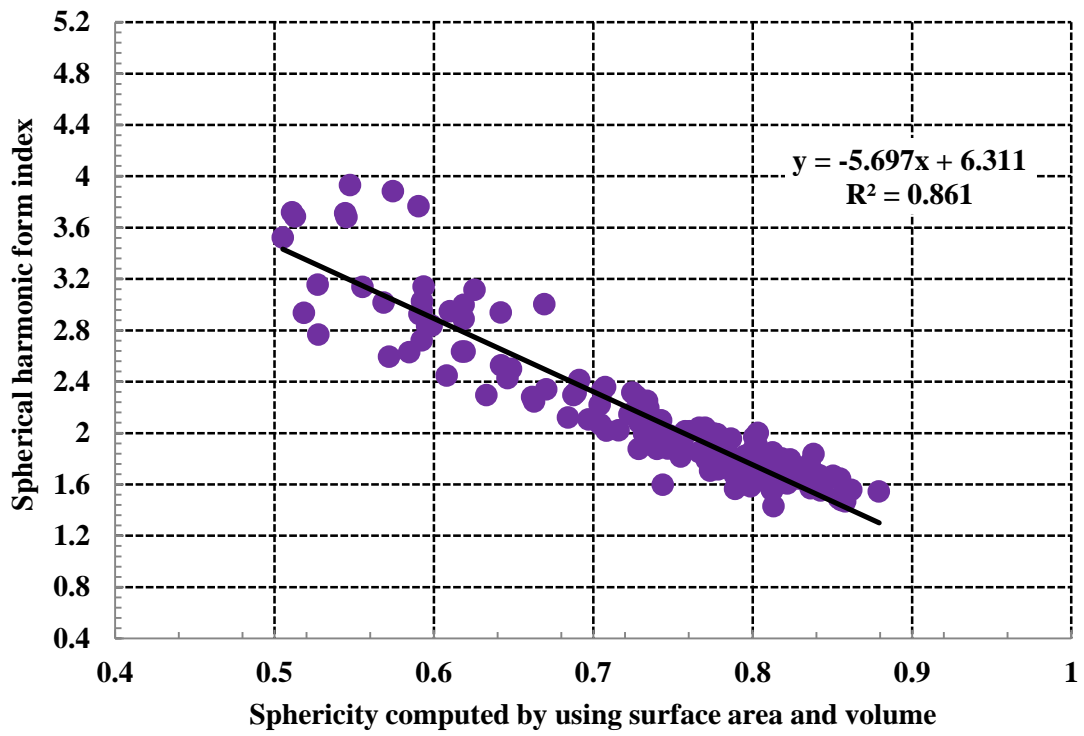


Figure 5.23: Spherical harmonic form index versus sphericity computed using volume and surface area for hornfels.

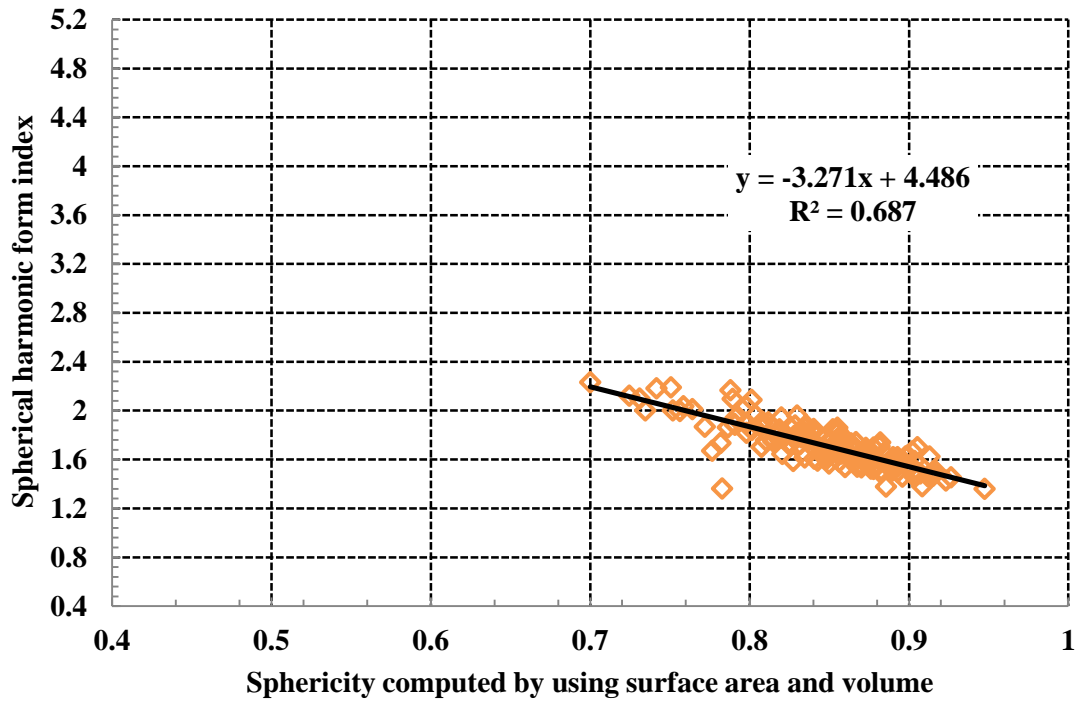


Figure 5.24: Spherical harmonic form index versus sphericity computed using volume and surface area for alluvial gravel.

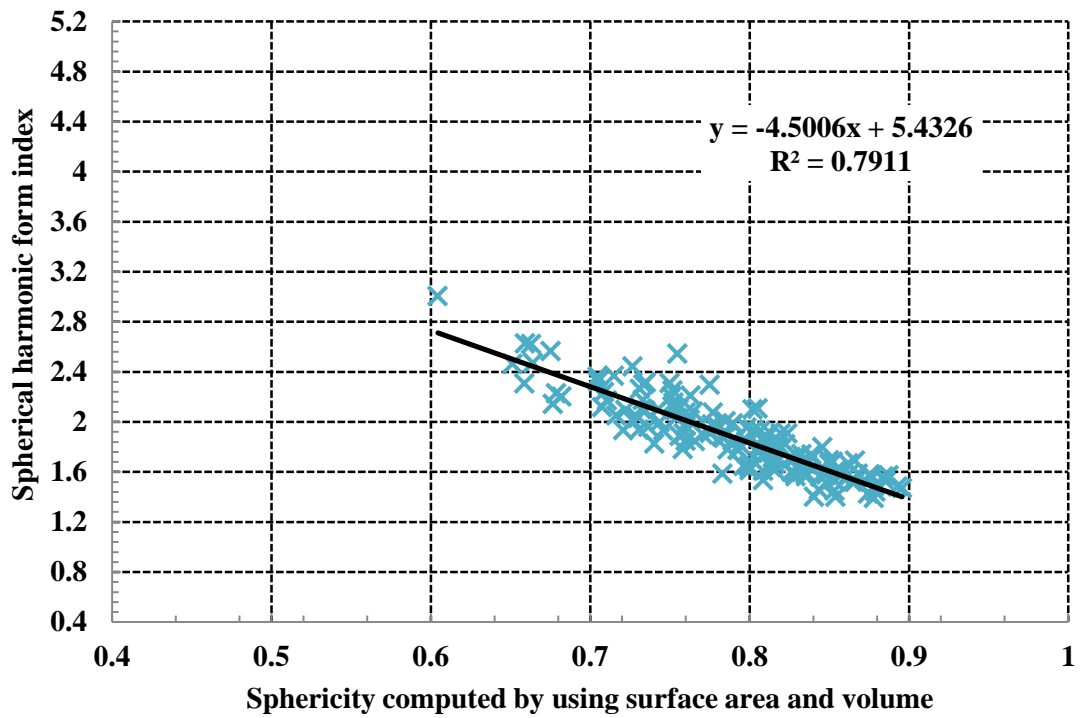


Figure 5.25: Spherical harmonic form index versus sphericity computed using volume and surface area for RA.

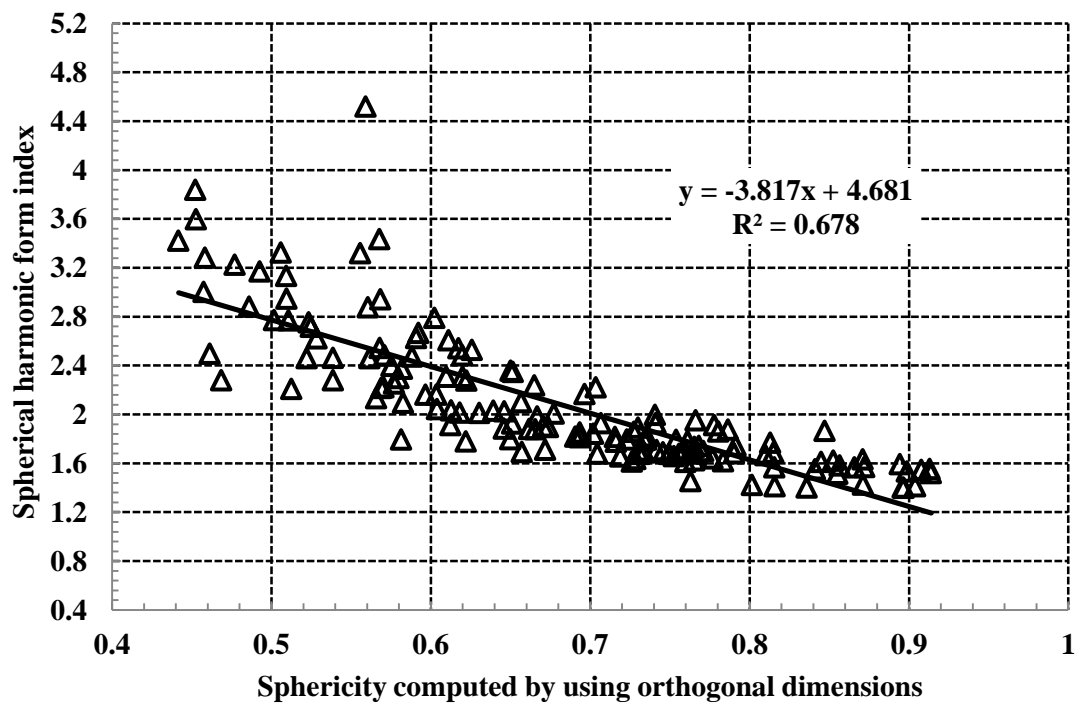


Figure 5.26: Spherical harmonic form index versus sphericity computed using orthogonal dimensions for granite.

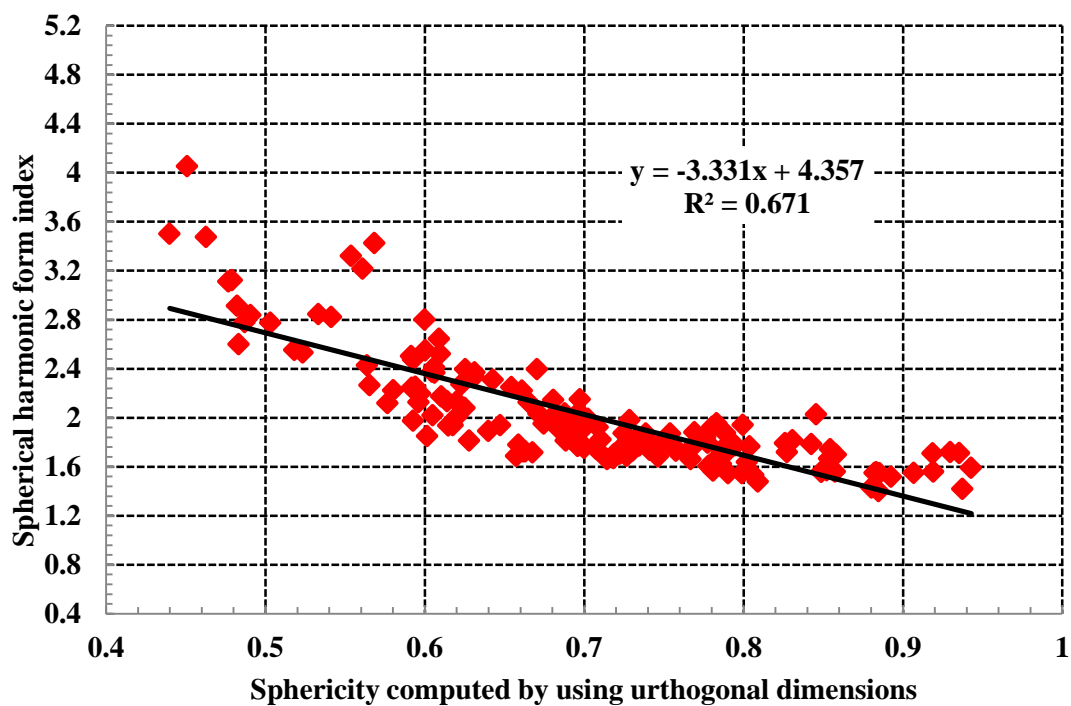


Figure 5.27: Spherical harmonic form index versus sphericity computed using orthogonal dimensions for tillite.

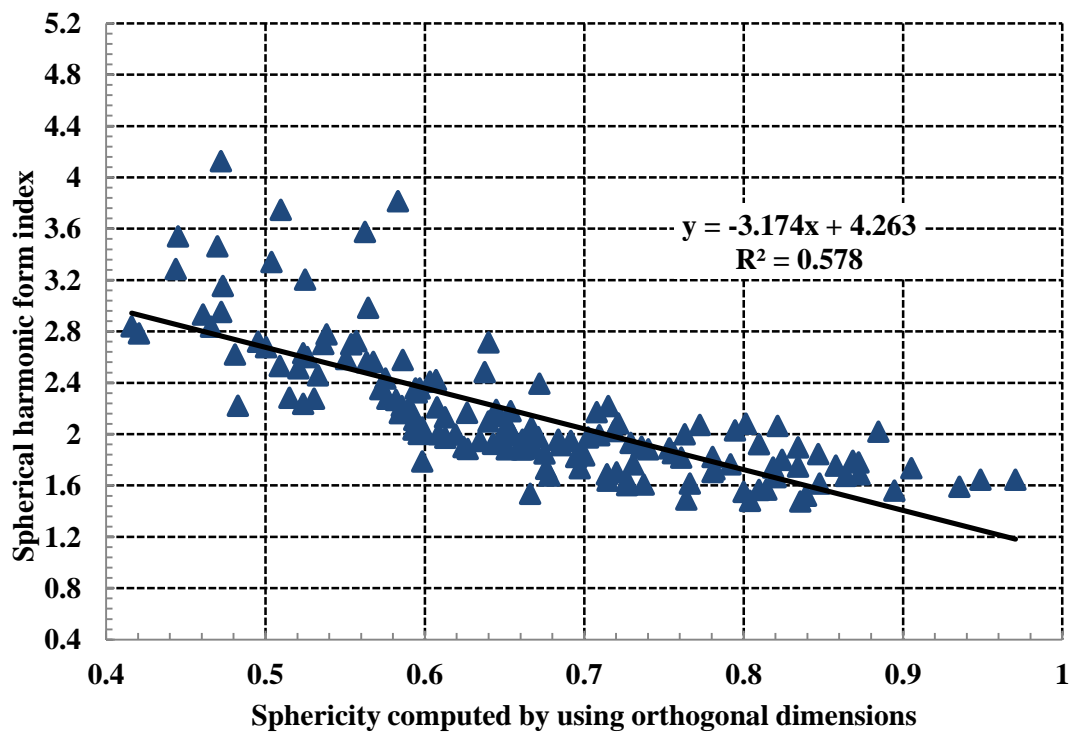


Figure 5.28: Spherical harmonic form index versus sphericity computed using orthogonal dimensions for quartzite.

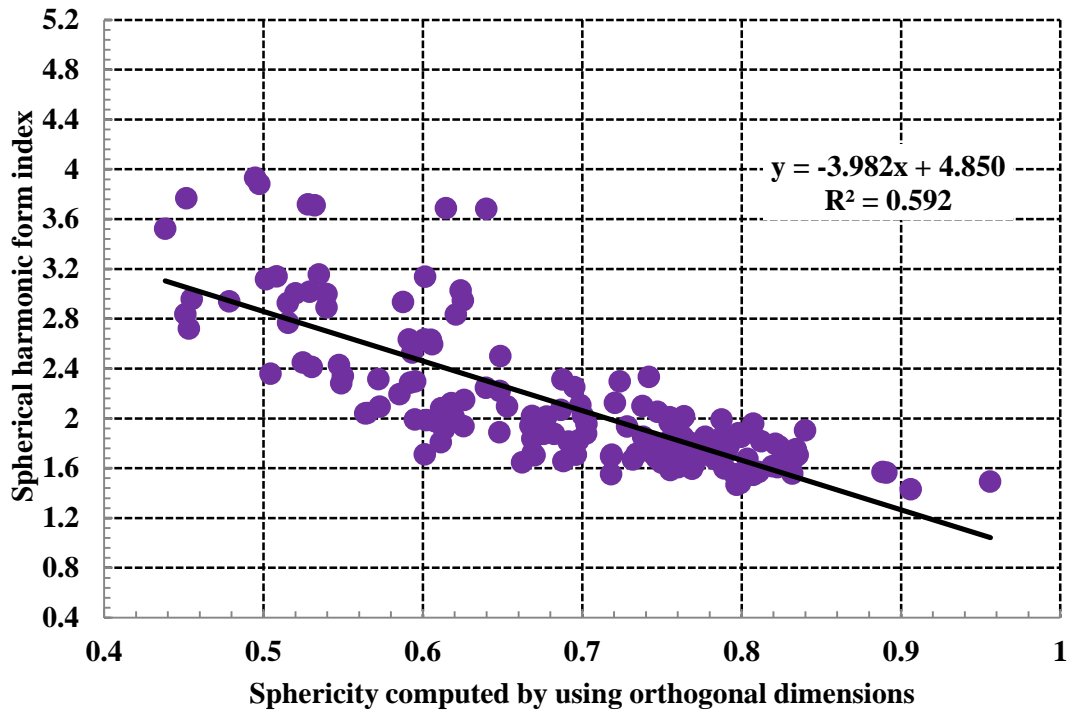


Figure 5.29: Spherical harmonic form index versus sphericity computed using orthogonal dimensions for hornfels.

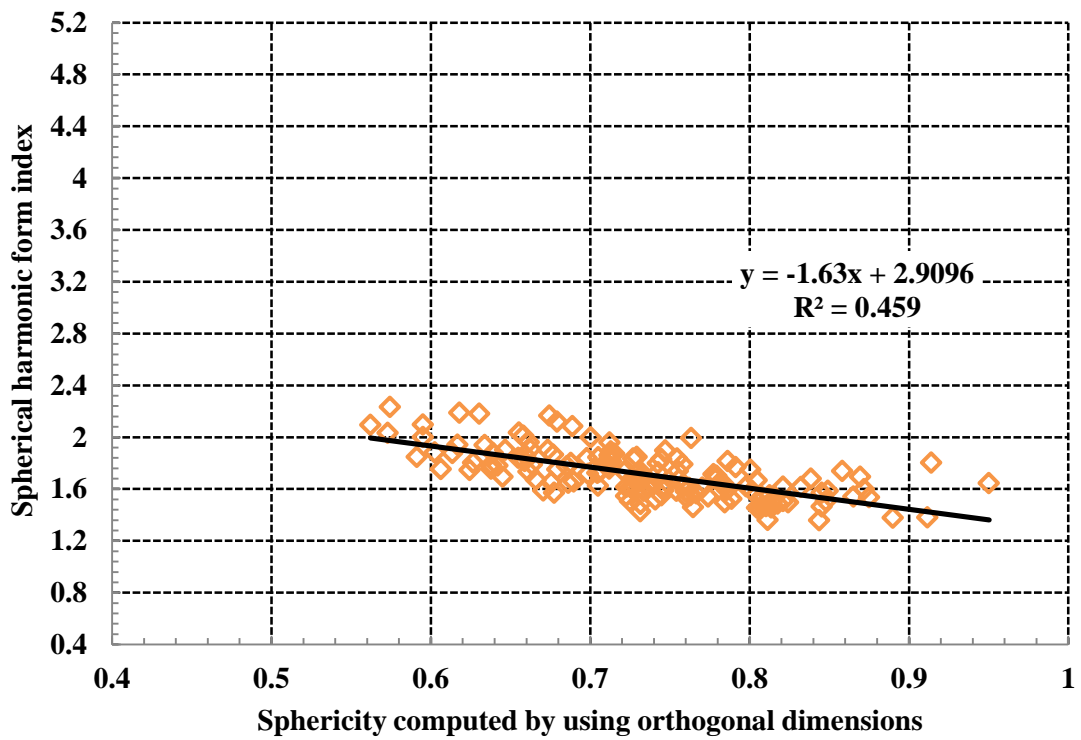


Figure 5.30: Spherical harmonic form index versus sphericity computed using orthogonal dimensions for alluvial gravel.



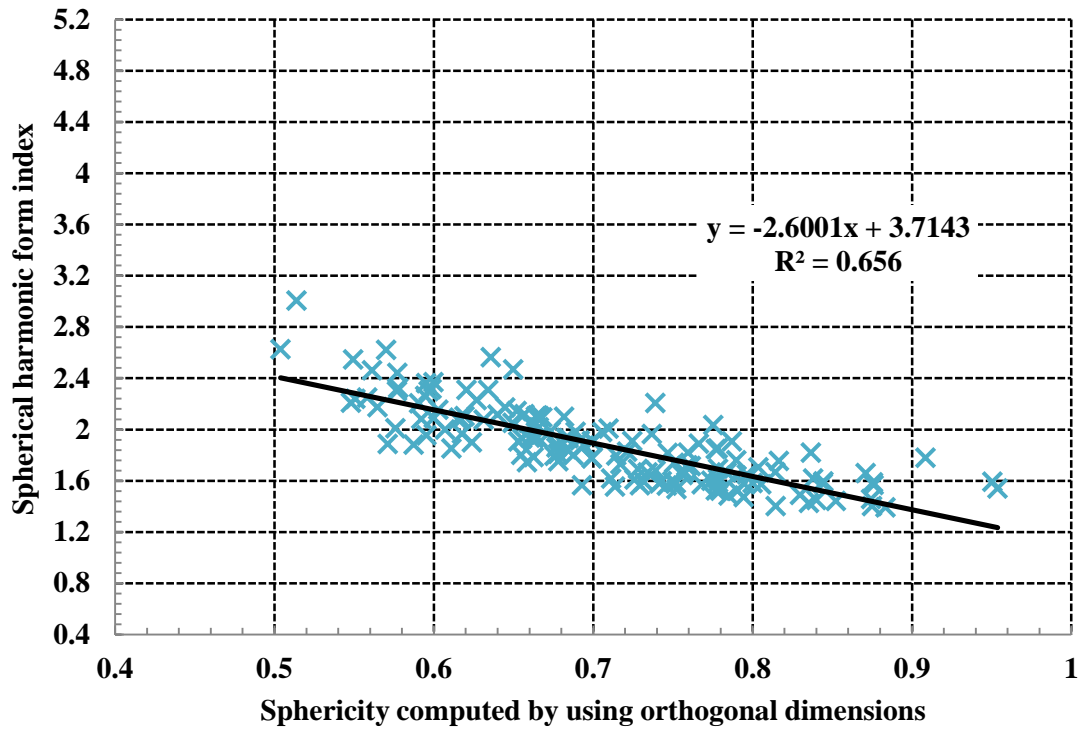


Figure 5.31: Spherical harmonic form index versus sphericity computed using orthogonal dimensions for RA.

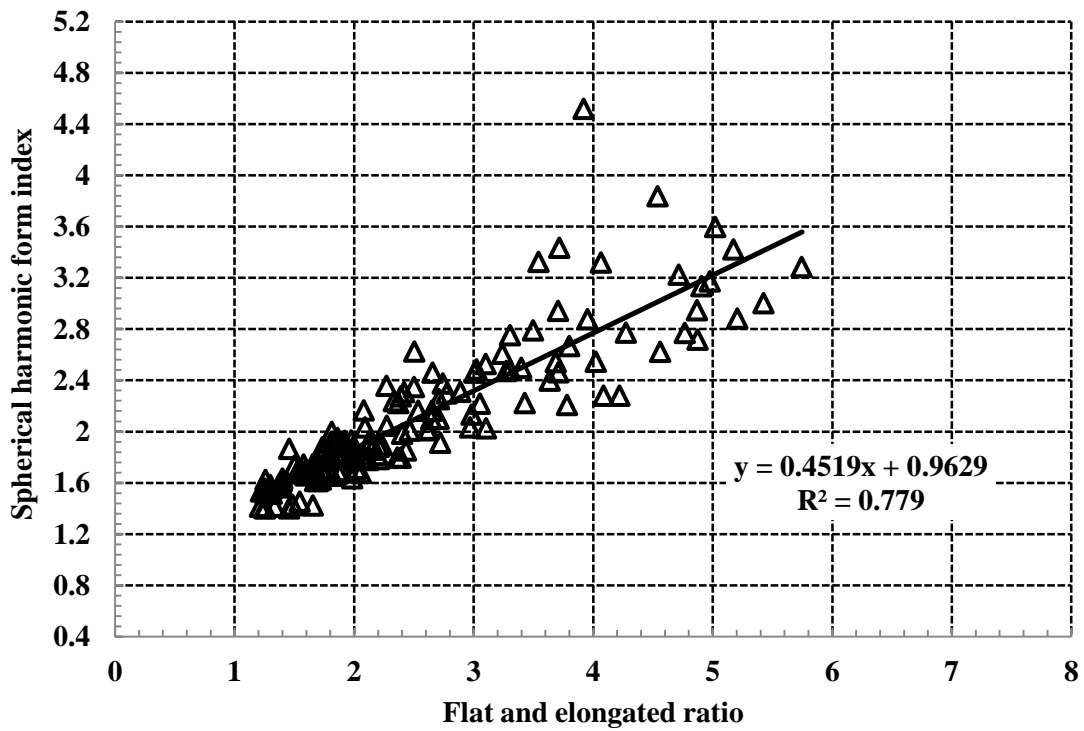


Figure 5.32: Spherical harmonic form index versus flat and elongated ratio for granite.

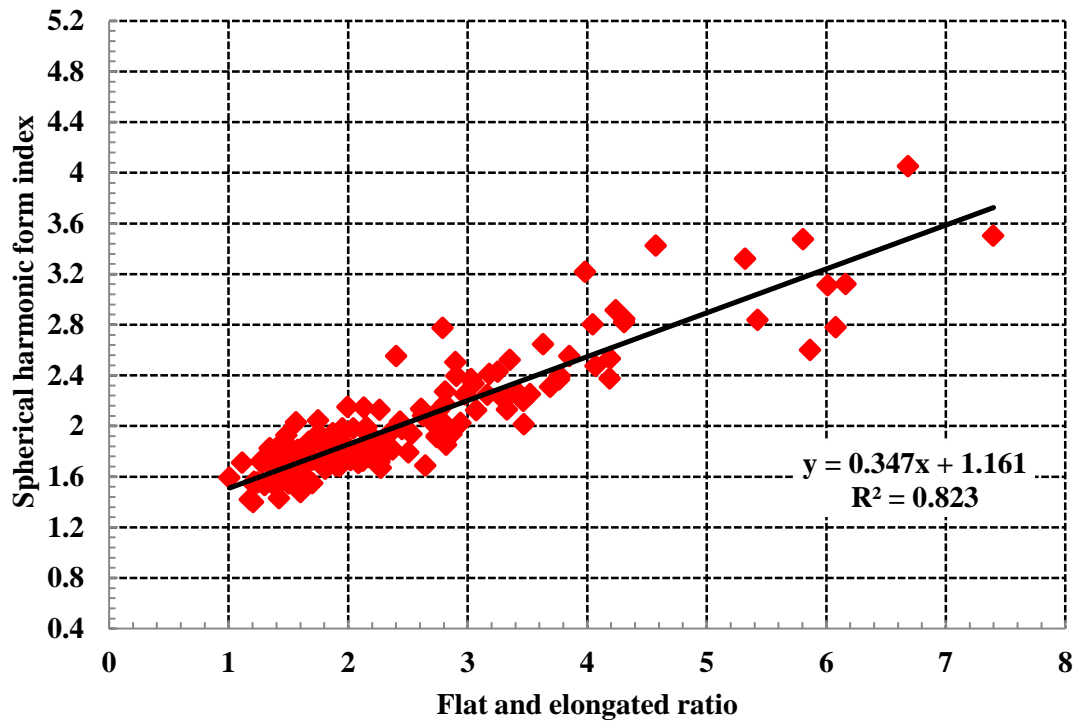


Figure 5.33: Spherical harmonic form index versus flat and elongated ratio for tillite.

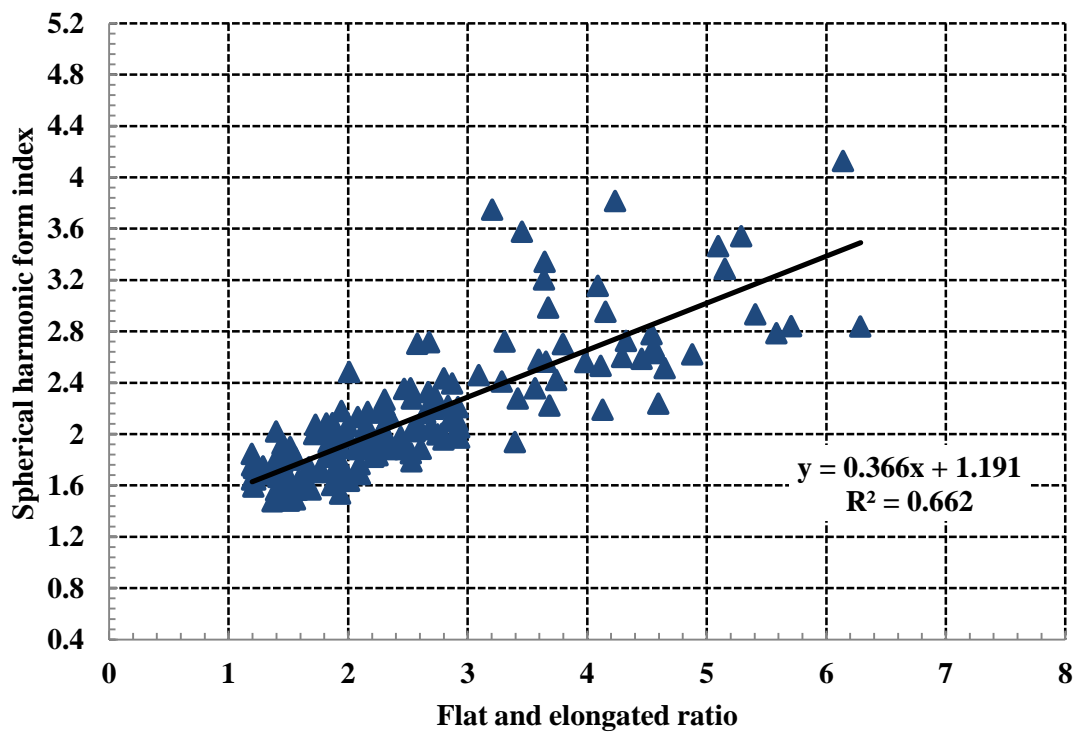


Figure 5.34: Spherical harmonic form index versus flat and elongated ratio for quartzite.

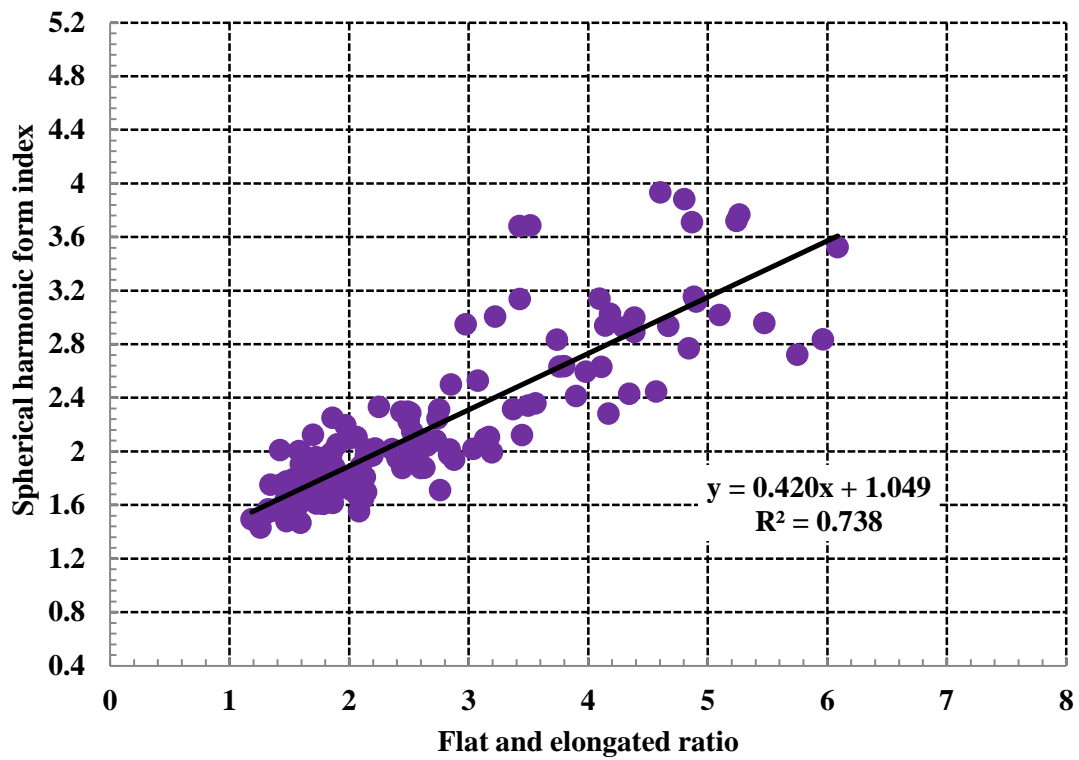


Figure 5.35: Spherical harmonic form index versus flat and elongated ratio for hornfels.

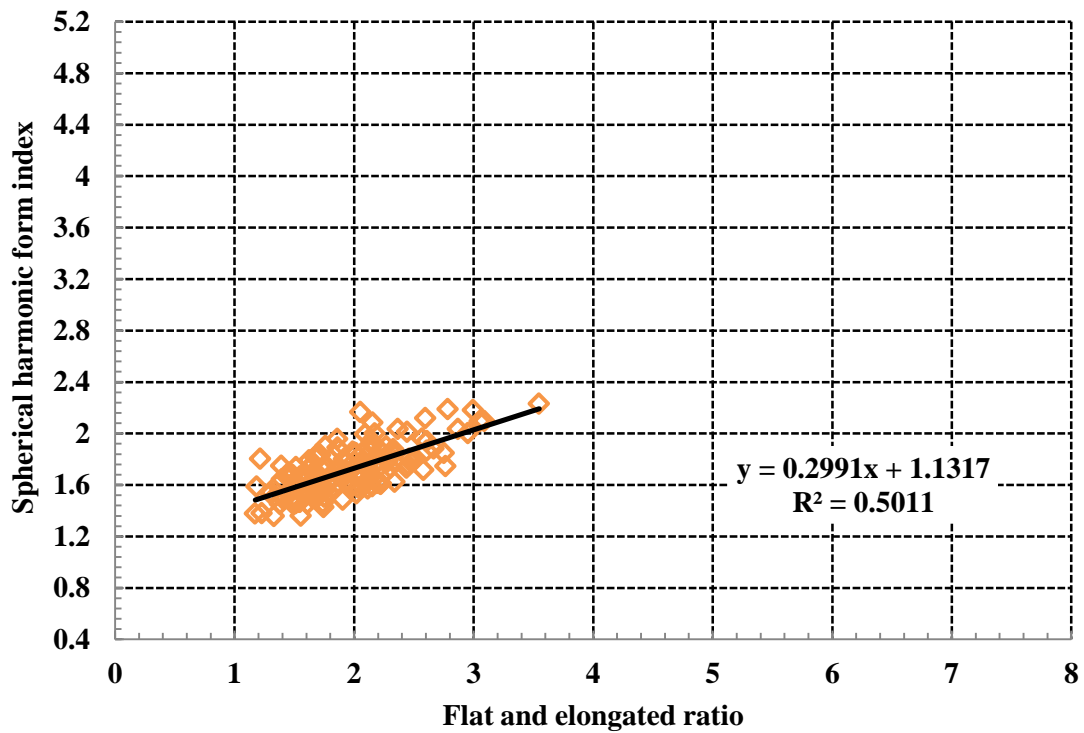


Figure 5.36: Spherical harmonic form index versus flat and elongated ratio for alluvial gravel.

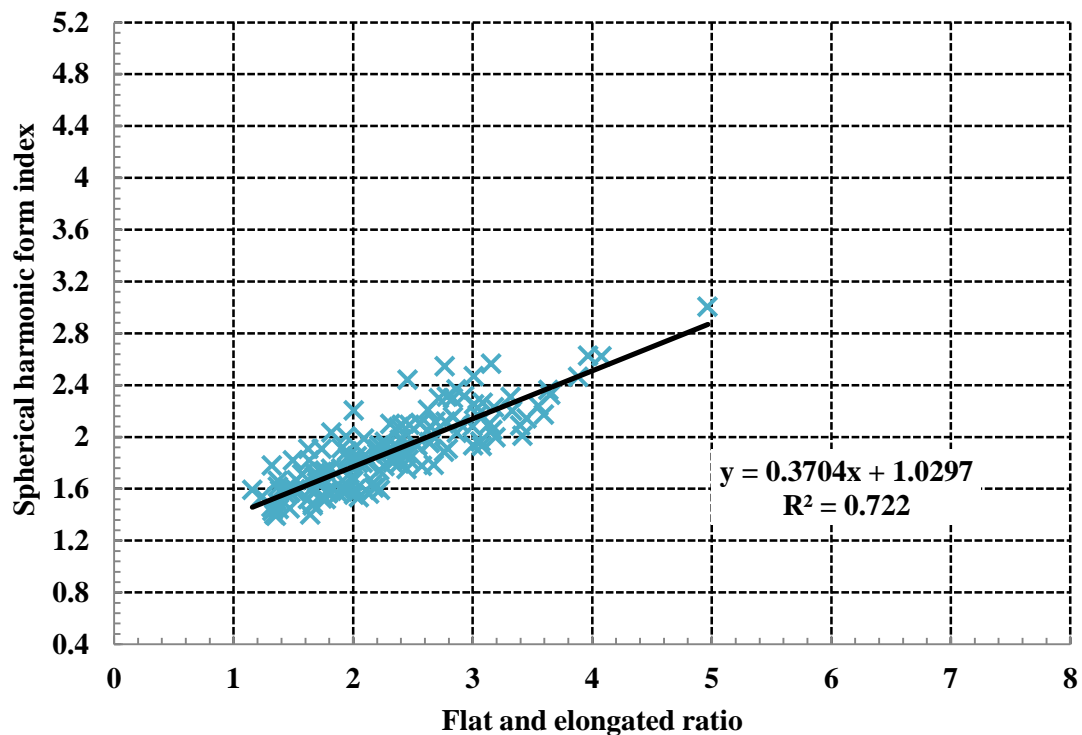


Figure 5.37: Spherical harmonic form index versus flat and elongated ratio for RA.

## 5.5 Validation of the laser-based form indices

To validate the capability of the laser-based form indices, two current standard tests used for characterisation of the aggregate form properties were conducted on the aggregates studied. These tests are the flakiness index test (TMH1 Method B3) which is commonly used in South Africa and flat and elongated particles ratio test (ASTM D 4791) used in the USA. In this section, the results of the flakiness index and flat and elongated particles ratio tests are correlated with laser-based aggregate form indices.

### 5.5.1 Correlation of flakiness index with laser-based form indices

Using the TMH1 Method B3 procedures for determination of flakiness index, a single flakiness index parameter is normally computed to represent the whole sample. The flakiness index results for each of the six types of aggregates studied were presented in Chapter 4 (Table 1). The flakiness index values were correlated with the average laser-based form indices presented in Tables 5.1 to 5.3, and 5.9.

Figures 5.38 to 5.41 show correlations of flakiness index with the sphericity computed by using the aggregate surface area and volume, the sphericity computed by using the aggregate orthogonal dimensions, flat and elongated ratio and spherical harmonic form index respectively. The trends of the plots agree with the theory underlying each of the form indices. The highest correlation was found between the flakiness index with the sphericity computed using the aggregate orthogonal dimensions ( $R^2 = 0.694$ ), followed by the flat and elongated ratio ( $R^2 = 0.632$ ), spherical harmonic form index ( $R^2 = 0.565$ ) and the sphericity computed by using aggregate surface area and volume ( $R^2 = 0.515$ ).

The overall trends of the plots in Figures 5.38 to 5.41 show linear relationships between the flakiness index and laser-based form indices. However, the data points appear to be much scattered. Possible reasons for the observed scatter could be the following:

- The plots include only the results of six types of aggregates used in this study. Inclusion of more aggregate samples could improve the correlations.
- The procedures for determination of flakiness index of individual aggregate sample yield a single flakiness index parameter to describe the form properties of the whole aggregate sample. In order to relate the flakiness index parameter with the laser-based form indices, average values to represent each aggregate type had to be calculated. A single parameter such as the computed average cannot clearly differentiate form properties of different aggregate types, particular for crushed aggregate, which appears to have similar form properties. Therefore, there is a need to employ advanced technique for accurate determination of aggregate form properties in order to distinguish the form properties of different types of aggregates.

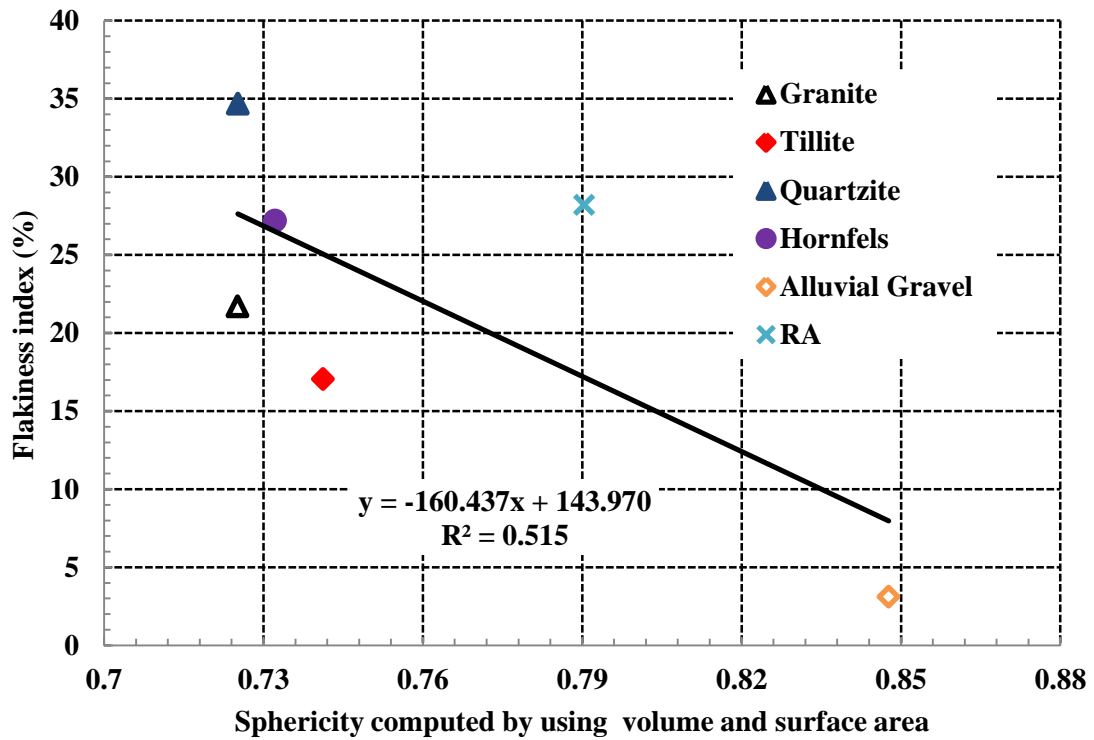


Figure 5.38: Flakiness index versus sphericity computed by using volume and surface area.

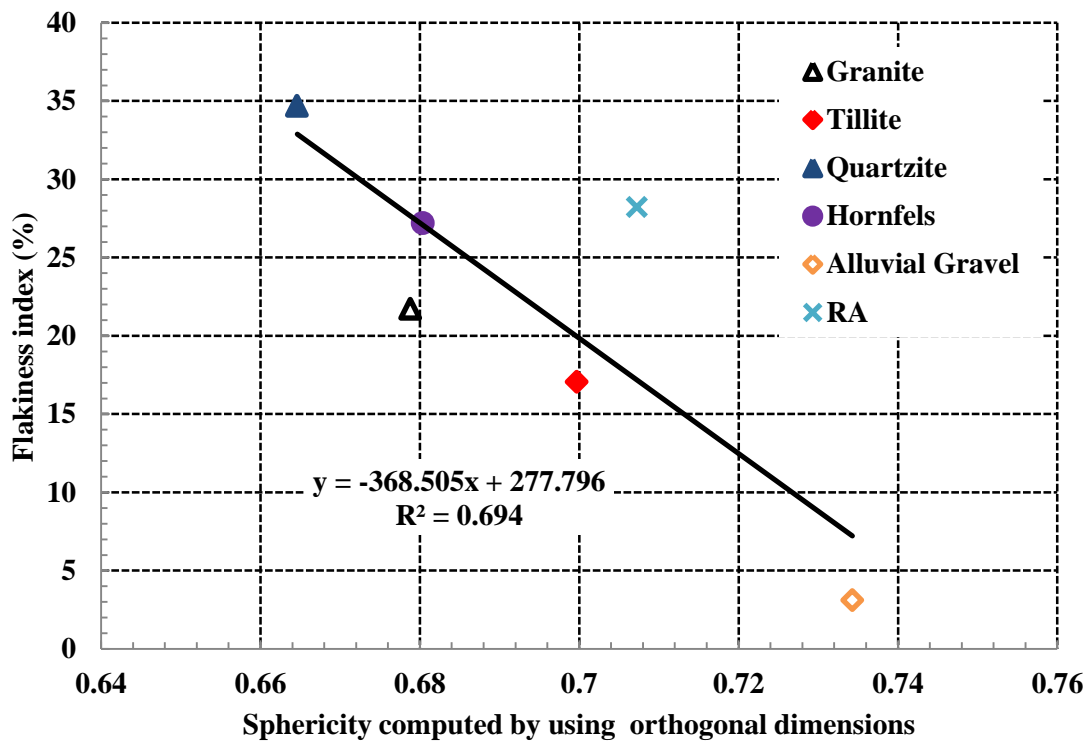


Figure 5.39: Flakiness index versus sphericity computed by using orthogonal dimensions.

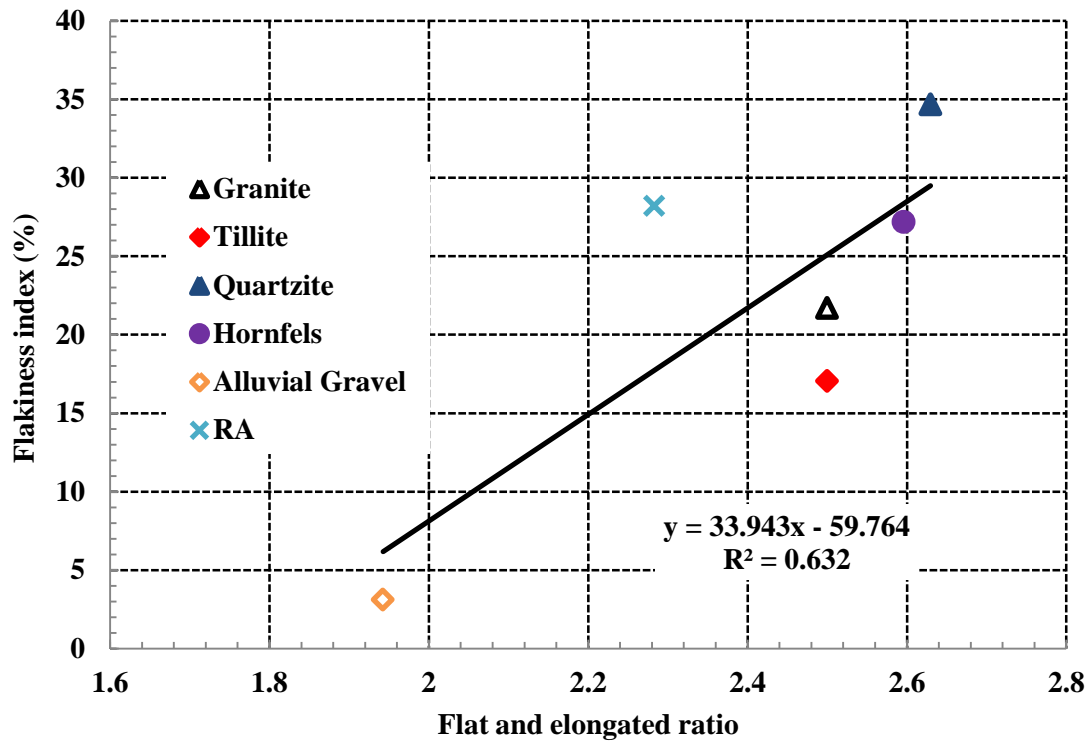


Figure 5.40: Flakiness index versus flat and elongated ratio.

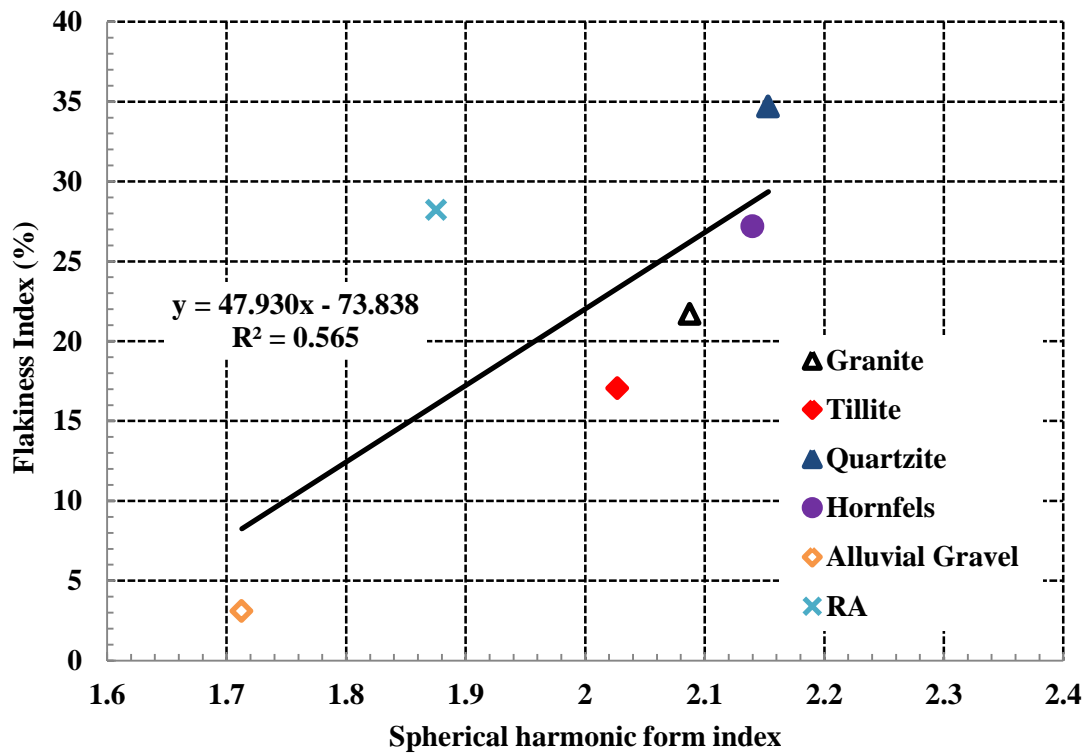


Figure 5.41: Flakiness index versus spherical harmonic form index.

## 5.5.2 Correlation of flat and elongated particles ratio with laser-based form indices

The standard test for determination of flat and elongated particles ratio (ASTM D 4791) requires the proportional caliper device to be set at a pre-defined ratio. It was indicated in Chapter 2 that SUPERPAVE recommends a ratio of 5:1. In this study, the flat and elongated particles ratio tests were carried out with the proportional caliper device set at three different ratios i.e. 5:1, 3:1 and 2:1. The results of flat and elongated particles ratio were presented in Chapter 4 (Table 1). The average laser-based form indices were presented in Tables 5.1 to 5.3 and 5.9.

Figures 5.42 to 5.53 show the correlation of the flat and elongated particles tests carried out using the current standard test procedures with laser-based form indices. The coefficients of determination ( $R^2$ ) ranging from 0.673 to 0.950 were obtained. Overall, the correlations with the flat and elongated particles ratio determined with the proportional caliper device set at a ratio of 3:1 were the best (Figures 5.46 to 5.49), followed by the 5:1 ratio (Figures 5.42 to 5.45) and the 2:1 ratio (Figures 5.50 to 5.53).

Similar to the correlation of the laser-based form indices with the flakiness index, in some figures the data points appears to be much scattered. Possible reasons for the observed scatter could be that only averages of a limited number of samples (six types of aggregates) were used in this study and plotted in Figures 5.50 to 5.53.

Despite the observed correlations, it is noted that the flat and elongated particles ratios of alluvial gravel and RA determined using the current standard method with the proportional caliper set at a ratio of 5: 1 are nearly zero (Figures 5.42 to 5.45). This is a clear indication of the limitation of the current standard methods to distinguish the shape properties of aggregates, which even visually can be identified to differ. Based on the observed results, further research to investigate the appropriateness of using the 5:1 ratio recommended in SUPERPAVE may be needed.

On the other hand, the distribution plots of various laser-based form indices presented earlier, clearly indicated that the alluvia gravel and the RA samples differ in terms of their shape properties. Therefore, the suitability of the aggregate laser scanning technique to determine aggregate shape properties is strengthened.



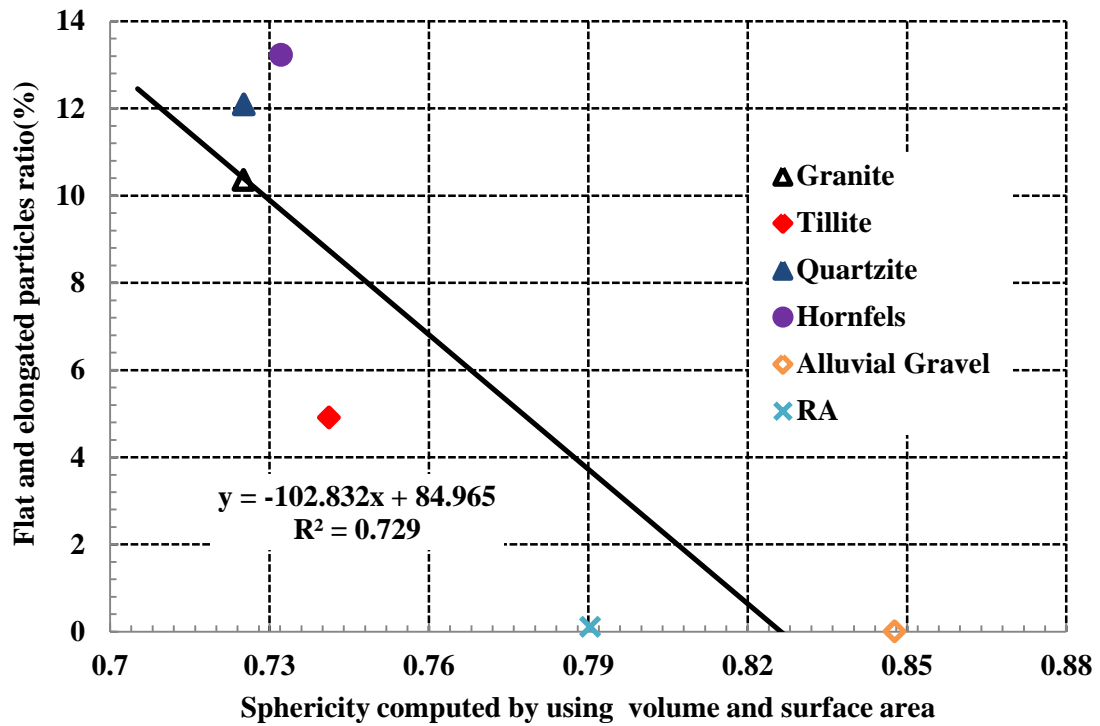


Figure 5.42: Flat and elongated particles ratio (proportional caliper set at 5:1) versus sphericity computed by using volume and surface area.

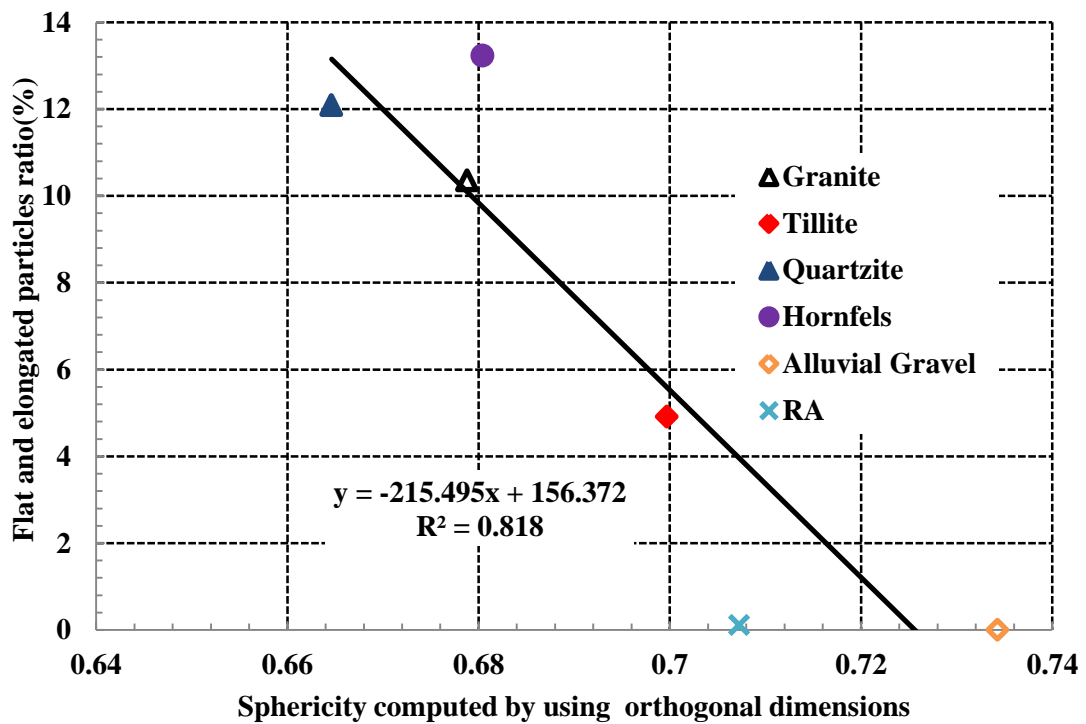


Figure 5.43: Flat and elongated particles ratio (proportional caliper set at 5:1) versus sphericity computed by using orthogonal dimensions.

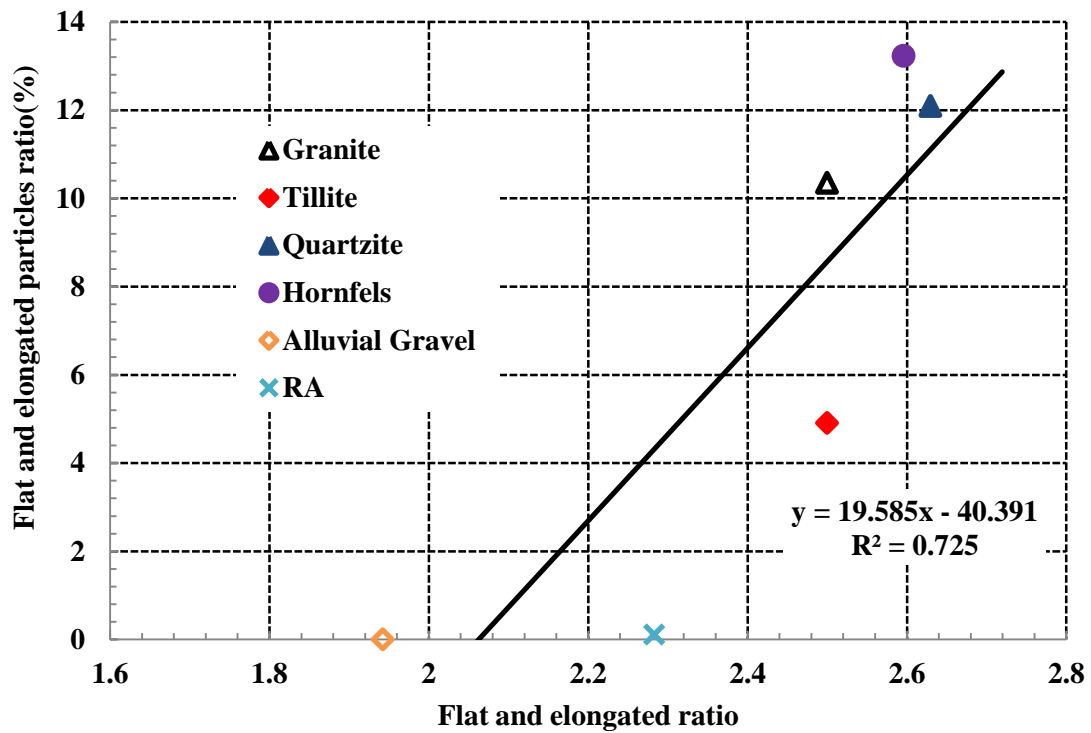


Figure 5.44: Flat and elongated particles ratio determined using the standard method (proportional caliper set at 5:1) versus the laser-based flat and elongated ratio.

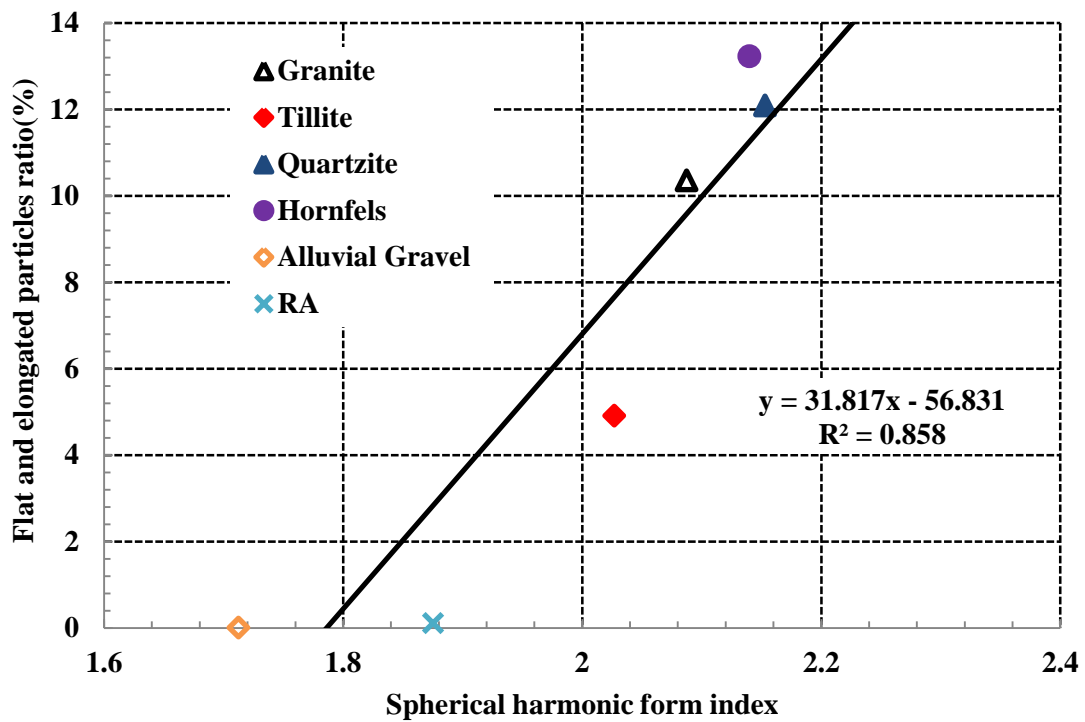


Figure 5.45: Flat and elongated particles ratio determined using the standard method (proportional caliper set at 5:1) versus spherical harmonic form index.

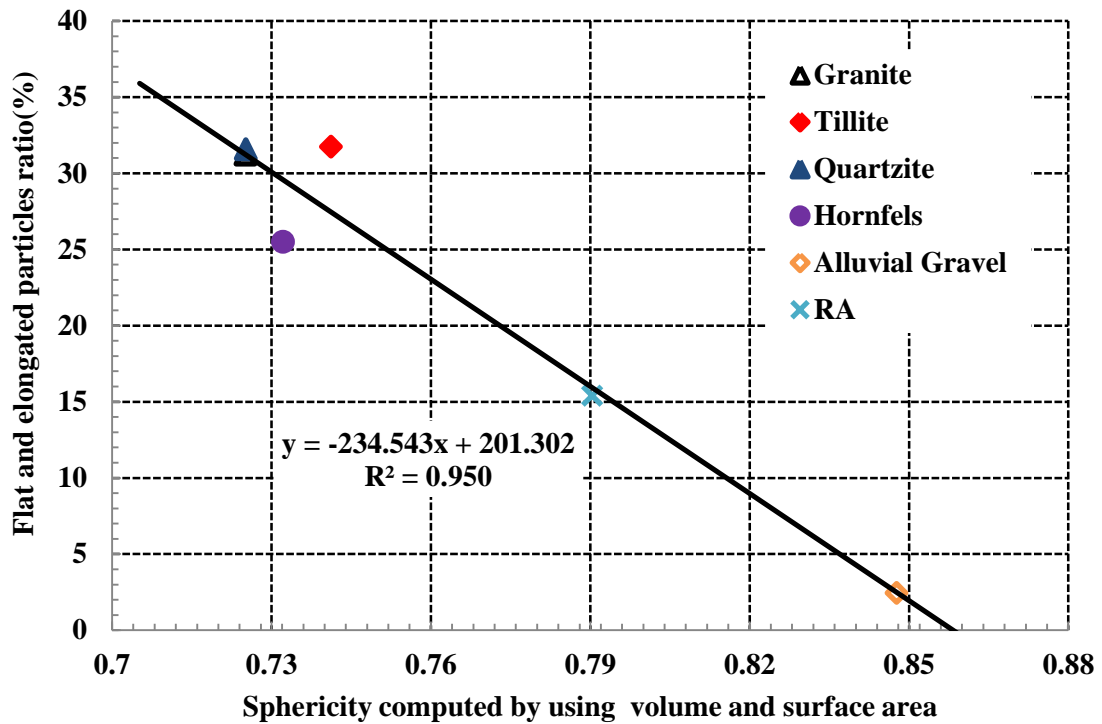


Figure 5.46: Flat and elongated particles ratio (proportional caliper set at 3:1) versus sphericity computed by using volume and surface area.

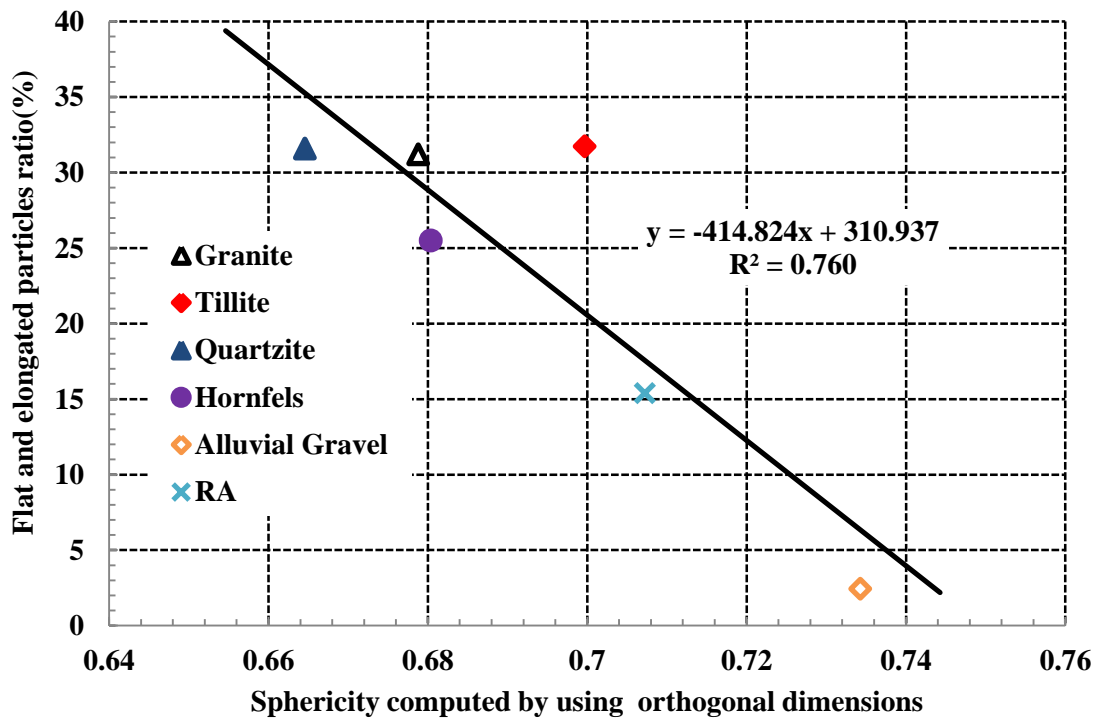


Figure 5.47: Flat and elongated particles ratio (proportional caliper set at 3:1) versus sphericity computed by using orthogonal dimensions.

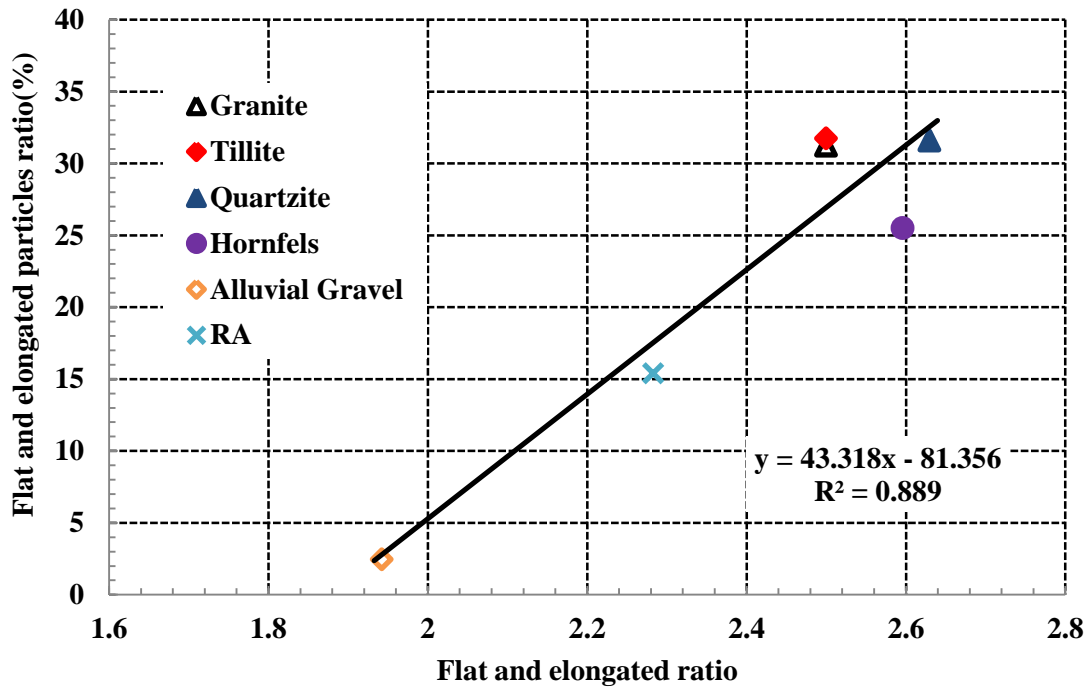


Figure 5.48: Flat and elongated particles ratio determined using the standard method (proportional caliper set at 3:1) versus laser-based flat and elongated ratio.

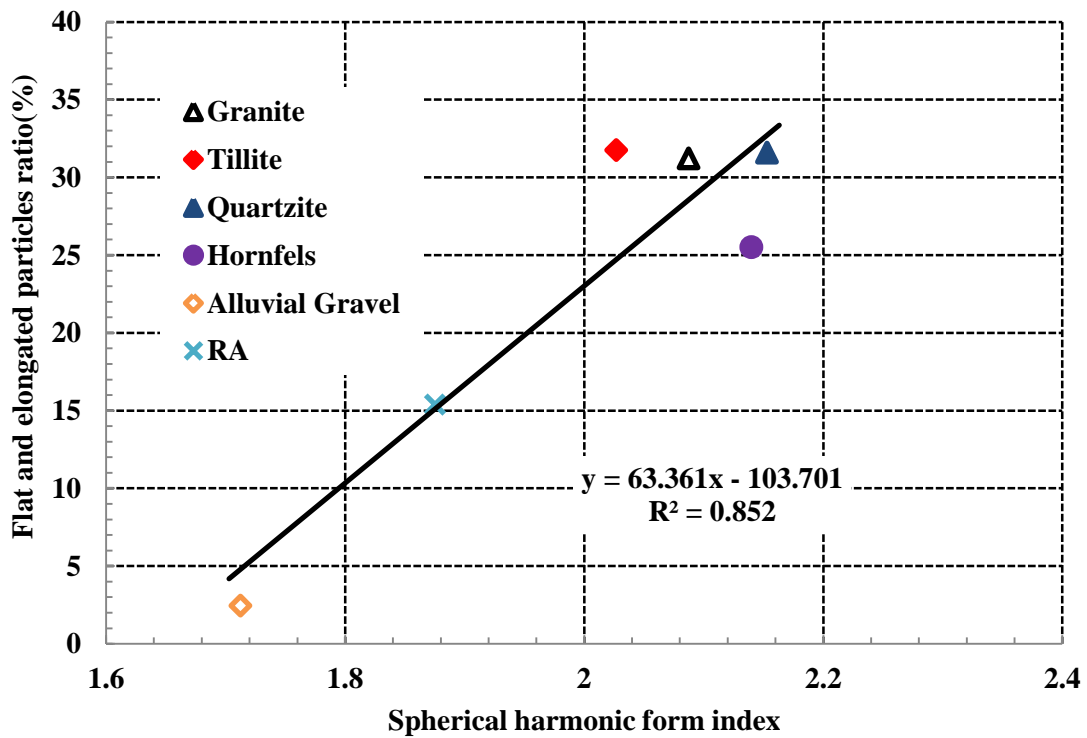


Figure 5.49: Flat and elongated particles ratio determined using the standard method (proportional caliper set at 3:1) versus spherical harmonic form index.

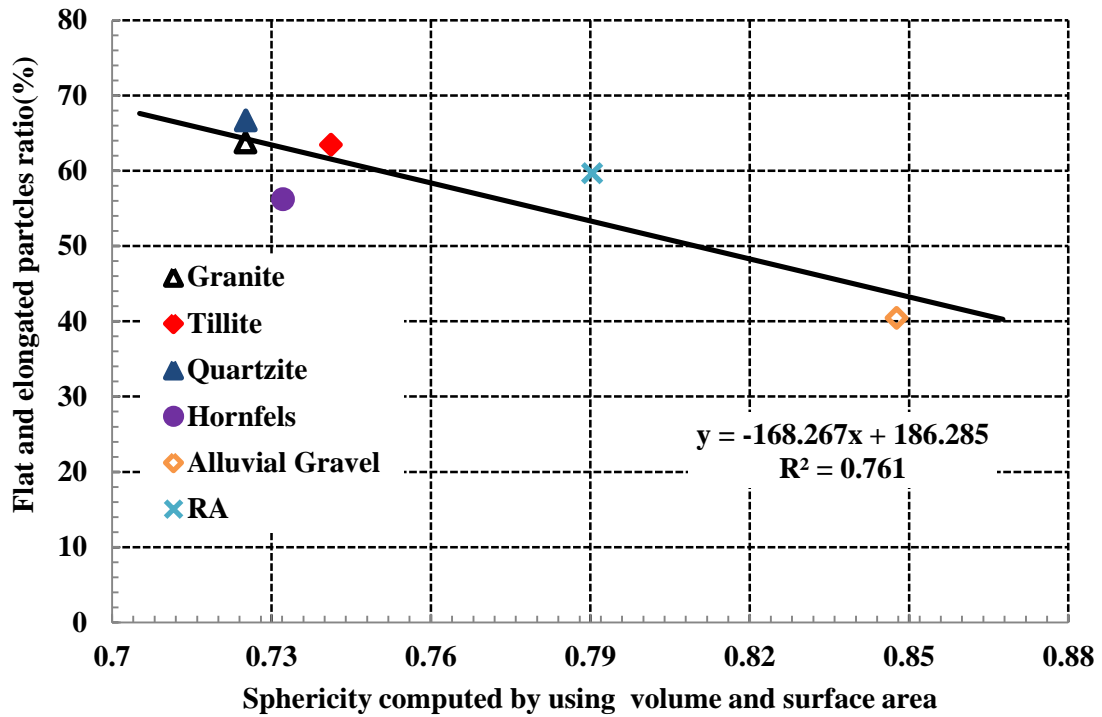


Figure 5.50: Flat and elongated particles ratio (proportional caliper set at 2:1) versus sphericity computed by using volume and surface area.

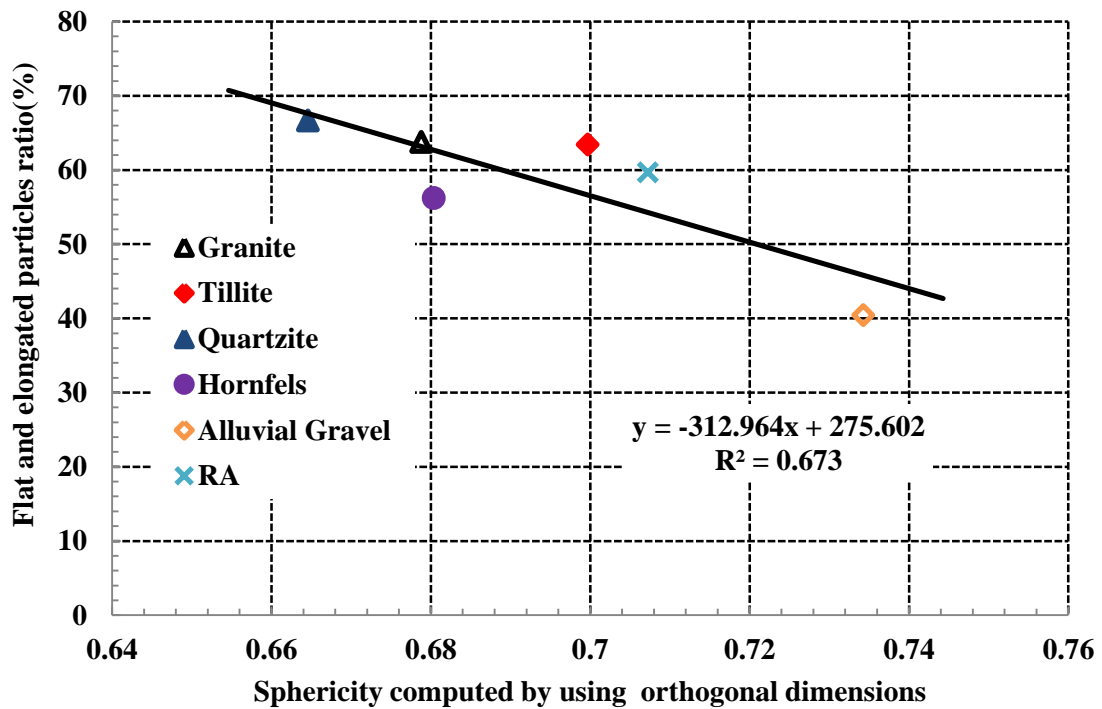


Figure 5.51: Flat and elongated particles ratio (proportional caliper set at 2:1) versus sphericity computed by using orthogonal dimensions.

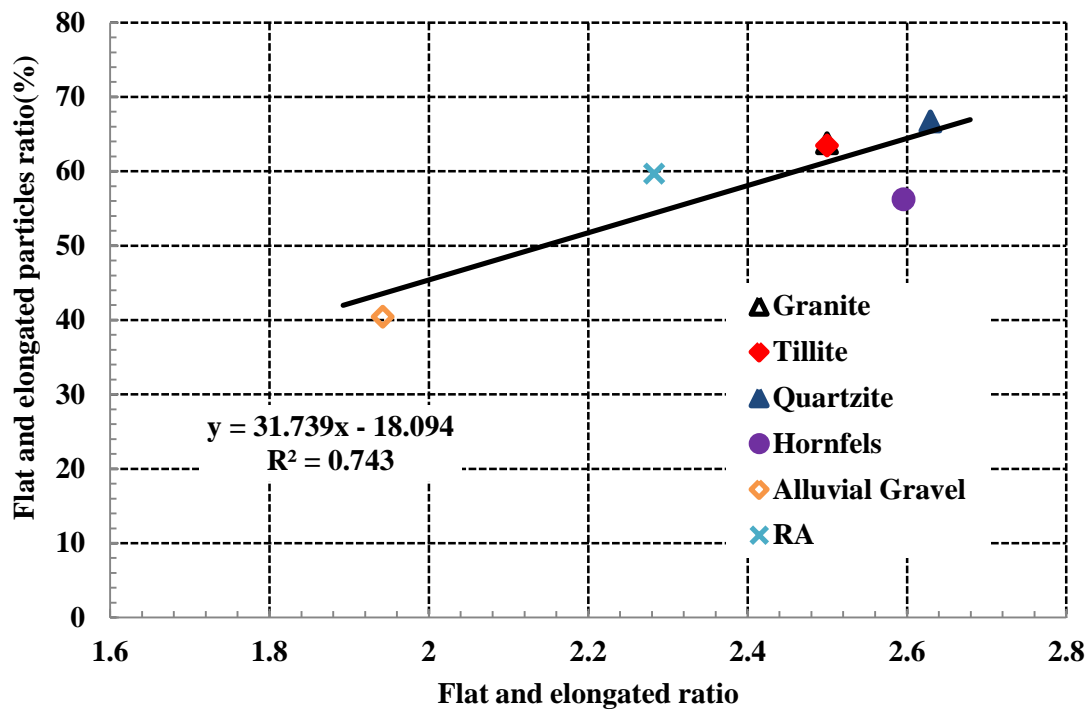


Figure 5.52: Flat and elongated particles ratio determined using the standard method (proportional caliper set at 2:1) versus laser-based flat and elongated ratio.

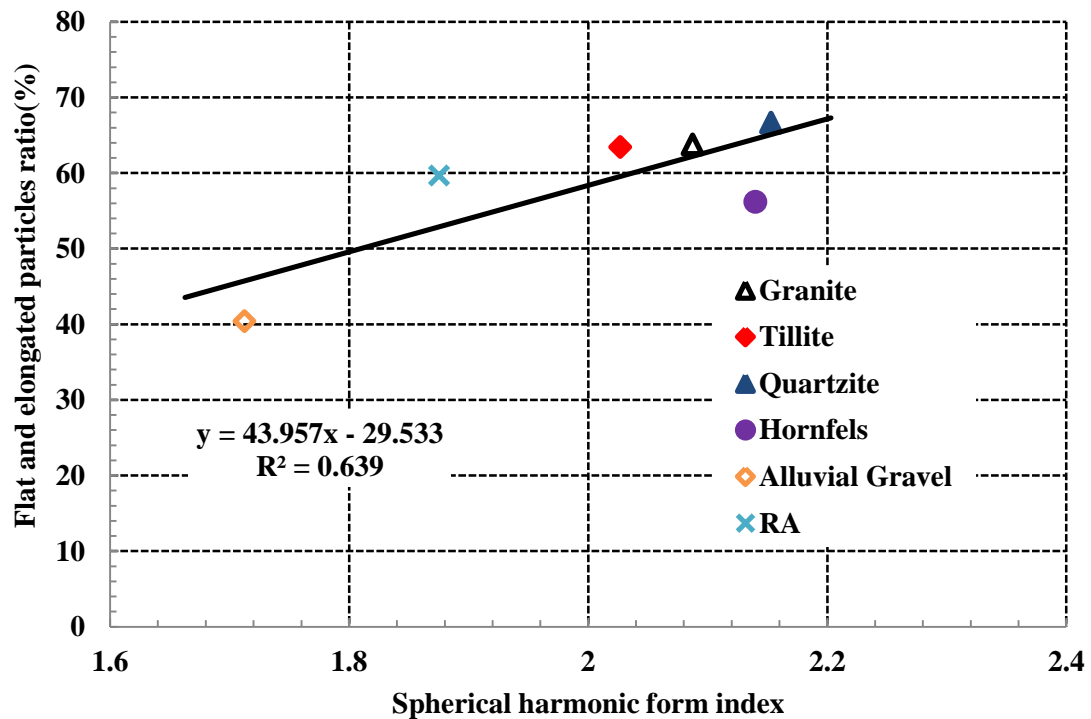


Figure 5.53: Flat and elongated particles ratio determined using the standard method (proportional caliper set at 2:1) versus spherical harmonic form index.

## 5.6 Selection of aggregates for pavement construction

Aggregate shape properties including form, angularity and surface texture influence the performance of pavements. Aggregate shape properties govern the behaviours of pavements including the ability to resist permanent deformation, shear resistance, skid resistance, stiffness properties, fatigue resistance, stability and workability of HMA mixes. Modern pavement design manuals and guidelines (i.e. SUPERPAVE) emphasise that the selection of aggregates should take into account whether the aggregates possess properties which improve pavement performance.

Equal-dimensional aggregate particles are preferred over the flat and elongated aggregates. Flat and elongated aggregate particles tend to lock up (resist re-orientation) resulting to difficulties in compaction. Furthermore, the tendency of flat and elongated particles to break during compaction may result into difficulties in achieving voids requirements in HMA mixes due to aggregate degradation which may change grading.

Angular aggregate particles are preferred over round-shaped aggregates. Angular aggregate particles improve mechanical interlock and provide better resistance to permanent deformation (rutting). Furthermore, the ability of angular aggregates to hold together when loaded increases the shear strength. On the other hand, round-shaped aggregates tend to slide over each other resulting into reduced shear strength.

Rough surface textured aggregate particles are preferred over smooth aggregates. Rough textured aggregates provided improve internal frictional compared to smooth textured aggregates. Internal friction properties improve shear resistance and ultimately the load carrying capacity.

Despite of the current knowledge on the influence of aggregate shape properties on the performance of the pavements, direct quantification of these shape properties using the current standard methods has been difficult. From the work presented in this study, it is evident that aggregate with varying shape properties can clearly be distinguished by using the laser scanning technique. This will enable selection of aggregates with desired properties to ensure improvements in the performance of pavements.

The laser scanning technique could be useful to ensure that the aggregates used for pavement construction have the desired shape properties. For example, one could use the laser scanning

technique at aggregate crushing plant to check periodically whether the crusher is still producing aggregates with desired shape properties. Wear and tear of the components of aggregate crushers results in the change or degradation of the shape properties and the quality of the produced aggregates. Checking the shape properties periodically with laser scanning technique could also be used as a tool for making a decision when to replace components of the crusher.

The application of laser scanning technique for determination of the aggregate shape properties has a benefit of improved accuracy. The laser scanning technique is suitable for research studies focusing towards improving the current understanding of the influence of aggregate shape properties on the performance of pavement. Furthermore, aggregate laser scanning can facilitate better understanding of the influence of the aggregates on the overall performance of pavements through numerical analysis and modelling of aggregates.

## **5.7 Summary**

This chapter presented the analysis of the laser scans data to determine indices to describe the aggregate shape properties. Two approaches were employed for analysis of the laser scans data. The first approach used the aggregate's physical properties (dimensions, surface area and volume) to compute sphericity and flat and elongated ratio indices. The second analysis approach employed spherical harmonic analysis of the laser scans data to compute aggregate form, angularity and surface texture indices.

Three different form indices were computed by using the aggregate's physical properties. These indices were the sphericity computed by using the surface area and volume of an aggregate particle, the sphericity computed by using the aggregate's orthogonal dimensions (longest dimension, intermediate dimension and shortest dimension) and the flat and elongated ratio computed by using the longest dimensions and the shortest dimension of an aggregate particle. The results showed that all the three indices were able to distinguish the form properties of the aggregates studied. The sphericity indices computed by using surface area and volume of an aggregate particle appeared to distinguish the form properties of the aggregates better. Possible explanation to this finding could be the ability of the laser scanning technique to measure the surface area and volume of irregular aggregate particles accurately.



Further analysis of the laser scans data were performed by using the spherical harmonic analysis technique. The spherical harmonic analysis technique was used to determine the aggregate form, angularity and surface texture indices. As part of the contribution of this study, a MATLAB™ code was developed to facilitate the analysis of the laser scans data by using the spherical harmonic analysis technique.

The form indices computed by using the aggregate's physical properties were further correlated with the form indices computed using spherical harmonic analysis technique. Good correlations were observed, indicating that both approaches could be used to determine the aggregate form indices. The time required to determine spherical harmonic form indices longer than the determination of the form indices based on the aggregate's physical properties. However, the spherical harmonic analysis technique has the advantage of being able to determine aggregate angularity and surface texture indices.

The laser-based form indices were further correlated with the flakiness index and flat and elongated particles ratio test results. Overall, the laser-based form indices correlated linearly with both, the flakiness index and flat and elongated particles ratio test results. However, in some cases the data points on the plots of the laser-based form indices versus the flakiness index and flat and elongated particles ratio test results appeared to be much scattered.

The study has demonstrated that various indices to describe the shape properties of aggregates could be determined by using the laser scanning technique. From the work presented in this study, it is evident that the limitations of the current standard methods could be addresses by employing advanced technologies such as the scanning technique.

## 6 CONCLUSIONS AND RECOMMENDATIONS

### 6.1 Conclusions

Aggregate shape properties including form, angularity and surface texture play a major role in the overall performance of pavements. Therefore, better characterisation of these properties is essential. This dissertation investigated improved techniques for determination of aggregate shape properties by using an advanced laser scanning technique. The following are the findings of the study:

- In this study, four different laser-based form indices were determined to describe form properties of aggregates from six different sources. The indices determined were; (a) sphericity computed using surface area and volume, (b) sphericity computed using three orthogonal dimensions, (c) flat and elongated ratio, and (d) spherical harmonic form index. Generally, all four form indices presented in this dissertation were able to rank the distribution of form properties of the six types of aggregates studied. The distribution of sphericity indices computed by using surface area and volume distinguished the form properties of the six types of aggregates clearer than other form indices. This could be due to the fact that the sphericity indices computed using volume and surface area represent the overall 3-D form of aggregates. On the other hand, the sphericity computed by using orthogonal dimensions and flat and elongated ratio indices are based on a the dimensions, which do not necessarily represent the overall 3-D form of aggregates;
- The spherical harmonic analysis technique was also used to determine angularity and surface texture indices for the six types of aggregate studied. A MATLAB<sup>TM</sup> code was developed for analysis of the laser scans data, using the spherical harmonic analysis technique to compute aggregate form, angularity and surface texture indices. The developed MATLAB<sup>TM</sup> code was found to be useful for analysis of the laser scans data to determine aggregate form, angularity and surface texture indices, and
- The spherical harmonic form indices correlated well with the laser-based form indices determined by using the aggregate's physical properties (volume, surface area, and orthogonal dimensions). The correlations between the spherical harmonic form indices with the sphericity indices computed by using volume and surface area were the best;
- Direct validation of the laser-based form indices was achieved by correlating with the results of the flakiness index and the flat and elongated particles ratio test, which are the

current standard methods used to evaluate form properties of aggregates. The laser-based form indices correlated linearly with both, the flakiness index and the flat and elongated particles ratio test results, and

- In chapter 4 Section 4.4, the laser scans data were used to determine the grading curves of the aggregates used in the study. The results compared well with the results of the current standard manual standard method (THM1 Method B4).

Based on the information contained in this dissertation, the following conclusions are drawn:

- The 3-D laser scanning technique is capable of measuring data required for the determination of form indices of coarse aggregates. This conclusion is supported by the laser scans data presented in chapter 4. This study has demonstrated that the laser scanning is a versatile technique for the determination of the various indices, based on 3-D data to describe the shape characteristics of aggregates, as well as the determination of the grading curves;
- Data obtained by using the 3-D laser scanning technique could be analysed using various approaches to determine indices describing the aggregate shape properties. This conclusion is supported by the results of correlations of various form indices performed in Chapter 5 Section 5.4. The coefficients of determination ( $R^2$ ) ranging between 0.459 and 0.861 were obtained. This is one of the major advantages of the laser scanning technique when compared with aggregate imaging;
- The sphericity indices computed by using volume and surface area properties appear to be more suitable in terms of describing the form of the aggregates than other form indices. This could be the result of the accurate measurement of the surface area and volume of the aggregates by using the laser scanning technique, and
- The capability of the spherical harmonic analysis technique to quantify all three aggregate shape properties (i.e. form, angularity, and surface texture) provides additional advantage over the use of the aggregate's physical properties.

Another major contribution of the dissertation is provision of a database of basic data to be used for on-going and future studies. Such studies include correlation of laser-based aggregate shape properties with pavement performance indicators, which was outside the scope of this dissertation. This data could also be used to investigate other techniques for quantification of aggregate shape properties. The laser scans data could also be used for numerical analysis and modelling of aggregates.

## 6.2 Recommendations

Based on the information contained in this dissertation, the following recommendations are made:

- This dissertation provided basic concepts for analysis of data of scanned aggregate particles. Limited types of aggregates were studied, including four types of crushed aggregates, RA and alluvial gravel. Although the analyses presented could differentiate the shape properties of the types of aggregates studied, further validation using aggregate materials from different sources is required. Future studies should for instance include RA and alluvial gravel from different sources, as well as other types of crushed aggregates and slag materials;
- Four laser-based form indices were used in this study, and their results appeared to be consistent, hence providing more confidence of the ability of the laser scanning technique for determination of the form of aggregates. On the other hand, angularity and surface texture were determined by using a spherical harmonic analysis technique only. Therefore, future studies should consider employing other analysis techniques such as wavelet analysis to validate the results obtained, and
- Lastly, further work is needed to correlate the laser-based aggregate shape indices with pavement performance indicators. Such studies may include:
  - Correlations of laser-based form indices with performance parameters of aggregates used in pavements;
  - Use of aggregate shape properties as basis for estimation of voids in compacted aggregates, and
  - Packing characteristic of different aggregate types, in relation to their shape properties.

## 7 REFERENCES

Al-Rousan T., Masad, E., Tutumluer, E. Pan, T. 2007. Evaluation of image analysis techniques for quantifying aggregate shape characteristics. *Construction and Building Materials Vol 21*, pp. 978-990.

Anochie-Boateng, J., Komba, J., Mukalenga, N., and Amrita, M. 2010. Evaluation of 3-D laser device for characterizing shape and surface properties of aggregates used in pavements. *29th Annual Southern African Transportation Conference*, Pretoria, August 2010.

Anochie-Boateng, J and Komba, J. 2010. Laser scanning protocol for determining aggregate shape and surface properties. TECHNICAL REPORT No: CSIR/BE/IE/IR/2010/0061/B

Anochie-Boateng, J. Komba, J. and Tutumluer, E. 2011a. Three-dimensional laser-based measurement of mineral aggregate surface area for South African hot-mix asphalt mixtures. *TRB 90th Annual Conference*, Washington D.C, USA, January 2011.

Anochie-Boateng, J., Komba, J., O'Connell, J. 2011b. Laser-based approach for determining flakiness index of aggregates used in pavements. *30th Annual Southern African Transportation Conference*, Pretoria, July 2011.

Anochie-Boateng, J. Komba, J. and Mvelase G. 2011c. Advanced and Automated Laser-based Technique to Evaluate Aggregates. IRF International Road Congress "Innovation in Road Infrastructure". Moscow, Russia. 22-24 November 2011.

Anochie-Boateng, J., Komba, J. and Tutumluer, E. 2012. Aggregate Surface Areas Quantified Through Laser Measurements for South African Asphalt Mixtures. *Journal of Transportation Engineering, ASCE*. Vol. 1(137).

Asphalt Institute. 1996. Superpave Mix Design. Superpave Series No.2 (SP-2). U.S.A.

Arasan, S., Yenera, E., Hattatoglu, F., Hinislioglu, S. and Akbuluta, S. 2011. Correlation between Shape of Aggregate and Mechanical Properties of Asphalt Concrete. *Road Pavement Material and Design*. Vol. 12, No. 2.

Arfken, B.G and Webber, H.J. Mathematical methods for physicists. 4th Edition, Academic press, San Diego. 1995.

ASTM D3398-00. 2006 Standard Test Method for Index of Aggregate Particle Shape and Texture. *Annual Book of ASTM Standards*, West Conshohocken, PA.

ASTM D 5821. 2006. Standard test method for determining the percentage of fractured particles in coarse aggregate. *Annual Book of ASTM Standards*, West Conshohocken, PA.

ASTM D 4791. 2010. Standard test method for flat particles, elongated particles, or flat and elongated particles in coarse aggregate. *Annual Book of ASTM Standards*, West Conshohocken, PA.

Barksdale, R.D., Pollard, C.O. Siegel, T. and Moeller, S. 1992. Evaluation of the Effect of Aggregates on Rutting and Fatigue of Asphalt. *Reserch Report, DOT Project 8812, GA Tech E20-835, Georgia Institute of Technology*, February 1992.

Barksdale, R. D., and Itani, S. Y.1994. Influence of Aggregate Shape on Base Behavior. *Transportation Research Record 1227*. Transportation Research Board, National Research Council, Washington, D.C. pp. 171-182.

Button, J. W., Perdomo, D., and Lytton, R. L. Influence of Aggregate on Rutting In Asphalt Concrete Pavements. *Transportation Research Record 1259*. Transportation Research Board, National Research Council, Washington D.C. pp. 141-152.

Chen, J.S., Lin, K.Y. and Chang, M.K. 2005. Influence of coarse aggregate shape on the strength of asphalt concrete mixtures. *Journal of the Eastern Asia Society for Transportation Studies*. Vol. 6, pp. 1062 - 1075

Collis, L. and Fox, R.A. 1985. Aggregates: Sand, Gravel & Crushed rock aggregates for construction purposes. *Geological Society of London. Engineering Geology Special Publication No 1*.

CSRA. 1998. Standard Specifications for Road and Bridge Work for State Road Authorities. South African Institution of Civil Engineers. South Africa.

DOT. 1987. Design and Use of Hot-Mix Asphalt in Pavements. Pretoria Department of Transport. Technical Recommendations for Highways; Draft TRH 8, 1987.

Garboczi, E.J. 2002. Three-dimensional mathematical analysis of particle shape using X-ray tomography and spherical harmonics: Application to aggregates used in concrete. *Concrete and Cement Research*, Vol. 32, No. 10, pp. 1621-1638.

Hayakawa, Y. and Oguchi T (2005). Evaluation of gravel sphericity and roundness based on surface-area measurement with a laser scanner. *Journal of Computer and Geosciences*, Vol 31(2005) pp. 735-741.

Kim, H., C.T. Haas, A.F. Rauch, and C. Browne. 2001. A Prototype Laser Scanner for Characterizing Size and Shape Parameters in Aggregates. *Proceedings of the 9<sup>th</sup> Annual Symposium, International Center for Aggregates Research*, Austin, TX.

Kim, H., C.T. Haas, A.F. Rauch, and C. Browne. 2002. Wavelet based Three-Dimensional Descriptors of Aggregate Particles. *Transportation Research Record 1787*. Transportation Research Board of the National Academies, Washington, DC, pp. 109–116.

Krumbein, W. C. 1941. Measurement and geological significance of shape and roundness of sedimentary particles. *Journal of Sedimentary Petrology*, 11(2) pp. 64-72.

Lin, C.L., and Miller, J.D. (2005), 3D Characterization and Analysis of Particle Shape Using X-Ray Microtomography (XMT). *Powder Technology 154*, pp. 61-69.

Masad, E. 2003. The Development of a Computer Controlled Image Analysis System for Measuring Aggregate Shape Properties. National Cooperative Highway Research Program NCHRP-IDEA Project 77 Final Report. Transportation Research Board, National Research Council, Washington, D.C.

Masad, E. 2004. Aggregate Imaging System (AIMS): Basics and applications. Pilot Implementation of the Aggregate Imaging System. Report 5-1707-01-1. Texas Transportation Institute.

Masad, E. and Button, J.W. 2000. Unified imaging approach for measuring aggregate angularity and texture. *International Journal of Computer-Aided Civil and Infrastructure Engineering – Advanced Computer Technologies in Transportation Engineering*, 15(4): 273-280.

Masad, E., Al-Rousan, T., Button, J., Little, D. and Tutumluer, E. 2007. Test Methods for Characterizing Aggregate Shape, Texture, and Angularity. NCHRP REPORT 555. TRB, Washington, D.C.

Masad, E., Olcott, D., White, T., and Tashman, L. 2001. Correlation of Imaging Shape Indices of Fine Aggregate with Asphalt Mixture Performance. *Transportation Research Record, No. 1757, TRB*, National Research Council, Washington, D.C. pp. 148-156.

Masad, E., Saadeh, S., Al-Rousan, T., Garboczi, E. and Little, D. 2005. Computation of particle surface characteristics using optical and X-ray CT images. *Computational Materials Science* 34(4) 406–424.

Prowell, B.D., Zhang, J. and Brown, E.R. 2005. Aggregate Properties and the Performance of Superpave Designed Hot Mix Asphalt. NCHRP Report Number 539. Transportation Research Board.

Pan, T. 2006. Investigation of Coarse Aggregate Morphology Affecting Hot Mix Behavior Using Image Analysis. PHD Thesis, University of Illinois at Urbana-Champaign.

Pan, T., and Tutumluer, E. and Carpenter, H. 2005. Effect of Coarse Aggregate Morphology on the Resilient Modulus of Hot Mix Asphalt. *TRB 84th Annual Conference*, Washington D.C, USA, January 2005.

Pan, T., Tutumluer, E. and Anochie-Boateng, J. 2006. Aggregate Morphology Affecting Resilient Behavior of Unbound Granular Materials. *Transportation Research Record, No. 1952, TRB*, National Research Council, Washington, D.C. pp. 12-20.

Pan, T., and Tutumluer, E. 2010. Imaging-based direct measurement of aggregate surface area and its application in asphalt mixture design. *International Journal of Pavement Engineering, Volume 11, Issue 5*, pp. 415-428



PAVEMENT INTERACTIVE. 2012. Coarse Aggregate Angularity. Pavement Tools Consortium, ([www.pavementinteractive.com](http://www.pavementinteractive.com)), University of Washington, (accessed on 11 June 2012).

Rahal, K. 2007. Mechanical properties of concrete with recycled coarse aggregate. *Journal of Building and Environment*. Vol 42 pp. 407–415.

Rao, C., Tutumluer, E., and Kim, I-T. 2002. Quantification of Coarse Aggregate Angularity based on Image Analysis,” *Transportation Research Record, No. 1787, TRB*, National Research Council, Washington, D.C. pp. 117-124.

Rao, C., Pan, T., and Tutumluer, E. 2003. Determination of Coarse Aggregate Surface Texture Using Image Analysis,” *Proceedings of the Pavement Mechanics Symposium at the 16th ASCE Engineering Mechanics Division Conference*, Seattle, Washington, July 16-18, 2003.

Rao, C., Tutumluer, E., and Stefanski, J. A. 2001. Coarse Aggregate Shape and Size Properties Using a New Image Analyzer. *ASTM Journal of Testing and Standard, Vol. 29, No. 5*, pp. 79-89.

Rao, C., Tutumluer, E., and Kim, I-T. 2002. Quantification of Coarse Aggregate Angularity based on Image Analysis. *Transportation Research Record (TRB)*, National Research Council, No. 1787, Washington, D.C., pp. 117-124.

Rittenhouse, G. 1943. A visual method of estimating two dimensional sphericity. *Journal of Sedimentary Petrology*, 13(2), pp. 79-81.

Saeed, A., Hall, J., and Barker, W. 2001. Performance-related tests of aggregates for use in unbound pavement layers. *NCHRP Report 453, TRB, National Research Council*, Washington, D.C.

SANS 3001-AG4. 2009. Determination of the flakiness index of coarse aggregates. SABS.

SBM. 2012. Effects of crusher operation on coarse aggregates shape. Downloadable from SBM website:<http://www.crusherasia.com/blog/effect-of-crusher-operation-on-coarse-aggregate-shape.html>. Accessed on 26 July 2012.

Taute, A., Verhaeghe, BMJA and Visser, AT. 2001. Interim guidelines for the design of Hot-Mix Asphalt in South Africa. Prepared as part of the Hot-Mix Asphalt Design Project. Pretoria. South Africa.

TMH 1. Standard Methods for Road Construction Materials. 1986. DoT, Pretoria, South Africa.

TMH 5. Sampling Methods for Road construction Materials. 1981. CSRA, Pretoria, South Africa.

TRH 21. Technical Recommendations for Highways. 2009. Hot mix recycled asphalt. SABITA, South Africa.

Tutumluer, E and Pan, T 2008. Aggregate Morphology Affecting Strength and Permanent Deformation Behavior of Unbound Aggregate Materials. *Journal of Materials in Civil Engineering*. Vol. 20, No. 9, pp. 617-627.

Tutumluer, E., Pan, T. and Carpenter S.H. 2003. Investigation of Aggregate Shape Effects on Hot Mix Performance using image analysis approach. Final Project Report on the Transportation Pooled Fund Study, TPF-5 (023). Civil Engineering Studies UILU-ENG-2005-2003, University of Illinois Urbana-Champaign, Urbana.

Tutumluer, E., Rao, C., and Stefanski, J. A. 2000. Video Image Analysis of Aggregates. Final Project Report, FHWA-IL-UI-278. Civil Engineering Studies UILU-ENG-2000-2015, University of Illinois Urbana-Champaign, Urbana.

Wang, L. B., Frost, J. D., and Lai, J. S. 1998. Fourier morphological descriptors of aggregate profiles. *Proc., 2nd International Conference on Imaging Technologies*, Davos, Switzerland, pp. 76-87.

Wang, L., Lane, D.S., Lu, Y. and Druta, C. 2008. Portable Image Analysis System For Characterizing Aggregate Morphology. Report No. FHWA/VTRC 08-CR 11. Virginia Transport Research Council.

Wang, L., X. Wang, L. Mohammad, and C. Abadie. 2005. Unified Method to Quantify Aggregate Shape Angularity and Texture Using Fourier Analysis. *Journal of Materials in Civil Engineering*, Vol.17, No. 5, pp. 498-504.

Yeggoni, M., Button J.W. and Zollinger D.G. 1994. Influence of Coarse Aggregates Shape and Surface Texture on Rutting of Hot Mix Asphalt. *Research Report 1244-6, Texas Transportation Institute, Texas A&M University System*, College Station, October 1994.

## 8 APPENDIX A: AGGREGATE SCAN RESULTS

**Table 8.1: Scan results of 19.0 mm granite aggregate particles.**

19.0 mm Sieve								
Particle No.	Dimensions (mm)			Centre of mass (mm)			Surface area (mm <sup>2</sup> )	Volume (mm <sup>3</sup> )
	d <sub>L</sub>	d <sub>I</sub>	d <sub>S</sub>	X	Y	Z		
1	39.22	31.87	16.10	-0.42	2.89	13.52	2558.46	7851.52
2	31.35	22.42	19.87	-1.13	2.13	15.66	2146.07	6699.91
3	34.65	27.34	18.50	-0.71	0.84	15.47	2524.83	8805.80
4	35.88	24.43	23.02	-1.48	1.39	16.13	2476.04	8460.95
5	34.01	28.49	19.31	0.62	2.51	14.30	2512.79	8635.04
6	28.02	22.99	21.35	0.38	-0.32	15.95	2035.34	6866.36
7	32.84	22.00	21.17	-1.69	1.49	15.16	1986.29	6128.76
8	26.78	26.33	18.01	-1.36	-0.44	14.85	1880.01	6082.07
9	30.57	21.01	19.76	-2.19	1.04	15.74	1919.39	6102.64
10	24.92	22.39	19.97	-0.90	1.81	15.32	1701.03	5380.24
11	37.00	28.36	15.00	0.66	1.50	13.26	2406.86	7387.02
12	32.56	23.58	14.82	0.37	2.93	13.17	1918.29	5462.13
13	34.41	28.82	18.49	-0.30	2.13	13.93	2231.51	6486.52
14	47.06	29.42	17.29	0.45	0.08	14.59	3298.66	11197.21
15	34.51	25.32	17.23	1.43	0.05	14.30	2331.67	7483.74
16	31.80	30.99	14.39	2.93	-1.44	13.79	2087.39	5896.26
17	48.88	25.45	18.03	1.83	0.05	14.12	2975.01	9593.82
18	46.08	31.87	18.42	3.77	-0.93	14.11	3179.23	9820.76
19	60.25	32.62	21.95	-1.35	-2.22	15.20	3888.95	13142.29
20	52.56	30.31	21.73	-4.05	-1.17	15.71	3149.90	10292.09
21	41.45	27.16	14.34	-0.70	1.74	13.38	2491.10	6882.31
22	37.39	30.87	15.77	-0.35	1.47	13.32	2229.72	5972.80
23	42.18	32.10	13.59	1.64	1.50	13.11	2684.04	6691.75
24	41.44	26.37	12.08	0.43	2.01	12.07	2260.93	5714.88
25	44.97	30.28	9.86	-0.03	1.10	11.07	2641.25	5574.31
26	54.29	30.05	9.45	-1.68	1.82	11.19	2761.07	5458.15
27	44.64	26.68	8.57	-2.00	1.37	10.64	2278.43	4344.42
28	44.55	28.31	9.34	-2.12	2.59	11.04	2505.89	5066.99
29	42.92	30.25	8.80	0.62	1.76	10.69	2053.62	3090.84
30	37.62	33.57	8.99	1.78	2.97	10.36	1799.19	2569.85

d<sub>L</sub> = Longest dimension, d<sub>I</sub> = Intermediate dimension and d<sub>S</sub> = Shortest dimension.

**Table 8.2: Scan results of 13.2 mm granite aggregate particles.**

13.2 mm Sieve								
Particle No.	Dimensions (mm)			Centre of mass (mm)			Surface area (mm <sup>2</sup> )	Volume (mm <sup>3</sup> )
	d <sub>L</sub>	d <sub>I</sub>	d <sub>S</sub>	X	Y	Z		
1	24.60	19.01	14.28	-0.86	0.29	13.29	1152.12	2836.57
2	29.56	21.32	17.94	-0.89	-0.71	14.02	1632.45	4329.93
3	23.16	22.27	18.38	0.46	1.14	13.96	1473.53	3965.38
4	23.37	19.10	17.98	3.87	1.80	14.87	1529.92	4151.22
5	23.39	20.95	16.95	1.82	-0.47	13.99	1380.64	3680.29
6	19.77	18.33	14.10	-2.40	-0.98	13.58	1066.58	2372.28
7	25.64	19.51	18.30	1.98	-0.16	15.15	1457.96	4019.48
8	25.02	21.07	17.92	-0.89	-2.74	13.69	1358.74	3016.46
9	22.05	18.05	12.96	-0.44	-0.45	12.41	1038.63	2333.14
10	20.72	20.41	15.04	-0.41	1.27	13.59	1214.91	2917.20
11	31.21	17.40	16.23	-0.75	-3.09	14.38	1508.34	3690.76
12	31.54	21.55	14.11	0.88	-0.76	13.30	1710.53	4472.12
13	31.08	20.65	18.50	1.47	-2.05	14.07	1665.41	4590.55
14	28.00	22.16	16.59	0.93	-2.05	14.33	1571.81	4133.94
15	28.40	22.87	14.36	-1.93	1.33	13.32	1392.40	3225.20
16	28.43	20.46	13.81	0.11	0.33	13.44	1390.17	3546.14
17	34.13	22.14	14.44	0.40	-1.11	12.83	1610.56	3848.36
18	27.36	22.91	8.81	0.98	-2.27	10.98	1181.18	2267.53
19	24.03	20.30	13.84	1.32	1.36	12.26	1232.06	1774.06
20	26.81	18.34	13.55	-2.59	0.80	12.46	1124.02	1397.28
21	32.25	21.89	16.78	3.36	2.94	13.30	1768.23	4789.89
22	48.12	24.52	12.72	2.16	1.90	12.78	2325.73	5892.25
23	39.48	26.88	10.65	0.18	1.26	11.39	1734.72	2884.92
24	40.69	17.43	13.53	0.28	-0.46	13.01	1600.52	3395.42
25	35.41	24.66	8.96	0.65	-1.01	10.60	1576.85	2445.39
26	41.26	22.29	9.65	3.01	2.02	10.76	1873.18	3223.28
27	41.05	27.95	11.04	3.15	0.38	11.08	1986.77	3365.83
28	30.91	26.82	8.38	1.44	0.39	10.57	1398.58	2337.58
29	39.41	25.55	8.03	-2.85	2.75	10.77	1527.55	2346.43
30	39.90	18.79	15.02	0.14	-2.22	14.56	1291.54	1714.43

d<sub>L</sub> = Longest dimension, d<sub>I</sub> = Intermediate dimension and d<sub>S</sub> = Shortest dimension.

**Table 8.3: Scan results of 9.5 mm granite aggregate particles.**

9.5 mm Sieve								
Particle No.	Dimensions (mm)			Centre of mass (mm)			Surface area (mm <sup>2</sup> )	Volume (mm <sup>3</sup> )
	d <sub>L</sub>	d <sub>I</sub>	d <sub>S</sub>	X	Y	Z		
1	18.40	12.51	11.54	-0.62	-1.04	11.37	631.98	1108.50
2	17.03	12.22	9.85	-1.18	-1.29	11.04	547.66	864.75
3	17.53	14.94	12.03	0.41	0.89	11.35	668.12	1228.40
4	18.48	13.90	11.26	-1.55	-0.64	11.24	660.26	1152.04
5	17.03	14.54	10.28	-0.76	-0.40	10.89	624.39	1078.11
6	13.99	12.70	10.22	-1.42	-0.76	10.74	525.04	797.24
7	14.31	12.97	11.39	-0.51	-1.48	11.28	524.73	844.97
8	13.33	10.42	10.57	-1.36	-1.51	10.22	422.92	568.04
9	13.32	11.94	10.98	-0.34	-0.75	10.72	459.36	701.60
10	11.45	10.91	9.15	-1.01	-1.58	10.35	387.84	546.05
11	21.37	13.34	9.41	-1.54	0.26	10.19	658.22	974.04
12	21.67	14.87	9.29	-1.87	0.17	10.64	778.52	1152.21
13	22.32	11.19	9.81	-0.84	0.30	10.90	668.44	1045.57
14	19.17	10.48	9.16	-1.67	-0.63	10.25	566.84	828.12
15	20.67	14.72	8.60	-2.94	-0.24	10.22	753.40	1112.40
16	17.34	13.31	6.40	-0.12	-0.08	9.57	460.67	554.56
17	21.16	12.20	8.85	-2.37	-1.53	10.03	575.42	792.35
18	20.04	16.60	9.31	-1.05	-0.28	10.20	687.71	1040.16
19	22.82	13.30	8.61	0.00	-1.21	10.03	553.90	731.02
20	15.35	13.04	8.51	-1.31	-0.58	9.80	495.98	685.07
21	27.01	15.21	8.93	0.86	-1.03	10.30	793.87	1174.09
22	40.84	13.63	12.01	0.31	0.19	11.59	1356.92	2515.76
23	33.45	17.28	13.36	-1.91	0.87	12.03	1209.46	2097.23
24	36.51	16.76	10.31	-1.50	0.69	12.35	1386.06	2408.34
25	32.99	13.86	7.27	-2.26	-1.03	9.88	977.56	1173.92
26	32.11	16.43	6.81	-0.53	-1.62	9.84	943.59	1033.47
27	21.65	16.56	6.19	-0.49	0.04	9.07	625.00	635.34
28	26.86	15.99	5.40	-1.30	-0.38	9.28	774.43	806.69
29	21.61	17.07	5.69	0.75	-0.85	9.12	600.11	593.81
30	25.87	16.67	5.31	1.13	-0.28	9.19	735.06	742.82

d<sub>L</sub> = Longest dimension, d<sub>I</sub> = Intermediate dimension and d<sub>S</sub> = Shortest dimension.

**Table 8.4: Scan results of 6.7 mm granite aggregate particles.**

6.7 mm Sieve								
Particle No.	Dimensions (mm)			Centre of mass (mm)			Surface area (mm <sup>2</sup> )	Volume (mm <sup>3</sup> )
	d <sub>L</sub>	d <sub>I</sub>	d <sub>S</sub>	X	Y	Z		
1	15.34	10.35	10.20	0.55	-0.74	10.20	371.97	439.09
2	13.62	8.16	8.87	-0.31	-0.63	10.07	349.27	438.98
3	16.07	8.66	8.46	-0.46	-0.89	10.21	410.98	582.85
4	14.07	10.98	8.90	-0.75	-1.12	9.95	377.77	473.98
5	13.30	9.66	9.95	-0.53	-0.82	10.82	384.86	562.76
6	13.31	9.91	7.84	-0.85	-0.08	9.66	345.12	443.52
7	15.07	12.38	9.09	-1.71	-0.67	10.23	405.11	539.75
8	13.33	11.33	8.50	-1.02	1.17	9.72	380.02	452.43
9	12.14	9.47	9.27	-0.52	-1.24	10.25	336.84	407.41
10	11.65	10.97	9.25	-0.29	-0.14	10.09	320.95	376.86
11	21.22	11.45	8.36	0.36	-1.50	10.17	550.55	750.12
12	16.63	8.42	9.96	-0.44	-1.35	10.73	454.39	638.46
13	18.59	10.00	9.31	-1.17	-0.79	9.83	445.85	529.04
14	16.49	9.23	8.88	-1.44	-1.79	10.15	403.89	454.89
15	15.17	11.65	7.64	-0.61	-0.61	9.85	413.14	542.75
16	13.38	10.31	6.87	-0.72	-0.74	9.17	329.72	375.56
17	17.60	11.53	6.74	-2.92	-1.33	9.48	463.63	569.40
18	17.70	10.41	8.31	-1.14	0.93	9.97	441.11	547.34
19	14.54	10.02	8.39	-0.18	-1.22	9.62	374.45	442.42
20	13.73	9.51	6.61	-0.66	-0.42	9.21	336.54	391.37
21	17.91	10.08	5.86	-2.11	-0.56	9.37	394.56	442.60
22	20.04	9.50	6.06	-2.07	-0.34	9.25	405.01	417.48
23	17.30	10.73	6.59	0.10	0.07	9.48	408.74	482.34
24	24.30	10.56	5.76	-2.79	-1.70	9.28	531.69	621.67
25	18.08	12.05	5.52	-1.28	-0.62	8.77	421.50	394.23
26	24.45	12.71	4.51	-1.88	0.25	8.75	532.43	532.99
27	16.47	12.15	4.09	-1.84	-0.35	8.55	372.63	325.47
28	22.49	10.49	4.48	-0.50	-0.20	8.83	454.97	419.39
29	24.81	11.06	4.79	-0.63	-1.04	8.80	449.67	364.49
30	20.15	13.82	5.14	-1.12	-0.52	8.30	406.14	284.26

d<sub>L</sub> = Longest dimension, d<sub>I</sub> = Intermediate dimension and d<sub>S</sub> = Shortest dimension.

**Table 8.5: Scan results of 4.75 mm granite aggregate particles.**

4.75 mm Sieve								
Particle No.	Dimensions (mm)			Centre of mass (mm)			Surface area (mm <sup>2</sup> )	Volume (mm <sup>3</sup> )
	d <sub>L</sub>	d <sub>I</sub>	d <sub>S</sub>	X	Y	Z		
1	9.14	6.57	4.95	-1.25	-0.48	8.28	142.53	114.35
2	9.38	7.36	5.35	-0.67	0.26	8.47	164.37	147.97
3	10.51	6.90	6.25	-2.00	-1.45	8.85	190.02	179.90
4	10.55	6.77	6.30	-0.63	-0.27	8.69	192.55	186.92
5	9.31	8.25	6.39	-0.96	-0.65	8.75	187.34	167.94
6	11.46	6.80	6.44	0.29	-1.34	9.07	207.07	195.04
7	9.75	6.55	5.48	-0.25	-1.37	8.41	151.69	127.50
8	9.21	6.24	5.06	-1.02	-0.54	8.29	137.10	118.66
9	6.99	6.20	5.73	-1.83	-1.78	8.63	134.56	118.41
10	8.62	7.43	5.31	-0.91	-1.02	8.12	146.92	119.62
11	9.79	8.06	4.85	-1.22	-0.72	8.62	179.12	157.97
12	12.17	5.72	5.09	-0.75	-0.65	8.63	188.58	174.66
13	9.63	8.56	4.64	-0.55	-0.32	8.13	167.67	139.06
14	12.12	5.81	6.08	-1.08	-1.85	8.68	194.61	183.27
15	11.91	8.38	5.72	-0.88	-1.59	8.44	201.64	177.88
16	8.13	7.80	4.56	-0.05	-0.44	8.28	154.17	129.05
17	10.73	6.99	4.86	-1.23	-0.67	8.38	169.85	144.20
18	10.28	7.57	5.67	-1.76	-1.10	8.48	180.07	152.54
19	9.98	7.24	5.47	-1.06	-1.48	8.29	165.79	145.58
20	9.72	7.57	4.58	-0.34	-0.64	8.29	148.68	126.88
21	15.98	8.64	5.35	-0.79	-0.79	8.85	284.21	275.58
22	12.43	6.51	4.70	-0.47	-1.00	7.99	175.36	143.38
23	13.51	7.31	4.87	0.52	-0.28	8.17	195.24	158.70
24	13.32	7.72	3.59	0.86	-0.66	8.09	192.49	132.97
25	11.54	7.89	3.88	0.06	-0.61	8.14	209.91	178.31
26	14.58	9.32	3.57	-1.72	-0.75	8.02	220.70	151.73
27	11.67	8.64	3.60	-0.42	-0.66	7.87	173.79	106.63
28	9.79	6.79	2.69	0.02	-0.40	7.74	134.56	74.06
29	12.43	8.68	3.06	-0.58	-0.20	7.57	165.14	89.18
30	9.68	7.62	2.93	0.24	-0.30	7.68	125.12	71.61

d<sub>L</sub> = Longest dimension, d<sub>I</sub> = Intermediate dimension and d<sub>S</sub> = Shortest dimension.



**Table 8.6: Scan results of 19.0 mm tillite aggregate particles.**

19.0 mm Sieve								
Particle No.	Dimensions (mm)			Centre of mass (mm)			Surface area (mm <sup>2</sup> )	Volume (mm <sup>3</sup> )
	d <sub>L</sub>	d <sub>I</sub>	d <sub>S</sub>	X	Y	Z		
1	26.08	25.92	20.34	-0.18	6.11	14.39	2066.79	6236.26
2	37.40	23.83	22.36	-2.65	0.21	16.28	2381.20	7984.79
3	32.35	27.05	26.80	-2.66	0.68	17.28	2602.50	9311.47
4	30.85	31.49	24.29	-2.27	-0.66	16.40	2574.39	8477.45
5	35.05	26.55	19.83	-2.76	0.38	14.66	2369.71	7394.19
6	35.21	24.75	22.59	2.04	1.22	15.92	2375.31	7657.07
7	26.38	22.26	26.19	0.86	-3.08	17.54	1979.07	5901.57
8	30.85	28.47	19.16	1.39	-2.51	14.25	2130.70	6424.22
9	33.76	31.34	22.63	2.99	8.71	15.01	2744.17	9054.77
10	32.17	24.50	19.90	-2.62	3.88	16.79	2506.99	8665.44
11	43.72	26.43	16.73	-3.76	3.67	13.35	2362.08	6989.75
12	40.20	26.80	17.75	-2.24	3.37	13.65	2668.39	8069.15
13	43.83	29.52	19.36	-3.30	-4.02	15.44	2883.58	9359.49
14	41.87	31.24	19.44	-6.22	-4.05	14.11	2671.86	8267.28
15	45.55	23.69	18.95	-2.87	1.31	13.83	2482.45	6267.29
16	38.88	30.85	21.19	-4.89	1.75	15.38	2775.92	9429.88
17	46.80	23.89	19.09	-3.34	-1.28	15.48	2586.79	7885.93
18	39.15	23.16	22.38	-1.65	0.95	14.97	2354.85	7064.03
19	45.21	28.69	23.25	0.67	3.78	16.67	3494.42	13372.66
20	33.51	31.72	21.40	-2.18	3.86	14.88	2635.45	8387.53
21	52.70	27.81	19.14	1.05	4.48	14.77	3523.03	11776.59
22	50.59	30.36	17.45	1.37	0.80	14.14	3239.58	10172.97
23	53.69	19.08	19.24	-3.91	1.70	13.65	3057.57	8760.01
24	33.83	33.00	12.34	-2.89	1.00	12.34	2284.12	6113.86
25	43.34	37.89	10.71	0.66	8.76	11.81	2863.07	6669.61
26	41.72	30.80	12.04	-2.90	2.11	12.13	2528.58	6768.45
27	43.53	28.81	7.42	-1.58	0.12	10.34	2099.35	3941.07
28	34.17	28.53	11.47	-2.82	1.11	11.85	1834.02	4083.05
29	36.23	23.59	11.79	-3.11	0.61	12.25	1595.14	3435.61
30	30.62	30.01	8.30	1.15	0.67	10.55	1534.91	2561.37

d<sub>L</sub> = Longest dimension, d<sub>I</sub> = Intermediate dimension and d<sub>S</sub> = Shortest dimension.

**Table 8.7: Scan results of 13.2 mm tillite aggregate particles.**

13.2 mm Sieve								
Particle No.	Dimensions (mm)			Centre of mass (mm)			Surface area (mm <sup>2</sup> )	Volume (mm <sup>3</sup> )
	d <sub>L</sub>	d <sub>I</sub>	d <sub>S</sub>	X	Y	Z		
1	21.64	18.12	17.94	3.67	0.91	14.42	1365.15	3536.27
2	25.30	18.69	16.31	0.35	0.72	14.23	1356.04	3512.52
3	27.00	19.79	16.66	0.88	2.41	14.22	1339.96	3208.97
4	23.70	20.93	16.91	-2.20	1.05	13.23	1282.18	3079.80
5	28.55	21.33	13.10	2.69	1.85	12.95	1440.52	3376.91
6	24.90	18.51	16.54	-1.08	-0.09	12.85	1158.90	2664.09
7	23.32	16.88	16.63	-0.24	-0.77	13.43	1241.58	3038.62
8	21.92	21.79	15.68	1.56	2.62	13.04	1146.61	2525.22
9	28.64	21.87	14.78	1.68	1.79	12.91	1352.26	3123.83
10	24.26	20.12	14.22	0.98	1.37	12.63	1166.19	2715.52
11	33.17	21.13	14.13	1.61	-0.08	12.96	1352.17	3112.43
12	35.46	20.65	15.95	3.08	3.02	13.68	1706.12	4314.91
13	31.63	25.08	12.99	-2.41	-0.13	12.47	1513.59	3569.02
14	31.65	27.77	11.54	1.52	0.17	11.91	1625.07	3564.98
15	30.64	20.40	10.69	-0.95	-2.05	11.72	1278.22	2753.38
16	28.43	21.37	10.74	-3.67	0.14	12.15	1344.35	3156.08
17	23.85	21.71	10.38	-0.57	2.48	11.36	1101.43	2252.56
18	29.98	23.79	9.00	1.25	0.02	11.17	1360.99	2974.52
19	27.66	16.49	10.93	-1.19	-0.63	14.25	1107.84	2275.41
20	25.18	16.92	11.81	0.43	1.42	11.08	983.10	1731.19
21	40.30	23.48	12.39	-0.57	-1.61	11.62	1931.41	4106.41
22	33.54	22.01	10.59	0.33	1.63	11.56	1513.17	3163.50
23	29.76	17.89	10.96	0.91	-0.96	11.41	1166.03	2310.51
24	33.03	25.33	10.82	-1.41	-3.48	11.69	1576.85	3280.61
25	42.96	28.08	9.96	-2.03	-1.10	10.68	1697.42	3083.75
26	21.04	20.00	6.39	-1.56	0.88	9.66	793.24	1114.79
27	32.09	23.71	9.11	-1.29	-1.41	11.29	1415.79	2838.92
28	29.73	22.60	8.86	-0.03	-1.86	11.21	1135.80	1915.50
29	28.60	25.83	5.37	-2.61	1.07	9.25	1240.92	1651.08
30	24.72	21.66	8.50	-0.18	0.62	10.74	1077.20	1875.45

d<sub>L</sub> = Longest dimension, d<sub>I</sub> = Intermediate dimension and d<sub>S</sub> = Shortest dimension.

**Table 8.8: Scan results of 9.5 mm tillite aggregate particles.**

9.5 mm Sieve								
Particle No.	Dimensions (mm)			Centre of mass (mm)			Surface area (mm <sup>2</sup> )	Volume (mm <sup>3</sup> )
	d <sub>L</sub>	d <sub>I</sub>	d <sub>S</sub>	X	Y	Z		
1	12.89	11.77	11.56	0.98	0.48	11.40	507.82	733.91
2	17.64	12.03	10.42	-1.29	-0.38	10.74	533.28	804.37
3	19.47	13.05	12.31	-0.21	-0.33	11.70	712.55	1258.79
4	14.15	11.09	8.76	1.39	1.56	10.56	411.62	583.20
5	13.98	11.86	8.73	-1.69	0.45	10.46	427.63	676.73
6	13.54	11.77	8.79	-0.16	-0.98	10.59	407.65	540.63
7	14.48	12.47	10.48	-0.53	-0.96	10.92	473.30	680.43
8	11.78	11.12	9.69	-0.47	-1.19	10.79	416.46	599.96
9	12.25	10.50	9.85	-1.08	-0.48	10.64	422.09	617.26
10	11.17	10.85	9.48	-1.17	-1.30	10.58	372.08	502.73
11	19.59	12.92	9.11	-1.27	-0.48	10.84	550.69	802.27
12	15.51	13.08	6.82	0.26	0.73	9.81	452.30	621.58
13	15.74	12.75	7.50	0.78	-0.37	9.78	456.63	633.47
14	17.34	15.36	9.45	0.95	-0.41	10.49	566.93	870.04
15	18.68	13.45	9.29	0.22	-0.26	10.61	510.52	760.04
16	15.15	14.86	7.76	-1.05	-1.82	10.24	497.71	714.77
17	13.60	13.02	7.26	-0.21	-0.01	10.08	415.67	547.77
18	16.90	12.79	7.42	-1.58	-0.54	10.18	452.81	637.66
19	15.49	12.24	7.58	-2.55	-1.26	9.73	406.35	494.90
20	14.81	12.34	8.72	0.29	0.40	10.37	437.40	622.32
21	19.79	12.15	7.02	-1.00	-1.59	10.12	530.25	758.87
22	25.61	13.72	6.65	-2.59	-2.62	9.76	666.34	926.63
23	20.57	18.65	7.28	-0.25	-0.05	9.88	670.86	1008.51
24	19.17	13.05	6.81	-0.80	-0.42	9.32	482.10	597.15
25	16.29	15.08	3.89	-1.04	0.02	8.78	427.86	378.15
26	25.78	15.50	6.15	1.46	-0.92	10.22	730.13	958.84
27	20.00	16.40	5.51	0.04	-1.02	9.18	571.14	625.27
28	25.09	14.45	4.32	-0.23	0.71	8.76	541.22	487.16
29	22.49	15.82	5.64	-1.77	-0.93	9.30	649.06	692.70
30	26.68	16.81	3.61	-0.55	0.20	8.74	582.89	521.69

d<sub>L</sub> = Longest dimension, d<sub>I</sub> = Intermediate dimension and d<sub>S</sub> = Shortest dimension.

**Table 8.9: Scan results of 6.7 mm tillite aggregate particles.**

6.7 mm Sieve								
Particle No.	Dimensions (mm)			Centre of mass (mm)			Surface area (mm <sup>2</sup> )	Volume (mm <sup>3</sup> )
	d <sub>L</sub>	d <sub>I</sub>	d <sub>S</sub>	X	Y	Z		
1	12.52	8.25	6.92	-1.34	-0.18	9.81	254.57	276.70
2	13.03	10.79	8.91	-0.78	-0.68	10.92	393.72	543.15
3	13.78	10.15	8.13	-1.03	-1.51	9.92	381.13	507.98
4	11.77	9.77	8.67	-1.75	-1.66	10.00	313.80	401.46
5	12.10	10.34	7.35	-1.23	-1.82	9.34	272.35	295.63
6	10.56	11.21	7.42	-0.79	-1.07	9.78	301.16	373.46
7	10.05	9.76	7.06	-0.42	-1.20	9.90	283.95	353.98
8	13.98	9.54	7.62	-0.47	-0.49	9.82	325.64	398.30
9	10.26	10.01	7.22	-1.43	-2.00	9.45	248.79	264.25
10	9.42	8.26	6.65	-1.07	-0.74	9.43	209.02	207.70
11	15.84	9.31	6.67	-1.05	-0.50	9.53	336.75	420.06
12	13.63	10.94	7.06	-0.36	-0.33	9.56	349.46	446.03
13	13.17	7.89	8.94	0.05	-0.79	9.93	312.28	390.35
14	13.71	11.15	6.44	-0.52	0.14	9.40	354.87	461.86
15	12.42	8.76	8.37	-1.83	-2.09	9.70	300.00	341.62
16	13.46	11.78	7.19	0.54	0.20	9.23	339.44	401.16
17	12.01	11.28	6.14	0.26	-0.07	8.95	280.17	301.60
18	13.99	10.19	7.37	0.52	0.66	9.75	297.73	349.89
19	12.46	8.78	5.96	-1.56	-1.43	9.16	258.22	270.43
20	11.57	9.00	6.14	-2.24	-0.78	9.17	248.68	279.27
21	12.98	9.20	4.08	-0.43	-1.17	8.41	232.27	185.20
22	11.46	8.73	3.78	-1.75	-1.16	8.52	204.03	166.04
23	13.62	8.86	4.09	-1.12	-0.60	8.67	233.20	206.23
24	13.12	10.87	3.78	-0.87	-0.43	8.44	264.86	249.95
25	13.40	11.24	3.56	-0.85	0.17	8.24	250.14	197.63
26	18.63	12.14	3.10	-0.55	-0.74	8.26	391.93	303.37
27	17.54	12.00	4.07	0.51	0.12	8.41	365.31	267.21
28	19.01	12.88	3.08	-0.79	-1.93	8.37	363.45	288.18
29	13.64	11.56	3.35	-0.11	0.74	8.03	279.64	195.64
30	14.30	9.17	2.64	0.59	-0.14	7.87	229.54	158.35

d<sub>L</sub> = Longest dimension, d<sub>I</sub> = Intermediate dimension and d<sub>S</sub> = Shortest dimension.

**Table 8.10: Scan results of 4.75 mm tillite aggregate particles.**

4.75 mm Sieve								
Particle No.	Dimensions (mm)			Centre of mass (mm)			Surface area (mm <sup>2</sup> )	Volume (mm <sup>3</sup> )
	d <sub>L</sub>	d <sub>I</sub>	d <sub>S</sub>	X	Y	Z		
1	11.22	6.05	6.07	-1.56	-0.95	9.07	200.13	185.07
2	9.29	6.48	6.26	-0.45	-0.33	9.17	198.16	176.28
3	9.22	7.44	5.64	-0.86	-1.03	9.11	156.32	132.70
4	10.56	7.04	7.21	-0.08	-0.12	8.99	187.90	177.36
5	10.15	6.48	6.62	-0.84	-1.79	9.12	160.81	128.75
6	9.38	5.27	5.35	-1.92	-1.95	8.91	150.83	120.69
7	7.94	5.42	6.10	-1.86	-1.19	9.17	148.58	138.64
8	7.10	6.47	4.91	0.28	-1.43	8.23	116.57	85.77
9	7.26	6.15	5.12	-1.49	-1.83	8.60	113.80	83.50
10	7.82	4.85	5.81	-0.89	-1.43	8.81	122.70	94.39
11	11.72	8.75	5.36	-0.10	-0.75	8.78	218.57	209.05
12	10.85	6.26	5.39	-1.90	-1.52	9.12	176.34	153.33
13	10.54	8.29	5.05	-0.61	-0.05	8.71	190.65	175.08
14	10.77	9.18	4.30	-0.14	-0.60	8.46	203.03	185.62
15	10.39	8.18	5.14	0.06	-0.78	8.54	185.54	175.87
16	10.02	6.45	5.13	-2.14	-2.74	8.90	143.41	113.72
17	10.37	6.39	4.88	-0.77	-1.43	9.10	158.32	135.66
18	10.45	7.08	5.23	-0.18	-0.71	8.46	151.60	116.69
19	9.00	7.81	5.29	-1.01	-1.61	8.72	163.11	153.90
20	9.09	5.16	5.68	-1.37	-1.93	8.88	143.11	118.66
21	9.53	8.86	3.24	-0.95	0.19	8.06	171.75	128.30
22	10.95	9.26	3.92	-1.37	-0.64	8.40	171.91	135.16
23	11.74	7.50	4.18	-1.32	-0.57	8.08	184.19	142.49
24	9.58	6.15	3.64	-0.94	-0.97	8.14	134.66	95.10
25	10.97	6.78	3.21	-1.47	-1.29	8.16	156.42	110.35
26	14.26	6.77	3.36	-2.04	-1.15	7.92	159.76	92.52
27	12.91	9.07	2.12	-1.51	-1.22	7.83	180.01	97.45
28	12.72	7.80	1.90	0.70	-0.51	7.73	157.25	47.75
29	10.72	9.01	2.34	-0.89	-0.42	7.62	143.44	62.92
30	8.97	8.28	2.38	-1.24	-0.48	7.57	123.19	67.81

d<sub>L</sub> = Longest dimension, d<sub>I</sub> = Intermediate dimension and d<sub>S</sub> = Shortest dimension.

**Table 8.11: Scan results of 19.0 mm quartzite aggregate particles.**

19.0 mm Sieve								
Particle No.	Dimensions (mm)			Centre of mass (mm)			Surface area (mm <sup>2</sup> )	Volume (mm <sup>3</sup> )
	d <sub>L</sub>	d <sub>I</sub>	d <sub>S</sub>	X	Y	Z		
1	32.43	21.58	18.23	0.18	-1.21	15.52	1952.69	5721.34
2	30.54	21.21	19.63	-1.43	-1.60	15.33	1708.10	4956.89
3	24.45	19.18	16.20	-1.41	0.17	13.60	1369.81	3609.96
4	25.83	23.90	17.00	0.40	0.70	13.40	1573.32	4059.83
5	28.40	25.90	16.83	3.87	1.46	14.75	2052.22	6348.66
6	29.41	24.59	20.80	-1.61	1.87	15.60	2013.06	5919.91
7	28.73	22.19	14.30	0.24	-0.56	13.84	1556.73	3935.11
8	25.84	20.45	15.53	-2.20	-1.23	13.79	1357.63	3369.23
9	27.62	26.59	19.04	0.37	-1.49	14.08	1758.02	4574.39
10	21.62	23.70	18.05	-1.40	2.44	13.67	1413.72	3509.64
11	38.05	25.54	18.26	-3.19	2.30	14.56	2251.80	6751.89
12	30.51	21.66	15.35	-0.32	5.07	13.49	1810.88	4717.01
13	46.20	27.56	16.18	3.82	-1.12	14.57	2207.33	5880.68
14	28.80	26.06	12.92	1.75	1.76	12.69	1772.65	4436.08
15	30.81	20.83	15.81	-3.35	-2.74	12.96	1593.87	4018.88
16	37.70	19.93	14.24	-1.40	-1.81	13.16	1568.37	3879.34
17	31.12	26.26	13.49	-0.68	3.21	11.76	1755.27	3998.05
18	27.94	30.97	13.97	-0.63	2.76	12.42	1671.88	3970.35
19	34.05	18.54	17.49	-2.21	1.10	14.21	1539.50	3990.70
20	32.43	24.86	15.43	-1.98	-1.32	13.62	1750.26	4739.69
21	41.56	21.24	12.15	1.44	-0.29	12.49	1967.35	4915.77
22	45.49	19.93	10.95	2.86	0.73	10.73	1664.52	3107.04
23	31.82	25.77	11.37	2.76	-0.34	12.56	1965.07	5043.12
24	28.86	31.98	6.99	-0.78	0.23	9.94	1375.37	2258.07
25	30.73	26.74	10.48	1.45	-1.09	11.64	1526.33	3154.55
26	51.39	27.06	14.12	-3.23	0.32	11.45	2341.87	4971.60
27	37.45	21.42	8.21	-1.03	0.30	11.02	1628.78	3228.28
28	38.09	25.01	8.34	-0.07	-1.46	10.67	1741.07	3054.96
29	35.99	23.26	5.86	2.05	-2.05	4.50	1366.46	1652.47
30	51.90	24.22	14.24	0.35	-1.59	11.56	2377.65	5074.65

d<sub>L</sub> = Longest dimension, d<sub>I</sub> = Intermediate dimension and d<sub>S</sub> = Shortest dimension.

**Table 8.12: Scan results of 13.2 mm quartzite aggregate particles.**

13.2 mm Sieve								
Particle No.	Dimensions (mm)			Centre of mass (mm)			Surface area (mm <sup>2</sup> )	Volume (mm <sup>3</sup> )
	d <sub>L</sub>	d <sub>I</sub>	d <sub>S</sub>	X	Y	Z		
1	22.05	15.16	14.14	-1.66	0.24	13.07	999.93	1962.61
2	27.94	20.76	12.62	1.38	1.37	12.30	1173.03	2551.86
3	22.40	17.29	15.41	-0.71	-0.86	13.18	1102.30	2343.34
4	24.23	18.95	17.09	-2.58	-0.34	12.53	1160.25	2593.45
5	18.66	18.09	13.34	-1.59	0.76	11.82	887.10	1670.51
6	15.30	15.16	12.65	-1.01	-1.47	12.02	720.79	1335.06
7	20.63	18.92	12.34	1.22	0.46	11.78	1005.58	2077.74
8	19.44	18.30	13.34	-1.63	0.96	12.48	962.15	1997.81
9	22.81	20.10	15.03	2.17	1.24	12.28	1107.83	2342.39
10	19.35	15.42	11.20	-1.63	0.02	11.13	796.96	1420.98
11	23.73	15.50	8.63	1.32	-0.08	10.71	703.20	1057.01
12	27.18	20.89	12.55	0.99	0.98	11.47	1184.81	2432.20
13	29.00	15.33	13.35	-0.66	-0.34	12.43	1103.29	2375.55
14	27.68	18.64	11.86	-1.10	-2.53	11.64	1243.34	2760.56
15	27.70	17.82	10.61	0.59	-1.07	11.48	1033.67	2009.41
16	29.06	14.12	11.47	0.64	-0.28	12.44	997.72	1885.08
17	24.80	15.95	13.10	1.10	-0.24	12.36	814.19	1462.07
18	21.59	19.16	11.57	0.35	1.06	11.27	838.06	1486.63
19	23.54	17.57	10.09	-1.98	2.71	11.04	824.10	1348.53
20	20.69	19.28	11.15	0.25	1.94	11.53	848.96	1532.06
21	27.89	18.45	7.59	2.77	0.01	9.71	853.65	1112.93
22	23.59	22.12	12.96	1.21	-8.38	12.39	1091.67	1813.50
23	23.70	18.14	8.12	1.45	0.77	9.96	782.99	1135.55
24	25.36	18.98	7.11	2.82	-0.02	10.03	833.41	1116.67
25	25.46	17.04	6.96	-1.43	-1.37	10.01	911.86	1368.46
26	21.61	18.84	7.53	-2.28	2.27	9.56	745.31	1059.24
27	23.55	16.80	5.91	-0.80	-1.64	9.56	658.15	804.31
28	22.41	20.72	6.60	-0.01	-1.21	9.96	857.91	1333.38
29	28.82	18.34	4.58	-1.01	0.82	9.25	778.50	944.56
30	19.63	16.49	4.63	-4.24	-0.58	8.93	569.77	464.30

d<sub>L</sub> = Longest dimension, d<sub>I</sub> = Intermediate dimension and d<sub>S</sub> = Shortest dimension.

**Table 8.13: Scan results of 9.5 mm quartzite aggregate particles.**

9.5 mm Sieve								
Particle No.	Dimensions (mm)			Centre of mass (mm)			Surface area (mm <sup>2</sup> )	Volume (mm <sup>3</sup> )
	d <sub>L</sub>	d <sub>I</sub>	d <sub>S</sub>	X	Y	Z		
1	18.32	16.75	13.14	1.75	-0.76	11.25	688.47	1128.69
2	17.85	12.97	14.93	-1.22	-0.41	12.25	743.30	1378.19
3	17.81	14.11	9.71	-2.39	0.68	10.64	578.98	937.95
4	13.43	11.58	10.36	-0.54	-1.37	11.05	550.42	826.97
5	17.62	13.45	10.26	-0.94	-1.77	10.52	578.62	872.96
6	17.73	14.96	10.05	-0.13	-2.49	10.66	586.45	915.77
7	19.61	11.47	10.37	0.74	-2.49	10.78	623.01	1046.45
8	18.54	13.10	13.03	-3.26	-2.42	12.52	653.20	1160.40
9	16.39	13.90	7.71	-0.45	0.17	9.74	461.53	663.82
10	14.60	12.20	9.28	1.21	-0.67	10.12	570.78	697.20
11	25.99	14.46	11.50	-1.09	-1.22	11.91	843.47	1484.56
12	27.12	10.13	9.93	-2.38	-1.69	11.05	710.00	1123.71
13	23.89	12.83	9.46	0.05	-1.78	10.79	670.80	984.52
14	26.62	12.11	11.54	0.22	-0.53	11.20	889.49	1485.21
15	21.97	14.40	7.52	-2.35	-0.72	10.04	652.63	987.17
16	25.13	13.65	9.65	-1.52	-1.36	11.40	863.92	1488.14
17	19.29	14.24	7.90	0.05	-0.18	10.03	590.08	883.07
18	23.96	11.48	11.50	-1.13	-2.92	11.24	689.84	948.65
19	22.86	11.91	11.37	-2.62	-1.58	11.32	661.39	1058.89
20	21.07	14.22	7.19	-1.54	-1.77	9.92	541.63	743.70
21	27.75	12.05	6.78	0.49	-0.68	9.72	644.20	743.83
22	24.80	13.48	6.03	-1.55	-0.40	9.36	525.88	650.74
23	23.20	9.86	7.23	-1.40	-1.25	9.13	446.78	424.04
24	24.50	15.82	6.45	-1.90	-0.98	9.49	650.83	696.38
25	21.25	14.93	7.93	-1.73	-2.74	9.49	508.76	538.73
26	22.72	12.34	4.66	-2.07	-1.27	9.15	481.18	510.10
27	35.79	16.73	6.76	3.38	-3.38	9.93	992.03	1208.24
28	24.92	13.19	4.89	-0.61	-1.14	9.37	575.64	536.73
29	17.04	12.68	3.82	-0.83	-0.75	8.53	390.72	353.98
30	21.90	14.46	4.77	-0.63	-1.07	8.96	458.93	516.94

d<sub>L</sub> = Longest dimension, d<sub>I</sub> = Intermediate dimension and d<sub>S</sub> = Shortest dimension.



**Table 8.14: Scan results of 6.7 mm quartzite aggregate particles.**

6.7 mm Sieve								
Particle No.	Dimensions (mm)			Centre of mass (mm)			Surface area (mm <sup>2</sup> )	Volume (mm <sup>3</sup> )
	d <sub>L</sub>	d <sub>I</sub>	d <sub>S</sub>	X	Y	Z		
1	14.81	9.49	9.27	-1.17	-1.53	11.02	410.39	545.62
2	11.22	10.11	9.24	-1.34	-1.02	10.32	341.36	412.31
3	13.07	8.70	6.66	-1.62	-1.01	10.15	304.13	357.18
4	10.47	7.20	6.86	-1.18	-3.18	10.32	247.23	269.04
5	12.50	7.25	7.87	-1.07	-1.72	10.21	266.07	298.43
6	10.07	10.53	8.22	-2.45	-2.21	10.22	271.40	302.37
7	13.41	11.17	6.89	-1.38	-0.37	9.55	326.62	384.96
8	9.97	9.99	7.13	-1.19	-1.19	9.67	249.34	272.07
9	11.06	9.44	7.26	-0.91	-1.45	9.75	252.63	261.35
10	12.17	9.02	8.41	-1.72	-0.92	9.68	276.63	333.07
11	18.04	9.78	7.10	-1.71	-1.79	10.20	424.92	551.67
12	16.49	8.81	5.88	-1.45	-1.76	9.41	314.56	300.11
13	17.08	8.17	7.46	-1.12	-1.92	10.25	448.24	554.04
14	17.17	11.22	5.93	0.08	-1.31	9.72	436.18	558.40
15	18.11	10.20	6.78	-0.13	-1.57	9.75	423.97	459.62
16	13.76	8.99	5.60	1.59	0.26	9.34	323.00	352.90
17	19.97	10.85	7.89	-1.15	-0.41	10.54	448.37	590.68
18	13.99	9.82	7.49	-1.98	-0.72	9.86	324.72	374.25
19	16.00	11.24	6.25	0.18	-0.12	9.27	371.92	431.40
20	14.44	10.30	7.86	-0.12	0.08	9.25	293.37	292.10
21	21.90	8.82	6.62	-0.96	-0.97	9.67	434.34	461.02
22	25.76	10.27	9.98	-0.41	-0.61	10.08	628.76	824.38
23	18.77	10.70	6.62	-0.80	-2.01	9.44	413.98	430.39
24	13.37	9.90	5.39	0.78	-1.13	9.04	300.31	313.11
25	17.91	7.43	4.86	-0.33	-1.22	9.05	282.95	261.02
26	23.60	10.65	4.58	-3.23	-1.12	8.85	488.24	435.07
27	16.60	11.76	3.66	-0.71	-1.41	8.76	334.93	297.81
28	24.12	9.92	4.23	0.23	-1.43	8.97	474.21	465.08
29	24.09	10.02	4.31	0.29	-1.41	8.97	479.70	467.45
30	18.05	11.30	4.20	-1.00	-0.54	8.88	345.25	301.42

d<sub>L</sub> = Longest dimension, d<sub>I</sub> = Intermediate dimension and d<sub>S</sub> = Shortest dimension.

**Table 8.15: Scan results of 4.75 mm quartzite aggregate particles.**

4.75 mm Sieve								
Particle No.	Dimensions (mm)			Centre of mass (mm)			Surface area (mm <sup>2</sup> )	Volume (mm <sup>3</sup> )
	d <sub>L</sub>	d <sub>I</sub>	d <sub>S</sub>	X	Y	Z		
1	9.39	5.37	4.86	-0.32	-1.25	8.60	107.26	86.14
2	11.43	7.05	5.79	-1.92	-1.02	9.53	206.58	176.24
3	7.95	5.71	4.25	-0.50	-1.02	8.51	113.82	84.77
4	8.27	6.61	6.04	0.52	-0.04	9.05	157.48	148.15
5	8.56	6.66	3.39	-0.18	-0.27	8.20	123.36	88.28
6	9.80	7.03	3.96	-0.78	-1.40	8.56	140.08	105.45
7	11.41	6.59	5.47	-1.05	-1.06	8.88	168.11	149.05
8	9.69	6.57	5.31	-1.85	-0.60	8.56	126.58	79.09
9	10.24	6.41	4.80	0.06	-1.04	8.70	141.22	110.40
10	6.91	5.17	5.36	0.12	-1.62	8.94	105.96	75.72
11	10.55	6.31	4.90	-1.65	-2.17	8.73	166.88	143.05
12	10.33	6.47	4.40	-0.40	-1.55	8.44	142.72	106.01
13	10.95	6.33	4.06	0.23	-1.50	8.32	151.98	119.15
14	9.89	6.30	4.37	-0.95	-1.26	8.45	139.72	106.42
15	10.83	6.08	3.98	-1.04	-1.53	8.45	148.87	112.78
16	9.87	7.23	4.46	0.04	-0.88	8.32	156.71	124.20
17	8.86	7.26	4.22	-1.03	-0.47	8.53	139.17	108.19
18	9.94	7.67	4.42	-0.72	-0.33	8.51	149.27	120.42
19	6.78	5.14	5.65	0.10	-1.64	8.92	106.97	76.71
20	10.67	6.67	4.37	-0.10	-0.83	8.43	156.15	119.63
21	11.06	5.19	3.57	-0.64	-1.56	8.28	122.19	76.04
22	12.27	5.68	4.96	-0.89	-1.58	8.38	146.17	99.10
23	10.56	6.24	3.79	0.28	-1.08	8.45	122.89	83.65
24	13.69	8.43	3.96	-1.37	-1.84	8.67	190.82	121.82
25	10.83	7.82	3.30	-1.88	-1.57	8.11	156.54	112.34
26	11.81	8.56	3.28	-0.95	-0.89	8.30	208.43	150.89
27	10.70	8.01	2.47	-0.70	-1.40	8.02	155.96	90.68
28	10.62	8.90	2.84	-0.04	-0.44	7.76	142.24	80.13
29	12.80	6.77	2.37	-1.02	-1.69	7.85	133.85	72.35
30	10.82	7.10	2.33	-0.64	-1.01	7.79	127.46	61.56

d<sub>L</sub> = Longest dimension, d<sub>I</sub> = Intermediate dimension and d<sub>S</sub> = Shortest dimension.

**Table 8.16: Scan results of 19.0 mm hornfels aggregate particles.**

19.0 mm Sieve								
Particle No.	Dimensions (mm)			Centre of mass (mm)			Surface area (mm <sup>2</sup> )	Volume (mm <sup>3</sup> )
	d <sub>L</sub>	d <sub>I</sub>	d <sub>S</sub>	X	Y	Z		
1	34.42	26.47	20.16	-1.68	-1.78	15.95	2361.07	7366.15
2	36.61	25.71	25.63	-0.31	3.28	16.75	2961.45	10911.61
3	27.53	25.59	20.77	-1.67	3.20	15.35	2160.33	6907.56
4	32.80	24.34	21.27	-0.67	2.82	15.70	2399.31	8533.14
5	28.46	26.70	22.58	-0.97	1.06	16.96	2452.79	8377.62
6	32.29	21.69	21.99	-1.89	2.58	15.74	2205.67	7163.70
7	32.63	22.50	21.53	-0.67	3.75	16.55	2216.69	7167.36
8	32.61	25.72	18.26	-2.11	1.09	14.65	1934.98	5739.01
9	27.89	20.42	19.19	-0.96	-0.33	15.66	1852.47	5799.32
10	32.57	22.89	20.59	-1.93	0.18	15.08	1842.78	5355.91
11	41.67	26.48	14.69	2.06	0.23	13.42	2376.51	7053.64
12	31.44	25.38	15.65	-0.21	0.85	13.08	1752.01	4413.38
13	34.12	23.19	16.37	-0.54	0.79	14.33	1876.43	5699.14
14	31.65	30.22	16.85	-2.78	1.34	14.30	2108.41	5877.84
15	36.52	27.57	14.93	-0.88	2.56	13.26	2320.20	7178.03
16	31.96	29.14	12.15	-2.51	0.45	12.84	2047.09	5418.16
17	37.96	25.85	15.19	-2.53	-0.51	12.49	2201.05	5738.70
18	28.31	24.90	16.05	-1.74	0.95	13.57	1768.27	4964.47
19	37.51	20.63	14.91	-6.31	-0.52	13.68	2029.75	5459.47
20	34.63	25.11	21.20	0.51	0.35	13.56	1923.11	4901.15
21	41.75	28.80	9.51	-3.51	4.38	10.63	2156.32	4583.07
22	31.91	24.86	11.19	2.12	4.02	12.07	1585.82	3100.99
23	33.92	30.03	8.52	-1.14	2.93	10.27	1837.37	3204.35
24	35.24	27.69	9.27	0.66	1.42	11.36	1674.09	3139.90
25	36.67	29.95	9.75	-1.22	2.24	11.53	2134.17	4502.05
26	39.50	35.46	11.53	2.12	1.87	10.79	2594.84	5003.91
27	40.52	26.75	8.87	-0.07	1.54	11.04	2064.45	4184.10
28	34.43	25.99	6.75	4.32	1.70	10.04	1764.17	2987.29
29	36.24	33.04	8.82	-3.85	0.22	11.39	1969.05	3673.69
30	34.42	26.47	20.16	-1.68	-1.78	15.95	2361.07	7366.15

d<sub>L</sub> = Longest dimension, d<sub>I</sub> = Intermediate dimension and d<sub>S</sub> = Shortest dimension.

**Table 8.17: Scan results of 13.2 mm hornfels aggregate particles.**

13.2 mm Sieve								
Particle No.	Dimensions (mm)			Centre of mass (mm)			Surface area (mm <sup>2</sup> )	Volume (mm <sup>3</sup> )
	d <sub>L</sub>	d <sub>I</sub>	d <sub>S</sub>	X	Y	Z		
1	19.07	18.58	13.84	-0.57	-1.41	13.36	1088.03	2365.69
2	24.36	16.65	12.02	-0.79	0.09	11.56	954.37	1957.09
3	23.50	19.07	14.39	-1.64	0.26	12.39	1153.49	2590.40
4	19.41	18.67	11.23	-1.06	-1.61	11.60	899.00	1874.70
5	25.92	18.26	12.56	0.47	-2.21	11.62	1009.62	1876.39
6	17.84	15.19	11.60	-1.08	0.72	11.80	758.00	1466.90
7	20.99	16.93	13.17	0.30	1.01	12.58	937.27	2145.12
8	17.56	18.18	14.82	0.83	0.31	13.05	953.25	2184.51
9	22.76	18.77	15.43	0.74	-0.36	12.98	1244.96	2938.70
10	25.30	20.46	15.46	2.04	-1.17	13.28	1334.37	3346.82
11	29.49	23.42	15.50	0.07	0.74	12.54	1526.18	3578.30
12	26.15	24.10	12.21	0.71	0.57	11.94	1245.62	2621.02
13	21.76	17.24	12.90	-0.01	-0.54	12.19	1056.96	2168.67
14	23.42	21.51	10.41	0.22	1.24	10.37	1064.78	1937.46
15	24.59	19.00	11.79	1.48	1.14	11.89	1010.81	2212.84
16	26.26	18.61	12.58	-2.06	0.01	12.02	1017.62	2165.97
17	22.88	18.92	8.80	0.43	0.39	10.43	805.31	1368.54
18	25.77	23.43	8.47	0.59	1.24	10.61	1072.59	1969.15
19	27.45	17.35	8.14	-0.91	-0.32	10.48	892.40	1546.66
20	23.06	18.76	6.69	0.74	0.49	10.28	800.45	1205.66
21	30.64	19.71	9.95	-1.66	0.64	11.04	1231.88	2092.88
22	26.44	18.97	9.65	-0.07	0.15	10.67	823.19	1198.89
23	32.93	19.39	7.65	1.33	-2.03	9.84	1104.49	1568.47
24	30.29	22.60	8.84	-1.08	0.66	9.62	1096.96	1414.02
25	19.62	18.53	7.87	-0.29	0.90	9.94	773.00	1017.77
26	29.45	18.25	6.00	1.59	-0.26	9.86	900.43	1257.03
27	26.69	19.42	8.97	-1.73	-0.63	9.93	866.15	1142.29
28	31.28	23.37	6.40	0.29	1.07	9.16	1257.97	1605.86
29	26.10	20.13	4.98	-0.31	1.21	8.92	822.54	810.63
30	31.77	23.33	6.53	0.63	1.25	9.23	1059.05	1301.74

d<sub>L</sub> = Longest dimension, d<sub>I</sub> = Intermediate dimension and d<sub>S</sub> = Shortest dimension.

**Table 8.18: Scan results of 9.5 mm hornfels aggregate particles.**

9.5 mm Sieve								
Particle No.	Dimensions (mm)			Centre of mass (mm)			Surface area (mm <sup>2</sup> )	Volume (mm <sup>3</sup> )
	d <sub>L</sub>	d <sub>I</sub>	d <sub>S</sub>	X	Y	Z		
1	19.73	15.04	10.73	-1.95	-0.76	11.46	664.82	1144.79
2	16.93	13.44	10.36	-0.83	0.19	10.75	522.78	832.22
3	15.73	14.28	9.12	-1.12	0.83	10.73	515.80	720.42
4	15.41	11.81	8.55	-0.81	-2.17	10.52	431.21	643.52
5	17.08	12.12	10.03	-0.82	-0.57	10.67	503.65	744.51
6	16.79	14.43	10.48	-1.31	0.73	10.45	557.22	811.36
7	20.33	11.62	9.68	-0.90	-0.79	10.58	532.19	828.08
8	15.52	12.03	9.84	-0.84	0.18	10.71	478.65	631.57
9	19.18	12.21	11.29	-0.65	-0.11	10.79	636.11	940.06
10	14.36	11.73	8.61	-1.84	-0.42	10.20	425.99	605.70
11	23.60	10.74	9.30	-1.90	0.28	11.16	676.57	1118.66
12	19.66	12.27	7.21	-3.42	-2.15	9.71	532.79	719.80
13	19.25	14.92	9.22	-0.74	-0.76	10.65	627.92	1006.51
14	23.21	12.10	9.24	-0.71	-0.41	10.35	652.96	972.89
15	19.28	14.70	8.69	-3.33	-2.78	11.04	563.97	763.01
16	19.81	14.34	8.24	0.03	0.70	10.08	569.43	826.84
17	17.11	12.76	7.96	0.97	0.77	10.51	572.24	897.72
18	18.71	11.71	10.04	-0.66	-2.25	10.32	570.32	805.25
19	18.27	12.63	11.45	-1.12	-1.03	10.59	562.64	857.45
20	18.51	13.10	10.53	-2.18	-0.98	11.35	579.06	896.71
21	22.57	14.01	8.92	-1.38	0.29	10.41	720.66	1118.04
22	24.31	16.37	7.61	-2.38	-1.05	10.44	796.54	1324.35
23	22.98	13.38	6.57	-0.59	-1.05	9.82	562.86	689.63
24	24.22	11.08	6.81	-0.95	-1.81	10.08	590.30	802.59
25	17.62	15.78	6.40	1.24	-0.07	9.63	544.55	683.40
26	23.39	15.53	4.83	1.77	-0.33	8.97	623.85	561.70
27	21.30	12.61	4.43	-0.57	-2.16	8.78	492.26	447.15
28	23.72	13.25	5.15	2.09	-0.01	8.82	571.73	520.77
29	18.43	15.05	5.24	2.49	-0.78	8.65	446.92	326.37
30	14.45	13.69	3.09	-0.35	0.59	8.16	344.81	224.87

d<sub>L</sub> = Longest dimension, d<sub>I</sub> = Intermediate dimension and d<sub>S</sub> = Shortest dimension.

**Table 8.19: Scan results of 6.7 mm hornfels aggregate particles.**

6.7 mm Sieve								
Particle No.	Dimensions (mm)			Centre of mass (mm)			Surface area (mm <sup>2</sup> )	Volume (mm <sup>3</sup> )
	d <sub>L</sub>	d <sub>I</sub>	d <sub>S</sub>	X	Y	Z		
1	10.67	8.40	5.93	-1.40	-1.53	9.43	223.79	214.33
2	12.14	8.02	7.92	0.14	-0.44	10.64	339.62	420.20
3	14.50	10.36	7.84	-1.28	-1.41	9.81	340.07	404.23
4	16.63	10.71	8.58	-0.22	-0.88	10.01	387.11	501.14
5	11.78	9.21	8.68	-2.01	-1.06	10.64	335.37	462.22
6	12.52	9.83	7.01	-3.04	-1.40	10.24	327.55	415.30
7	10.31	9.35	5.55	-1.43	-1.04	8.96	231.18	226.77
8	11.15	6.84	7.84	-1.50	-1.74	9.83	244.53	227.63
9	11.66	8.78	7.90	-1.28	-0.64	9.67	263.12	317.70
10	10.61	10.04	6.64	-0.71	-0.48	9.02	219.50	199.76
11	14.83	9.03	7.29	-0.74	-0.26	10.37	396.26	544.08
12	11.53	6.01	6.66	-0.50	-0.75	9.90	243.82	270.40
13	13.37	11.26	6.61	-2.26	-0.32	9.79	360.11	435.22
14	16.62	7.95	6.27	0.32	-0.86	9.66	328.71	376.16
15	10.84	9.84	6.11	-1.67	-0.88	9.22	251.18	253.95
16	13.21	8.81	6.16	-1.30	-0.36	9.28	250.15	245.39
17	13.40	10.64	6.25	-1.27	-0.87	9.46	295.73	365.63
18	13.96	10.04	5.41	-1.78	-0.30	9.06	285.29	289.65
19	14.86	10.48	5.16	-0.97	-0.39	9.34	296.62	315.74
20	12.96	8.71	5.89	-1.42	-0.25	9.10	238.03	247.67
21	13.72	11.81	5.16	-1.93	0.33	8.92	307.01	299.26
22	13.30	7.86	4.23	-0.39	-0.08	8.86	241.53	224.27
23	16.32	12.16	5.15	0.11	0.31	9.05	370.67	390.67
24	16.27	11.23	3.90	0.44	0.26	8.86	358.44	343.60
25	12.13	12.76	5.14	-1.48	0.07	8.92	286.79	291.28
26	23.35	11.98	3.84	1.30	0.26	8.63	423.44	294.27
27	21.97	11.77	3.82	0.34	-1.92	8.77	407.93	353.26
28	19.52	8.86	4.71	-0.21	-1.69	8.82	310.94	265.30
29	20.42	11.18	3.42	-1.09	-0.98	8.58	356.05	292.67
30	11.72	11.90	2.80	-0.84	-1.30	8.29	247.79	167.33

d<sub>L</sub> = Longest dimension, d<sub>I</sub> = Intermediate dimension and d<sub>S</sub> = Shortest dimension.

**Table 8.20: Scan results of 4.75 mm hornfels aggregate particles.**

4.75 mm Sieve								
Particle No.	Dimensions (mm)			Centre of mass (mm)			Surface area (mm <sup>2</sup> )	Volume (mm <sup>3</sup> )
	d <sub>L</sub>	d <sub>I</sub>	d <sub>S</sub>	X	Y	Z		
1	10.25	7.30	6.19	-0.45	-0.79	9.04	192.10	171.78
2	8.57	6.69	6.38	-0.53	-0.04	8.94	176.96	159.42
3	10.50	5.52	5.94	-0.25	-0.58	9.06	158.66	127.54
4	10.41	6.06	5.91	0.94	-0.97	8.74	158.75	138.26
5	6.59	6.65	3.81	-0.91	-1.26	8.52	120.55	87.14
6	10.51	8.23	6.22	-0.71	-0.15	9.20	205.40	201.07
7	10.04	6.75	6.55	-0.84	-0.77	9.41	199.00	207.07
8	9.14	7.18	6.05	-1.02	-0.89	8.89	171.58	155.99
9	8.81	6.12	6.67	-1.07	-1.25	9.33	166.17	166.10
10	9.04	7.00	6.23	-0.82	-0.28	8.85	153.75	137.15
11	12.40	7.41	4.79	-0.42	-1.18	8.63	189.48	176.38
12	10.18	8.39	4.84	-1.26	-1.07	8.71	176.52	157.27
13	8.45	8.62	4.78	-1.10	-1.27	8.96	167.51	148.59
14	10.37	5.05	4.86	-0.49	-1.73	8.87	139.06	112.20
15	11.10	6.98	5.28	-0.43	-0.56	8.81	190.22	189.40
16	10.01	7.55	5.26	-0.83	-1.51	8.95	189.75	168.80
17	8.72	8.94	4.68	-1.24	-0.11	8.80	166.19	156.55
18	10.02	7.51	5.94	-1.54	-0.87	9.00	185.44	164.04
19	10.98	6.75	5.19	-1.35	-2.29	9.35	189.10	193.33
20	9.02	6.81	5.04	-1.35	-1.56	8.85	144.37	123.22
21	14.61	6.63	4.53	-0.80	-1.52	8.68	209.62	156.33
22	15.05	7.74	6.17	-1.42	-2.39	8.98	243.10	203.22
23	13.67	5.40	6.94	1.92	0.61	9.14	227.83	203.66
24	10.82	6.49	3.92	-1.48	-1.52	8.49	165.40	148.58
25	10.18	6.88	3.58	-1.69	-0.77	8.22	137.51	100.59
26	13.67	6.64	2.60	-0.94	-0.56	7.94	150.30	78.63
27	14.46	7.78	3.53	-0.72	-1.12	7.97	191.18	113.70
28	14.08	7.26	2.57	-0.62	-1.15	8.10	176.65	100.71
29	12.55	8.96	2.89	-1.74	-1.41	8.28	188.17	126.09
30	11.62	6.77	2.98	-0.23	-1.07	8.01	141.17	90.67

d<sub>L</sub> = Longest dimension, d<sub>I</sub> = Intermediate dimension and d<sub>S</sub> = Shortest dimension.

**Table 8.21: Scan results of 19.0 mm alluvial gravel aggregate particles.**

19.0 mm Sieve								
Particle No.	Dimensions (mm)			Centre of mass (mm)			Surface area (mm <sup>2</sup> )	Volume (mm <sup>3</sup> )
	d <sub>L</sub>	d <sub>I</sub>	d <sub>S</sub>	X	Y	Z		
1	30.05	21.23	18.33	-3.57	0.22	14.71	1792.90	5762.12
2	24.75	20.38	15.99	-3.47	-1.60	13.86	1401.91	4303.82
3	24.91	22.72	16.49	-0.47	3.10	13.46	1491.92	4424.92
4	26.06	21.22	17.23	-3.06	-0.81	14.81	1592.13	5065.99
5	25.50	22.11	17.93	-1.71	-0.72	14.12	1511.83	4587.57
6	32.02	23.17	17.40	-0.13	2.38	14.43	1784.77	5869.67
7	31.18	21.06	17.41	0.27	1.38	14.78	1791.06	6101.96
8	31.35	21.63	18.49	0.04	-1.58	15.13	1734.83	5589.79
9	27.15	25.97	17.94	-1.66	2.24	13.86	1854.05	6218.35
10	36.50	22.35	23.14	-0.24	-1.00	16.93	2324.63	8599.04
11	38.79	24.30	18.01	1.11	-1.32	14.46	2284.17	7461.34
12	33.19	23.48	16.45	-0.08	-2.06	13.38	1705.39	4907.92
13	33.58	23.69	13.77	-0.71	1.13	13.46	1786.92	5566.68
14	37.57	20.24	18.09	-2.96	-0.06	15.13	2255.06	7347.14
15	35.38	30.10	15.93	-3.09	-0.12	14.54	2248.11	7725.78
16	43.41	25.32	16.28	-1.08	-1.17	14.19	2760.39	9592.80
17	37.92	27.03	17.45	-2.01	1.03	14.57	2315.84	8385.31
18	42.39	20.73	22.64	-4.60	-0.26	15.39	2628.97	9560.51
19	27.91	24.19	13.90	-2.55	-0.15	12.89	1595.77	4102.85
20	29.64	27.60	14.17	-2.06	2.36	12.46	1854.30	4939.92
21	38.49	23.97	13.03	-1.19	-1.05	12.45	2027.73	5407.49
22	43.99	29.59	12.40	-2.34	1.00	13.43	2799.42	8158.51
23	47.45	25.70	15.56	-0.15	0.19	13.96	2708.76	9298.90
24	25.72	23.85	21.18	0.41	-0.19	15.13	1736.79	5202.96
25	30.81	24.07	20.31	-1.61	0.30	16.14	2113.67	7848.61
26	27.25	26.07	18.72	0.15	-2.22	15.05	1816.56	5939.50
27	26.85	22.19	22.90	-0.76	1.47	17.06	1968.98	6847.33
28	30.46	23.48	21.60	1.76	-1.37	16.44	2011.05	7432.10
29	33.24	24.10	28.07	-0.11	-0.03	18.39	2558.63	10259.89
30	26.02	19.25	19.46	0.80	1.72	15.09	1460.95	4606.71

d<sub>L</sub> = Longest dimension, d<sub>I</sub> = Intermediate dimension and d<sub>S</sub> = Shortest dimension.



**Table 8.22: Scan results of 13.2 mm alluvial gravel aggregate particles.**

13.2 mm Sieve								
Particle No.	Dimensions (mm)			Centre of mass (mm)			Surface area (mm <sup>2</sup> )	Volume (mm <sup>3</sup> )
	d <sub>L</sub>	d <sub>I</sub>	d <sub>S</sub>	X	Y	Z		
1	22.76	20.58	13.93	0.83	-0.15	13.08	1208.20	3331.69
2	22.91	19.92	13.39	-2.73	-0.94	12.46	1118.91	2896.83
3	27.82	22.89	16.75	-0.97	-0.17	13.19	1436.23	3763.03
4	19.86	18.47	16.19	-0.01	-0.56	14.61	1239.26	3551.53
5	24.49	17.47	17.62	-2.87	-0.91	14.60	1388.28	3844.76
6	23.36	20.31	18.00	-0.64	-0.91	13.99	1336.93	3666.09
7	26.69	19.73	15.48	-3.13	-1.13	13.37	1312.83	3655.13
8	19.20	23.02	13.74	-0.63	2.22	13.05	1266.70	3151.15
9	23.75	21.19	11.70	0.36	0.29	12.20	1178.54	3015.57
10	22.21	18.64	13.80	-0.21	-0.50	13.75	1045.24	2730.17
11	22.75	16.90	12.19	-0.51	-1.60	12.91	1028.23	2603.59
12	35.19	23.12	12.64	-2.40	-0.58	12.89	1613.88	3966.55
13	32.13	19.37	14.09	0.51	2.22	13.44	1430.64	3865.19
14	32.46	22.25	15.30	-3.76	-0.99	14.03	1772.94	5578.06
15	29.14	15.97	11.86	-0.33	-0.28	12.39	1201.44	3110.48
16	29.01	15.62	12.46	0.59	-0.57	12.35	1170.67	2877.06
17	27.89	20.59	16.24	0.90	-1.74	13.53	1407.41	3923.59
18	29.03	18.46	14.08	1.90	-2.28	13.47	1458.27	4354.31
19	25.31	19.95	13.15	0.68	-1.69	12.32	1139.86	2873.77
20	27.31	20.27	14.29	-1.95	-4.32	13.10	1288.93	3564.34
21	25.53	18.45	12.74	-2.09	-0.71	12.28	1106.73	2705.10
22	19.86	18.44	11.98	0.17	0.00	12.13	962.75	2369.97
23	26.46	23.33	14.20	-5.31	-0.14	12.99	1422.57	3662.14
24	25.88	19.30	11.92	-2.35	2.01	11.41	1203.69	2560.33
25	27.94	22.73	10.76	1.45	-0.55	11.23	1315.12	2766.93
26	34.86	21.08	14.18	0.53	-1.35	13.74	1628.05	4720.09
27	25.75	20.21	11.70	-1.01	-1.09	12.06	1313.70	3305.97
28	28.27	19.24	13.03	-1.96	-1.95	12.89	1218.53	3062.04
29	30.84	23.13	10.30	-4.34	0.94	11.74	1395.95	3133.14
30	25.59	16.77	15.47	-2.39	-0.38	13.27	1209.88	3079.42

d<sub>L</sub> = Longest dimension, d<sub>I</sub> = Intermediate dimension and d<sub>S</sub> = Shortest dimension.

**Table 8.23: Scan results of 9.5 mm alluvial gravel aggregate particles.**

9.5 mm Sieve								
Particle No.	Dimensions (mm)			Centre of mass (mm)			Surface area (mm <sup>2</sup> )	Volume (mm <sup>3</sup> )
	d <sub>L</sub>	d <sub>I</sub>	d <sub>S</sub>	X	Y	Z		
1	19.87	12.07	8.78	-0.89	0.53	11.07	619.56	1124.68
2	18.73	12.39	10.62	-1.85	-1.39	11.56	620.03	1087.97
3	20.63	12.55	13.69	-1.94	-1.36	12.88	771.39	1717.85
4	21.59	14.41	12.33	-1.84	-0.97	11.92	801.13	1789.47
5	19.58	11.28	11.55	-1.26	-0.96	11.53	642.97	1177.21
6	19.57	15.40	9.83	-0.90	-1.13	11.55	684.34	1412.37
7	14.35	12.43	8.89	-0.59	-1.20	10.60	474.00	787.87
8	17.30	14.08	10.34	0.86	0.76	10.69	569.32	945.20
9	21.63	14.61	11.61	-0.54	0.96	11.51	820.37	1553.80
10	17.03	11.97	11.44	-0.90	-1.44	11.02	504.57	860.68
11	18.65	12.41	7.89	-0.48	0.34	9.83	514.03	724.14
12	16.67	13.52	10.86	-0.54	-0.47	11.42	622.00	1254.15
13	16.12	15.23	9.84	-1.20	-0.52	10.87	633.63	1143.72
14	19.46	13.29	11.15	-1.42	-2.25	11.88	622.20	1294.64
15	19.30	14.45	10.13	-1.22	-0.40	11.40	700.43	1501.57
16	19.10	15.33	11.45	-0.73	-0.24	11.87	777.27	1663.88
17	18.31	15.09	10.89	-0.80	-0.75	11.42	689.13	1395.49
18	20.96	13.07	10.94	-1.06	-1.09	11.50	721.56	1410.96
19	21.26	15.21	12.36	-1.92	-1.31	12.21	845.07	1892.50
20	18.68	16.79	13.77	-0.29	-0.75	11.98	812.94	1779.38
21	19.31	15.80	9.32	-0.47	-0.52	10.98	731.78	1401.17
22	19.96	17.56	7.74	-1.15	0.28	10.85	719.64	1361.14
23	22.71	15.09	8.70	-2.13	-1.10	10.63	760.53	1388.59
24	18.27	11.13	8.85	0.99	-1.06	10.77	581.90	1050.37
25	17.96	15.89	8.47	-2.20	-1.07	10.36	652.61	1136.78
26	17.19	14.08	7.35	-0.98	-0.03	10.31	575.65	1014.52
27	20.33	15.83	10.13	-0.04	-1.11	11.04	775.79	1598.88
28	19.09	16.53	8.63	-1.13	-0.95	10.79	732.82	1482.52
29	18.12	13.83	8.57	-0.91	-0.18	10.71	582.88	1038.06
30	22.73	15.16	9.78	-1.18	-1.20	11.07	792.41	1600.32

d<sub>L</sub> = Longest dimension, d<sub>I</sub> = Intermediate dimension and d<sub>S</sub> = Shortest dimension.

**Table 8.24: Scan results of 6.7 mm alluvial gravel aggregate particles.**

6.7 mm Sieve								
Particle No.	Dimensions (mm)			Centre of mass (mm)			Surface area (mm <sup>2</sup> )	Volume (mm <sup>3</sup> )
	d <sub>L</sub>	d <sub>I</sub>	d <sub>S</sub>	X	Y	Z		
1	10.37	9.27	7.00	0.53	-0.60	9.48	252.12	329.45
2	10.21	8.48	6.48	-1.64	-1.74	9.27	243.82	289.34
3	11.87	9.86	7.63	-1.41	-1.40	10.14	276.38	299.26
4	12.10	9.17	7.30	-0.60	-1.14	9.94	292.78	396.38
5	12.91	10.04	7.42	-1.65	-0.50	10.27	341.32	516.55
6	12.95	10.07	7.73	-0.17	-0.23	10.18	320.86	456.07
7	13.50	8.82	7.94	-1.19	-1.47	10.02	319.98	425.72
8	12.16	9.16	7.84	-1.82	-0.85	10.07	301.71	414.47
9	12.76	9.52	6.70	-0.62	-1.42	9.91	290.49	402.32
10	13.64	10.05	8.09	-1.72	-0.41	10.22	408.89	632.38
11	14.25	11.07	6.65	-0.52	-1.08	9.59	361.91	451.57
12	14.09	8.87	6.86	-1.46	-1.14	9.83	275.70	301.19
13	13.78	9.70	6.40	1.37	-0.34	9.40	279.98	316.00
14	13.35	9.44	8.22	-1.14	-0.99	10.03	357.43	478.79
15	15.41	8.99	7.56	-1.19	-1.65	9.85	368.46	525.86
16	13.82	9.89	7.97	-1.00	-1.18	10.05	324.25	453.48
17	12.68	10.90	6.53	-2.10	-1.07	9.72	305.59	392.73
18	14.33	8.80	6.31	-0.20	-0.90	9.45	276.51	308.28
19	15.97	10.51	8.49	-0.59	-0.86	10.48	406.74	585.07
20	13.94	9.37	7.49	-0.63	-1.41	9.37	306.04	380.59
21	15.53	11.33	6.22	-0.54	-0.26	9.63	364.98	488.98
22	14.13	10.60	8.36	-0.12	-1.54	11.04	415.00	655.77
23	14.95	11.34	8.15	-0.54	-1.65	10.09	373.86	517.62
24	13.37	10.33	7.09	-1.22	-2.73	9.75	354.39	503.68
25	16.67	9.01	5.81	-1.59	-1.19	9.30	311.02	367.68
26	15.79	7.95	7.35	-0.01	-1.02	9.67	330.48	419.57
27	13.96	11.28	5.36	-0.84	-0.26	9.15	313.76	354.54
28	15.99	11.48	8.05	-0.68	-1.57	10.36	436.80	678.82
29	19.47	11.08	7.08	-1.41	-1.41	10.15	484.97	773.68
30	17.01	12.66	6.62	-0.55	-0.94	9.76	445.60	637.28

d<sub>L</sub> = Longest dimension, d<sub>I</sub> = Intermediate dimension and d<sub>S</sub> = Shortest dimension.

**Table 8.25: Scan results of 4.75 mm alluvial gravel aggregate particles.**

4.75 mm Sieve								
Particle No.	Dimensions (mm)			Centre of mass (mm)			Surface area (mm <sup>2</sup> )	Volume (mm <sup>3</sup> )
	d <sub>L</sub>	d <sub>I</sub>	d <sub>S</sub>	X	Y	Z		
1	8.80	7.46	6.72	-0.39	-0.96	9.14	190.18	207.77
2	8.97	6.50	6.49	-0.61	-1.76	9.47	169.51	185.09
3	10.87	7.43	6.36	-1.66	-1.38	9.40	200.71	233.24
4	8.72	6.98	5.88	-0.16	-0.59	8.75	154.60	149.66
5	8.99	7.15	5.09	-1.02	-1.38	8.94	161.80	151.66
6	7.79	6.29	5.03	-1.26	-0.79	8.60	127.35	115.80
7	10.06	7.70	5.14	-0.44	-0.73	8.77	188.63	200.36
8	8.81	7.84	4.36	-0.70	-0.71	8.50	159.25	153.41
9	9.23	8.36	4.87	-0.04	-1.11	8.75	166.58	157.74
10	9.93	6.48	5.84	-1.12	-1.75	9.10	170.36	163.23
11	7.36	5.88	5.54	-0.41	-0.38	8.69	119.15	112.81
12	7.68	6.51	5.33	-1.27	0.02	8.57	125.72	107.10
13	7.98	6.50	4.73	-1.41	-0.91	8.49	124.23	111.62
14	8.12	6.66	4.66	-0.61	-1.47	8.63	128.36	109.48
15	8.14	6.41	4.58	-1.40	-2.08	8.59	125.33	106.91
16	8.95	6.64	5.02	-0.04	-0.97	8.83	138.33	130.19
17	8.08	6.69	3.69	-1.37	-1.42	8.39	124.50	101.86
18	9.53	7.73	4.13	-1.66	-1.37	8.21	136.17	103.31
19	8.50	7.23	3.82	-1.90	-1.18	8.30	132.66	115.13
20	8.80	7.14	3.96	-0.46	-0.88	8.26	119.79	89.36
21	8.76	6.99	3.54	-0.99	-1.27	8.39	126.57	99.58
22	10.38	6.83	4.91	-1.23	-1.32	8.90	161.73	163.48
23	9.62	6.25	4.47	-1.67	-1.57	8.88	151.41	135.56
24	9.11	7.47	4.02	-1.86	-0.35	8.96	154.23	128.42
25	10.31	5.54	5.85	0.05	-0.38	8.97	158.42	137.12
26	9.12	5.97	3.92	-1.38	-1.34	8.41	126.23	95.73
27	9.95	6.05	4.24	-1.01	-0.01	8.71	146.65	127.56
28	12.19	8.49	4.99	-1.31	-1.53	8.85	219.08	203.67
29	10.94	7.12	3.54	-1.66	-1.27	8.21	145.10	102.76
30	8.92	6.01	3.23	-1.12	-0.17	8.35	112.87	82.96

d<sub>L</sub> = Longest dimension, d<sub>I</sub> = Intermediate dimension and d<sub>S</sub> = Shortest dimension.

**Table 8.26: Scan results of 19.0 mm RA aggregate particles.**

19.0 mm Sieve								
Particle No.	Dimensions (mm)			Centre of mass (mm)			Surface area (mm <sup>2</sup> )	Volume (mm <sup>3</sup> )
	d <sub>L</sub>	d <sub>I</sub>	d <sub>S</sub>	X	Y	Z		
1	26.58	25.45	16.27	1.52	0.31	13.23	1549.12	4276.44
2	26.51	24.07	19.31	0.48	-1.45	14.78	1704.97	5060.75
3	30.84	26.50	18.14	-0.90	-1.42	14.15	1844.33	5293.09
4	28.10	24.78	16.54	2.87	0.14	13.32	1638.73	4602.88
5	27.68	24.59	16.84	-0.88	-1.90	14.90	1614.55	4814.32
6	30.83	21.15	21.20	0.77	-0.74	15.00	1764.66	4989.07
7	32.37	22.34	18.57	1.12	-0.32	14.41	1711.81	5220.09
8	21.84	23.50	17.61	1.38	-0.23	14.32	1550.01	4517.38
9	23.81	23.58	18.03	3.52	-2.63	13.74	1586.39	4142.20
10	27.26	25.12	13.96	1.21	0.29	13.63	1580.54	4095.18
11	34.35	25.19	14.85	0.27	-2.76	13.10	1823.05	5255.90
12	30.21	24.59	11.92	2.46	0.08	12.17	1579.75	4027.84
13	35.58	24.74	18.31	-1.21	-1.45	14.37	2017.22	5926.61
14	31.26	23.10	14.18	2.26	0.61	12.75	1533.32	3917.87
15	31.07	20.59	17.85	-2.96	-0.03	13.63	1610.27	4509.27
16	30.18	22.90	12.70	0.71	0.10	12.67	1510.90	3937.34
17	28.58	25.29	14.99	-0.08	0.29	14.01	1558.20	4345.67
18	30.91	23.94	13.65	0.87	-0.14	12.84	1514.89	3917.03
19	26.25	24.64	13.79	0.71	0.11	12.85	1401.96	3569.07
20	28.13	21.26	12.76	4.42	-1.36	11.78	1289.12	3032.38
21	25.30	23.79	11.64	1.89	-0.03	12.16	1438.90	3669.98
22	29.62	28.38	14.57	0.65	-4.52	13.04	1607.14	4014.31
23	29.16	25.68	11.32	-0.28	0.80	12.04	1582.85	4177.85
24	28.86	25.35	14.79	0.01	-0.18	12.28	1446.82	3402.50
25	27.50	22.25	10.83	0.51	-1.39	11.54	1328.62	2786.67
26	39.56	23.86	13.94	-2.10	-3.74	12.28	1870.75	4779.89
27	28.69	22.36	10.72	-0.23	-0.55	11.63	1524.86	3697.06
28	40.03	23.78	11.27	-0.84	-0.64	11.59	1760.03	4142.53
29	28.89	25.08	9.12	3.58	1.63	11.19	1309.13	2701.30
30	36.52	23.71	11.84	0.91	-1.75	12.19	1783.66	4430.11

d<sub>L</sub> = Longest dimension, d<sub>I</sub> = Intermediate dimension and d<sub>S</sub> = Shortest dimension.

**Table 8.27: Scan results of 13.2 mm RA aggregate particles.**

13.2 mm Sieve								
Particle No.	Dimensions (mm)			Centre of mass (mm)			Surface area (mm <sup>2</sup> )	Volume (mm <sup>3</sup> )
	d <sub>L</sub>	d <sub>I</sub>	d <sub>S</sub>	X	Y	Z		
1	21.10	20.31	14.74	1.71	-0.19	12.79	1145.80	2784.87
2	25.20	19.84	18.30	-1.02	-0.70	14.75	1419.67	4141.67
3	25.76	20.63	13.00	1.06	-0.01	12.49	1277.32	3377.71
4	26.21	21.25	15.25	1.30	-0.30	13.48	1331.87	3581.55
5	28.13	18.06	16.18	2.24	-1.48	13.08	1282.33	3263.95
6	25.55	19.31	15.32	-2.01	-0.42	13.38	1280.44	3420.48
7	25.92	20.04	19.56	-0.09	-1.15	14.29	1341.24	3777.69
8	21.12	19.30	11.85	0.65	-0.51	12.24	1054.03	2456.68
9	24.26	21.35	16.58	-1.28	0.29	14.16	1330.16	3563.29
10	22.75	21.27	16.78	0.29	-1.73	14.20	1215.42	3278.78
11	27.96	20.62	11.71	-0.89	-1.99	12.23	1387.85	3520.86
12	30.25	18.14	12.70	0.30	-0.62	11.93	1184.43	2625.96
13	25.55	21.27	11.74	-0.83	0.35	12.62	1192.78	2816.79
14	23.56	19.40	11.92	-0.90	0.51	12.15	1112.12	2547.71
15	21.94	19.15	10.71	-0.56	-0.09	11.92	1041.68	2298.36
16	23.87	17.85	13.51	2.80	-1.84	12.65	1037.95	2416.10
17	26.55	24.06	11.71	2.39	0.17	11.81	1272.05	2939.32
18	25.48	23.41	13.01	0.28	1.77	12.24	1273.90	2865.14
19	22.82	19.85	11.58	-0.85	0.46	12.00	993.07	2163.28
20	22.14	21.38	11.05	2.30	-0.86	12.29	1079.82	2459.75
21	25.11	23.27	10.18	0.16	1.07	11.59	1243.91	2627.57
22	23.76	19.27	10.02	1.72	-1.84	11.26	950.71	1881.26
23	32.28	23.07	10.11	1.73	-1.59	11.61	1453.89	3343.08
24	25.43	20.59	12.67	-0.90	-1.15	12.48	1215.02	2592.67
25	27.25	19.72	8.88	-0.91	-1.00	11.05	1011.17	2003.22
26	29.39	22.07	11.14	-0.50	0.83	11.36	1317.23	2841.06
27	24.16	19.02	8.70	0.72	-0.19	10.30	971.82	1695.36
28	25.26	20.49	8.00	0.52	-2.89	10.56	1036.43	1740.76
29	30.32	20.84	9.10	-1.98	-1.04	10.78	1319.19	2538.01
30	24.63	20.85	7.42	0.53	1.94	10.13	945.32	1461.21

d<sub>L</sub> = Longest dimension, d<sub>I</sub> = Intermediate dimension and d<sub>S</sub> = Shortest dimension.

**Table 8.28: Scan results of 9.5 mm RA aggregate particles.**

9.5 mm Sieve								
Particle No.	Dimensions (mm)			Centre of mass (mm)			Surface area (mm <sup>2</sup> )	Volume (mm <sup>3</sup> )
	d <sub>L</sub>	d <sub>I</sub>	d <sub>S</sub>	X	Y	Z		
1	15.98	14.39	11.89	-2.30	-0.26	12.98	609.22	1089.53
2	18.96	13.16	11.51	0.56	-0.05	11.49	618.40	1130.27
3	16.95	12.89	11.18	-0.07	-0.20	11.43	591.72	1109.40
4	15.28	12.61	10.00	-0.99	-1.97	11.16	440.40	658.78
5	15.85	14.51	10.43	1.15	-1.32	10.79	541.83	905.28
6	15.61	13.68	8.80	0.27	-0.05	10.50	484.78	806.24
7	15.97	12.34	10.81	0.20	-2.02	11.15	479.29	824.62
8	14.02	12.35	10.64	-0.47	-0.34	11.37	453.62	703.88
9	11.90	10.38	8.09	-0.68	-0.43	10.27	348.75	482.83
10	13.52	11.54	9.80	-1.09	0.19	11.29	451.75	744.09
11	27.05	14.49	11.52	-0.38	-1.50	11.78	915.55	1826.63
12	21.67	14.67	10.41	-1.44	-0.57	11.22	737.11	1463.74
13	16.49	13.08	10.13	-1.08	-0.15	10.83	549.29	905.23
14	20.30	14.84	10.10	1.25	-1.49	11.58	696.73	1420.15
15	19.05	12.60	8.98	0.29	-0.83	10.73	530.68	832.44
16	14.52	14.44	12.55	-1.27	-0.54	11.80	611.49	1106.39
17	20.39	14.38	7.58	-0.08	-1.18	10.47	606.55	917.44
18	20.13	15.82	7.57	-1.56	-0.42	10.33	590.38	898.28
19	18.93	15.74	6.60	-0.41	-0.88	9.86	615.50	895.56
20	15.49	14.81	7.99	-0.59	0.88	10.34	516.19	809.26
21	17.52	13.88	7.96	-1.17	-1.45	10.71	542.55	875.87
22	14.90	14.75	8.20	0.40	-0.56	10.50	518.51	812.26
23	19.45	12.71	5.69	0.27	-0.48	9.68	510.23	671.80
24	20.49	11.43	7.76	-0.92	-1.03	10.41	533.27	825.79
25	20.65	14.55	5.65	-0.54	-0.84	9.57	521.61	662.94
26	20.30	16.56	6.67	-0.46	0.24	9.84	635.45	902.44
27	18.53	17.74	5.37	-0.68	0.24	9.44	603.47	775.90
28	17.24	12.88	5.48	0.12	-0.60	9.77	428.25	533.56
29	17.36	13.61	5.46	0.30	0.33	9.32	435.19	477.28
30	20.00	13.74	5.15	-0.32	-0.45	9.27	454.81	479.42

d<sub>L</sub> = Longest dimension, d<sub>I</sub> = Intermediate dimension and d<sub>S</sub> = Shortest dimension.

**Table 8.29: Scan results of 6.7 mm RA aggregate particles.**

6.7 mm Sieve								
Particle No.	Dimensions (mm)			Centre of mass (mm)			Surface area (mm <sup>2</sup> )	Volume (mm <sup>3</sup> )
	d <sub>L</sub>	d <sub>I</sub>	d <sub>S</sub>	X	Y	Z		
1	15.48	9.23	8.65	-1.50	-1.90	10.49	334.33	433.73
2	13.83	10.59	7.85	0.83	-0.44	10.12	330.39	452.03
3	13.96	10.29	8.30	-0.33	-1.40	10.20	335.96	434.73
4	13.11	8.55	6.24	-1.61	-2.23	9.39	255.20	269.77
5	12.26	9.92	8.93	-1.06	-1.75	10.51	363.62	515.31
6	13.32	9.78	7.40	-1.47	-1.65	9.98	309.52	409.90
7	12.81	11.37	6.00	-0.93	1.14	9.67	288.73	357.93
8	12.57	10.23	6.57	0.92	0.40	9.74	271.08	343.82
9	13.23	9.64	7.05	-1.26	-1.07	9.93	304.44	415.26
10	12.65	8.21	7.53	0.61	0.42	9.69	259.34	316.63
11	21.91	11.28	7.93	-1.07	0.44	10.62	533.39	801.67
12	19.51	9.70	7.95	-1.43	-1.07	10.69	473.64	705.66
13	19.39	12.07	6.83	-1.25	-0.99	9.68	408.85	507.30
14	17.12	10.97	7.54	-1.49	-1.39	9.92	392.07	528.96
15	15.80	11.65	6.39	-0.58	-0.33	9.45	401.43	464.23
16	16.18	10.09	5.39	-1.38	-1.23	9.42	361.33	431.78
17	15.53	9.93	7.42	-1.65	-1.40	9.95	340.04	413.88
18	12.47	9.71	4.46	-0.76	0.09	8.92	253.54	250.89
19	15.24	12.94	5.26	-0.64	-0.07	9.57	345.83	378.87
20	13.19	9.94	5.15	-0.79	-1.63	9.21	271.40	303.73
21	17.92	8.47	7.30	-0.83	-0.23	9.55	360.10	397.97
22	15.41	12.15	6.40	-2.35	-1.01	9.79	372.97	475.01
23	13.39	11.37	7.36	-2.80	-2.00	9.54	290.55	305.04
24	15.58	8.78	6.47	-0.89	-2.24	9.58	303.00	324.56
25	15.24	8.89	6.35	0.70	-0.46	9.49	285.48	306.81
26	14.78	12.22	4.91	-0.23	-1.52	9.34	313.82	283.01
27	13.60	12.04	4.52	0.18	-0.85	9.03	304.46	311.95
28	14.06	8.84	4.80	-0.63	-1.43	8.98	271.55	265.20
29	14.27	10.49	4.20	-1.50	-2.15	9.13	294.00	298.52
30	15.48	9.23	8.65	-1.50	-1.90	10.49	334.33	433.73

d<sub>L</sub> = Longest dimension, d<sub>I</sub> = Intermediate dimension and d<sub>S</sub> = Shortest dimension.



**Table 8.30: Scan results of 4.75 mm RA aggregate particles.**

4.75 mm Sieve								
Particle No.	Dimensions (mm)			Centre of mass (mm)			Surface area (mm <sup>2</sup> )	Volume (mm <sup>3</sup> )
	d <sub>L</sub>	d <sub>I</sub>	d <sub>S</sub>	X	Y	Z		
1	10.32	6.78	6.88	-0.32	-0.89	9.41	171.56	149.47
2	10.06	6.92	6.38	-0.05	-0.65	9.50	198.52	202.32
3	7.48	6.98	5.38	-1.21	-1.01	8.87	138.37	123.77
4	9.91	7.98	5.96	0.40	-1.74	9.48	183.13	196.65
5	9.49	7.32	5.84	0.63	-0.61	9.23	158.65	151.45
6	9.63	8.04	5.78	-0.90	-0.97	9.33	178.42	189.99
7	8.70	6.19	3.81	-0.68	-0.76	8.35	116.24	86.09
8	8.35	7.29	3.75	0.27	-0.23	8.58	138.02	114.88
9	8.09	6.61	4.64	-0.48	-0.51	8.73	116.70	98.80
10	7.55	6.27	3.73	0.29	-0.23	8.37	106.49	78.50
11	11.27	7.15	5.08	0.72	-0.68	9.22	184.75	179.44
12	11.76	7.53	5.29	-0.87	0.10	8.97	191.53	179.21
13	11.44	7.50	4.90	-1.35	-0.98	8.95	203.34	201.70
14	10.90	8.33	4.45	-0.71	-0.34	8.69	171.57	153.98
15	11.54	8.60	5.65	-1.74	-0.82	9.21	195.44	186.40
16	13.72	6.30	4.96	0.22	-0.19	8.89	195.51	168.57
17	13.22	8.34	6.94	0.83	-1.07	9.43	232.53	244.30
18	13.71	7.20	4.55	-0.78	-1.10	8.61	196.35	168.66
19	11.14	5.82	4.10	0.09	-1.14	8.57	155.65	124.60
20	12.63	5.46	4.81	-0.83	-1.38	8.82	176.10	146.47
21	16.90	8.58	4.26	-1.31	-1.68	8.87	259.35	210.16
22	11.16	6.90	4.21	0.33	-0.94	8.64	161.68	128.05
23	10.38	8.73	4.34	-0.59	0.10	8.69	180.31	155.76
24	11.53	7.47	3.21	-0.50	-0.05	8.33	156.67	115.77
25	10.38	7.96	2.85	-0.59	-0.23	8.24	150.25	102.45
26	11.08	8.39	4.32	0.64	0.08	8.72	177.12	145.60
27	12.56	8.37	4.51	-0.76	-0.19	8.64	182.53	150.61
28	11.09	6.87	3.87	-0.77	-0.11	8.32	137.53	91.70
29	11.42	8.64	2.80	-1.46	-0.64	8.34	149.10	92.42
30	10.68	7.20	2.15	-0.71	-0.59	8.02	119.65	57.83

d<sub>L</sub> = Longest dimension, d<sub>I</sub> = Intermediate dimension and d<sub>S</sub> = Shortest dimension.

## 9 APPENDIX B: MATLAB CODE FOR ANALYSIS OF LASER SCAN DATA

% Laser Data Processing  
% Get file from disk

```
clear
close all
cd ('D:\laser scan data\');
ANUM = input('Enter FILE NAME (no ext) ','s');
LNUM = input('Enter the L value to process ','s');
LL = str2num(LNUM);
File1 = strcat(ANUM, '.asc');

FixX = input('Enter Fixed point for X ','s');
FixY = input('Enter Fixed point for Y ','s');
FixZ = input('Enter Fixed point for Z ','s');
FixX = str2num(FixX);
FixY = str2num(FixY);
FixZ = str2num(FixZ);

DATA1 = load (File1);      % ascii file

fil = 1;
[M N] = size(DATA1);

% First ZZ data
DataA(:, :) = decimate(DATA1(:, :), fil);
clear DATA1;
DataX(:, :) = DataA(1:M, 1) - FixX;
DataY(:, :) = DataA(1:M, 2) - FixY;
DataZ(:, :) = DataA(1:M, 3) - FixZ;
clear DataA;
DataB = zeros(M, N);
DataB(1:M, 1) = (DataX);
DataB(1:M, 2) = (DataY);
DataB(1:M, 3) = (DataZ);
RadiusA = (((DataX(:, :).^2) + (DataY(:, :).^2) + (DataZ(:, :).^2)).^0.5);
```

% This routine selects a Quadrant (1 - 4 is where Z is Positive and 5 - 8 is where Z is negative)

```
Quadr(:, :) = zeros(M, 1);
for i = 1:1:M
if DataX(i, 1) > 0 && DataY(i, 1) > 0 && DataZ(i, 1) > 0
    Quadr(i, 1) = 1;
elseif DataX(i, 1) < 0 && DataY(i, 1) > 0 && DataZ(i, 1) > 0
    Quadr(i, 1) = 2;
elseif DataX(i, 1) < 0 && DataY(i, 1) < 0 && DataZ(i, 1) > 0
    Quadr(i, 1) = 3;
elseif DataX(i, 1) > 0 && DataY(i, 1) < 0 && DataZ(i, 1) > 0
    Quadr(i, 1) = 4;
elseif DataX(i, 1) > 0 && DataY(i, 1) > 0 && DataZ(i, 1) < 0
```

```

    Quadr(i,1) = 5;
elseif DataX(i,1) < 0 && DataY(i,1) > 0 && DataZ(i,1) < 0
    Quadr(i,1) = 6;
elseif DataX(i,1) < 0 && DataY(i,1) < 0 && DataZ(i,1) < 0
    Quadr(i,1) = 7;
elseif DataX(i,1) > 0 && DataY(i,1) < 0 && DataZ(i,1) < 0
    Quadr(i,1) = 8;
end
end

```

#### % Calculating angle Alpha (Angles are in RADIANS)

```

AngleAlpha (:,:) = zeros(M,1);
for i = 1:1:M
    if Quadr(i,1) == 1;
        AngleAlpha(i,1) = atan(abs(DataY(i,1)/DataX(i,1)));
    elseif Quadr(i,1) == 2;
        AngleAlpha(i,1) = ((pi/2)+atan(abs(DataX(i,1)/DataY(i,1))));
    elseif Quadr(i,1) == 3;
        AngleAlpha(i,1) = (pi+atan(abs(DataY(i,1)/DataX(i,1))));
    elseif Quadr(i,1) == 4;
        AngleAlpha(i,1) = ((3/2*pi)+atan(abs(DataX(i,1)/DataY(i,1))));
    elseif Quadr(i,1) == 5;
        AngleAlpha(i,1) = atan(abs(DataY(i,1)/DataX(i,1)));
    elseif Quadr(i,1) == 6;
        AngleAlpha(i,1) = ((pi/2)+atan(abs(DataX(i,1)/DataY(i,1))));
    elseif Quadr(i,1) == 7;
        AngleAlpha(i,1) = (pi+atan(abs(DataY(i,1)/DataX(i,1))));
    elseif Quadr(i,1) == 8;
        AngleAlpha(i,1) = ((3/2*pi)+atan(abs(DataX(i,1)/DataY(i,1))));
    end
end

```

#### % Calculating angle Beta (Angles are in RADIANS)

```

AngleBeta (:,:) = zeros(M,1);
for i = 1:1:M
    AngleBeta(i,1) = (acos(DataZ(i,1)/RadiusA(i,1)));
end

```

#### % values of l m and xx

```

l = LL;
xx = (l+1)^2;

```

#### % Setting up file sizes

```

Ylm (:,:) = zeros(M,xx);
anbd (:,:) = zeros(xx,3);

```

#### % value of l is 0

```

l = 0;
m = 0;
x = 1; % x is a counter for columns in the file Ylm (column 1 is l=0 ans m = 0)
for i = 1:1:M
    Plm = legendre(l,cos(AngleBeta(i,1)));
    if l~=0
        Plm = squeeze(Plm(abs(m)+1,,:));
    end
end

```

```

end
Y1 = ((2*l+1)/(4*pi));
Y2 = factorial(l-abs(m))/factorial(l+abs(m));
Y3 = sqrt(Y1*Y2);
if m >= 0
    Ylm(i,x) = Y3*Plm*exp((-1)^(1/2)*m*AngleAlpha(i,1));
elseif m<0
    Ylm(i,x) = (-1)^abs(m)*Y3*Plm*exp((-1)^(1/2)*m*AngleAlpha(i,1));
end
end

```

**% Main loop**

```

for l = 1:1:LL;
    if l == 1 m = -l; x = l*l+1; mx = x+l+l; end
    if l == 2 m = -l; x = l*l+1; mx = x+l+l; end
    if l == 3 m = -l; x = l*l+1; mx = x+l+l; end
    if l == 4 m = -l; x = l*l+1; mx = x+l+l; end
    if l == 5 m = -l; x = l*l+1; mx = x+l+l; end
    if l == 6 m = -l; x = l*l+1; mx = x+l+l; end
    if l == 7 m = -l; x = l*l+1; mx = x+l+l; end
    if l == 8 m = -l; x = l*l+1; mx = x+l+l; end
    if l == 9 m = -l; x = l*l+1; mx = x+l+l; end
    if l == 10 m = -l; x = l*l+1; mx = x+l+l; end
    if l == 11 m = -l; x = l*l+1; mx = x+l+l; end
    if l == 12 m = -l; x = l*l+1; mx = x+l+l; end
    if l == 13 m = -l; x = l*l+1; mx = x+l+l; end
    if l == 14 m = -l; x = l*l+1; mx = x+l+l; end
    if l == 15 m = -l; x = l*l+1; mx = x+l+l; end
    if l == 16 m = -l; x = l*l+1; mx = x+l+l; end
    if l == 17 m = -l; x = l*l+1; mx = x+l+l; end
    if l == 18 m = -l; x = l*l+1; mx = x+l+l; end
    if l == 19 m = -l; x = l*l+1; mx = x+l+l; end
    if l == 20 m = -l; x = l*l+1; mx = x+l+l; end
    if l == 21 m = -l; x = l*l+1; mx = x+l+l; end
    if l == 22 m = -l; x = l*l+1; mx = x+l+l; end
    if l == 23 m = -l; x = l*l+1; mx = x+l+l; end
    if l == 24 m = -l; x = l*l+1; mx = x+l+l; end
    if l == 25 m = -l; x = l*l+1; mx = x+l+l; end

for x = x:1:mx;
    for i = 1:1:M
        Plm = legendre(l,cos(AngleBeta(i,1)));
        if l~=0
            Plm = squeeze(Plm(abs(m)+1,.,:));
        end
        Y1 = ((2*l+1)/(4*pi));
        Y2 = factorial(l-abs(m))/factorial(l+abs(m));
        Y3 = sqrt(Y1*Y2);
        if m >= 0
            Ylm(i,x) = Y3*Plm*exp((-1)^(1/2)*m*AngleAlpha(i,1));
        elseif m<0
            Ylm(i,x) = (-1)^abs(m)*Y3*Plm*exp((-1)^(1/2)*m*AngleAlpha(i,1));
        end
    end
end

```

```

    end
  end
  anbd(x,:) = ([l, m, x]);
  m = m + 1;
end
end
A = RadiusA(:,:);
B = Ylm(:,:);
BB=real(B);
C=mldivide(BB,A);
D=C(1);

```

### % Calculating Form, Angularity and Texture Indices

```

if LL == 5
  E = sum(abs(C(1:36)));
  Form = abs(E/D)
elseif LL == 20
  E = sum(abs(C(37:441)));
  Angularity = abs(E/D)
elseif LL == 25
  E = sum(abs(C(442:676)));
  Texture = abs(E/D)
end

```

10 APPENDIX C: EFFECT OF DEGREE ( $l$ ) VALUE ON CONVERGENCE

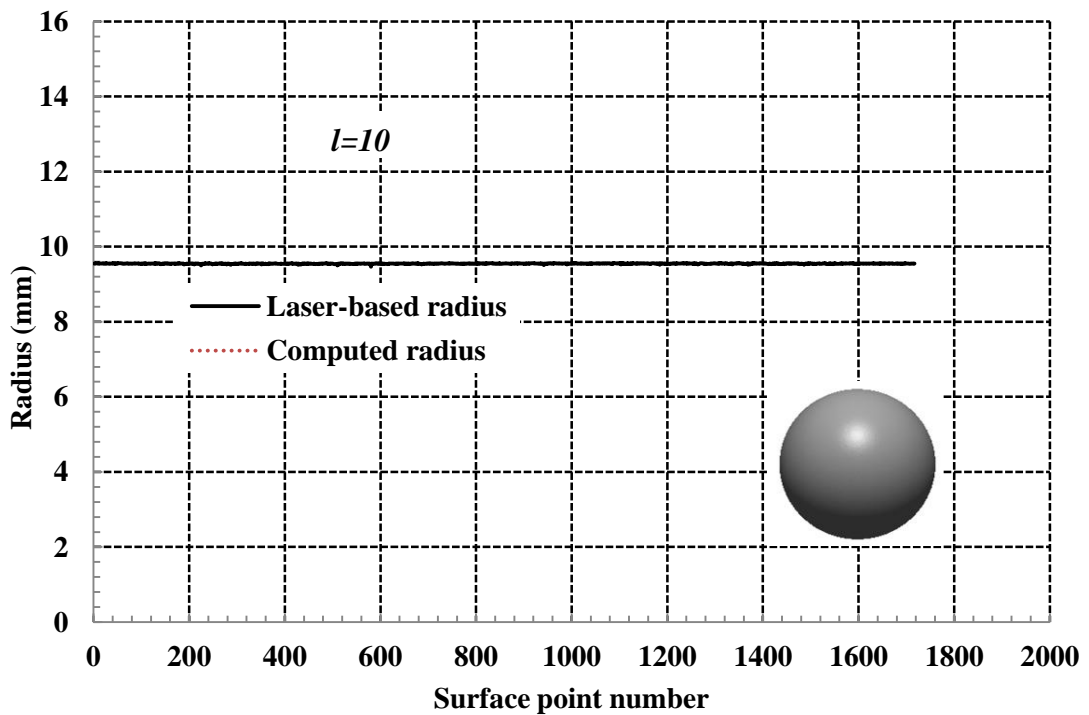
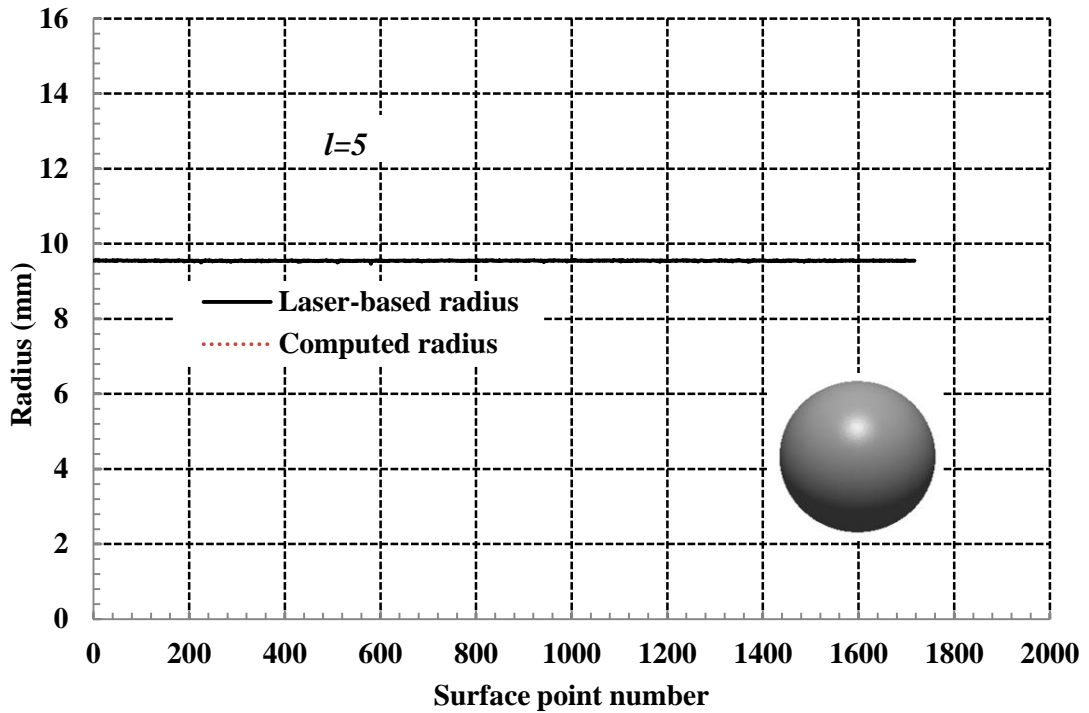


Figure 10.1: Radii determined from laser scans and radii computed using spherical harmonic technique for 19 mm spherical object ( $l=5$  and 10).

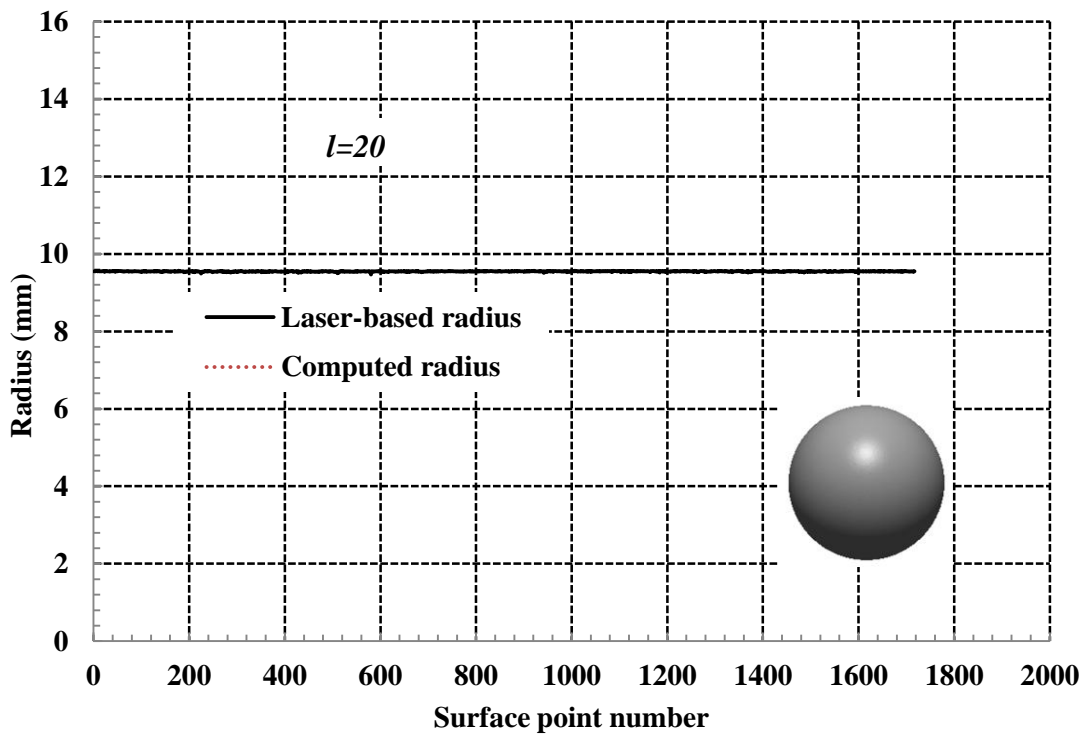
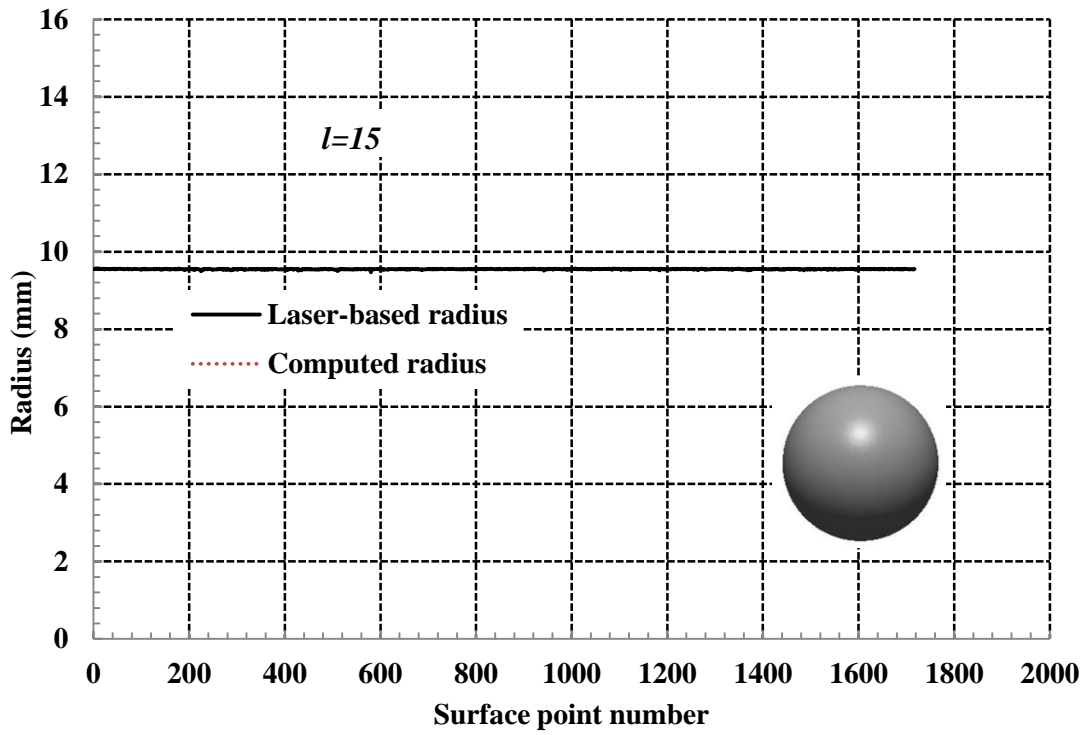


Figure 10.2: Radii determined from laser scans and radii computed using spherical harmonic technique for 19 mm spherical object ( $l=15$  and 20).

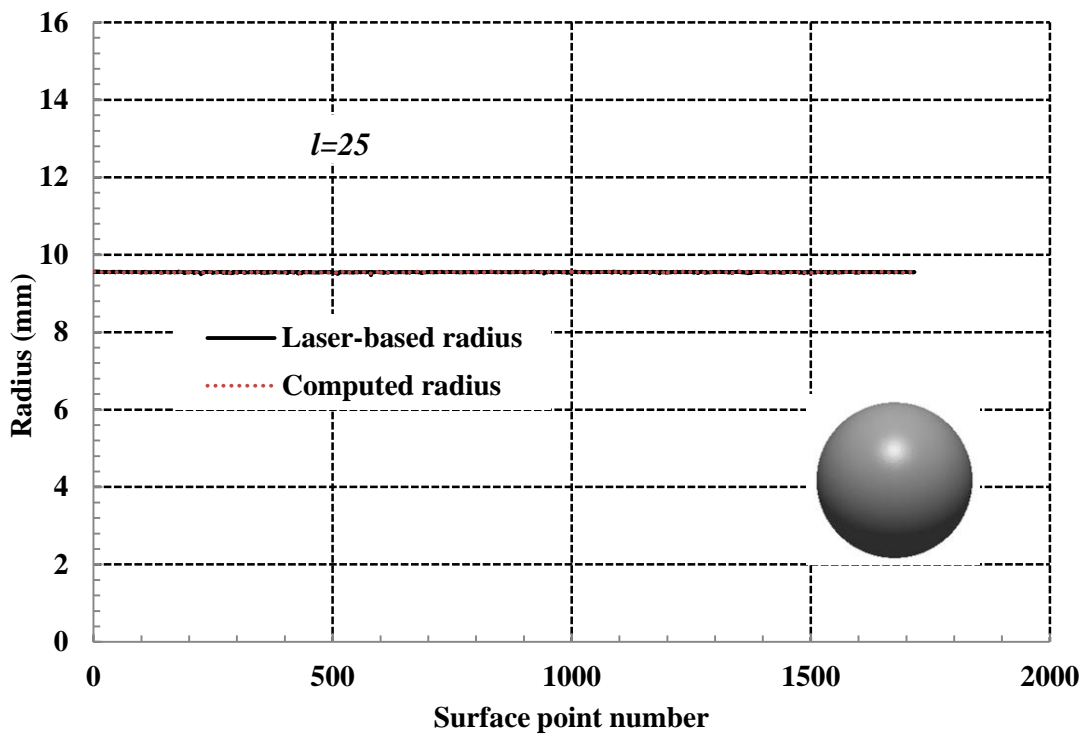


Figure 10.3: Radii determined from laser scans and radii computed using spherical harmonic technique for 19 mm spherical object ( $l=25$ ).



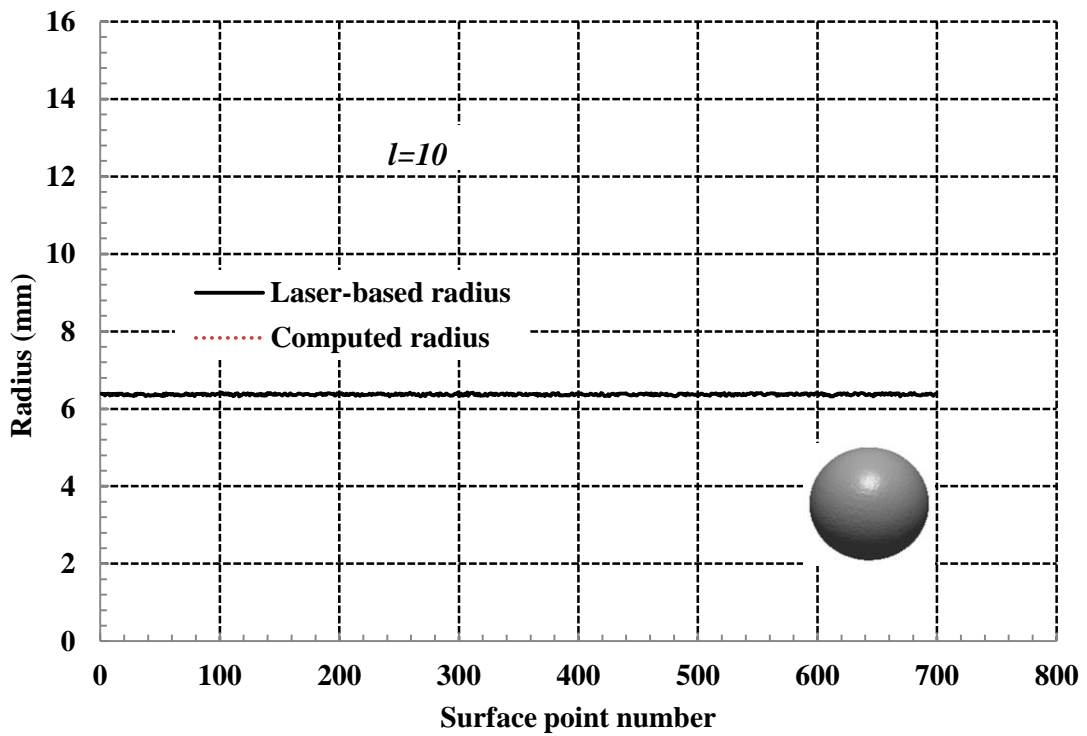
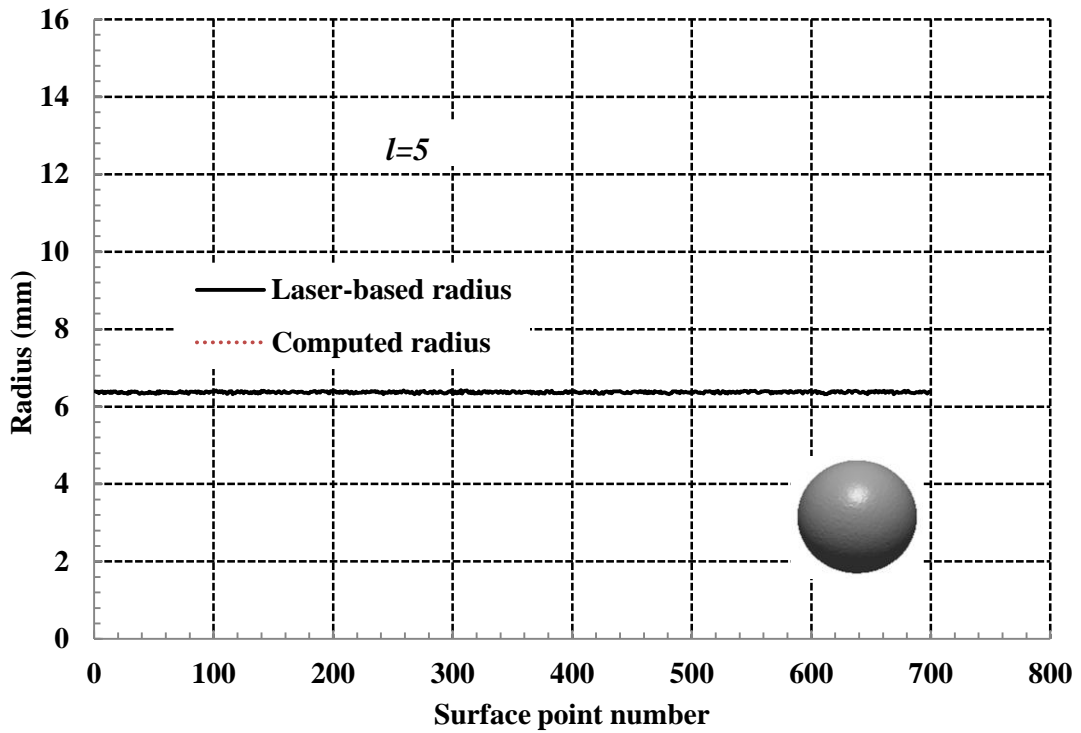


Figure 10.4: Radii determined from laser scans and radii computed using spherical harmonic technique for 13 mm spherical object ( $l=5$  and 10).

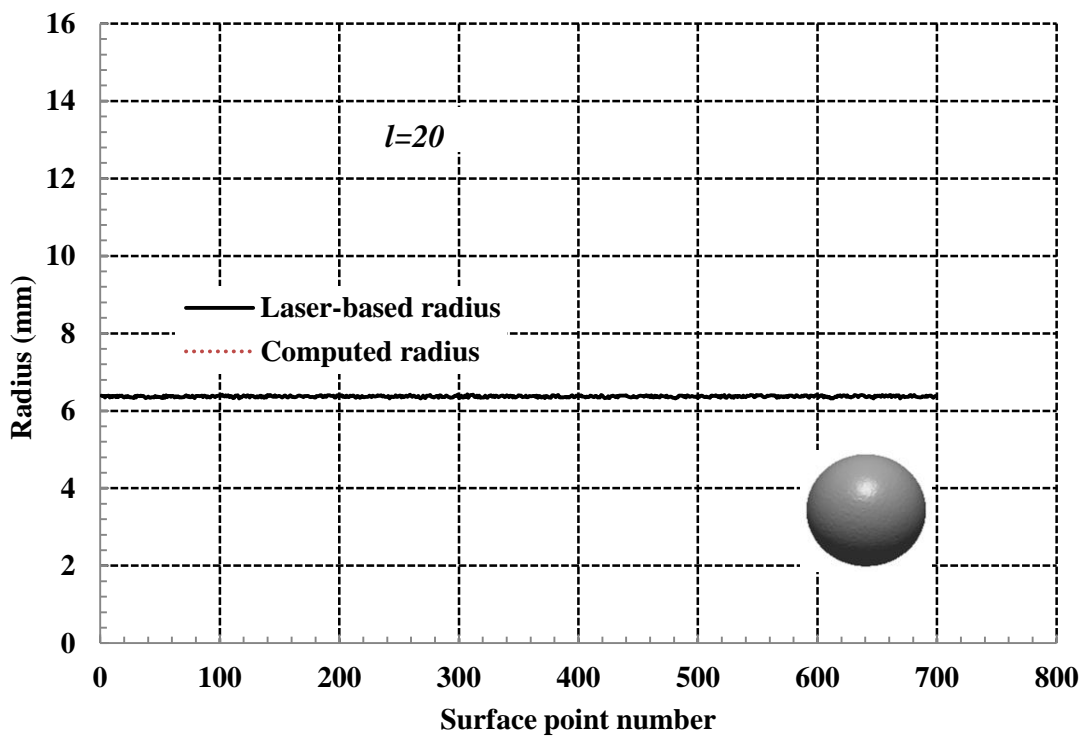
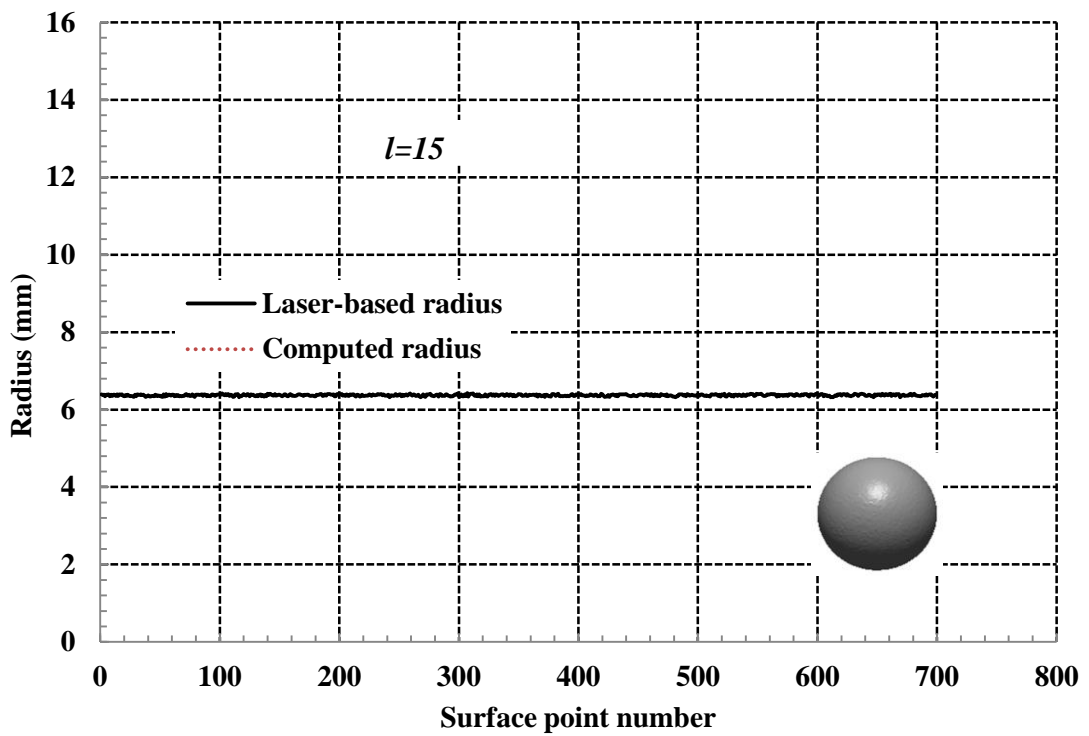


Figure 10.5: Radii determined from laser scans and radii computed using spherical harmonic technique for 13 mm spherical object ( $l=15$  and  $20$ ).

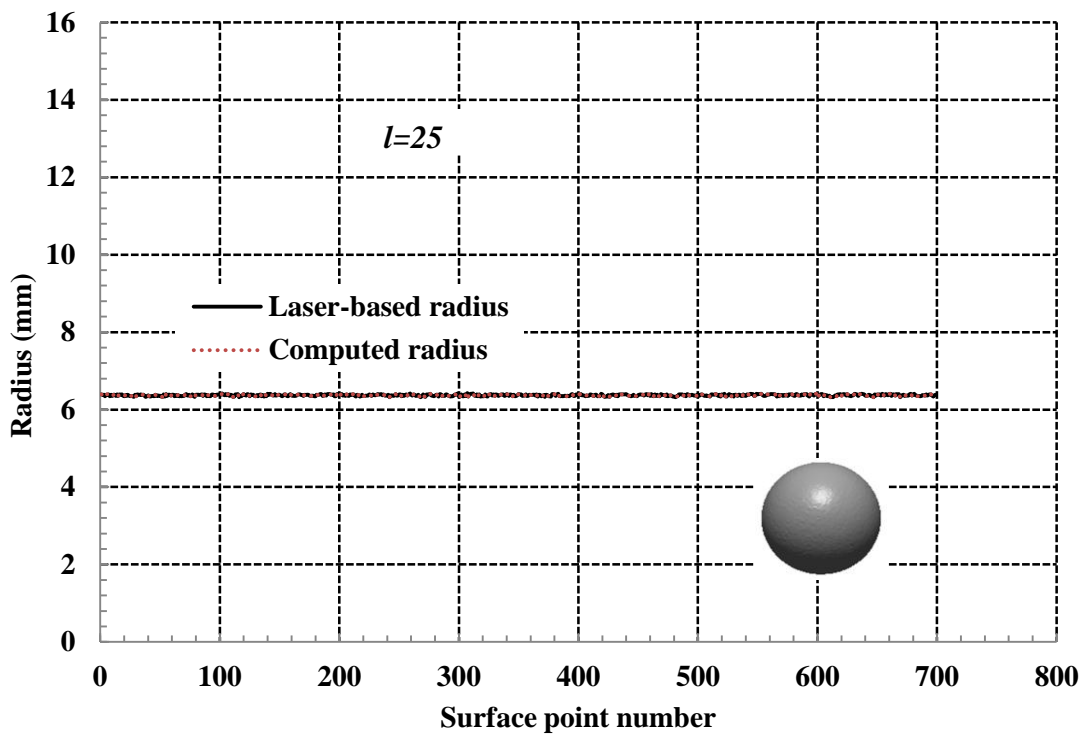


Figure 10.6: Radii determined from laser scans and radii computed using spherical harmonic technique for 13 mm spherical object ( $l=25$ ).

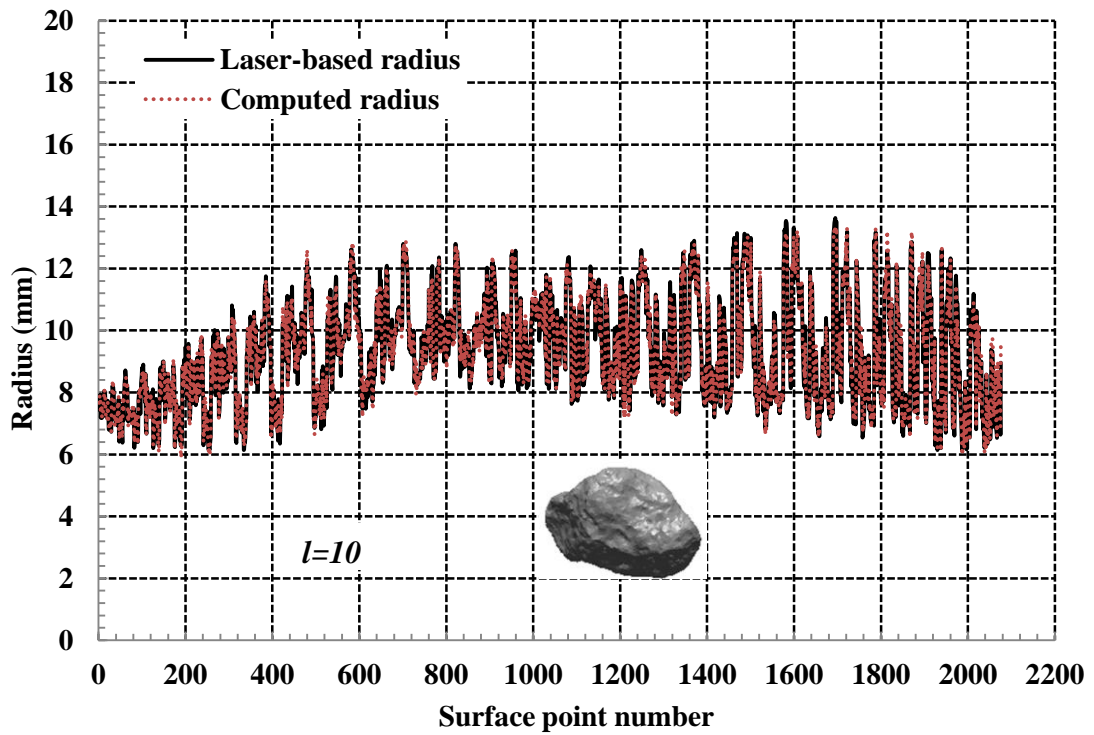
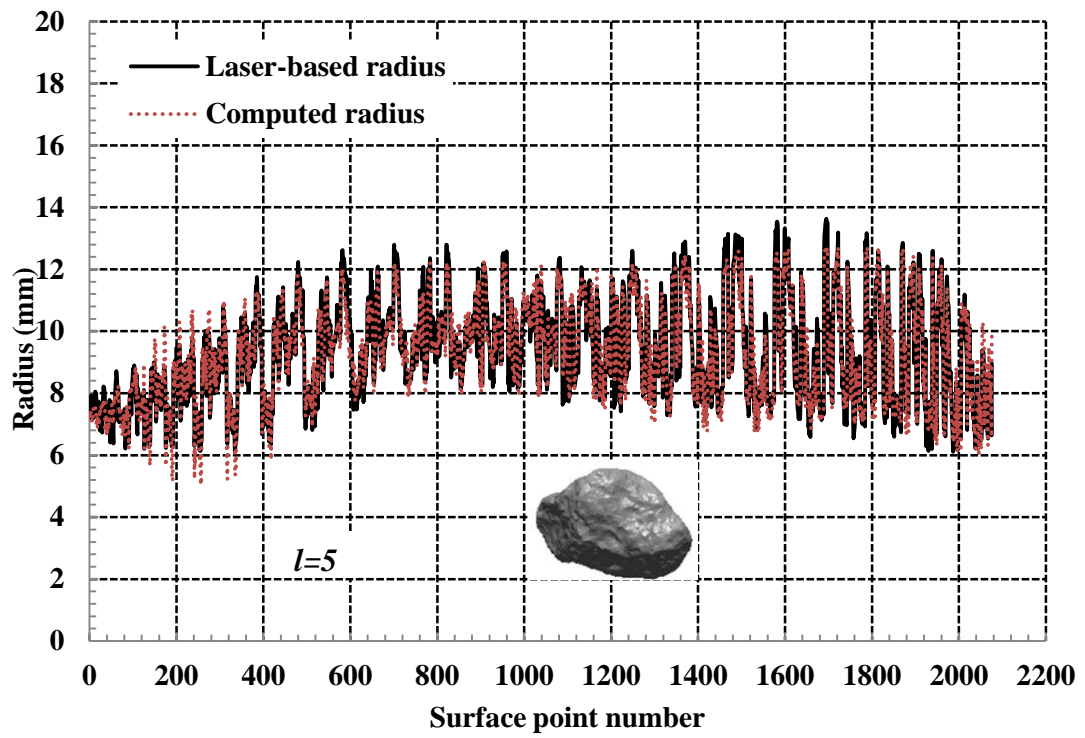


Figure 10.7: Radii determined from laser scans and radii computed using spherical harmonic technique for 13.2 mm aggregate particle ( $l=5$  and 10).

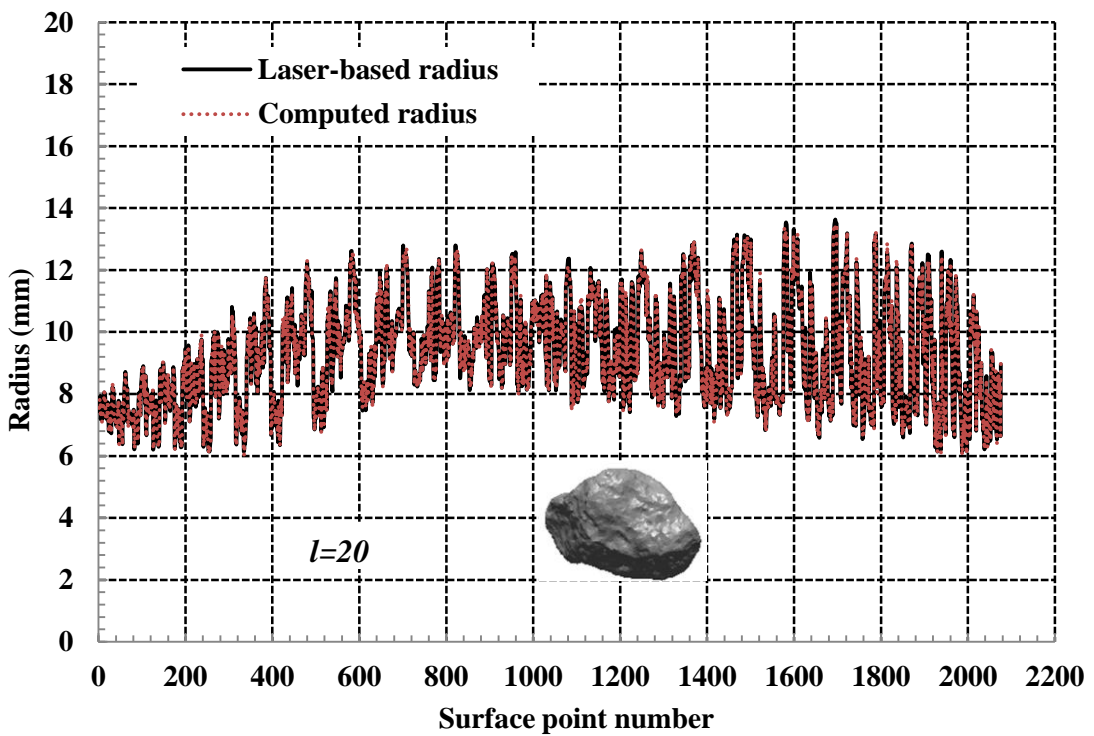
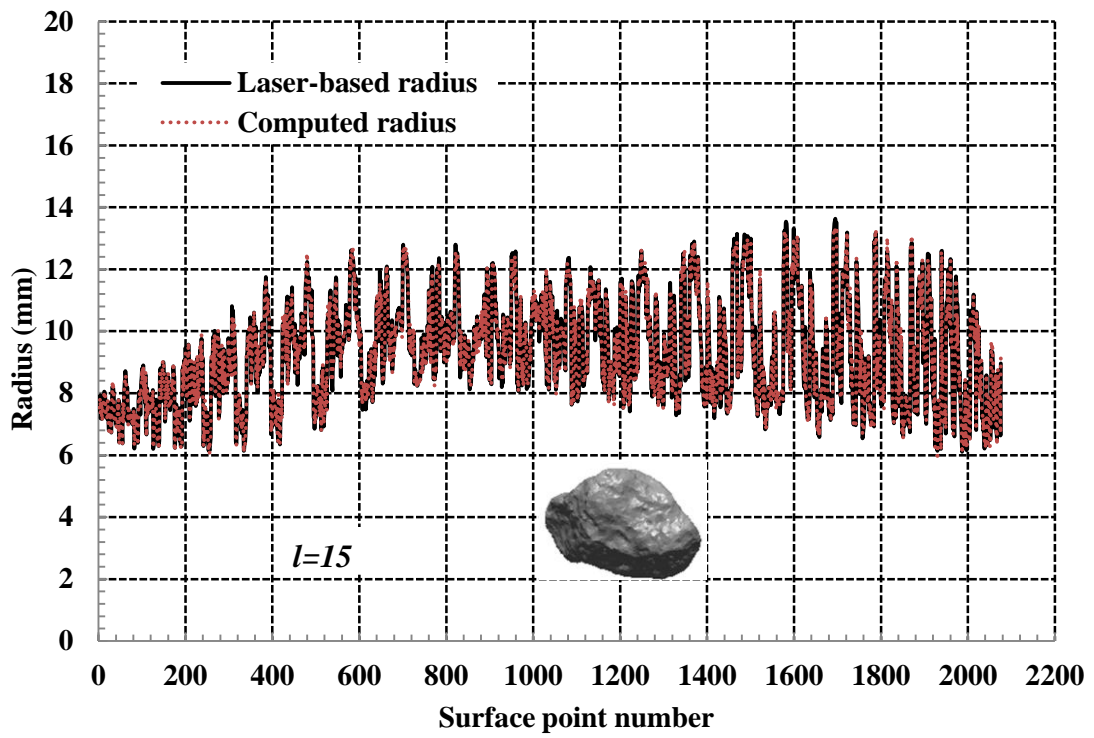


Figure 10.8: Radii determined from laser scans and radii computed using spherical harmonic technique for 13.2 mm aggregate particle ( $l=15$  and 20).

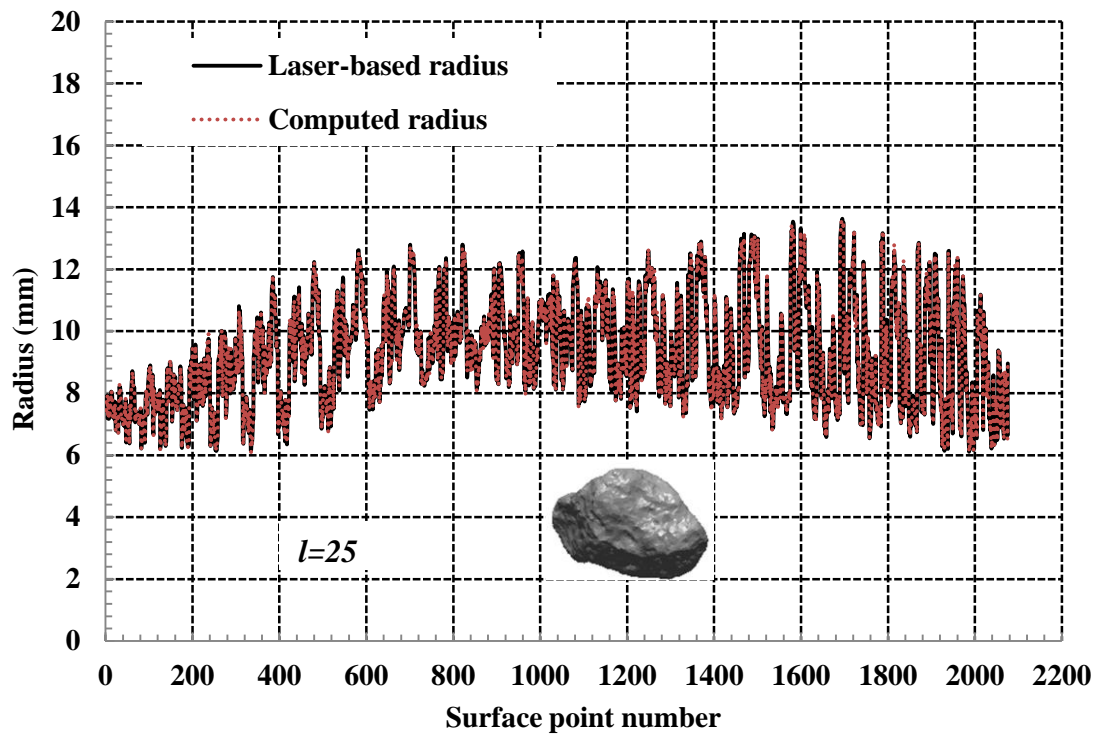


Figure 10.9: Radii determined from laser scans and radii computed using spherical harmonic technique for 13.2 mm aggregate particle ( $l=25$ ).

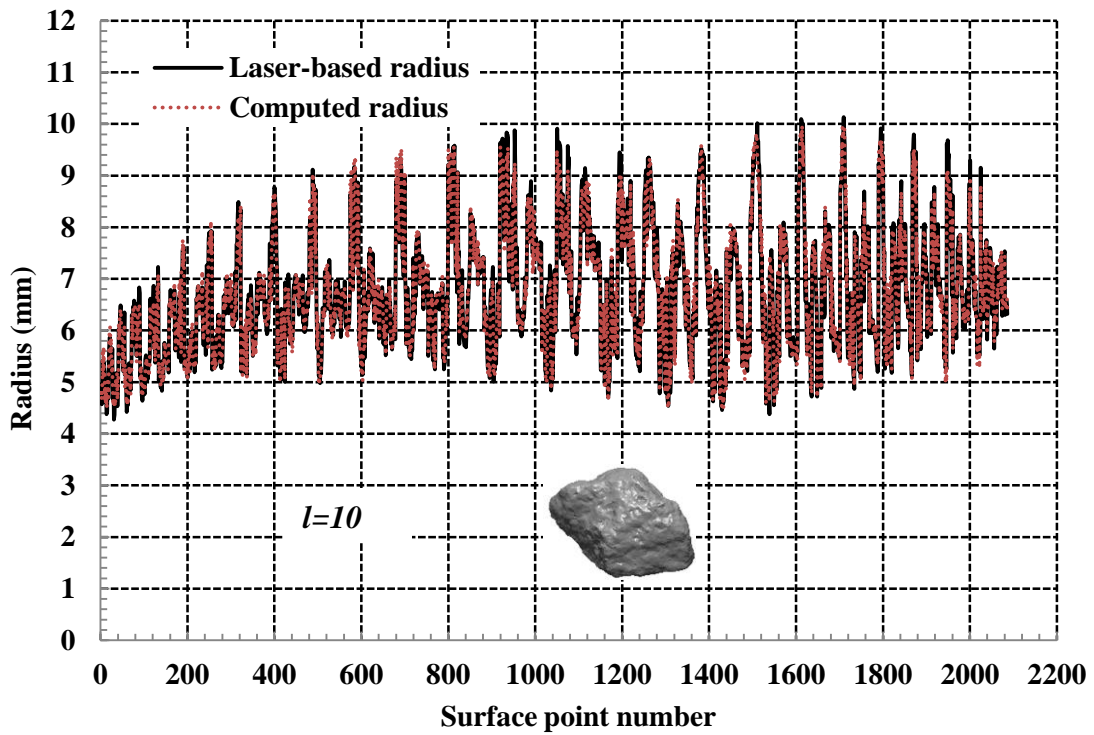
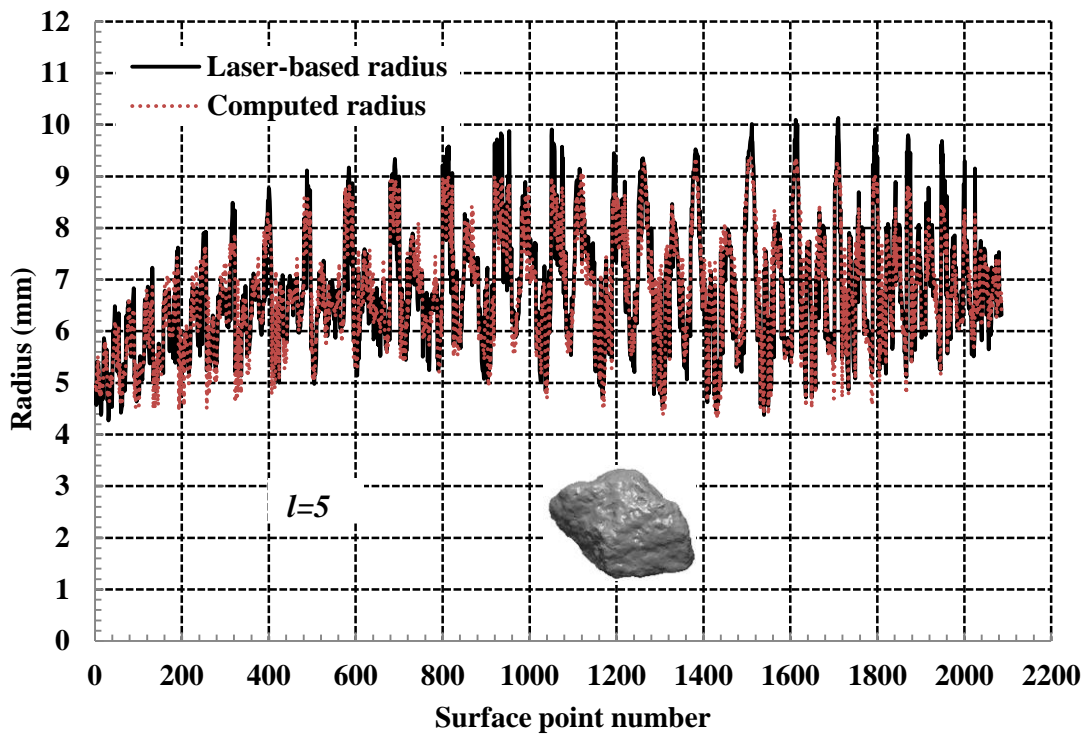


Figure 10.10: Radii determined from laser scans and radii computed using spherical harmonic technique for 9.5 mm aggregate particle ( $l=5$  and 10).

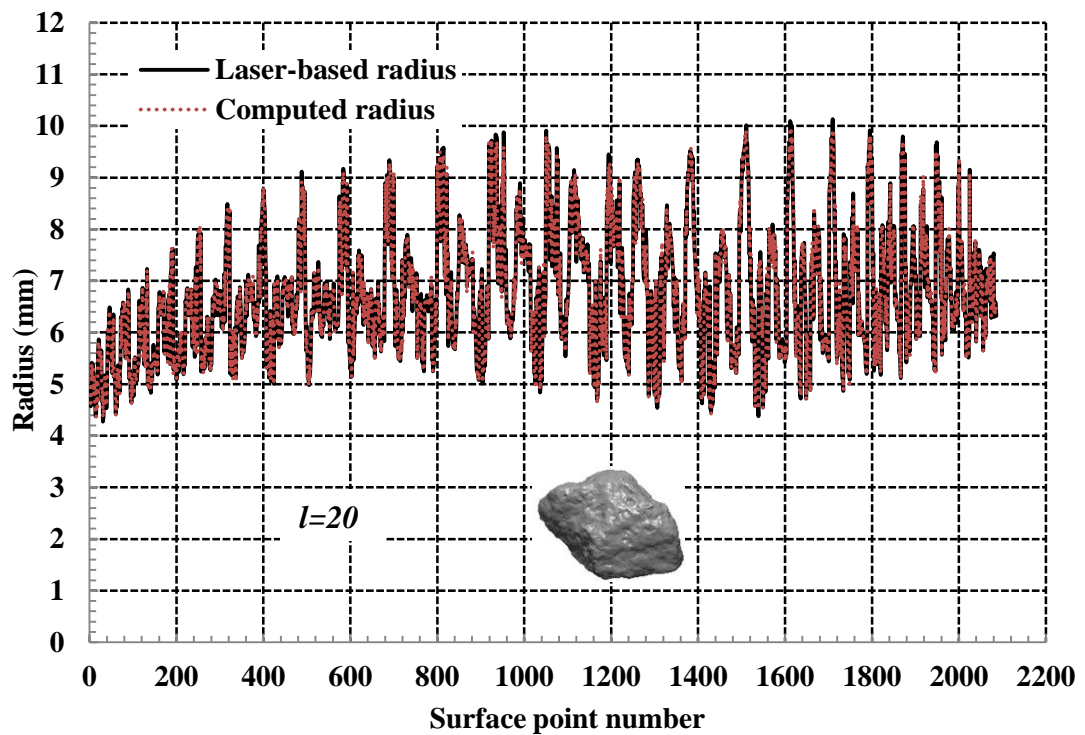
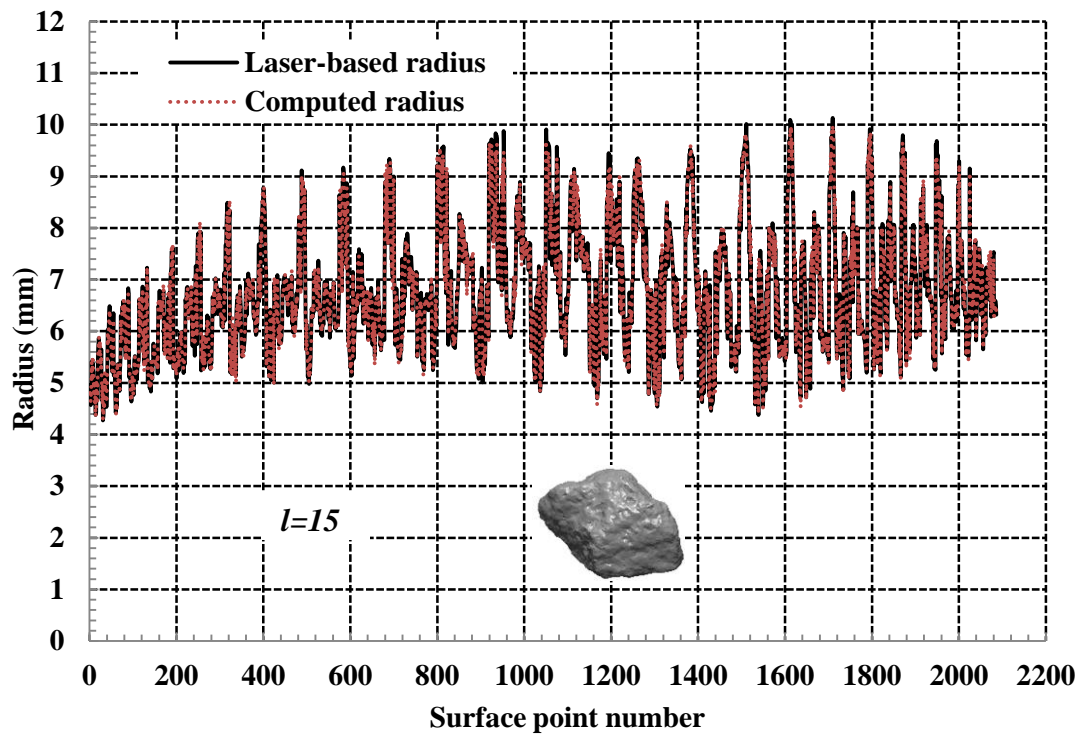


Figure 10.11: Radii determined from laser scans and radii computed using spherical harmonic technique for 9.5 mm aggregate particle ( $l=15$  and 20).



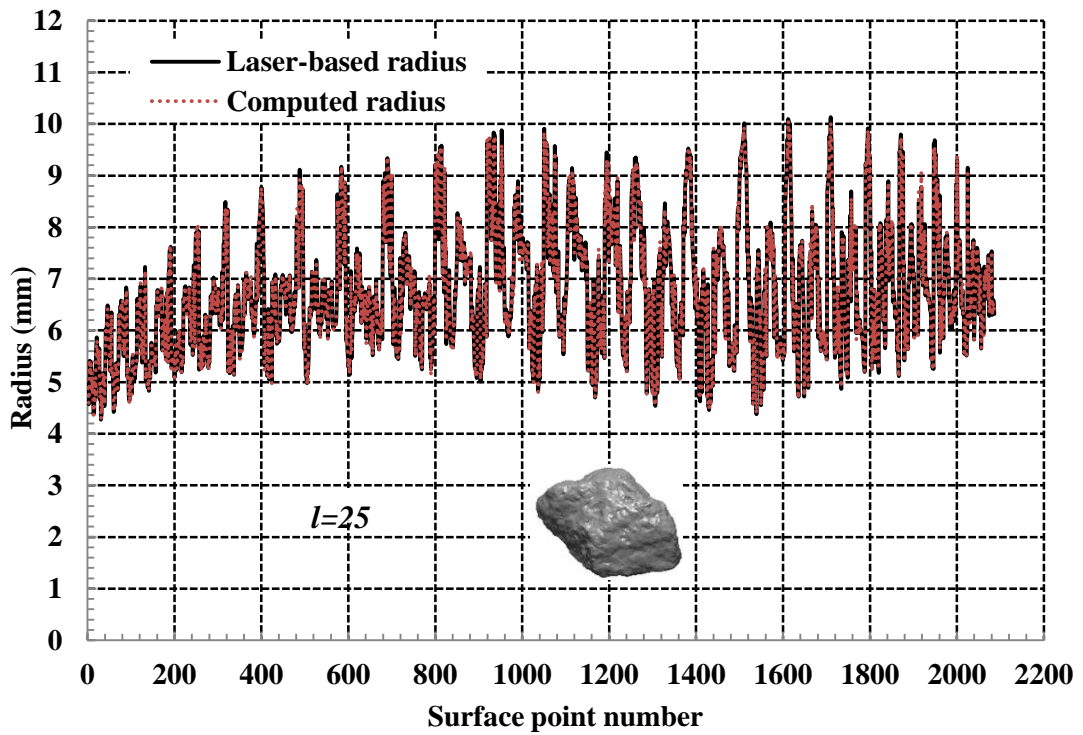
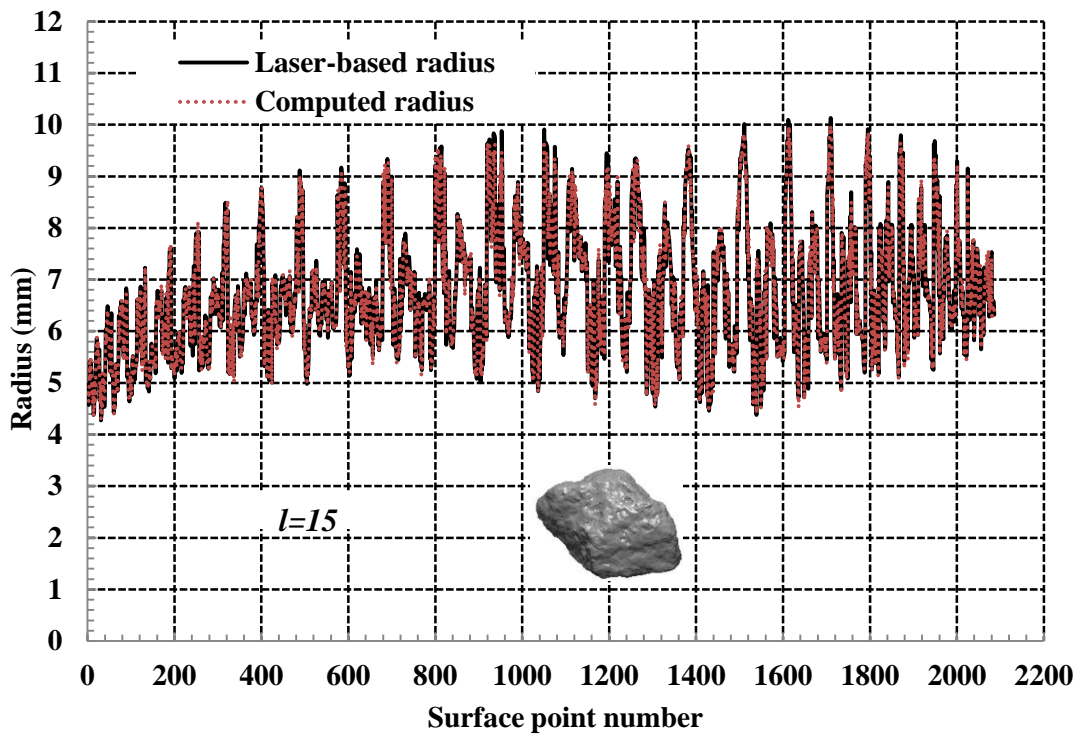


Figure 10.12: Radii determined from laser scans and radii computed using spherical harmonic technique for 9.5 mm aggregate particle ( $l=25$ ).

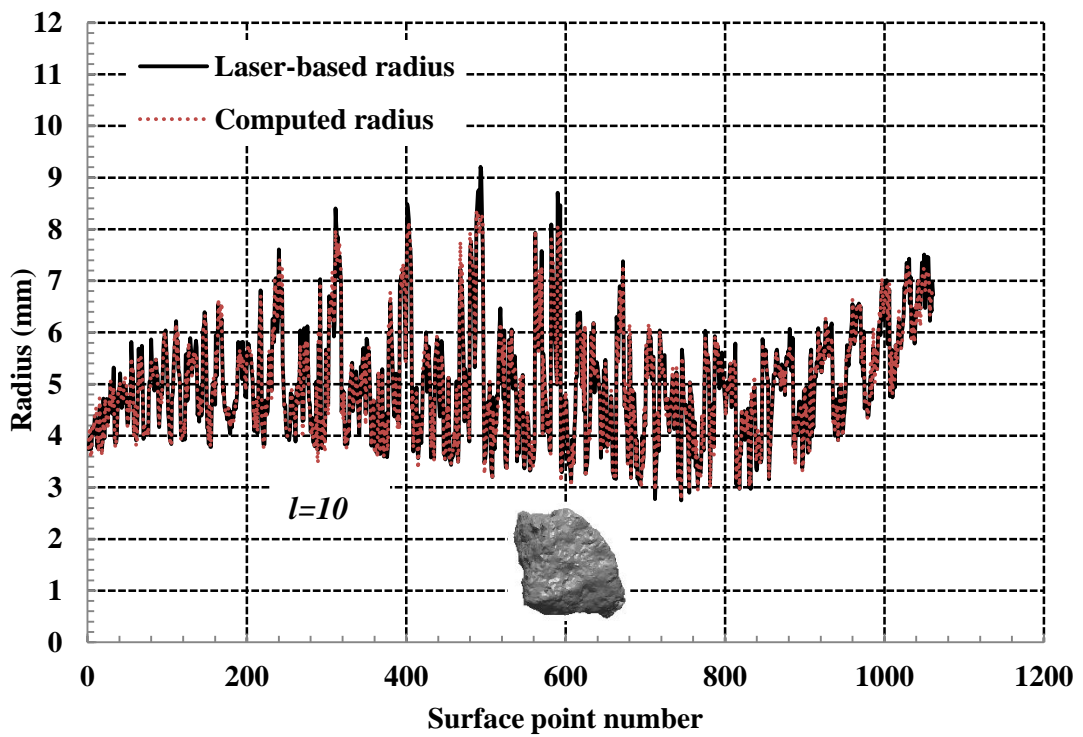
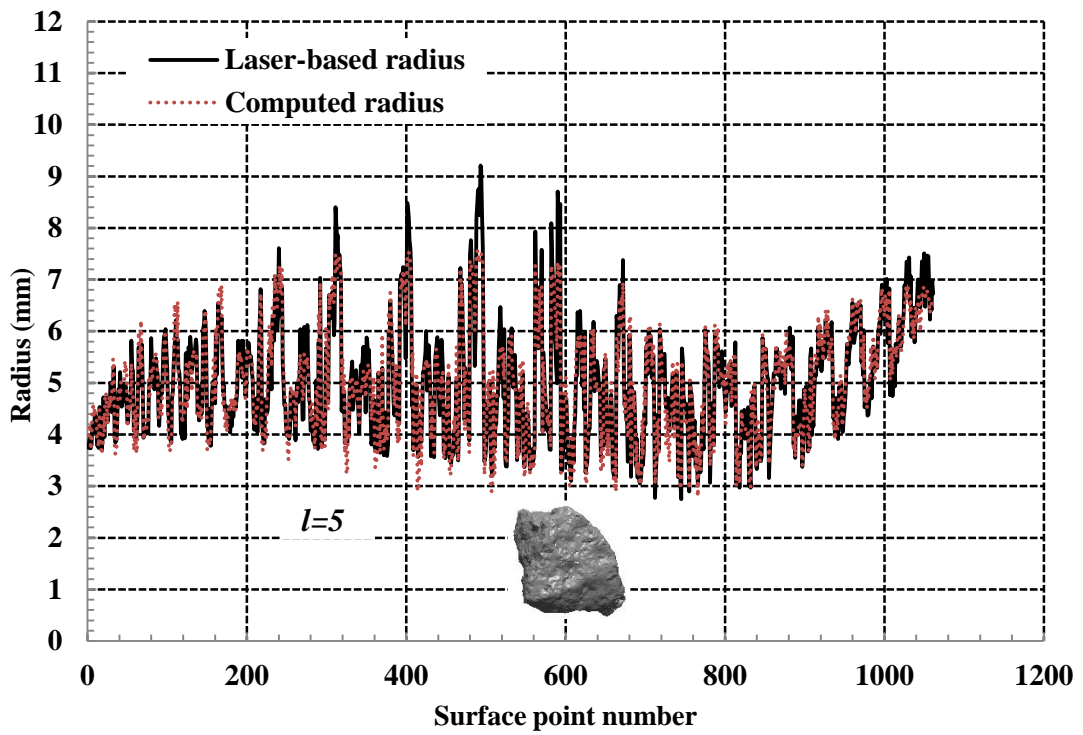


Figure 10.13: Radii determined from laser scans and radii computed using spherical harmonic technique for 6.7 mm aggregate particle ( $l=5$  and 10).

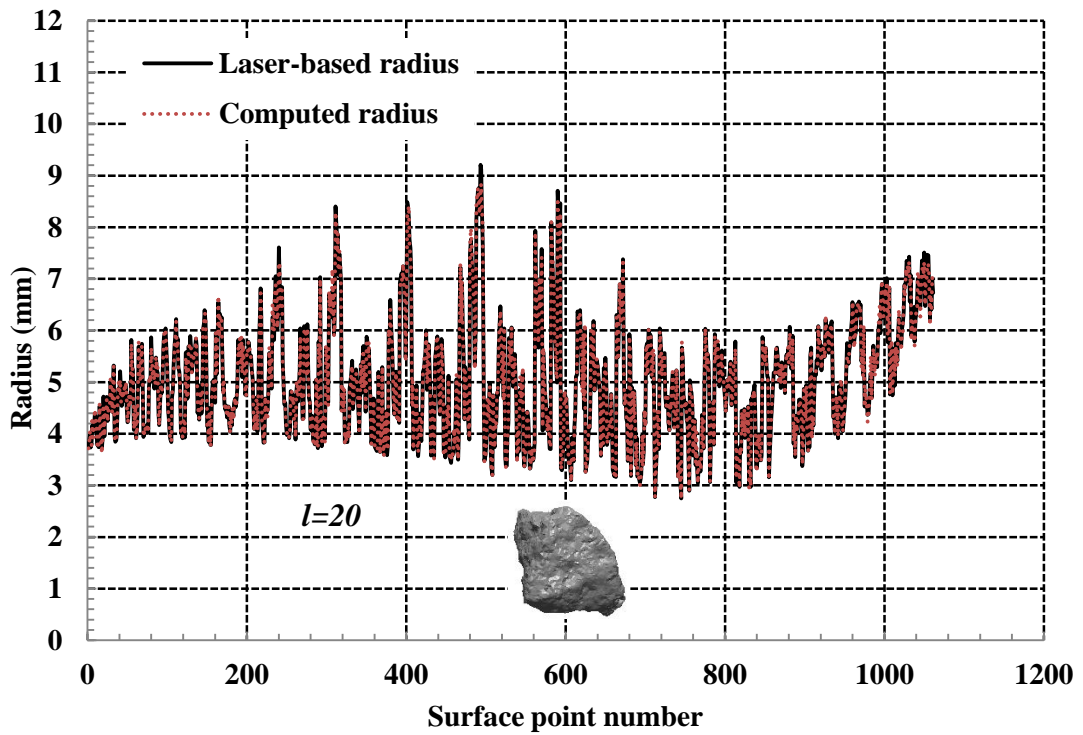
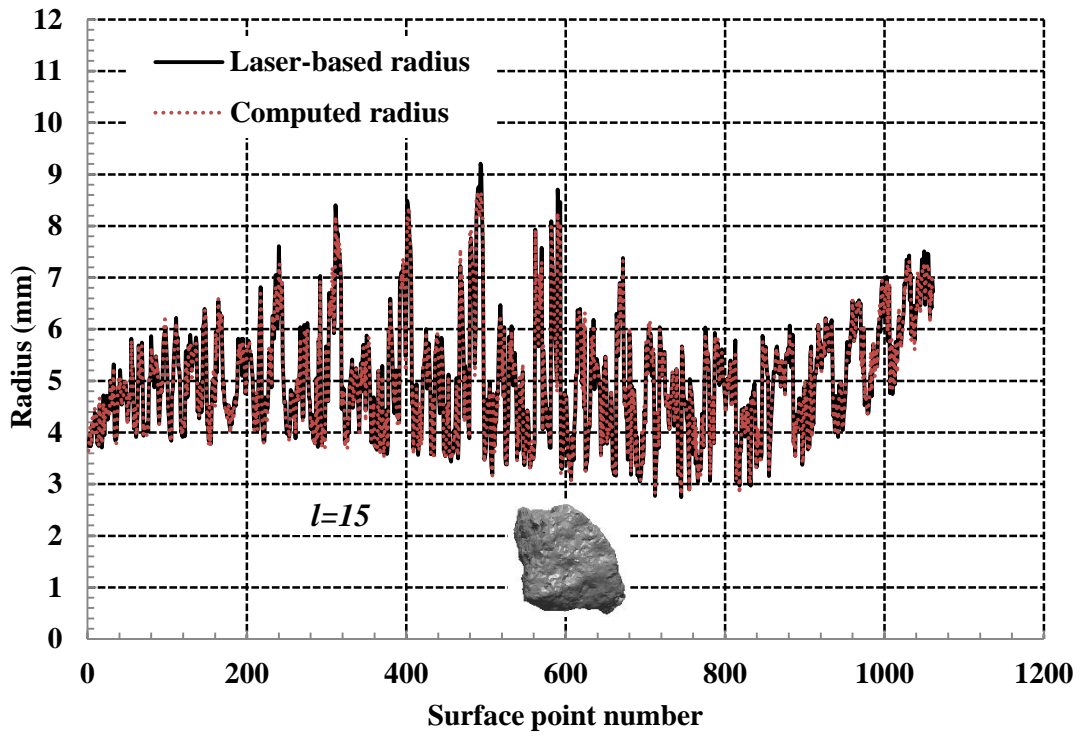


Figure 10.14: Radii determined from laser scans and radii computed using spherical harmonic technique for 6.7 mm aggregate particle ( $l=15$  and 20).

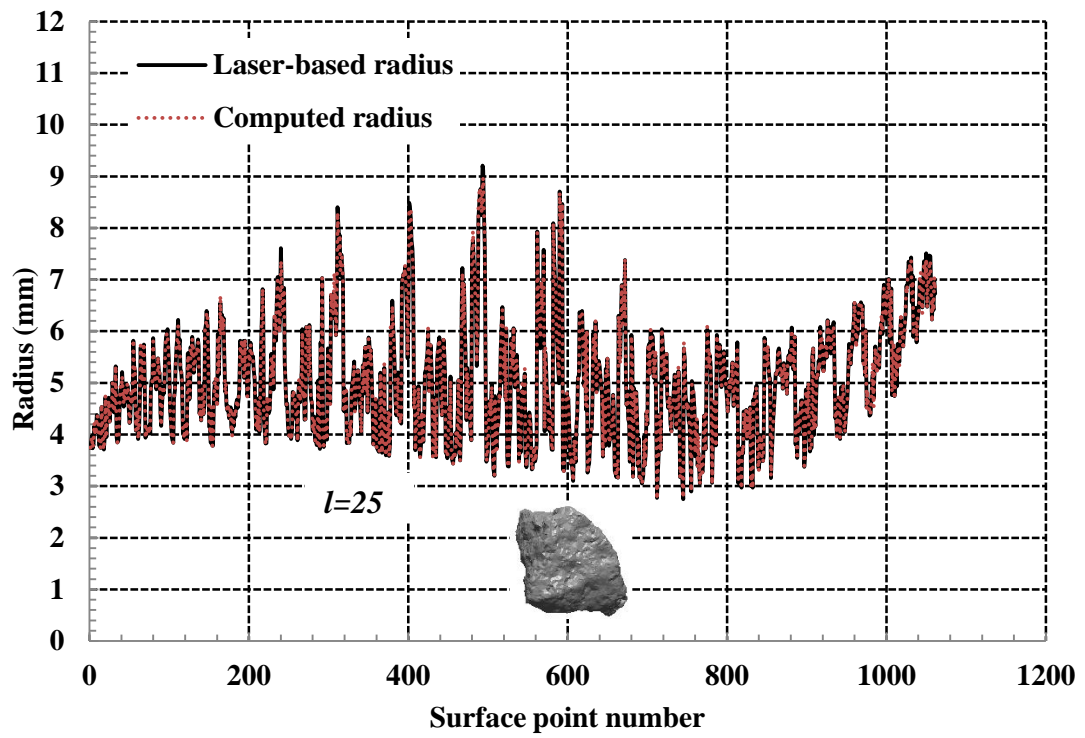


Figure 10.15: Radii determined from laser scans and radii computed using spherical harmonic technique for 6.7 mm aggregate particle ( $l=25$ ).

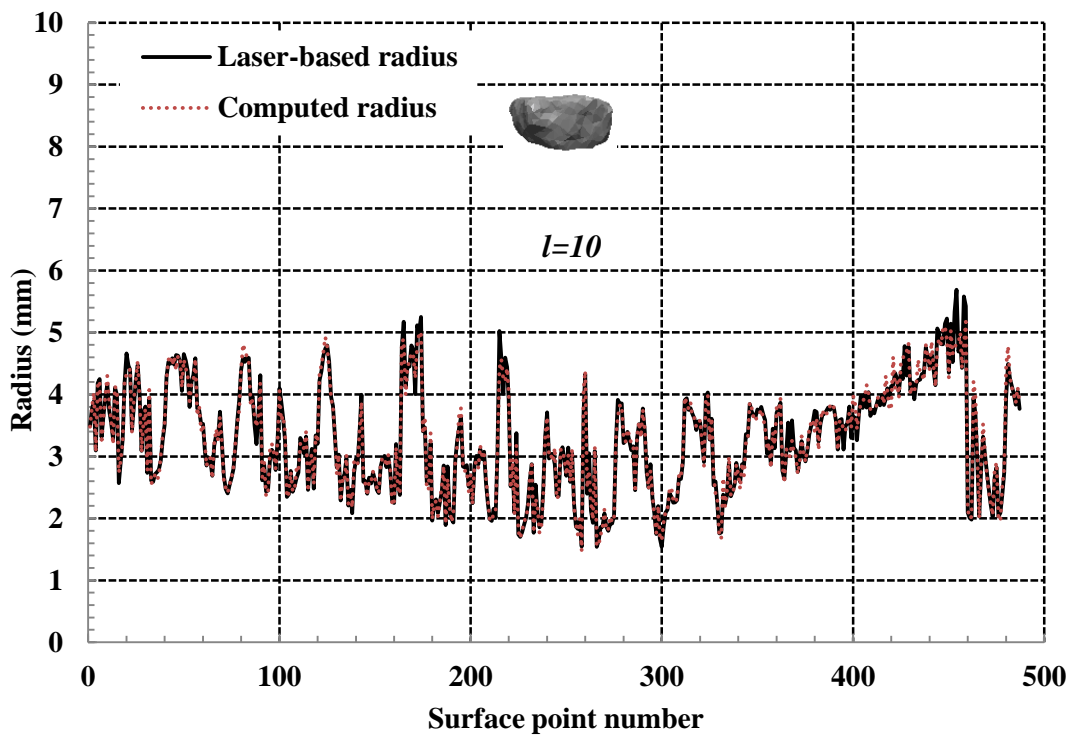
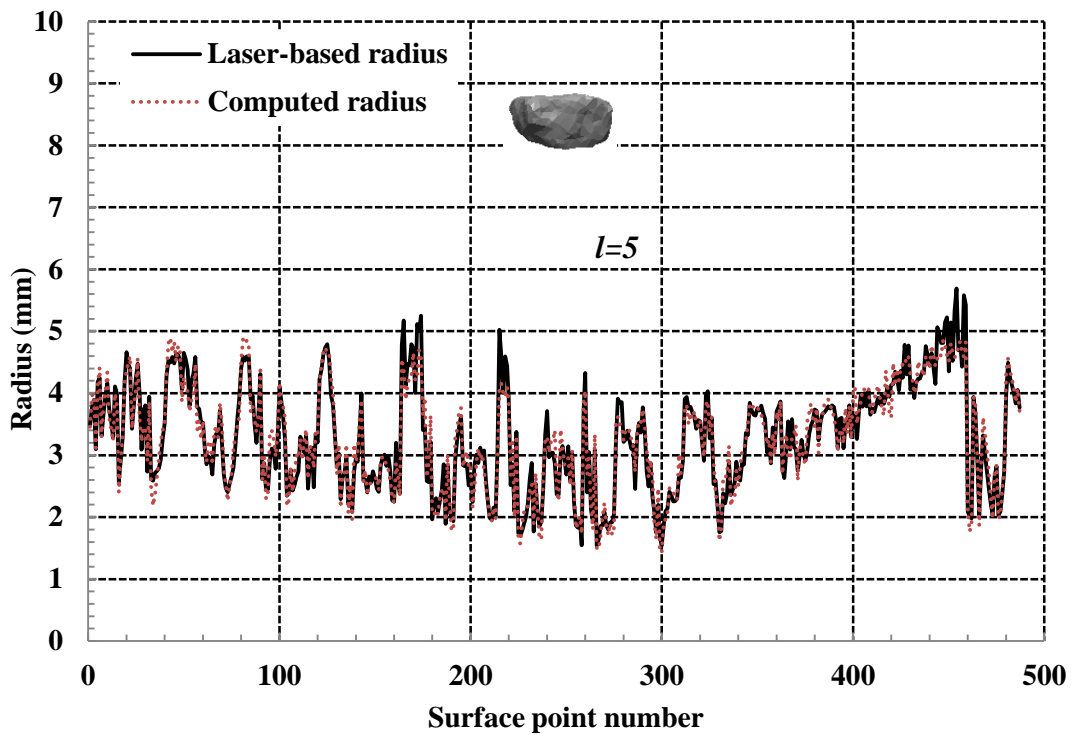


Figure 10.16: Radii determined from laser scans and radii computed using spherical harmonic technique for 4.75 mm aggregate particle ( $l=5$  and 10).

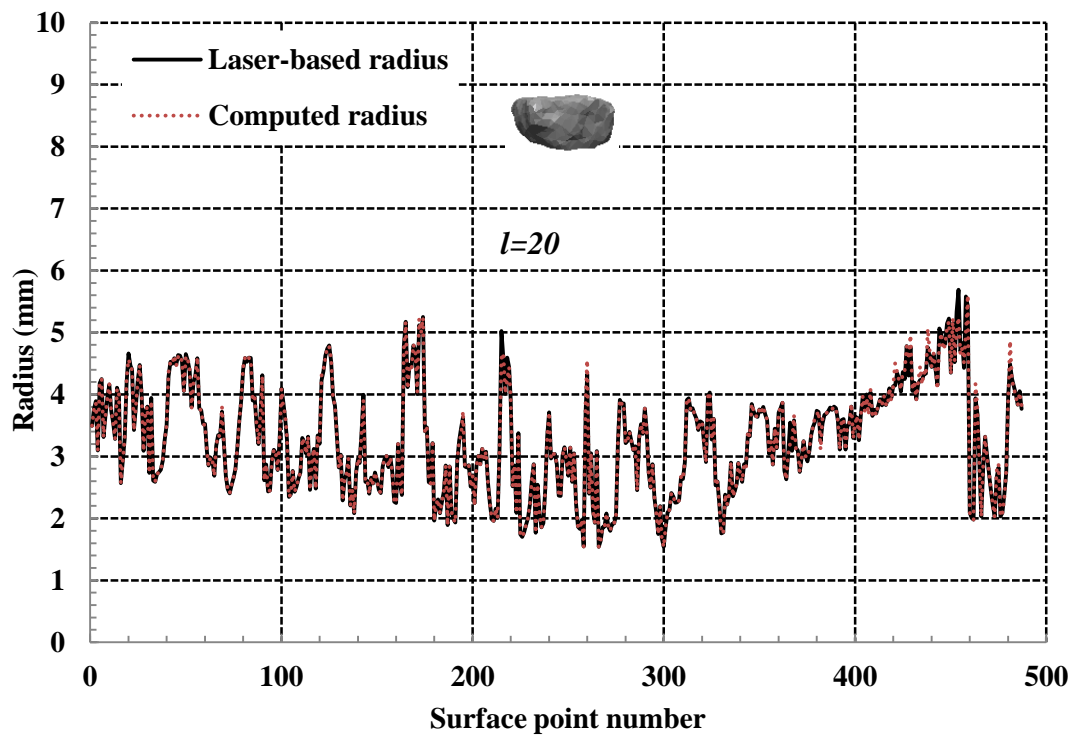
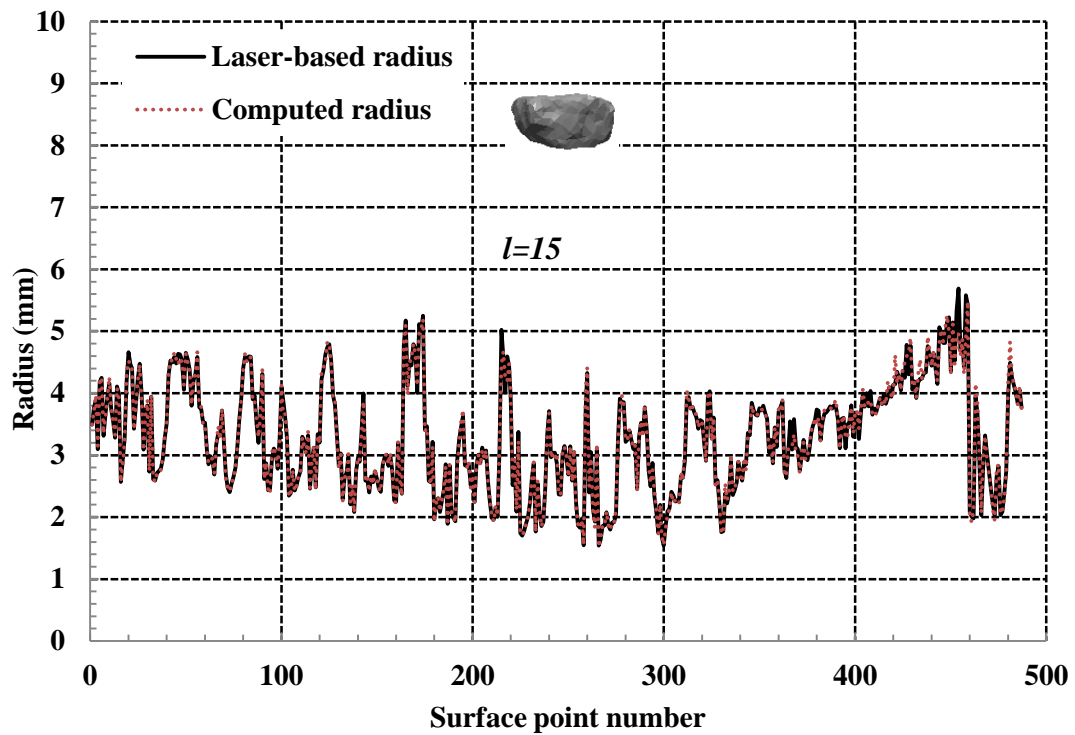


Figure 10.17: Radii determined from laser scans and radii computed using spherical harmonic technique for 4.75 mm aggregate particle ( $l=15$  and 20).

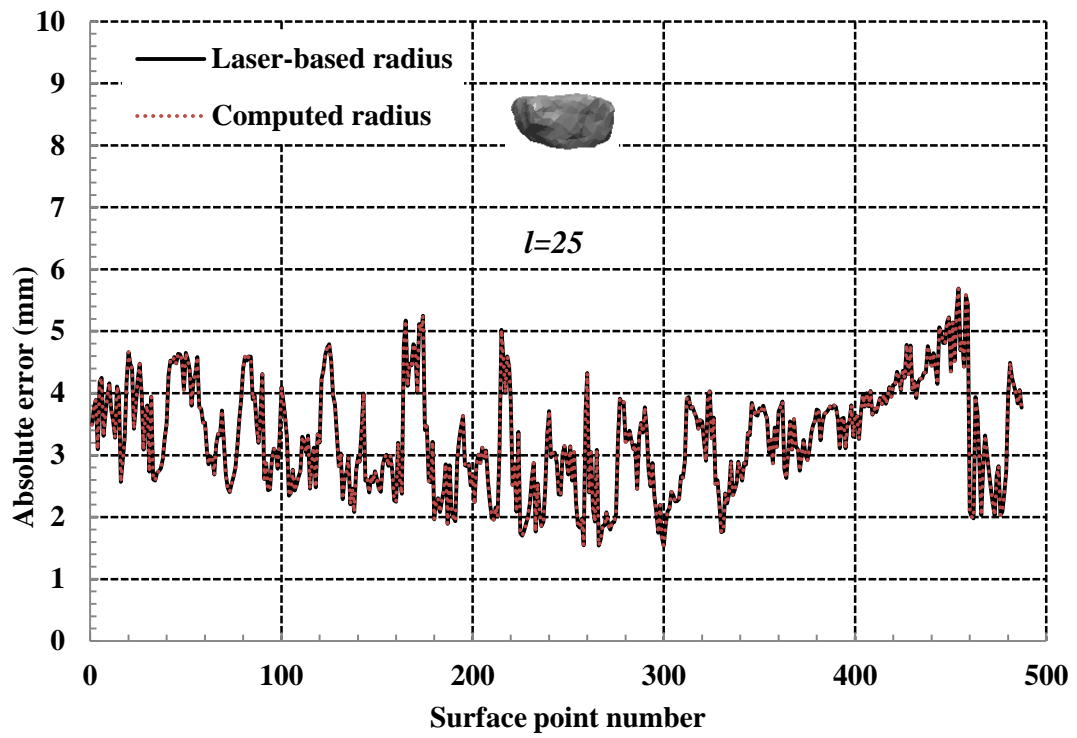


Figure 10.18: Radii determined from laser scans and radii computed using spherical harmonic technique for 4.75 mm aggregate particle ( $l=25$ ).